Ontario

Ontario Geological Survey
Open File Report 6160

An Integrated Study of Intrusive Rocks Spatially Associated with Gold and Base Metal Mineralization in the Abitibi Greenstone Belt, Timmins Area and Clifford Township: Discover Abitibi Initiative

2005

Ontario

ONTARIO GEOLOGICAL SURVEY

Open File Report 6160

An Integrated Study of Intrusive Rocks Spatially Associated with Gold and Base Metal Mineralization in the Abitibi Greenstone Belt, Timmins Area and Clifford Township: Discover Abitibi Initiative

by

P.J. MacDonald, S.J. Piercey and M.A. Hamilton

2005

Parts of this publication may be quoted if credit is given. It is recommended that reference to this publication be made in the following form:

MacDonald, P.J., Piercey, S.J. and Hamilton, M.A. 2005. An integrated study of intrusive rocks spatially associated with gold and base metal mineralization in the Abitibi greenstone belt, Timmins area and Clifford Township: Discover Abitibi Initiative; Ontario Geological Survey, Open File Report 6160, 190p.

Discover Abitibi
Découvrons l'Abitibi

Discover Abitibi
A project of innovation, cooperation and revitalization

Découvrons l' Abitibi
Un projet d'innovation, de coopération et de renouvellement

Discover Abitibi Initiative
The Discover Abitibi Initiative is a regional, cluster economic development project based on geoscientific investigations of the western Abitibi greenstone belt. The initiative, centred on the Kirkland Lake and Timmins mining camps, will complete 19 projects developed and directed by the local stakeholders. FedNor, Northern Ontario Heritage Fund Corporation, municipalities and private sector investors have provided the funding for the initiative.

Initiative Découvrons l'Abitibi
L'initiative Découvrons l'Abitibi est un project de développment économique régional dans une grappe d'industries, projet fondé sur des études géoscientifiques de la ceinture de roches vertes de l'Abitibi occidental. Cette initiative, centrée sur les zones minières de Kirkland Lake et de Timmins mènera à bien 19 projets élaborés et dirigés par des intervenants locaux. FedNor, la Société de gestion du Fonds du patrimoine du Nord de l'Ontario, municipalités et des investisseurs du secteur privé ont fourni les fonds de cette initiative.

FedNor
Canada

Timmins

KIRKLAND LAKE

Ontario
Northern Ontario Heritage Fund
Fonds du patrimoine du Nord de l'Ontario

© Queen's Printer for Ontario, 2005

© Queen's Printer for Ontario, 2005.

Open File Reports of the Ontario Geological Survey are available for viewing at the Mines Library in Sudbury, at the Mines and Minerals Information Centre in Toronto, and at the regional Mines and Minerals office whose district includes the area covered by the report (see below).

Copies can be purchased at Publication Sales and the office whose district includes the area covered by the report. Although a particular report may not be in stock at locations other than the Publication Sales office in Sudbury, they can generally be obtained within 3 working days. All telephone, fax, mail and e-mail orders should be directed to the Publication Sales office in Sudbury. Use of VISA or MasterCard ensures the fastest possible service. Cheques or money orders should be made payable to the *Minister of Finance.*

Mines and Minerals Information Centre (MMIC) Tel: (416) 314-3800
Macdonald Block, Room M2-17
900 Bay St.
Toronto, Ontario M7A 1C3

Mines Library Tel: (705) 670-5615
933 Ramsey Lake Road, Level A3
Sudbury, Ontario P3E 6B5

Publication Sales Tel: (705) 670-5691(local)
933 Ramsey Lake Rd., Level A3 1-888-415-9845(toll-free)
Sudbury, Ontario P3E 6B5 Fax: (705) 670-5770
E-mail: pubsales@ndm.gov.on.ca

Regional Mines and Minerals Offices:

Kenora - Suite 104, 810 Robertson St., Kenora P9N 4J2

Kirkland Lake - 10 Government Rd. E., Kirkland Lake P2N 1A8

Red Lake - Box 324, Ontario Government Building, Red Lake P0V 2M0

Sault Ste. Marie - 70 Foster Dr., Ste. 200, Sault Ste. Marie P6A 6V8

Southern Ontario - P.O. Bag Service 43, 126 Old Troy Rd., Tweed K0K 3J0

Sudbury - Level B3, 933 Ramsey Lake Rd., Sudbury P3E 6B5

Thunder Bay - Suite B002, 435 James St. S., Thunder Bay P7E 6S7

Timmins - Ontario Government Complex, P.O. Bag 3060, Hwy. 101 East, South Porcupine P0N 1H0

Toronto - MMIC, Macdonald Block, Room M2-17, 900 Bay St., Toronto M7A 1C3

This report has not received a technical edit. Discrepancies may occur for which the Ontario Ministry of Northern Development and Mines does not assume any liability. Source references are included in the report and users are urged to verify critical information. Recommendations and statements of opinions expressed are those of the author or authors and are not to be construed as statements of government policy.

If you wish to reproduce any of the text, tables or illustrations in this report, please write for permission to the Team Leader, Publication Services, Ministry of Northern Development and Mines, 933 Ramsey Lake Road, Level B4, Sudbury, Ontario P3E 6B5.

Cette publication est disponible en anglais seulement.

Parts of this report may be quoted if credit is given. It is recommended that reference be made in the following form:

MacDonald, P.J., Piercey, S.J. and Hamilton, M.A. 2005. An integrated study of intrusive rocks spatially associated with gold and base metal mineralization in the Abitibi greenstone belt, Timmins area and Clifford Township: Discover Abitibi Initiative; Ontario Geological Survey, Open File Report 6160, 190p.

105-04875/

Contents

Abstract xv

Chapter 1: Overview 1
  Introduction 1
  Methodology and Approach 1
  Report Layout 2
  Acknowledgments 2
  References 3

Chapter 2: Porphyry Intrusions of the Timmins Gold Camp: An Examination of Intermediate to Felsic Intrusions Associated with Gold Mineralization along the Porcupine–Destor Deformation Zone 6
  Introduction 6
  Previous Work 6
  Regional Geology 7
  Geology: Quartz-Feldspar Porphyry Intrusions 8
    Central Trend 8
      Field Relationships 8
      Petrography 9
      Alteration, Veining and Mineralization 10
      Deformation 11
      Geochemistry 11
      Geochronology 12
    Northern Trend 12
      Field Relationships 12
      Petrography 13
      Alteration, Veining and Mineralization 13
      Deformation 14
      Geochemistry 15
      Geochronology 16
    Western Trend 16
      Field Relationships 16
      Petrography 17
      Alteration, Veining and Mineralization 17
      Deformation 18
      Geochemistry 18
      Geochronology 19
    Southern Trend 19
      Field Relationships 19
      Petrography 20
      Alteration, Veining and Mineralization 20
      Deformation 21
      Geochemistry 21
      Geochronology 22

Eastern Trend 22
Field Relationships 22
Petrography 23
Alteration, Veining and Mineralization 23
Deformation 24
Geochemistry 24
Geochronology 25
Geology: The Krist Formation 26
Field Relationships and Petrography 26
Alteration, Veining, Mineralization and Deformation 26
Geochemistry 27
Geochronology 27
Comparison of Porphyry Trends 27
Comparison of the Krist Formation with Porphyry Intrusions 28
Discussion 29
Geochemical and Timing Relationships of Porphyries with Gold Mineralization 29
Relationship of Porphyries to Gold and Copper Mineralization and Exploration Implications 29
Summary 31
References 32

Chapter 3: The Setting and Importance of Subvolcanic Intrusions in the Blake River Group of Ontario 95
Introduction 95
Regional Geologic and Tectonic Setting 95
Previous Work 96
Geology and Stratigraphic Relationships 98
Alteration and Mineralization Styles 99
Lithogeochemistry: Petrogenetic Aspects 100
Alteration and Metamorphism: Constraints on Elemental Utility 101
Results: Blake River Group 101
Results: Clifford Stock and Equivalents 102
Uranium–Lead Geochronology 103
Age of Clifford Stock 103
Age of Felsic Dikes 103
Exploration Implications and Recommendations 104
Summary 105
References 106

Appendix A. Lithogeochemical Analytical Methods, Quality Control and Quality Assurance 161

Appendix B. Analytical Methods for Uranium–Lead Geochronology 187

Metric Conversion Table 190

FIGURES

1.1. Assemblage map of the Ontario portion of the Abitibi greenstone belt with assemblage boundaries with locations of the porphyry project localities and the base-metal portion of the subproject. 4

1.2. Geographic map of the study area 5

2.1. Stratigraphic column of the Timmins area of the southern Abitibi greenstone belt including the Deloro, Tisdale, Porcupine and Timiskaming assemblages 35

2.2. Simplified regional geology map of the Timmins portion of the southern Abitibi greenstone belt with the locations of the 5 geographical porphyry trends shown 36

2.3. Simplified surface geology map of the central trend showing the names and locations 37

2.4. Simplified surface geology map of the northern trend showing the names and locations 38

2.5. Surface geology map of the Crown porphyry breccia, Shania Twain Centre showing northward extension 39

2.6. Map showing location relationship of Hollinger–McIntyre gold mineralization and sericite–calcium carbonate alteration to the northern trend porphyries 40

2.7. Simplified surface geology map of the western trend showing the names and locations 41

2.8. Simplified surface geology map of the southern trend showing the names and locations 42

2.9. Simplified surface geology map of the eastern trend showing the names and locations 43

2.10. Simplified surface geology map of the Krist Formation showing the locations of the samples collected 44

2.11. Standard Harker plots for the 5 geographical porphyry trends as well as the Krist Formation (A to L).. 45

2.12. Major element alteration plots for the 5 geographical porphyry trends as well as the Krist Formation, including A) Na_2O versus Al_2O_3/Na_2O plot; B) alteration box-plot; and C) Hughes plot 47

2.13. Classification plots for rocks of the 5 geographical porphyry trends as well as the Krist Formation: A) Nb/Y versus Zr/TiO_2 discrimination diagram; B) SiO_2 versus alkali plot showing alkaline versus subalkaline fields; C) alkali–FeO–MgO (AFM) plot; and D) Y versus Zr/Y 49

2.14. Classification plots for rocks of the 5 geographical porphyry trends as well as the Krist Formation: A) typical normative feldspar diagram; and B) Al_2O_3 versus Yb diagram for classifying different types of tonalite-trondhjemite-granodiorite (TTG) 51

2.15. Primitive mantle normalized plots for rocks of the 5 geographical porphyry trends as well as the Krist Formation: A) Group A; B) Group B; C) Group C; D) Group D; E) Groups E1 and E2; F) Group F; and G) Group G 52

2.16. Concordia plots for porphyry U/Pb geochronology samples: A) sample 03LAH-0627 (Mt. Logano porphyry (southern trend)); and B) sample 03PJM-131 (Pamour porphyry (eastern trend)). 56

3.1. Regional distribution of the Blake River Group, with locations of major felsic volcanic complexes of the central Blake River Group, synvolcanic intrusions of the Blake River Group, and younger, Lac Dufault age intrusions. 112

3.2. Geological map of the Clifford stock and Blake River Group, Clifford Township 113

3.3. Schematic stratigraphic column for rocks of the Blake River Group in Clifford Township. 114

3.4. Major element alteration plots for the Blake River Group Rocks in Clifford Township, including A) Na_2O versus Al_2O_3/Na_2O plot; B) alteration box-plot; C) Hughes plot 115

3.5. Geochemical classification diagrams for the Blake River Group rocks. A) Nb/Y versus Zr/TiO_2 diagram; B) standard AFM diagram; C) Y versus Zr/Y diagram 117

3.6. Standard Harker plots for the Blake River Group volcanic and intrusive rocks (A to P) 119

3.7. Primitive mantle normalized plots for rocks of the Blake River Group: A) cycle 1, unit 1, contaminated E-MORB-like; B) cycle 1, unit 1, E-MORB-like; C) cycle 1, unit 2, transitional arc (basaltic tuffs); D) cycle 1, unit 2, E-MORB-like; E) cycle 1, unit 2, contaminated E-MORB-like; F) cycle 2, unit 4, contaminated E-MORB-like; G) cycle 2, unit 4, E-MORB-like; H) cycle 2, unit 5, transitional to calc-alkalic rhyolites; I) synvolcanic gabbro and diabase, contaminated E-MORB like; and J) synvolcanic gabbro and diabase, E-MORB like 122

3.8. Trace element plots illustrating relationship of the size of the negative Nb anomaly (Nb/Th_{pmN}) to contamination sensitive elements and element ratios: A) Nb/La_{pmN} versus Nb/Th_{pmN}; B) La/Sm versus Nb/Th_{pmN}; C) SiO_2 versus Nb/Th_{pmN}; and D) Nb/U versus Nb/Th_{pmN}. 124

3.9. Major element alteration plots for the Clifford stock and equivalent rocks from Clifford Township: A) Na_2O versus Al_2O_3/Na_2O plot with designations for least-altered samples; B) alteration box-plot; C) Hughes plot 125

3.10. Classification plots for the rocks of the Clifford stock and equivalents. A) typical normative feldspar diagram; B) alkali–FeO–MgO (AFM) plot; C) Nb/Y versus Zr/TiO_2 discrimination diagram; and D) Al_2O_3 versus Yb diagram 127

3.11. Trace element plots for rocks of the Clifford stock and equivalents: A) Y versus Zr/Y diagram; B) primitive mantle normalized plot; and C) Y versus Sc plot 128

3.12. Standard Harker plots for rocks of the Clifford stock and equivalents (A to O) 129

3.13. Concordia diagram summarizing U/Pb results for samples: A) 03SJP-115; and B) 03SJP-059-1 131

3.14. Geochemical diagrams that effectively discriminate the Clifford stock from the older Blake River Group rocks, including: A) Y versus Zr/Y; B) Yb versus La/Yb; C) Yb versus Al_2O_3/Yb; and D) Nb/Y versus Zr/Y 132

A1. Schematic of the standard scatterplot (A) and Thompson–Howarth plot (B) 166

PHOTOS

2.1. Selected photos and photomicrographs of the intrusions of the central trend (A to O) 57

2.2. Selected photos and photomicrographs of the intrusions of the northern trend (A to I) 60

2.3. Selected photos and photomicrographs of the intrusions of the western trend (A to D) 62

2.4. Selected photos and photomicrographs of the intrusions of the southern trend (A to F) 63

2.5. Selected photos and photomicrographs of the intrusions of the eastern trend (A to L) 64

2.6. Selected photos and photomicrographs of the intrusions of the Krist Formation (A to E) 66

3.1. Photographs of rocks from the Blake River Group (A to G) 133

3.2. Photographs of rocks from the Clifford stock and equivalent units (A to D) 134

3.3. Photographs of alteration types and styles from Clifford Township (A to H) 135

TABLES

2.1. The porphyry intrusions included in this study; information includes the porphyry name, geographical trend as explained in the report (central, northern, western, southern or eastern), age of emplacement (if known) and source for age.......... 67

2.2. Summary of the field relationships, petrology, alteration, veining, mineralization, deformation, geochemistry and geochronology for quick comparison of the 5 geographical porphyry trends 68

2.3. Geochemical data for rocks of the porphyry intrusion suite examined within this project.......... 71

3.1. Geochemical data for rocks of the Blake River Group and Clifford stock and equivalents.......... 139

3.2. Key element ratios for rocks of the Blake River Group and Clifford stock and equivalents.......... 146

A1. Precision and accuracy data for major elements by fused disc XRF at the Ontario Geoscience Laboratories.......... 167

A2. Precision and accuracy data for major elements by fused disc XRF at Activation Laboratories.......... 170

A3. Precision and accuracy data for trace elements by pressed pellet XRF at the Ontario Geoscience Laboratories.......... 173

A4. Precision and accuracy data for trace elements by pressed pellet XRF at Activation Laboratories.......... 174

A5. Precision and accuracy data for trace elements by ICP–ES at the Ontario Geoscience Laboratories.......... 175

A6. Precision and accuracy data for trace elements by ICP–MS at the Ontario Geoscience Laboratories.......... 180

Abstract

This report presents the results of the intrusion subproject of the Discover Abitibi Initiative, a project aimed at understanding the relationship of intrusions to base metal and gold mineralization in the Abitibi greenstone belt of Ontario. The first part of this report deals with intrusions associated with gold in the Timmins camp and the second part of the report deals with the relationship of the Clifford stock and the Blake River Group in eastern Ontario to base metal and gold mineralization in Clifford Township.

Porphyry intrusions in the Timmins camp were studied from Bristol Township, west of Timmins, through the Timmins camp proper, across to Carr Township, east of Timmins, so as to compare porphyries within the main gold camp to those outside of the main camp. The porphyry intrusions in the Timmins camp and area have been subdivided into 5 trends depending on geographic location. These trends are east-trending belts ranging from 4 to 20 km long that are typically composed of numerous intrusions ranging from small dikes a few hundred metres long to oval bodies that are up to 11 km long. The porphyry intrusions generally intrude into the Vipond Formation of the Tisdale assemblage, but also at the Deloro–Tisdale and Tisdale–Porcupine assemblages contacts; the porphyry intrusions are generally semi-conformable to stratigraphy. The majority of the porphyry intrusions were emplaced predominantly at 2687 to 2691 Ma (Ayer et al. 2003a; Corfu et al. 1989), although the Aquarius porphyry was emplaced at 2705 Ma (Corfu et al. 1989), and the Pamour porphyry was emplaced at 2677.5 Ma (this study). The bulk of the gold-associated intrusions are high-aluminum (high-Al) tonalite-trondhjemite-granodiorite (TTG) suite intrusions with light rare earth element (LREE)-enrichment, heavy rare earth element (HREE) and yttrium depletion, and high Al_2O_3 contents; these signatures are very similar to modern-day adakitic magmas. The porphyry intrusions in the Timmins camp, even though spatially associated with gold and copper mineralization, have no genetic relationship to gold largely because 1) gold-bearing veins crosscut both the porphyry intrusions and the rocks that host the porphyries; 2) they are hosted in structurally controlled vein arrays; and 3) recent Re/Os ages obtained from gold-associated molybdenite (Ayer et al. 2003a) illustrate that the porphyries are 17 to 30 million years younger than the gold mineralization event. Nonetheless, gold mineralization is typically associated with 1) clusters of porphyry intrusions (e.g., Dome and Hollinger–McIntyre mines) with high-Al TTG signatures; 2) porphyries that have strong associations with major structures; and 3) porphyries that have undergone sericite (±carbonate) alteration (significant sodium losses and potassium metasomatism).

The rocks of the Blake River Group in Clifford Township consist predominantly of basalt to andesite with lesser rhyolite, and associated synvolcanic, high level rhyolitic intrusive rocks, and synvolcanic gabbro and diabase. The Blake River Group rocks have lithogeochemical signatures similar to modern enriched mid-ocean ridge basalt (E-MORB) and many have evidence for crustal contamination (contaminated E-MORB). The Clifford stock and age equivalent east-northeast-trending dikes from Clifford Township crosscut the Blake River Group and represent a distinctively younger pulse of magmatic activity within northeastern Ontario. Contrary to previous assertions, the Clifford stock has yielded a U/Pb zircon age of 2686.9±1.2 Ma, and an age equivalent east-northeast-trending dike has yielded an age of 2688.5±2.3 Ma. These ages are younger than the Blake River Group magmatism in this area (ca. 2700–2696 Ma; Péloquin and Piercey 2005), but are similar to other late tectonic TTG plutons in the southeastern Abitibi greenstone belt (e.g., Clarice Lake, Lac Dufault; Corfu and Noble 1992; Mortensen 1993). The Clifford stock and equivalent rocks have very distinctive lithogeochemical signatures typical of high-Al TTG suites, and have very distinctively low Y (<10 ppm) and Yb (<2 ppm), and high Zr/Y (>7), Nb/Y (>0.4), Al_2O_3/Yb (>10), and La/Yb (>10) ratios, as compared to the older Blake River Group rocks; these features can be used to geochemically discriminate felsic magmatism associated with the Blake River Group from younger TTG-related magmatism associated with the Clifford stock and other TTG magmatism (ca. 2690 Ma).

Mineralization in Clifford Township consists of an older volcanogenic massive sulphide (VMS) related style of mineralization, and a younger, overprinting porphyry copper-molybdenum-gold (Cu-Mo-Au) style of mineralization. The VMS-related mineralization consists of epidote-quartz-pyrite-chlorite assemblages, typical of semi-conformable-style alteration associated with permeable zones (e.g., amygdules, pillow margins and interpillow regions) in the volcanic rocks of the Blake River Group. There are also some zones of higher temperature chlorite-quartz-chalcopyrite-pyrite assemblages typical of pipe-like alteration. The younger porphyry Cu-Mo-Au style mineralization occurs as a series of breccia pipes and stockwork vein systems. This latter style of mineralization is associated with a complex array of veinlet and vein-styles of alteration that is quite distinctive from VMS mineralization. The fact that this mineralization is hosted in the Clifford stock and associated dikes that are circa 2690 million years old suggests that this mineralization represents a distinctly younger magmatic-hydrothermal event, distinctive from the early VMS-related event. Recommendations for exploration for both types of commodities (VMS versus porphyry Cu-Mo-Au) are provided within this report.

REFERENCES

Ayer, J.A., Barr, E., Bleeker, W., Creaser, R.A., Hall, G., Ketchum, J.W.F., Powers, D., Salier, B., Still, A. and Trowell, N.F. 2003a. Discover Abitibi. New geochronological results from the Timmins area: implications for the timing of late-tectonic stratigraphy, magmatism and gold mineralization; *in* Summary of Field Work and Other Activities 2003, Ontario Geological Survey, Open File Report 6120, p.33-1 to 33-11.

Corfu, F., Krogh, T.E., Kwok, Y.Y. and Jensen, L.S. 1989. U-Pb zircon geochronology in the southwestern Abitibi greenstone belt, Superior Province; Canadian Journal of Earth Sciences, v.26, p.1747-1763.

Corfu, F. and Noble, S.R. 1992. Genesis of the southern Abitibi greenstone belt, Superior Province, Canada; evidence from zircon Hf isotope analyses using a single filament technique; Geochimica et Cosmochimica Acta, v.56, p.2081-2097.

Mortensen, J.K. 1993. U-Pb geochronology of the eastern Abitibi Subprovince. Part 2: Noranda–Kirkland Lake area; Canadian Journal of Earth Sciences, v.30, p.29-41.

Péloquin, A.S. and Piercey, S.J. 2005. Geology and base metal mineralization in Ben Nevis, Katrine and Clifford townships: Discover Abitibi; Ontario Geological Survey, Open File Report 6161.

An Integrated Study of Intrusive Rocks Spatially Associated with Gold and Base Metal Mineralization in the Abitibi Greenstone Belt, Timmins Area and Clifford Township: Discover Abitibi

P.J. MacDonald[1], S.J. Piercey[2] and M.A. Hamilton[3]
Ontario Geological Survey
Open File Report 6160
2005

---

[1] Mineral Exploration Research Centre, Department of Earth Sciences,
Laurentian University, 935 Ramsey Lake Road, Sudbury, Ontario P3E 2C6

Correspondence should be addressed to
[2] Mineral Exploration Research Centre, Department of Earth Sciences,
Laurentian University, 935 Ramsey Lake Road, Sudbury, Ontario P3E 2C6
Telephone: 705.675.1151 ext.2364; Facsimile: 705.675.4898; Email: spiercey@laurentian.ca

[3] Jack Satterly Geochronology Laboratory, Department of Geology
University of Toronto, Earth Sciences Centre, 22 Russell Street, Toronto, Ontario M5S 3B1

Chapter 1: Overview

INTRODUCTION

The Abitibi greenstone belt is one of the most prolific metallogenic provinces in the world (e.g., Card and Poulsen 1998), with world-class gold deposits (e.g., Timmins and Kirkland Lake districts; Card and Poulsen 1998), magmatic nickel-copper mineralization in komatiitic rocks (e.g., Alexo: Barnes and Naldrett 1985), and world-class volcanogenic massive sulphide (VMS) deposits (e.g., Noranda camp: Gibson and Watkinson 1990; Kidd Creek: Hannington and Barrie 1999, and references therein). These districts have produced significant base and precious metals over the last century; however, even with a century of mining, fundamental questions still exist with respect to the regional stratigraphic, structural and geochemical controls on the localization of these deposits in the Abitibi greenstone belt. This poor understanding of the regional controls on ore systems has hampered recent exploration efforts and has led to a dearth of new discoveries in recent years. The Discover Abitibi Initiative was designed with these problems in mind, and is a multi-disciplinary geological, geophysical and geochemical program aimed at enhancing the understanding of the regional setting of mineral deposits within the Abitibi greenstone belt of Ontario (e.g., Ayer et al. 2003b, 2004).

This report summarizes the results of a subproject within the Discover Abitibi Initiative aimed at understanding the role that intrusions have played in the localization and genesis of gold and base metal deposits within the Abitibi greenstone belt, Ontario. The report will consist of 3 parts: an overview and 2 studies. The first study (Chapter 2) is of the role of felsic "porphyry" suite intrusions and their relationship to orogenic gold within the Porcupine gold camp (Figure 1.1); and the second study (Chapter 3) is aimed at understanding the role of felsic intrusions in the generation of massive sulphide and gold mineralization within the Blake River Group of Ontario (*see* Figure 1.1). Initial results of this project have been previously reported (MacDonald and Piercey 2003; MacDonald, Piercey and Hamilton 2004; Péloquin and Piercey 2003; Piercey et al. 2004), and this report constitutes the final field results, and a preliminary assessment of the geochemical and U/Pb geochronological database for the intrusion subproject. Outlined below are the methodology and approach taken in this project, an outline of the layout of this report, and acknowledgments. The goals and objectives of each subproject within the intrusion project will be discussed in the respective sections.

METHODOLOGY AND APPROACH

This subproject involved a combination of field and laboratory work. Field work was conducted in the Timmins area and in Clifford Township (Figure 1.2) in both 2003 and 2004 and involved a combination of geological (approximately 1:5000) and outcrop-scale mapping, coupled with studies of diamond drill core. In addition to field work, major, trace and rare-earth element geochemistry were conducted in support of the field mapping and drill core studies; details on the instrumentation, methodology, precision and accuracy are presented in Appendix A. As well, certain key units were sampled and submitted for geochronological analyses; ages were obtained for these units. The U/Pb geochronological analyses on zircons were conducted at the Jack Satterly Geochronology Laboratory at the University of Toronto; details on the methodology and instrumentation are presented in Appendix B.

REPORT LAYOUT

Due to the breadth and diversity of the intrusion subproject, this report will be divided into 2 parts: one part on the relationship of porphyries to gold in the Timmins camp (Chapter 2), and a second part on the Clifford stock and its relationship to base-metal and gold mineralization in Clifford Township (Chapter 3). Each part will be self contained with its own introduction, main body of geological and analytical data, and summary and discussion followed by the relevant figures, photos and tables. The end of the report contains 2 appendixes describing the analytical methods and quality control and quality assurance information for the lithogeochemistry (Appendix A) and U/Pb geochronology (Appendix B).

ACKNOWLEDGMENTS

This subproject was supported by the Discover Abitibi Initiative, which is funded by the private sector (a consortium of mining, exploration, and mining and exploration services companies), municipalities, and the federal and provincial governments (respectively Industry Canada through FedNor and the Ontario Ministry of Northern Development and Mines through the Northern Ontario Heritage Fund). One of the authors (SJP) and his research group are also supported by a Natural Sciences and Engineering Research Council of Canada (NSERC) Discovery Grant. Phil Thurston and John Ayer are thanked for their administrative and scientific contributions during the length of this project. Marcus Burnham and James Schweyer are thanked for numerous discussions about laboratory protocol, and precision and accuracy information for the Ontario Geoscience Laboratories; Eric Hoffman is thanked for similar discussions and information from Activation Laboratories Limited. For the Blake River portion of the project, Wallbridge Mining Company Ltd. provided access to their properties, to drill core, and provided logistical support during field work in 2004. Discussions with Shirley Péloquin, Eric Chaloux, Doug Hunter, Dave Melling, John Watkins and Ian Fraser are gratefully acknowledged. Field assistance was provided by Andrew Shannon (2003), Chuck Lemieux (2003), Ivan Burton (2004) and Tyler Ruks (2004). For the porphyry portion of the project, the Porcupine Joint Venture (Alastair Still, Keith Green, Peter Harvey, Erik Barr, Bill MacRae, Steve Harding and Michael Nerup), Falconbridge Limited (Damien Duff and Cliff David), Kinross Gold Corporation (Ryburn Norman), Lakeshore Gold Corporation (Henry Marsden and Jacques Samson) and Tom Exploration Inc. (Chris Dupont) are acknowledged for access to drill core, property and logistics. Staff from the Ontario Geological Survey, including Brian Atkinson of the Resident Geologist office, and Lindsay Hall and crew, are thanked for geological discussions and sharing their knowledge of the Timmins region. Roger Bateman of the Discover Abitibi Initiative along with Dave Rhys of Panterra Geoservices Inc. are also acknowledged for insight into the structural geology of the area. Etienne Dinel of the University of Ottawa is thanked for sample collection of porphyry within the Hoyle Pond deposit.

REFERENCES

Ayer, J., Amelin, Y., Corfu, F., Kamo, S., Ketchum, J., Kwok, K. and Trowell, N. 2002. Evolution of the Southern Abitibi greenstone belt based on U-Pb geochronology: autochthonous volcanic construction followed by plutonism, regional deformation and sedimentation; Precambrian Research, v.115, p.63-95.

Ayer, J.A., Barr, E., Bleeker, W., Creaser, R.A., Hall, G., Ketchum, J.W.F., Powers, D., Salier, B., Still, A. and Trowell, N.F. 2003a. Discover Abitibi. New geochronological results from the Timmins area: implications for the timing of late-tectonic stratigraphy, magmatism and gold mineralization; *in* Summary of Field Work and Other Activities 2003, Ontario Geological Survey, Open File Report 6120, p.33-1 to 33-11.

Ayer, J.A., Thurston, P.C., Dubé, B., Fowler, A.D., Gibson, H.L., Hudak, G., Lafrance, B., Lesher, C.M., Piercey, S.J., Reed, L.E. and Thompson, P.H. 2003b. Overview of the Discover Abitibi Greenstone Architecture Project: subprojects, goals and results; *in* Summary of Field Work and Other Activities 2003, Ontario Geological Survey, Open File Report 6120, p.32-1 to 32-12.

Ayer, J.A., Thurston , P.C., Dubé, B., Gibson, H.L., Hudak, G.J., Lafrance, B., Lesher, C.M., Piercey, S.J., Reed, L.E. and Thompson, P.H. 2004. Discover Abitibi Greenstone Architecture Project: overview of results and belt-scale implications; *in* Summary of Field Work and Other Activities 2004, Ontario Geological Survey, p.37-1 to 37-15.

Barnes, S.-J. and Naldrett, A.J. 1985. The fractionation of the platinum-group elements at the Alexo komatiite, Abitibi greenstone belt, northern Ontario; The Canadian Mineralogist, v.23, p.295.

Card, K.D. and Poulsen, K.H. 1998. Archean and Paleoproterozoic geology and metallogeny of the southern Canadian Shield; Exploration and Mining Geology, v.7, p.181-215.

Gibson, H.L. and Watkinson, D.H. 1990. Volcanogenic massive sulphide deposits of the Noranda cauldron and shield volcano, Quebec; *in* The northwestern Quebec polymetallic belt: a summary of 60 years of mining exploration, Canadian Institute of Mining and Metallurgy, Special Volume 43, p.119-132.

Hannington, M.D. and Barrie, C.T. eds. 1999. The Giant Kidd Creek volcanogenic massive sulfide deposit, western Abitibi Subprovince, Canada; Society of Economic Geologists, Economic Geology Monograph 10, 672p.

MacDonald, P.J. and Piercey, S.J. 2003. Discover Abitibi. Gold Subproject 3. Preliminary regional geological assessment of porphyry intrusions spatially associated with gold deposits in the western Abitibi Subprovince, Timmins, Ontario; *in* Summary of Field Work and Other Activities 2003, Ontario Geological Survey, Open File Report 6120, p.36-1 to 36-7.

MacDonald, P.J., Piercey, S.J. and Hamilton, M.A. 2004. Discover Abitibi. Gold Subproject 3. Regional geological assessment of porphyry intrusions spatially associated with gold deposits along the Porcupine–Destor deformation zone, western Abitibi Subprovince, Timmins, Ontario; *in* Summary of Field Work and Other Activities 2004, Ontario Geological Survey, Open File Report 6145, p.43-1 to 43-7.

Péloquin, A.S. and Piercey, S.J. 2003. Discover Abitibi. Base Metal Subproject 3. Geology and base metal mineralization in Ben Nevis, Katrine, and Clifford townships; *in* Summary of Field Work and Other Activities 2003, Open File Report 6120, Ontario Geological Survey, p.41-1 to 41-8.

Piercey, S.J., Hamilton, M.A., Péloquin, A.S. and Chaloux, E. 2004. Discover Abitibi. Intrusion Subproject. Updates on studies of the Clifford stock and Blake River Group, Clifford Township; *in* Summary of Field Work and Other Activities 2004, Ontario Geological Survey, Open File Report 6145, p.44-1 to 44-14.

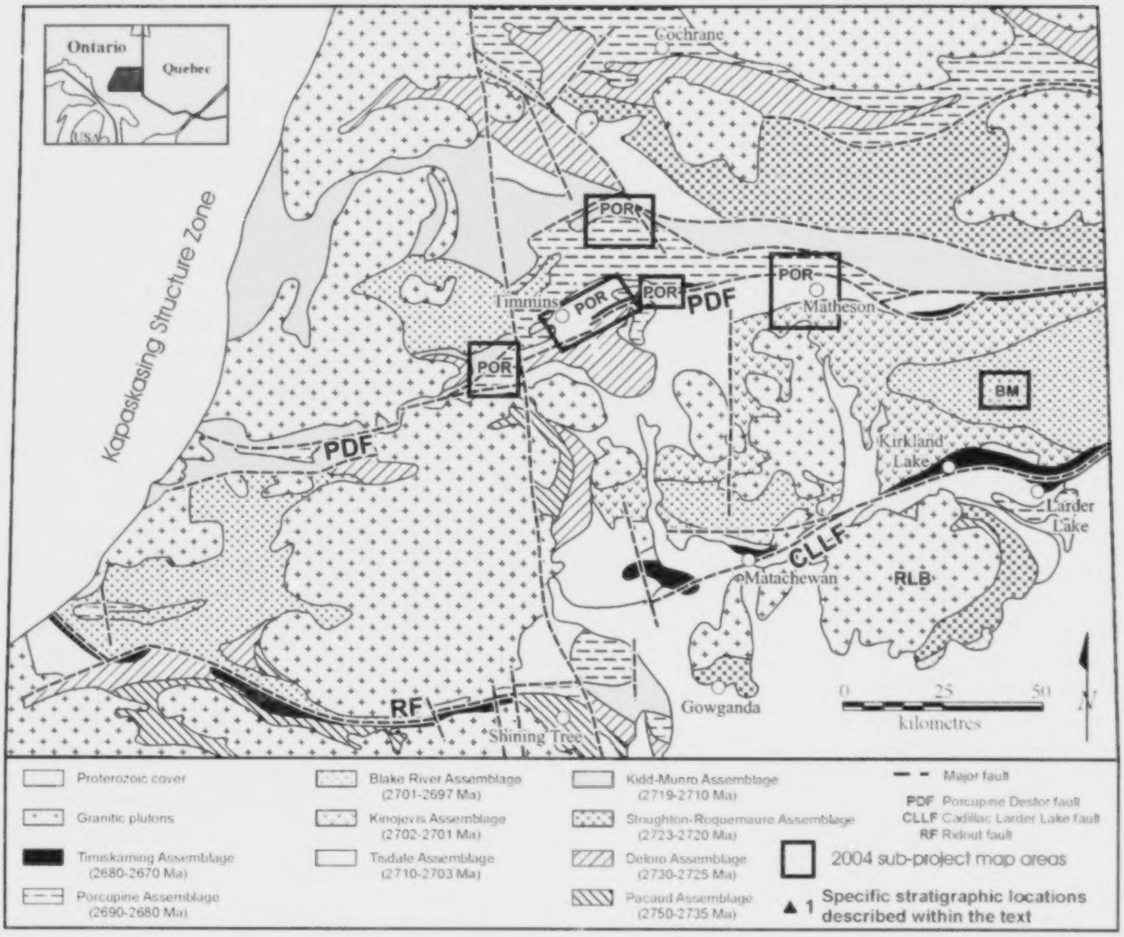
Ontario
Quebec
USA
Cochrane
Kapaskasing Structure Zone
POR
POR
POR
POR
POR
Timmins
PDF
Matheson
BM
Kirkland Lake
Larder Lake
PDF
CLLF
Matachewan
RLB
RF
Shining Tree
Gowganda
0
25
50
kilometres
N
Proterozoic cover
Granitic plutons
Timiskaming Assemblage (2680-2670 Ma)
Porcupine Assemblage (2690-2680 Ma)
Blake River Assemblage (2701-2697 Ma)
Kinojevis Assemblage (2702-2701 Ma)
Tisdale Assemblage (2710-2703 Ma)
Kidd-Munro Assemblage (2719-2710 Ma)
Stoughton-Roquemaure Assemblage (2723-2720 Ma)
Deloro Assemblage (2730-2725 Ma)
Pacaud Assemblage (2750-2735 Ma)
Major fault
PDF Porcupine Destor fault
CLLF Cadillac Larder Lake fault
RF Ridout fault
2004 sub-project map areas
▲ 1 Specific stratigraphic locations described within the text

Figure 1.1. Assemblage map of the Ontario portion of the Abitibi greenstone belt with assemblage boundaries (*from* Ayer et al. 2002), with locations of the porphyry project localities (POR) and the base-metal (BM) portion of the subproject.

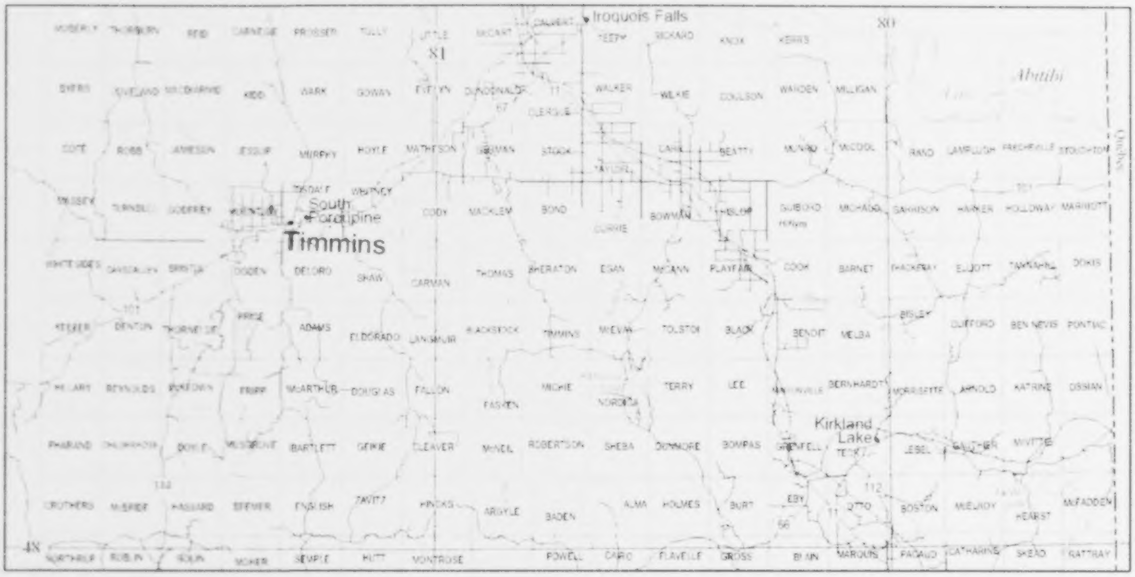
Iroquois Falls
Abitibi
Quebec
South Porcupine
Timmins
Kirkland Lake
81
80
48
101
11
67
144
112
66

Figure 1.2. Geographic map of the study area, providing, for reference, the township names mentioned in this report.

Chapter 2: Porphyry Intrusions of the Timmins Gold Camp: An Examination of Intermediate to Felsic Intrusions Associated with Gold Mineralization along the Porcupine–Destor Deformation Zone

INTRODUCTION

As part of the two-year Discover Abitibi Initiative (Intrusion Subproject), this chapter presents observations of porphyry intrusions spatially associated with gold deposits along the Porcupine–Destor deformation zone (PDDZ) in the vicinity of the Timmins gold camp, near Timmins, Ontario. Even though most of the porphyry bodies have been the partial focus of numerous past studies (Davies and Luhta 1978; Gorman, Kerrich and Fyfe 1981; Mason and Melnik 1986; Wood et al. 1986; Burrows and Spooner 1986; Brisbin 1997; Gray and Hutchinson 2001), much debate exists on various aspects of their understanding. It is the aim of this project to 1) compare and contrast field relations, petrology, geochemistry and geochronology of the porphyry intrusions; 2) distinguish differences between mineralized and barren porphyry intrusions; 3) test correlations of the porphyry intrusions with the extrusive Krist Formation; 4) create a regional lithogeochemical data set on the various porphyry intrusions.

The format of this chapter will begin with briefly discussing the previous work done on the porphyry intrusions (herein referred to as "porphyries") of the Timmins camp. The regional geology will then be briefly addressed, followed by a report on observation collected over 2003 and 2004 on each of the 5 geographical porphyry intrusion trends previously reported on by MacDonald and Piercey (2003) and MacDonald, Piercey and Hamilton (2004). The Krist Formation will then be briefly discussed followed by a comparison of the porphyry intrusion trends and Krist Formation volcanic rocks. This chapter will be concluded by a summary and discussion of the observations collected and how the porphyry intrusions trends compare to each other and the implications for gold exploration.

PREVIOUS WORK

The spatial association between gold mineralization and felsic porphyry bodies has long been recognized in the Timmins gold camp (Burrows 1924, 1925). Over the years since discovery, much of the research done on the camp has lead to the belief that the porphyry bodies were intrusive in nature (Hurst 1936; Holmes 1944; Griffis 1962). This idea came under scrutiny by Davies (1977) who suggested that the porphyries represented felsic volcanic rocks that were deposited in local topographic lows. Davies and Luhta (1978) later suggested that these felsic porphyritic volcanic rocks were not originally porphyritic in texture, but, rather, the porphyritic texture was a result of metasomatism by gold- and copper-rich mineralizing fluids that were not genetically related to the felsic porphyritic bodies; coincidentally, these results were debated in the literature (e.g., Griffis 1978; Davies and Luhta 1978).

In Pyke's (1982) regional overview of the geology of the Timmins area, he suggested that the porphyries were intrusive in origin and that they may represent subvolcanic intrusions, but he also suggested that they could possibly represent felsic domes.

A second debate on the porphyry bodies of Timmins began in 1986 with Mason and Melnik (1986) suggesting that the gold and copper mineralization within the Hollinger–McIntyre deposits was a result of an Archean porphyry-type hydrothermal system, similar to those present in Phanerozoic porphyry-copper deposits of the Cordillera of North, Central and South America. Wood et al. (1986) and Burrows and Spooner (1986) opposed this view, suggesting that the gold and copper mineralization occurred late syntectonic to posttectonic, whereas the porphyries were pre- to early syntectonic intrusions forming a time gap indicating that porphyry magmatism and gold mineralization were not coeval and were unrelated. Broadly coincident with the latter work was work by Corfu et al. (1989) who illustrated that there was a temporal separation of at least 15 million years between porphyry emplacement and gold mineralization (Corfu et al. 1989), hence, gold mineralization was a distinctly younger event in relation to the porphyry magmatism. Following this research, porphyry magmatism was no longer thought of as being the heat engine of the porphyry-type hydrothermal system that resulted in gold mineralization, but rather a later albitite diking event that was interpreted to be the engine of the hydrothermal system and the cause of gold mineralization (Melnik-Proud 1992; Brisbin 1997, 2000). The debate continued with Burrows et al. (1993) suggesting that the mineralization was a result of structural favourable zones or traps and not intrusion-related hydrothermal systems.

Further insight into the porphyry bodies was presented by Gray (1994) who combined the earlier 2 ideas on mineralization and suggested that there was 1) an early copper-gold mineralization as a result of intrusion-related hydrothermal activity; and 2) a later structural gold mineralization event responsible for the bulk of the gold mineralization within the Timmins camp. Gray and Hutchinson (2001) further suggested that there were 2 separate porphyry intrusions types: quartz-feldspar phenocrystic porphyries and feldspar phenocrystic porphyries. This hypothesis was later discarded by an internal study by Placer Dome, which used geochemistry to show that there were not 2 separate porphyry intrusion types (Wells 2001).

Recent Re/Os molybdenite geochronology has further dismissed the possibility of a genetic relationship between porphyry magmatism and gold-copper mineralization. An age of 2672±7 Ma at the McIntyre Mine (Bateman et al. 2004) illustrates that the gold mineralization is greater than 15 million years younger than the porphyry intrusions.

REGIONAL GEOLOGY

The oldest rocks within the Timmins gold camp are the calc-alkaline volcanic rocks of the Deloro assemblage (ca. 2730 Ma), which occur south of the Porcupine–Destor deformation zone (PDDZ; Figures 2.1 and 2.2; Ayer, Ketchum and Trowell 2002). Most gold deposits of the Timmins camp occur, however, not within this older stratigraphy, but rather north of the PDDZ, and are hosted within volcanic flows of the Tisdale assemblage (2710–2703 Ma; Ayer, Ketchum and Trowell 2002; *see* Figures 2.1 and 2.2). The volcanic flows of the Tisdale assemblage range in composition from ultramafic at the bottom of the assemblage (Hersey Lake Formation) through tholeiitic (Central, Vipond and Gold Centre formations) in the middle to upper units (Pyke 1982; Brisbin 1997).

Prior to gold mineralization, the Tisdale assemblage volcanic rocks were intruded by numerous porphyritic felsic bodies during the period of 2687 to 2691 Ma (Corfu et al. 1989; Ayer et al. 2003). Coeval with the porphyry intrusions are the felsic metavolcanic rocks of the Krist Formation (ca. 2687 Ma), which form the base of the Porcupine assemblage; this assemblage lies unconformably on top of the Tisdale assemblage within the Timmins camp (Ayer, Ketchum and Trowell 2002; *see* Figure 2.1).

Postdating the intermediate to felsic magmatism of the porphyry intrusions and Krist Formation metavolcanic rocks, but predating gold mineralization, are clastic sedimentary rocks of the Porcupine assemblage, which formed circa 2687 Ma (Ayer, Ketchum and Trowell 2002; *see* Figure 2.1). These sedimentary rock units regionally overlie the Krist Formation within structurally controlled basins such as the Porcupine syncline. Further clastic sedimentation of the Timiskaming assemblage postdates the Porcupine assemblage and was deposited within isolated topographical lows (ca. 2679±4 Ma: Ayer et al. 2003; *see* Figures 2.1 and 2.2). Further intrusive magmatism occurred at 2673+6/–2 Ma with the emplacement of late albitite dikes (Corfu et al. 1989).

The majority of gold mineralization event in the Timmins camp postdate albitite dike emplacement at 2673+6/–2 Ma (Marmont and Corfu 1989) as the gold-bearing veins crosscut the albitite dikes (Melnik-Proud 1992; Brisbin 1997, 2000). Recent Re/Os molybdenite geochronology further supports this assertion as molybdenite from the Dome Mine gold zone has an age of 2670±10 Ma (Ayer et al. 2003) and from the McIntyre Mine copper zone has an age of 2672±7 Ma (Bateman et al. 2004). Although the albitite dikes are crosscut by the copper-gold veins, the McIntyre Mine copper zone age (2672 Ma) is similar to the emplacement age of the albitite dike (2673 Ma: Corfu et al. 1989), which suggests that some copper-gold mineralization may be genetically related to hydrothermal activity generated by albitite dike emplacement, as previously suggested by Melnik-Proud (1992) and Brisbin (1997, 2000).

GEOLOGY: QUARTZ-FELDSPAR PORPHYRY INTRUSIONS

Quartz-feldspar porphyries associated, and not associated, with gold deposits occur over an area of approximately 100 km in length along the PDDZ (*see* Figure 2.2) from Bristol Township in the east to Carr Township in the west (*see* Figure 1.2). As part of this project, 28 different quartz-feldspar porphyry intrusions were examined during the summers of 2003 and 2004 with further petrographic and geochemical data collected during the autumn and winter of these years. These intrusions were geographically grouped into 5 trends as shown on Figure 2.2 and in Table 2.1. The 5 trends are the central, northern, western, southern and eastern trends. Descriptions of each trend are presented below, which include the location, field relationships; petrography; alteration, veining and mineralization; deformation; geochemistry; and geochronology. A comparative summary of these data for the 5 trends is provided in Table 2.2.

Central Trend

The central trend of quartz-feldspar porphyries includes any intrusions directly along the PDDZ or its immediate splay faults (e.g., Dome fault) between the Mattagami River fault (western boundary) and the Burrows–Benedict fault (eastern boundary) spanning across Ogden, Deloro and Tisdale townships (*see* Figure 2.2). The intrusions discussed within this trend include (from east to west) Dome Fault Zone, Preston, Paymaster, West (West Preston), Northwest (Paymaster South and Paymaster 2-3), Edwards (at Vedron deposit), Buffalo Ankerite #5, Naybob and Porphyry Hill intrusions (Figure 2.3). Three intrusions within the central trend are not discussed—Buffalo Ankerite, Aunor and Delnite porphyry bodies—as they were not examined due to inaccessibility to outcrop or drill core.

FIELD RELATIONSHIPS

The 12 intrusions of the central trend form a west-southwest to east-northeast linear belt approximately 11 km long and 2 km wide (*see* Figure 2.3). The intrusions of the eastern half of this trend (Dome Fault Zone, Preston, Paymaster, West and Northwest) are known to plunge eastwards and coalesce at depth (E. Barr, Porcupine Joint Venture, personal communication, 2003). Although the porphyry intrusions join at depth, a batholith-scale intrusion that may have been the source of these porphyries has yet to be identified. The central trend of porphyries intrude into 3 different stratigraphic levels of the Tisdale assemblage: along the northern margin of the PDDZ (Buffalo Ankerite, Aunor, Delnite, Naybob and

Porphyry Hill); below or at the Hersey Lake–Central formations contact (West, Northwest, Vedron and Buffalo Ankerite #5); and into the Central and Vipond formations (Dome Fault Zone, Preston and Paymaster). The porphyry intrusions are generally semi-conformable with stratigraphy, except for the Preston porphyry, which crosscuts stratigraphy at a high angle. As well, the central trend porphyry intrusions show a weak correlation with pillowed units of the Tisdale assemblage stratigraphy and alteration zones, known within the camp as 'carb rock'. Furthermore, zones of deformation are also proximal to areas where the porphyry intrusions have been emplaced. For example, intrusions are present in deformation zones in both the Porcupine–Destor deformation zone (e.g., Buffalo Ankerite, Aunor, Delnite, Naybob and Porphyry Hill intrusions), and in the Dome fault zone (e.g., Dome Fault Zone, Preston and Edwards intrusions).

The porphyry intrusions of the central trend display 3 groupings with respect to size and shape. The most common occurrence of the intrusions is as small dikes, sills and plugs up to 1 km long and 0.3 km wide, but typically only a few hundreds metres long and tens of metres wide. These types include the Northwest, Edwards, Buffalo Ankerite #5, Buffalo Ankerite, Aunor, Delnite, Naybob and Porphyry Hill intrusions. The second most common group of intrusions are elongate porphyries, for example, the Dome Fault Zone, Preston and Paymaster porphyries range from 1 to 2 km long and from 100 to 300 m wide. The third grouping encompasses the largest porphyry of the central trend, the West porphyry, which occurs as an oval-shaped intrusion approximately 1200 by 600 m.

The central trend porphyry intrusions typically have sharp contacts with the host Tisdale assemblage mafic volcanic stratigraphy where observable (Dome Fault Zone, Preston, Paymaster, Northwest, Vedron and Buffalo Ankerite #5). Metre-scale apophyses are present at both the Northwest and Edwards porphyries (Photo 2.1A). Two exceptions to sharp contacts within the central trend are 1) the northern contact of the Edwards porphyry, where subrounded porphyry fragments are present in a fine-grained chloritic matrix forming a roof breccia (Photo 2.1B); and 2) the western nose of the Paymaster porphyry where large (up to 15 cm in diameter), subangular flow-banded porphyry fragments and large (up to 15 cm in diameter) subrounded mafic volcanic fragments are hosted within a fine-grained chloritic matrix forming a basal breccia (Photo 2.1C).

PETROGRAPHY

The porphyry intrusions of the central trend dominantly show porphyritic textures (Photo 2.1D Naybob; also Dome Fault Zone, Preston, Paymaster, West and Northwest) but locally exhibit aphanitic textures (Photo 2.1E) (Edwards and Buffalo Ankerite #5) and equigranular textures (Photo 2.1F) (Porphyry Hill). The porphyritic textured intrusions have 15 to 45% phenocrysts surrounded by a quartz-feldspar-rich, very fine-grained matrix. The phenocrysts are generally one-third moderately strained subhedral quartz, and two-thirds subhedral to anhedral plagioclase, ranging from 1 to 5 mm in diameter. The Naybob porphyry differs slightly from the latter in containing a matrix that is slightly coarser grained. Aphanitic samples of intrusions are similar to the porphyritic intrusion, but lack the phenocrysts (e.g., <5% phenocrysts). The minor phenocrysts within the aphanitic samples are always small subhedral to euhedral quartz crystals that do not exceed 1 mm in diameter. Equigranular intrusions have feldspar grains (1–5 mm plagioclase) with interstitial quartz. Primary minerals abundant in minor amounts within all the intrusions include 0.5 mm crystals of colourless apatite; up to 1 mm long blades of tourmaline; and submillimetre, subhedral to euhedral pyrite crystals are typically disseminated throughout the porphyry intrusions. Although pyrite is the most common sulphide mineral, both pyrrhotite and chalcopyrite are locally observed. Foreign material, including suspected xenoliths of ultramafic rock that have undergone green mica alteration, is present in most of the intrusions. These green mica fragments are typically a few centimetres in length, but may range up to 10 cm long (Photo 2.1G). The foreign fragments are most abundant near the margins of the intrusions and are elongate with the dominant structural fabric. Flow banding defined by mineral alignment is present in the western nose of the Paymaster porphyry (Photo 2.1H).

Metamorphic minerals are rarely observed within the porphyry intrusions of the central trend. Although metamorphic biotite has been observed in the porphyries in the vicinity of the Dome Mine (Thompson 2003), none was observed during this project. The only metamorphic mineral observed was stilpnomelane, which occurs as long blades up to 1 mm in length within the Edwards porphyry (*see* Photo 2.1E).

ALTERATION, VEINING AND MINERALIZATION

The porphyries of the central trend have all undergone alteration of differing types and degrees. The most common alteration affecting all the porphyries to some degree is white mica (sericite) alteration of feldspar phenocrysts and their feldspathic matrixes. Depending on the degree of alteration, relict feldspar phenocrysts may or may not be visible (Photos 2.1I and 2.1J). The most intense white mica alteration is present in the most eastern porphyries of the central trend (Dome Fault Zone, Preston and Paymaster). For example, in the vicinity of the Dome Mine, the feldspars of these porphyry intrusions are completely replaced by sericite. Often coupled with, but also occurring locally separate from, the white mica alteration is a calcium-carbonate alteration, typically resulting in the feldspathic mineralogy having a cloudy grayish-brown appearance (Photo 2.1K). Rocks that are often described as "bleached" exhibit the most pervasive calcium-carbonate alteration and, like sericite alteration, carbonate alteration is strongest on the most eastern intrusions of the central trend (Dome Fault Zone, Preston and Paymaster). Chlorite alteration occurs in minor abundance in all of the intrusions as euhedral to anhedral, up to 1 mm laths (Photo 2.1L). Iron-carbonate (ankerite) alteration is also common (Photo 2.1M). The porphyries within the central part of the trend exhibit the most intense ankerite alteration (West, Northwest and Buffalo Ankerite #5).

Three different types of veins are hosted within the porphyry intrusions of central trend, including quartz-tourmaline, quartz-ankerite and monomineralic quartz veins. Quartz-tourmaline veins are the most common, generally occurring as subvertical, south-southeast-trending veins that crosscut stratigraphy and structural fabrics. Quartz-tourmaline veins are typically 10 to 20 cm wide (Photo 2.1N) and 5 to 15 m long, although smaller veins are observed in the Northwest porphyry. No alteration envelopes are present around the quartz-tourmaline veins. The second most common vein type is quartz-ankerite veins. These veins are generally subparallel to stratigraphy and are 10 to 20 cm thick, but only 1 to 5 m long. Alteration associated with the quartz-ankerite veins includes 10 cm wide zones of green mica outside of the porphyry intrusions, and metre-scale pervasive ankerite alteration within the porphyry intrusions. Pyrite enrichment is typically associated with the ankerite alteration envelopes. The least common vein type present is chaotic clusters of white quartz within the Edwards porphyry. These centimetre-size quartz veins are present in randomly oriented localized zones, and are not associated with alteration envelopes. Timing relationships between these veins and the quartz-tourmaline veins and quartz-ankerite veins are uncertain.

The porphyry intrusions of the central trend show a close spatial association with gold enrichment. For example, the most eastern of the porphyries of the central trend (Dome Fault Zone, Preston and Paymaster) join in a triple point precisely where the Dome Super Pit is located, and plunge in the same general direction as mineralization (E. Barr, Porcupine Joint Venture, personnel communication, 2003). The intrusions at Dome also have the strongest sericite-carbonate alteration. Other intrusions of the central trend show a similar spatial association to gold mineralization, but the abundance of mineralization is exponentially lower.

DEFORMATION

The porphyry intrusions of the central trend show varying degrees of deformation. The deformation ranges from non-existent in the westernmost intrusions (Naybob and Porphyry Hill), to at least 2 separate phases of deformation in the eastern and central intrusions of the trend (Dome Fault Zone, Preston, Paymaster, West, Northwest, Edwards and Buffalo Ankerite #5). No significant structural fabrics are present in the most western intrusions of the central trend (Naybob and Porphyry Hill).

The more recognizable and dominant fabric is an east-southeast-trending millimetre- to centimetre-scale spaced cleavage (Photo 2.1O) developed approximately axial planar to the South Tisdale anticline. Present work by Bateman et al. (2004) suggests the South Tisdale anticline is a D_2 structure and, thus, the axial planar spaced cleavage discussed above was also a result of the D_2 deformation event.

An older, more penetrative foliation is observed within microlithons that occur between planes of the younger D_2 spaced cleavage discussed above. This older foliation is oriented subparallel to the younger spaced cleavage (generally east-southeast striking). The D_1 generation of deformation resulted in the formation of this penetrative foliation (Bateman et al. 2004).

GEOCHEMISTRY

Geochemical data for the porphyry intrusions of the central trend are presented in Figures 2.11 to 2.15 and in Table 2.3.

Standard major element Harker plots for TiO_2, Al_2O_3, Fe_2O_3 and MgO (Figures 2.11A to 2.11D) form decreasing arrays with SiO_2 increase exhibiting compatibility with fractionation of oxides, hornblende and pyroxene as well as little to no mobility during alteration. Scatter of CaO, Na_2O and K_2O data (Figures 2.11E to 2.11G) suggests incompatibility during crystal fractionation and/or some mobility of these elements during alteration. The trace element Harker plots (Figures 2.11H to 2.11N) of the central trend intrusions display 3 trends: 1) V, Sc, Nb and Y (*see* Figures 2.11H, 2.11I, 2.11L and 2.11M) show decreasing arrays representing compatibility during crystal fractionation and the fractionation of oxides, hornblende and pyroxene; 2) Sr and Rb (*see* Figures 2.11J and 2.11K) show scatter representing mobility during alteration; and 3) Th (*see* Figure 2.11N) shows a slightly increasing array indicating incompatibility during crystal fractionation.

Alteration plots of the central trend intrusions indicate that the porphyries have undergone various degrees of alteration. Most of the central trend intrusions display fresh to weakly altered signatures and plot in the least-altered field on an alteration box plot (Figures 2.12A to 2.12C). However, sodium loss (*see* Figure 2.12A) coupled with potassium metasomatism (sericite alteration) (*see* Figures 2.12B and 2.12C) is exhibited within the intrusions at the Dome Mine (Dome Fault Zone, Preston and Paymaster porphyries). As well, sodium-alteration and/or metasomatism (albite alteration) are present in the Northwest, Edwards and Buffalo Ankerite #5 porphyries (*see* Figures 2.12A to 2.12C).

Trace element ratios suggest the intrusions of the central trend are rhyodacite to dacite in composition (Figure 2.13A). The intrusions are subalkalic (Figures 2.13A and 2.13B) displaying calc-alkaline trends (Figures 2.13C and 2.13D) with Zr/Y ratios greater than 7 (*see* Figure 2.13D). Triangular CIPW normative plots of feldspars (Figure 2.14A) suggest that the central trend intrusions range from trondhjemite to tonalite to granodioritic (TTG) in composition with the more potassium-metasomatized intrusions yielding high orthoclase values that are interpreted to be secondary and reflecting high sericite content. The central trend intrusions are further separated into high-Al TTG, excluding the Naybob porphyry and Porphyry Hill granodiorite, which are low-Al TTG (Figure 2.14B). Yttrium values are below 18 ppm, indicating TTG magmatism similar to modern-day adakitic magmatism (*see* Figure 2.11M).

Extended primitive mantle normalized multi-element plots of the central trend intrusions yield 2 separate geochemical groups based on their primitive mantle normalized patterns. The more common group (group A) encompasses all of the central trend intrusions (Dome Fault Zone, Preston, Paymaster, West, Northwest, Edwards and Buffalo Ankerite #5 porphyries) except the Naybob porphyry and Porphyry Hill granodiorite (group B). The group A intrusions display moderate fractionation of the REE with heavy REE (HREE) depletion. As well, the group A intrusions display Nb and Ti negative anomalies and Zr, Hf and Al positive anomalies (Figure 2.15A). Group B intrusions display moderate to strong fractionation (Figure 2.15B) with greater light REE (LREE)–enrichment, more HREE depletion compared to group A, and a more pronounced negative Nb anomaly (*see* Figure 2.15B).

GEOCHRONOLOGY

Uranium-lead geochronology was previously reported on 2 of the eastern porphyritic intrusions of the central trend (*see* Table 2.1). Corfu et al. (1989) obtained ages of 2690±2 Ma for the Paymaster porphyry, and circa 2690 Ma for the Preston porphyry (although the latter age was considered a probable age due to discordance in the U/Pb data). Gray and Hutchinson (2001) obtained an age of 2688±2 Ma for the Dome Fault Zone porphyry.

Northern Trend

The northern trend of quartz-feldspar porphyry bodies includes any intrusions that are located along the Hollinger shear zone between the Mattagami River fault (western boundary) and the Burrows–Benedict fault (eastern boundary) (*see* Figure 2.2), north of the central trend in Tisdale Township. The northern trend includes 8 porphyry intrusions as shown on Figure 2.4. Within this trend, the 4 intrusions discussed in this report are, from east to west, Crown, Pearl Lake, Gillies Lake and Coniaurium porphyries. At least 4 other quartz-feldspar porphyry intrusions were not examined, including the Millerton, Miller Lake, Acme and Northern porphyries, due to an inability to access the Hollinger Property where these porphyry bodies crop out because of safety reasons (sink holes).

FIELD RELATIONSHIPS

The 8 felsic porphyritic intrusions of the northern trend form a southwest-northeast linear belt approximately 4 km long and 1 km wide (*see* Figure 2.4). The porphyries plunge to the northeast and coalesce at depth (P. Harvey, Porcupine Joint Venture, personal communication, 2003). Although the porphyry intrusions join at depth, no large-source batholith, which might be the source of the intrusions, is known to exist at depth.

The porphyry bodies of the northern trend have intruded mafic volcanic rocks of the Central and Vipond formations of the Tisdale assemblage. The intrusions lie subparallel to the volcanic stratigraphy and form numerous elongated, irregularly shaped porphyry bodies that are generally semi-conformable with stratigraphy. Similar to the central trend, the northern trend intrusions show a weak correlation with pillowed units of the Tisdale assemblage stratigraphy. Furthermore, zones of deformation are localized in proximity to porphyritic intrusions (e.g., Hollinger shear zone). The Millerton, Acme, Pearl Lake and Coniaurium porphyries are all located along the linear Hollinger shear (deformation) zone. The northern trend porphyries have intruded into the hinges of the Northern Anticline (Gillies Lake porphyry), the

McIntyre syncline (Northern and Miller Lake porphyries) and the Hollinger–Coniaurium anticline (Millerton, Acme, Pearl Lake and Coniaurium porphyries) (Ferguson 1966; Piroshco and Kettles 1991).

The porphyry intrusions of the northern trend can be divided into 3 groups based on their size and shape. Irregularly shaped bodies ranging from 500 m to 1 km long and a few hundred metres wide are the most common type of intrusion in the northern trend, and include the Crown, Miller Lake, Gillies Lake and Coniaurium porphyries. The second most common group of intrusions are small elongate intrusions a few hundred metres long and less than 100 m wide, and include the Millerton, Northern and Acme porphyry bodies. The third group encompasses the largest porphyry of the northern trend, the Pearl Lake porphyry, which is an elongate oval-shaped intrusive body approximately 2 km long and 500 m wide.

The contacts of porphyry bodies within the northern trend and the host mafic volcanic rocks are sharp (Photo 2.2A) and are intrusive or tectonic boundaries, with the exception of the Crown porphyry, where subrounded, stretched clasts of porphyry and mafic volcanic rocks are hosted within a fine-grained chloritic matrix (Photo 2.2B). Mapping around this marginal breccia unit illustrates that the Crown porphyry extended northward, cross-cutting stratigraphy (Figure 2.5).

PETROGRAPHY

The unaltered and undeformed intrusions of the northern trend exhibit a porphyritic texture (Photo 2.2C), with the porphyry bodies typically containing 15% highly strained, subhedral quartz, and 30% 1 to 8 mm feldspar phenocrysts that are in a fine-grained quartzo-feldspathic matrix. Subhedral to anhedral feldspar phenocrysts are dominantly plagioclase, although black orthoclase phenocrysts (Photo 2.2D) are present in the Gillies Lake porphyry. Primary minerals present in minor amounts within the northern trend porphyries include tourmaline, apatite and pyrite. Although pyrite is the most common sulphide mineral in all of the northern trend porphyries, the Pearl Lake porphyry also contains chalcopyrite, pyrrhotite, molybdenite and bornite as disseminated submillimetre grains, millimetre-thick stringers and 3 to 4 cm thick clusters (Photo 2.2E). Xenoliths of 'carb rock' are also common in the northern trend porphyries. These green mica-rich fragments are typically a few centimetres in length, but range up to 10 cm long, and are most abundant near the margins of the Pearl Lake porphyry and are elongate with the dominant structural fabric in the porphyry. Internal, hydrothermal breccias also occur in the Pearl Lake porphyry and are distinguished by centimetre to decimetre fragments of porphyry in a feldspathic- to tourmaline-rich matrix (Photo 2.2F). The best example of an unaltered, primary porphyry body is the Gillies Lake porphyry (*see* Photo 2.2C).

ALTERATION, VEINING AND MINERALIZATION

The porphyry intrusions of the northern trend have all undergone alteration of differing types and degrees. The most common alteration affecting all the porphyries is white mica alteration of feldspar phenocrysts and the feldspathic matrices. White mica alteration forms an elongate zone that is both bordered and cored by the northern trend of porphyry bodies (Figure 2.6). Depending on the degree of sericite alteration, relict feldspar phenocrysts are or are not visible. The Crown and Gillies Lake porphyries border the white mica alteration zone and show only weak white mica alteration (Photo 2.2G), whereas the Pearl Lake and Coniaurium porphyries that core the white mica alteration zone show the strongest alteration with the feldspar phenocrysts and feldspathic matrix nearly completely obliterated (Photo 2.2H). These porphyry bodies within the white mica alteration zone are best described as quartz-sericite schists, rather than true igneous porphyries. Coupled with the white mica alteration in some places, and also occurring separately from the white mica alteration in others, is calcium-carbonate alteration, which, like the white mica alteration, is most predominant in the Pearl Lake porphyry. Calcium-carbonate alteration can be recognized by the feldspars of the porphyry having a cloudy, brownish-grey appearance (*see* Photo 2.2G) and the rocks having a distinctive bleached white colouration (Photo 2.2I). The Pearl Lake porphyry, which was best observed in diamond-drill core, also shows zones of pervasive hematite (pink), patchy ankerite (beige), and pervasive chlorite (green to grey) alteration facies.

Multiple generations of veins are present within the porphyries of the northern trend. The most commonly observed veins are quartz-tourmaline veins that occur as 10 to 30 cm wide vein sets. The quartz-tourmaline veins generally trend northwest and are not related positively to any of the deformation events discussed below. Numerous other vein types are present within the northern trend (dominantly the Pearl Lake porphyry), such as quartz-ankerite, quartz-calcium carbonate and monomineralic quartz; however, no timing or genetic relationships could be determined for these veins.

Both gold and copper mineralization are spatially associated with the porphyries of the northern trend. Gold enrichment is strongest within the central parts of the northern trend (*see* Figure 2.6). For example, the bulk of the Hollinger–McIntyre ore zones existed within the mafic volcanic flows of the Tisdale assemblage along the contact between the flows and the margins of the porphyry bodies, although mineralized veins often extended into the porphyries as well (Melnik-Proud 1992). Gold enrichment within the northern trend also shows a strong association to sericite altered porphyries (Millerton, Acme, Pearl Lake and Coniaurium) (Mason and Melnik 1986), even though all of the intrusions do exhibit anomalous gold (P. Harvey, Porcupine Joint Venture, personal communication, 2003). Copper mineralization occurred within the centre of the Pearl Lake porphyry and was typically associated with hematite (pink) alteration, with chalcopyrite and bornite the dominant copper ore minerals (Melnik-Proud 1992). Gold veins typically crosscut the hematite alteration, suggesting copper mineralization predated gold enrichment (P. Harvey, Porcupine Joint Venture, personal communication, 2004).

DEFORMATION

The porphyry intrusions of the northern show at least 3 generations of structural fabrics with varying degrees of intensity depending on the location of the porphyries and the degree of alteration present in the porphyries.

The oldest fabric is a steeply dipping (near vertical), generally east-striking penetrative foliation observed within microlithons between planes of a younger fabric. This foliation is related to D_1 deformation event (Bateman et al. 2004).

The most dominant fabric observed within the northern trend porphyries is a east-striking, steeply dipping spaced cleavage that is subparallel to the older foliation and is observable in all of the northern trend intrusions. This fabric is related to the D_2 deformation event (Bateman et al. 2004) and is characterized by cleavage planes that are typically spaced between 1 and 5 mm.

Locally present along the dominant spaced cleavage plane in the northern trend porphyries is an east-plunging, 50° steep lineation. This lineation is best exhibited as a strong stretching lineation of clasts within a heterolithic breccia that surrounds the Crown porphyry (*see* Photo 2.2B), and is also present as mineral elongations within the Pearl Lake porphyry. The generation of deformation related to this lineation is unknown at present (Bateman et al. 2004).

The youngest structural fabric is a shallowly dipping to flat-lying foliation observed within the Pearl Lake porphyry; this foliation is related to the D_6 deformation event that is suspected to be a result of late orogenic collapse (Bateman et al. 2004).

All 3 fabrics discussed above are recognizable within the Pearl Lake porphyry, which is located within the central part of the northern trend and shows the strongest alteration and, thus, has the best mineralogy for structural fabric development. In contrast, the Gillies Lake porphyry located on the northern margin of the northern trend shows very little deformation with only a weakly developed D_2 fabric. The lack of deformation within the Gillies Lake porphyry is due to a lack of alteration and thus minerals favourable to exhibit structural fabric.

GEOCHEMISTRY

Geochemical data for the porphyry intrusions of the northern trend are presented in Figures 2.11 to 2.15 and in Table 2.3.

Standard Harker plots for the northern trend porphyries are presented in Figure 2.11. Standard major element Harker plots for TiO_2 and Al_2O_3 display flat arrays (*see* Figures 2.11A and 2.11B), with decreasing Fe_2O_3, MgO and CaO (*see* Figures 2.11C to 2.11E) suggesting fractionation of pyroxenes and hornblende, as well as little to no mobility during alteration. Scatter of Na_2O and K_2O data (*see* Figures 2.11F and 2.11G) suggests incompatibility during crystal fractionation and mobility of these elements during alteration. The trace element Harker plots (*see* Figures 2.11H to 2.11N) of the northern trend intrusions display 3 trends: 1) V, Sc, Nb and Y (*see* Figures 2.11H, 2.11I, 2.11L and 2.11M) show flat arrays; 2) Sr and Rb (*see* Figures 2.11J and 2.11K) show scatter representing mobility during alteration; and 3) Th (*see* Figure 2.11N) shows a slightly increasing array indicating incompatibility during crystal fractionation.

Alteration plots of the northern trend intrusions indicate the porphyries have undergone various degrees of alteration. Most of the northern trend intrusions display strongly altered signatures and plot outside the least-altered field on an alteration box plot (*see* Figures 2.12A to 2.12C). Sodium loss (*see* Figure 2.12A) coupled with potassium metasomatism (sericite alteration) (*see* Figures 2.12B and 2.12C) is the dominant alteration type within all of the Pearl Lake porphyry samples. The Gillies Lake and Crown porphyries differ, exhibiting fresh to weak sodium alteration and/or metasomatism (albite alteration) (*see* Figures 2.12A to 2.12C).

Trace element ratios suggests that the intrusions of the northern trend are rhyodacite to dacite in composition (*see* Figure 2.13A). The intrusions are subalkalic (*see* Figure 2.13B) displaying calc-alkaline trends (*see* Figures 2.13C and 2.13D) with Zr/Y ratios greater than 7 (*see* Figure 2.13D). Triangular CIPW normative plots of feldspars (*see* Figure 2.14A) suggest that the unaltered northern trend intrusions range from trondhjemite to tonalite to granodioritic (TTG) in composition, with the potassium-altered samples of the Pearl Lake porphyry plotting with high orthoclase values reflecting sericite content, rather than orthoclase. The northern trend intrusions have low Yb and high Al_2O_3, similar to high-Al TTG (*see* Figure 2.14B), and have Y less than 8 ppm, similar to modern-day adakitic magmatism (Figure 2.11M).

Extended primitive mantle normalized multi-element plots for the northern trend are similar to the group A samples from the central trend. The northern trend intrusions have moderate depletion of heavy REE (HREE) and have LREE-enrichment, negative Nb and Ti anomalies, and positive Zr, Hf and Al peaks (*see* Figure 2.15A).

GEOCHRONOLOGY

Uranium-lead geochronological analyses have been previously reported on 3 of the porphyritic intrusions of the northern trend: Corfu et al. (1989) obtained ages of 2688±2 Ma, 2691±3 Ma, and 2689±1 Ma, respectively, for the Crown, Millerton and Pearl Lake porphyries.

Western Trend

The western trend of quartz-feldspar porphyries includes any intrusions west of the Mattagami River fault that are along where the PDDZ is suspected to extend (*see* Figure 2.2), spanning across the western side of Ogden Township and all of Bristol Township (*see* Figure 1.2). The western trend includes 6 intrusions as shown on Figure 2.7, including (from east to west) Bristol Township, Bristol Lake, South Bristol Lake and Holmer porphyries, as well as the Thunder Creek and Southwest Bristol Township syenites.

FIELD RELATIONSHIPS

The 6 intrusions of western trend form an east-west linear belt approximately 13 km long. The intrusions of the eastern half of this trend (Bristol Township, Bristol Lake and South Bristol Lake) are known to plunge westwards (C. Dupont, Tom Exploration Inc., personal communication, 2004), but the plunges of the Holmer porphyry, Southwestern porphyry and Thunder Creek syenite are unknown. The porphyry and syenite intrusions of the western trend are typically located along the boundary between the Tisdale assemblage metavolcanic rocks and the Porcupine assemblage clastic metasedimentary rocks (*see* Figures 2.1 and 2.7; Vaillancourt, Pickett and Dinel 2001). The Bristol Township porphyry intrudes along the southern margin of a sliver of Tisdale assemblage mafic volcanic rocks at the contact with Porcupine assemblage metasedimentary rocks (*see* Figure 2.7). The Bristol Lake, South Bristol Lake and Holmer porphyry bodies intrude along the northern contact of the Tisdale and Porcupine assemblages (*see* Figure 2.7), south of the Kamiskotia Intrusive Complex. The syenite intrusions similarly intrude the northern contact of the Tisdale–Porcupine assemblages, but slightly further west than the porphyry intrusions (*see* Figure 2.7).

The largest porphyry body in the western trend is the Bristol Township porphyry. This body is a large intrusive body roughly 5 km long (east to west) and 3 km wide (north to south). Smaller porphyry dikes extend west from the Bristol Township porphyry and include the Bristol Lake, South Bristol Lake and Holmer porphyries. The larger 2 porphyry dikes off the Bristol Township porphyry (Bristol Lake and South Bristol Lake porphyries) are elongate in shape, approximately 3 km long (east to west), and 0.5 to 1 km wide (north to south). The Holmer intrusion is the smallest porphyry in the western trend and is approximately 0.5 km long (northeast-southwest) and only a few metres to a few tens of metres wide. The syenite intrusions of the western trend include an irregularly shaped body, the Southwest Bristol Township syenite, approximately 2 km in diameter, and the smaller, slightly less quartz deficient Thunder Creek syenite that occurs as a north-trending dike. The smaller Thunder Creek syenite is distinct and not spatially continuous with the Southwest Bristol Township syenite.

The boundaries of the Bristol Township porphyry are generally sharp with the surrounding country rocks, although breccia units flank the intrusion in some localities (C. Dupont, Tom Exploration Inc., personnel communication, 2004). The eastern margin of the Bristol Township porphyry is extremely sharp and cut by the Mattagami River fault (*see* Figure 2.7). The margins of smaller Bristol Lake and South Bristol Lake intrusions were not observable. The margins of the Holmer porphyry contain heterolithic breccia with angular blocks of porphyry, mafic volcanic rocks and siliciclastic metasedimentary rocks (Photo 2.3A) up to a few metres in diameter, although the extent of the breccia is unknown due to it only being observed in moderately spaced drill core. The margins of the syenites, where observed, are sharp.

PETROGRAPHY

The intrusions of the western trend range in texture from porphyritic to equigranular. The porphyritic intrusions (Bristol Township, Bristol Lake, South Bristol Lake and Holmer) have 1 to 5 mm subhedral phenocrysts of plagioclase feldspars ranging from 10 to 25 modal %, along with 1 to 3 mm phenocrysts of moderately strained euhedral to subhedral quartz ranging from 5 to 20 modal % (Photo 2.3B). Pyrite is the dominant sulphide mineral in all of the porphyritic intrusions of the western trend occurring as euhedral to anhedral, up to 1 mm in diameter disseminated pyrite grains (trace to 5%); however, chalcopyrite is present with pyrite within the large Bristol Township porphyry as both millimetre-thick stringers and lenses up to a few centimetres in length. Arsenopyrite is present as submillimetre euhedral crystals within the Holmer porphyry.

The Southwest Bristol Township syenite of the western trend consist of fine- to medium-grained feldspars up to 3 mm in diameter interlocking to form an equigranular texture (Photo 2.3C). The feldspar grains are dominantly orthoclase (60–70 modal %) with lesser plagioclase (30–40 modal %). The slightly less quartz-deficient Thunder Creek syenite displays a porphyritic texture with clusters of intergrown, 1 to 2 mm equigranular feldspars (orthoclase and plagioclase) that are up to 3 cm in diameter (30–40 modal %); subhedral 1 to 2 mm plagioclase phenocrysts (15–30 modal %); and minor quartz phenocrysts (1–5 modal %) within a fine-grained feldspathic matrix. Trace to 3% euhedral to subhedral, 0.5 to 3 mm disseminated pyrite is also a primary constituent of the Thunder Creek syenite.

ALTERATION, VEINING AND MINERALIZATION

The porphyry and syenite intrusions of the western trend show various types and degrees of alteration. The porphyritic intrusions all display varying degrees of sericite alteration, ranging from weak in the Holmer porphyry (~2 modal %) to strong in the Bristol Township porphyry (10–20 modal %); depending on the degree of sericite alteration, relict feldspar phenocrysts may or may not be visible. Weak to moderate chlorite alteration is the second most common alteration, occurring as 0.5 mm anhedral to subhedral laths ranging from 2 to 20 modal %. Weak calcium-carbonate alteration is associated with sericite alteration, particularly in the Bristol Township porphyry. The calcium-carbonate alteration is recognizable by a bleached appearance in hand sample and a clouded brownish-grey appearance of feldspar phenocrysts and matrices in thin section (Photo 2.3D). The large Bristol Township porphyry intrusion also locally shows weak pervasive hematite alteration distinguishable by a light pink colouration and radial acicular blades of leucoxene. The syenite intrusions of the western trend show weak to moderate sericite and chlorite alteration similar to the porphyritic intrusions. The syenites also show ankerite and hematite alteration ranging from weak to moderate in intensity.

Minimal quartz veining is present within the western trend of porphyry and syenite intrusions. The most common vein type is white quartz veins with minor calcium-carbonate ranging from 1 to 10 cm wide. Most commonly observed in the Bristol Township porphyry, these quartz veins typically have minor pyrite (±chalcopyrite) enrichment within their vein envelopes; the timing of these veins is uncertain. A second type of vein present in the porphyritic intrusions are millimetre-thick white quartz veinlets, best described as quartz sweats.

Although no gold mines are associated with the intrusions of the western trend, the porphyritic intrusions have been the focus of years of exploration with numerous zones of anomalous gold known to exist (C. Dupont, Tom Exploration Inc., personal communication, 2004). The Holmer porphyry shows the weakest association with no known gold enrichment (J. Samson, Lakeshore Gold Corporation, personal communication, 2004). Mining claims are presently centred on both the Bristol Lake and South Bristol Lake porphyries; however, no significant mineralization has been documented to the authors' knowledge. The larger Bristol Township porphyry has had numerous intersections of anomalous gold associated with sulphide minerals (C. Dupont, Tom Exploration Inc., personal communication, 2004). In addition, some anomalous copper exists in the Bristol Township porphyry as chalcopyrite is present. The syenite intrusions of the western trend (Southwestern Bristol Township and Thunder Creek intrusions) have no known gold or copper enrichment known.

DEFORMATION

The western trend of porphyry and syenite intrusions generally show little to no deformation. The Bristol Township porphyry shows the strongest degree of deformation within the western trend displaying one weakly developed penetrative foliation observed within microlithons that is cut by a later and moderately dominant spaced cleavage. These two structural fabrics are also present in outcropping of the Bristol Lake and South Bristol Lake porphyry bodies. The older foliation is steeply dipping with an east to west trend; this structural fabric is suspected to be related to the D_1 deformation event to the east in Tisdale Township discussed by Bateman et al. (2004). The younger spaced cleavage is also steeply dipping and strikes east subparallel to the older foliation, with a slightly more east-southeast trend. The younger cleavage is characterized by 1 to 3 mm spaced cleavage planes and is suspected to be related to the D_2 deformation event to the east in Tisdale Township discussed by Bateman et al. (2004).

GEOCHEMISTRY

Geochemical data for the porphyry intrusions of the western trend are presented in Figures 2.11 to 2.15 and in Table 2.3.

Standard major element Harker plots for TiO_2, Al_2O_3, Fe_2O_3, MgO and CaO with increasing SiO_2 (*see* Figures 2.11A to 2.11E) are consistent with fractionation of feldspars, ferromagnesian minerals and oxides, as well as little to no mobility during alteration. Scatter of Na_2O and K_2O data (*see* Figures 2.11F and 2.11G) suggests mobility of these elements during alteration. Trace element Harker plots (*see* Figures 2.11H to 2.11N) of the western trend intrusions display 3 trends: 1) V, Sc, Nb and Y (*see* Figures 2.11H, 2.11I, 2.11L, and 2.11M) show decreasing arrays likely due to pyroxene, oxide ± hornblende fractionation; 2) Sr and Rb (*see* Figures 2.11J and 2.11K) show scatter representing mobility during alteration; and 3) Th (*see* Figure 2.11N) shows a slightly increasing array indicating incompatibility during crystal fractionation. Of note, 2 samples of the Holmer porphyry (04-PJM-258 and 04-PJM-259) show higher than average V, Sc, Sr, Nb, Y and Th and lower than average Rb values; the Southwest Bristol Township syenite also shows higher than average Rb, Nb, Y and Th values (*see* Table 2.3).

Alteration plots of the western trend intrusions indicate the porphyries have undergone various degrees of alteration. Most of the western trend intrusions display fresh to weakly altered signatures and plot in the least-altered field on an alteration box plot (*see* Figures 2.12A to 2.12C). However, sodium loss (*see* Figure 2.12A) coupled with potassium metasomatism (sericite alteration) (*see* Figures 2.12B and 2.12C) is exhibited within the 2 samples of the Bristol Township porphyry (04-PJM-283 and 04-PJM-286). As well, sodium alteration and/or metasomatism (albite alteration) is exhibited by the Bristol Lake, South Bristol Lake and Holmer porphyries (*see* Figures 2.12A to 2.12C).

Trace element ratios suggest that the intrusions of the western trend are trachyandesite to andesite in composition (*see* Figure 2.13A). The intrusions are subalkalic, except for the Holmer porphyry samples, which display an alkalic trend (*see* Figures 2.11A and B). Excluding the alkalic samples, all of the western trend intrusions display a calc-alkaline trend (*see* Figures 2.13C and 2.13D) with Zr/Y ratios greater than 7 (*see* Figure 2.13D). Triangular CIPW normative plots of feldspars (*see* Figure 2.14A) show that the western trend intrusions range from trondhjemite to tonalite to granodiorite (TTG) in composition. The western trend intrusions are further separated into high-Al TTG, excluding the some samples of the Holmer porphyry, which plot in low-Al TTG field (*see* Figure 2.14B).

Extended primitive mantle normalized multi-element plots yield 4 separate groups. The most common group (group A) encompasses Bristol Township, Bristol Lake and South Bristol Lake porphyries of the western. The group A intrusions display moderate fractionation with LREE-enrichment with HREE-depletion, coupled with negative Nb and Ti troughs, and positive Zr, Hf and Al anomalies (*see* Figure 2.15A). The Holmer porphyry, Southwest Bristol Township syenite and Thunder Creek syenite are divided into 3 other groups. Some of the Holmer porphyry samples (04-PJM-258 and 04-PJM-259) and the Southwest Bristol Township syenite form one of the groups (group C) (Figure 2.15C). These intrusions show moderate fractionation with greater LREE and HREE enrichment than group A intrusions, and have similar negative Nb and Ti anomalies, but do not have the positive Zr, Hf and Al anomalies (*see* Figure 2.15C). Group D of the western trend intrusions includes the Thunder Creek syenite (Figure 2.15D). This group (group D) shows a relatively flat pattern with low Ti, V and Sc, and positive anomalies of Th, Zr, Hf and Al (*see* Figure 2.15D). The last group (group E1) of western trend intrusions encompasses the other samples of the Holmer porphyry (04-PJM-262 and 04-PJM-263) (Figure 2.15E–Group E1). Group E1 intrusions have lower total trace element contents with weak LREE-enrichment and HREE-depletion, less well-developed negative Nb and Ti anomalies, and positive Zr, Hf and Al anomalies (*see* Figure 2.15E–Group E1).

GEOCHRONOLOGY

The Bristol Township porphyry is the only porphyry in the western trend that has had an age determined: Ayer et al. (2003) obtained a U/Pb zircon age of 2687.7±1.4 Ma. The other porphyry intrusions (Bristol Lake and South Bristol Lake porphyries) are suspected to be the same age based on similarities in the field relations, petrology and geochemistry. An age of emplacement for the Holmer porphyry, Thunder Creek syenite and Southwest Bristol Township syenite intrusions is unknown.

Southern Trend

The southern trend of porphyry intrusions includes intrusive bodies south of the PDDZ (*see* Figure 2.2), which form part of the swarm of porphyry intrusions that surround the Shaw Dome. This project focussed on the area spanning across Deloro and Shaw townships and examined 2 areas of this swarm: a porphyry dike swarm in northern Deloro Township and the large Mt. Logano porphyry intrusions in northeast Shaw Township (Figure 2.8; *see also* Figure 1.2 for township locations).

FIELD RELATIONSHIPS

The porphyry intrusions of the southern trend consist of 2 separate patterns of intrusive bodies: 1) a porphyry dike swarm; and 2) the Mt. Logano porphyry intrusion.

The porphyry dike swarm of northern Deloro Township consists of numerous (at least 5) separate metre-scale dikes with a general east-west strike that extend several hundred metres to a few kilometres in length (*see* Figure 2.8). The dike swarm has intruded at or near the contact between the top of the older Deloro assemblage metavolcanic rocks and the younger Tisdale assemblage metavolcanic rock units along the northern margin of the Shaw Dome (*see* Figure 2.1). The dikes crosscut stratigraphy and show sharp margins with the host-metavolcanic rocks (Photo 2.4A), although this relationship is not well exposed in all localities.

The Mt. Logano porphyry body consists of one large, possibly composite, elongate oval-shaped intrusive body (*see* Figure 2.8). The Mt. Logano porphyry is much larger then the Deloro Township dikes, being approximately 6 km or longer (east-southeast to west-northwest) and 1 to 1.5 km wide (*see* Figure 2.8). This porphyry has intruded near the Deloro–Tisdale assemblages contact, along the northeast margin of the Shaw Dome (*see* Figure 2.8). The contacts of the Mt. Logano porphyry have not been observed, but, near the western margin of the intrusive body, an internal breccia exists consisting of centimetre- to decimetre-size subrounded porphyry fragments supported in a porphyry matrix (Photo 2.4B).

PETROGRAPHY

Both the northern Deloro Township porphyry dike swarm and the Mt. Logano porphyry have similar primary petrography. The intrusions display a porphyritic texture with 1 to 5 mm phenocrysts of quartz and plagioclase feldspars, ranging from 20 to 45% of the rock, within a very fine-grained matrix (Photo 2.4C). The feldspar phenocrysts are generally subhedral in shape, with varying degrees of alteration resulting in the grains having slightly corroded textures (*see* Photo 2.4C) with partial to complete replacement by white mica (Photo 2.4D). Quartz phenocrysts are typically euhedral to subhedral in shape and exhibit minor strain extinction. All of the southern trend porphyry intrusions contain 0.5 to 1.5 mm, euhedral to subhedral disseminated pyrite crystals.

ALTERATION, VEINING AND MINERALIZATION

All of the southern trend porphyry intrusions (northern Deloro Township swarm and Mt. Logano) have white mica and chlorite alteration to varying degrees, along with locally preserved carbonate alteration. White mica alteration of feldspars and feldspathic matrices is weakly to moderately developed in all the intrusions, characterized by sericite trains consisting of approximately 0.3 mm muscovite blades (Photo 2.4E) and corroded feldspars; the white mica alteration ranges from 2 to 5 modal %. The margins of the Mt. Logano porphyry show the strongest sericite alteration with the alteration generally decreasing inward from the margins of the porphyry. Chlorite alteration is equally common as sericite within the southern trend, ranging from weakly to moderately developed 0.5 to 2 mm, euhedral to anhedral chlorite laths (Photo 2.4F). The amount of chlorite ranges from 2 to 5 modal %. The porphyry dike swarm of northern Deloro Township displays the strongest chlorite alteration of the southern trend, but this is within individual dikes of the swarm and not the entire swarm. Weak calcium-carbonate alteration is often coupled with the areas of moderate sericite alteration giving phenocrysts and relict phenocrysts of feldspar a clouded brownish-grey appearance (*see* Photo 2.4E).

Two types of veins are present in the porphyries of the southern trend and both are very rare. The more common veins are millimetre-thick white quartz sweats within the porphyry intrusions (especially the Mt. Logano porphyry). These quartz sweats have no recognizable preferred orientation. The second type of veins are present in the most northern dikes of the northern Deloro Township swarm and consists of white quartz with minor calcium-carbonate. The thickness of the veins ranges from 1 to 20 cm and the veins are typically a few metres to tens of metres long. These veins have a dominantly northwest to southeast orientation and are more common within the host metavolcanic rocks surrounding the porphyry bodies, than within the porphyry dikes themselves. Angular wall rock fragments up to a centimetre in diameter are present in these veins along with minor pyrite and chalcopyrite in and around the quartz veins.

No gold or copper mineralization is known to be spatially associated with southern trend of porphyry intrusions. Quartz veins containing approximately 5% chalcopyrite are present in the area of the northernmost Deloro Township porphyry dikes, suggesting a possible spatial association to anomalous copper.

DEFORMATION

Two phases of deformation are visible within the porphyry intrusions of the southern trend. The most dominant structural fabric is a steeply dipping, millimetre-spaced cleavage, which is moderately developed in the northern Deloro Township porphyry dike swarm, and weakly to moderately developed in the Mt. Logano porphyry. This spaced cleavage is related to D_2 regional deformation event discussed by Bateman et al. (2004). Locally visible microlithons within porphyry dikes of northern Deloro Township swarm display a penetrative foliation that is older the D_2 spaced cleavage discussed above. This foliation is related to the D_1 regional deformation event discussed by Bateman et al. (2004).

GEOCHEMISTRY

Geochemical data for the porphyry intrusions of the southern trend are presented in Figures 2.11 to 2.15 and in Table 2.3.

Standard major element Harker plots for TiO_2, Al_2O_3, Fe_2O_3 and MgO (*see* Figures 2.11A to 2.11D) form decreasing arrays with increasing SiO_2 suggesting fractionation of ferromagnesian minerals and oxides, as well as little to no mobility during alteration. Increasing CaO, Na_2O and K_2O with SiO_2 (*see* Figures 2.11E to 2.11G) suggest incompatibility during crystal fractionation and the associated scatter in the data suggests variable mobility of these elements during alteration. Trace element Harker plots (*see* Figures 2.11H to 2.11N) of the southern trend intrusions display 3 trends: 1) V, Sc, Nb and Y (*see* Figures 2.11H, 2.11I, 2.11L and 2.11M) decrease with increasing SiO_2 consistent with oxide and ferromagnesian mineral fractionation; 2) Sr and Rb (*see* Figures 2.11J and 2.11K) show scatter representing variable mobility during alteration; and 3) Th (*see* Figure 2.11N) shows a flat array.

Alteration plots of the southern trend intrusions indicate the porphyries have only undergone minor alteration. Most of the southern trend intrusions display fresh to weakly altered signatures (*see* Figures 2.12A to 2.12C) and plot in the least-altered field of a Hughes plot (Hughes 1973). However, sodium alteration and/or metasomatism (albite alteration) is present in 2 samples of the northern Deloro Township dike swarm porphyries (*see* Figures 2.12A to 2.12C).

Trace element ratios suggest that the intrusions of the southern trend are rhyodacite to dacite in composition (*see* Figure 2.13A). The intrusions are subalkalic (*see* Figure 2.13B) with calc-alkaline trends (*see* Figures 2.13C and 2.13D) and Zr/Y>7 (*see* Figure 2.13D). Triangular CIPW normative plots of feldspars (*see* Figure 2.14A) illustrate that the southern trend intrusions range from trondhjemite to tonalite to granodioritic (TTG) in composition. The southern trend intrusions straddle the line that separates high-Al TTG and low-Al TTG intrusions (*see* Figure 2.14B).

Extended primitive mantle normalized multi-element plots of the southern intrusions are all similar to other group A intrusions in the central and northern trends. The southern trend intrusions have LREE-enriched and heavy REE (HREE)-depleted patterns with negative Nb and Ti anomalies, and positive Zr, Hf and Al anomalies (*see* Figure 2.15A).

GEOCHRONOLOGY

The southern trend intrusions have not previously had ages determined. As part of this study, one sample, collected by L.A.F. Hall and M.G. Houlé, OGS, was submitted to the Jack Satterly Geochronology Laboratory, University of Toronto, for geochronological analysis using U/Pb on zircons using the methods outlined in Appendix B. Sample 03LAH-0627 yielded high-quality slender, elongate, pale brown to colourless well-terminated prismatic zircons, as well as rarer needle or acicular forms, and flat prisms. The highest quality, air abraded, slender prisms yielded a very tight agreement of $^{207}Pb/^{206}Pb$ ages with 2 fractions overlapping each other and on concordia, whereas a third fraction was somewhat reversely concordant (possibly due to analytical problems)(Figure 2.16A). All 3 fractions gave a well-defined age of 2689.0±1.4 Ma (weighted mean $^{207}Pb/^{206}Pb$ age; *see* Figure 2.16A). Given the similarity in chemistry and field relationships of the intrusions on the northern margin of the Shaw Dome, it is likely that this age is the age of all southern trend intrusions.

Eastern Trend

The eastern porphyry bodies include any intermediate to felsic intrusions along the PDDZ west of the Burrows–Benedict fault, from near South Porcupine in the west, to Matheson in the east (*see* Figures 2.2 and 1.2). The eastern porphyry body consists of 9 intrusions, which occur within Whitney, Macklem and Carr townships (*see* Figure 1.2), including (from west to east) Pamour porphyry, Hoyle Pond porphyry, Bob's Lake granodiorite, Aquarius porphyry, Aquarius Mine porphyry, Homestead porphyry, Crowley porphyry, Pominex porphyry and Carr Township porphyry (Figure 2.9).

FIELD RELATIONSHIPS

Three geographical groups of intrusions exist within the eastern trend. The westerly group of intrusions is located in Whitney and Hoyle townships and includes the elongate Pamour porphyry, Hoyle Pond porphyry and Bob's Lake granodiorite (*see* Figure 2.9). The second group of intrusions forms an east to west belt spanning across northern Macklem Township in proximity to the Aquarius Mine (*see* Figure 2.9), and include the Aquarius, Aquarius Mine, Homestead, Crowley and Pominex porphyries. The Carr Township porphyry is in a group by itself and is the most easterly porphyry of this study (*see* Figure 2.9).

All of the eastern trend intrusions have intruded either the Tisdale or Porcupine assemblages (*see* Figure 2.1). The Whitney and Hoyle townships intrusions (Pamour porphyry, Hoyle Pond porphyry and Bob's Lake granodiorite), and the Macklem Township intrusions (Aquarius, Aquarius Mine, Homestead, Crowley and Pominex porphyries) have intruded near the base of the Tisdale assemblage within the Hersey Lake and Central formations (*see* Figure 2.1). The Carr Township porphyry is different from the other intrusion groups of the eastern trend: this porphyry intrudes the Porcupine assemblage along the contact between siliciclastic metasediments of the Porcupine assemblage and a thin sliver of mafic metavolcanic rocks, the latter of which are most likely part of the lower to middle units of the Tisdale assemblage (*see* Figure 2.1).

The size and shape of each of the eastern trend intrusions differs considerably. The largest intrusion, the Carr Township porphyry, is an oval-shaped body spanning over 12 km in length (east to west) and greater than 5 km in width (north to south) (*see* Figure 2.9). The second largest intrusion, the Bob's Lake granodiorite, is elongate and irregularly shaped, spanning more than 5 km in length and approximately 2 km in width (*see* Figure 2.9). The next largest intrusions are the Crowley and Pominex porphyry dikes in Macklem Township; these are elongate in shape and are at least 3 km long and approximately 100 m wide (*see* Figure 2.9). The elongate Pamour and Hoyle Pond porphyries in Whitney and Hoyle townships are the next largest intrusions of the eastern trend and are less than 1 km long and 100 m wide (*see* Figure 2.9). The Aquarius, Homestead and Aquarius Mine porphyries in Macklem Township are the smallest eastern trend intrusions occurring as oval-shaped bodies that are 100 to 300 m in diameter (*see* Figure 2.9).

The eastern trend of porphyries either have sharp intrusive (Photo 2.5A) or tectonic boundaries; exceptions to this are the margins of both the Aquarius and Carr Township porphyries. The Aquarius porphyry margin (where observed) is a transitional contact between the intrusion and host mafic volcanic rocks. A gradation from porphyry with very little chlorite, to chlorite-rich porphyry, to quartz-feldspathic-rich, chloritic volcanic rock, to chloritic volcanic rock is present over a distance of a 15 cm (Photo 2.5B). The contact of the Carr Township porphyry consists of a 1 m wide breccia unit with porphyry fragments up to 8 cm long within a very fine-grained chloritic matrix (Photo 2.5C).

PETROGRAPHY

The intrusions of the eastern trend all exhibit a porphyritic texture (Photo 2.5D), except for the Bob's Lake granodiorite (Photo 2.5E). Phenocrysts of plagioclase (5–35%) and quartz (0–20%) in the porphyries range from 1 to 6 mm long; larger phenocrysts, up to 15 mm in diameter (Photo 2.5F), are present within the Carr Township porphyry. The plagioclase phenocrysts are euhedral to subhedral and range from unaltered to completely altered, occurring as relict crystals (Photo 2.5G). The quartz phenocrysts are euhedral to subhedral with weak to moderate strain extinction. The matrix that surrounds the phenocrysts consists of fine-grained quartzo-feldspathic material. The equigranular Bob's Lake granodiorite (*see* Photo 2.5E) consist of 60%, 1 to 4 mm subhedral to euhedral plagioclase; 30%, 1 to 2 mm, interstitial, weakly strained quartz; and 10% fine-grained quartzo-feldspathic matrix. Trace to 5% euhedral to subhedral pyrite is present in all of the intrusions of the eastern trend ranging from disseminated grains approximately 1 mm in size to millimetre-thick stringers and centimetre-size clusters (Photo 2.5H). Trace chalcopyrite is present in the Carr Township porphyry associated with pyrite stringers and clusters. The Carr Township porphyry also contains internal breccias that consist of multiple centimetre-size rounded porphyry fragments within a porphyry matrix (Photo 2.5I), suggesting the Carr Township porphyry is a composite intrusive body.

Metamorphic minerals are present in 2 of the eastern trend intrusions (Pamour and Aquarius porphyries). Biotite ranges from 10 to 20 modal % of the Pamour porphyry and is present as both disseminated submillimetre, subhedral laths, as well as clusters 5 to 20 mm in size (Photo 2.5J). Retrograde chlorite is also present in the Pamour porphyry altering the biotite. Metamorphic biotite coupled with muscovite occurs as 1 to 3 cm wide rotated clusters in the Aquarius porphyry (Photo 2.5K).

ALTERATION, VEINING AND MINERALIZATION

The eastern trend of porphyry intrusions has a range of alteration types with differing intensity. The most prominent alteration present in all of the intrusions is white mica alteration, which is often coupled with weak calcium-carbonate alteration. The white mica (sericite) alteration ranges from 1 to 10 modal % and occurs as submillimetre-size clusters and trains within the matrix of the eastern trend porphyries (*see* Photo 2.5G). White mica alteration also occurs as approximately 1 cm wide clusters of muscovite in the Bob's Lake granodiorite. Calcium-carbonate alteration is recognized by bleaching of the intrusions along with a clouded brownish-grey appearance of feldspars and matrices in thin section. Chlorite alteration is the second most common alteration facies being developed locally in most of the intrusions. The chlorite occurs as disseminated 0.5 mm euhedral to subhedral laths. Weak to moderate pervasive hematite (Aquarius and Carr Township porphyries) and patchy ankerite (Aquarius Mine porphyry) alteration facies are also present in the eastern trend of porphyry intrusions. Silicification and albitization are strongly developed in the Crowley and Pominex porphyries (Photo 2.5L) near the Aquarius Mine.

Three types of veins are present in the eastern trend intrusions. The most common veins are white quartz sweats and are present in most of the eastern trend intrusions. These sweats are 1 to 2 mm wide and are not accompanied by alteration of the surrounding wall rock. The second and more significant vein type is white quartz with minor calcium carbonate. These types of veins are centimetres to decimetres in width, and often are accompanied by wall rock alteration and sulphide mineralization. The Aquarius Mine porphyry also contains quartz-ankerite veins. These veins are similar in every respect to the quartz–calcium carbonate veins discussed above, excepting ankerite is present instead of calcium carbonate.

Both anomalous gold and copper are spatially associated with porphyritic intrusions of the eastern trend. Gold mineralization shows the strongest spatial association with the sericite–carbonate-altered Hoyle Pond porphyry and the ankerite-altered Aquarius Mine porphyry (R. Norman, Kinross Gold Corp., personal communication, 2004). The strong degree of deformation may also play a key role in the association between gold and porphyry magmatism at Hoyle Pond. Anomalous copper values also exist within the Carr Township porphyry (up to 2187 ppm Cu – sample # 03-PJM-142i). The copper enrichment is spatially associated with hematite alteration zones and the presence of chalcopyrite with pyrite in stringers and centimetre-size lenses.

DEFORMATION

Only the Hoyle Pond and Pamour porphyry intrusions of the eastern trend display significant structural fabrics. The Hoyle Pond porphyry exhibits strong, penetrative foliation. The Pamour porphyry has weak to moderately developed foliation near the margins of the intrusion, which is suspected to be the same generation as the foliation in the Hoyle Pond porphyry. The generation and orientation of the foliation is unknown due to the fact that the Hoyle Pond porphyry samples were provided by another person (E. Dinel, University of Ottawa, personal communication, 2004), and the Pamour porphyry was only observed in poorly oriented drill core.

GEOCHEMISTRY

Geochemical data for the porphyry intrusions of the eastern trend are presented in Figures 2.11 to 2.15 and in Table 2.3.

Standard major element Harker plots show decreasing TiO_2, Al_2O_3, Fe_2O_3, MgO and CaO with increasing SiO_2 (*see* Figures 2.11A to 2.11E) compatible with ferromagnesian mineral, oxide ± feldspar fractionation and little to no mobility of these elements during alteration. Scatter of Na_2O and K_2O data (*see* Figures 2.11F and 2.11G) suggests incompatibility and mobility of these elements during alteration.

Trace element Harker plots (*see* Figures 2.11H to 2.11N) of the eastern trend intrusions display 2 trends: 1) V and Sc (*see* Figures 2.11H and 2.11I) show decreasing arrays representing compatibility during oxide fractionation; and 2) Sr, Rb, Nb, Y and Th (*see* Figures 2.11J to 2.11N) show scatter as a product of various intrusion types, but also represent incompatibility during crystal fractionation and, in the case of Rb and Sr, mobility during alteration.

Alteration plots of the eastern trend intrusions indicate the porphyries have undergone various degrees of alteration. Most of the eastern trend intrusions display sodium alteration and/or metasomatism (albite alteration) (*see* Figures 2.12A to 2.12C). However, some samples display fresh to weakly altered signatures (*see* Figure 2.12A to 2.12C) and plot in the least-altered field of a Hughes plot (Hughes 1973).

Trace element ratios suggests the intrusions of the eastern trend are andesite to dacite in composition (*see* Figure 2.13A). The intrusions are predominantly subalkalic except for a few samples of the Aquarius and Crowley porphyries (*see* Figures 2.13A and 2.13B). The eastern trend intrusions also display calc-alkaline trends (*see* Figures 2.13C and 2.13D) with Zr/Y ratios greater than 7 (*see* Figure 2.13D). Triangular CIPW normative plots of feldspars (*see* Figure 2.14A) illustrate that the eastern trend intrusions range from trondhjemite to tonalite to granodiorite (TTG) in composition, and they are transitional between high-Al TTG and low-Al TTG (*see* Figure 2.14B).

The extended primitive normalized mantle multi-element signatures for the eastern trend porphyries can be divided into 4 separate groups. The first group (group A) includes the Aquarius, Aquarius Mine, Homestead, Crowley and Pominex porphyry intrusions. These intrusions (group A) show moderate LREE enrichment and HREE-depletion with negative Nb anomalies and positive Zr, Hf and Al anomalies (*see* Figure 2.15A). The second group (group B) encompasses the Pamour porphyry and the Bob's Lake granodiorite. These intrusions (group B) display moderate to strong LREE-enrichment and HREE-depletion with negative Nb and Ti anomalies, and positive Zr, Hf and Al anomalies (*see* Figure 2.15B). The third group (group E2) includes the Hoyle Pond porphyry, which has a relatively weakly LREE-enriched and HREE-depletion pattern, with only weakly developed negative Nb and Ti anomalies, and weakly positive Al, Zr and Hf anomalies (*see* Figure 2.15E–Group E2). The last group (group F) consists of the Carr Township porphyry, which has weak to moderate LREE-enrichment and HREE-depletion, but with small negative Nb and Ti anomalies, and very small positive Zr, Hf and Al anomalies (Figure 2.15F).

GEOCHRONOLOGY

Uranium-lead zircon geochronology has been conducted on the Pamour porphyry and the Aquarius porphyry. The U/Pb age of the Aquarius porphyry reported by Corfu et al. (1989) (*see* Table 2.1) was poorly constrained at 2705±10 Ma, although 2 zircons analyzed were near concordant; a lack of zircons as well as inheritance and/or complex lead loss caused the poor constraint. Two of the other porphyritic intrusions of Macklem Township (Aquarius Mine and Homestead porphyries) are likely to be the same age as the Aquarius porphyry due to similar field relationships, petrology and chemistry. The Hoyle Pond porphyry has a preliminary U/Pb age of circa 2683 Ma (Hamilton as cited *in* Dinel and Fowler 2004, p.46-3).

As part of this study, a sample from the Pamour porphyry (03PJM-131) was collected and submitted to the Jack Satterly Geochronology Laboratory, University of Toronto, for U/Pb geochronological analysis on zircons using the methods outlined in Appendix B. This sample yielded very diverse zircon grains that were not of great quality, consisting primarily of mostly small, square bipyramids, pale to medium brown in colour, but often cracked, frosty or turbid; some of the larger grains looked slightly rounded (resorbed xenocrysts?). The best, clearest, inclusion- and crack-free grains were strongly abraded and analyzed, but yielded discordant results: 3 fractions lie on or near concordia between 2690 and 2703 Ma (2 of these fractions have large errors), whereas 2 darker brown single grains are both highly discordant. A final fraction (A1f on Figure 2.16B) provided the best estimate for the age of the sample, and is only slightly discordant (0.5%): the $^{207}Pb/^{206}Pb$ age is 2677.5±1.0 Ma. This age is interpreted to be the best estimate of the age of the Pamour porphyry and is a minimum age.

GEOLOGY: THE KRIST FORMATION

The Krist Formation forms the basal member of the Porcupine assemblage (*see* Figure 2.1) and typically observed to uniformly fill paleotopographic lows (Porcupine and Kayorum synclines) to an approximate thickness of 200 m (Brisbin 2000)(Figures 2.3 and 2.10). A fundamental question that exists within the Timmins camp is the relationship between the porphyries and the Krist Formation. In an attempt to test this relationship, the Krist Formation was briefly examined and sampled at 3 localities to be compared both geologically and geochemically with the porphyry intrusions. The 3 locations are shown on Figure 2.10 and include outcrop locations within the Porcupine syncline, near a power line along the southern side of Highway 101 between Schumacher and South Porcupine; the Kayorum syncline in a small outcrop within a trailer park between the Shania Twain Centre and Moneta Road; and a thin band of felsic volcanic rocks south of the PDDZ directly south of the Aunor gold mine.

Field Relationships and Petrography

The Krist Formation is dominantly a volcaniclastic package that is composed of conglomeritic volcaniclastic rocks that consist of subrounded to rounded porphyry fragments up to a few centimetres in diameter supported in a feldspar-phyric, intermediate to felsic, lapilli tuff matrix (Photo 2.6A). Mafic volcanic fragments, similar in size and shape to the porphyry fragments, are locally observed near the base of the Krist Formation within the Kayorum syncline (Photo 2.6B). Angular to subrounded sulphide (pyrite) fragments up to 2 cm in diameter are also common in both the Porcupine and Kayorum synclines (Photo 2.6C). The matrix contains minor quartz phenocrysts, with alteration minerals including white mica and chlorite. The outcropping of the Krist Formation in northern Deloro township consists of a lapilli tuff with no porphyry or mafic clasts.

Alteration, Veining, Mineralization and Deformation

Alteration of the Krist Formation includes weak to moderately developed sericite-carbonate alteration. This alteration assemblage affected the feldspathic portion of the matrix predominantly, resulting in a cloudy brownish-grey appearance of feldspars in thin section (Photo 2.6D). Minor chlorite alteration is also present within the Krist Formation.

No significant veining or mineralization is associated with the Krist Formation, although the sulphide fragments present within the formation do contain minor chalcopyrite.

A spaced cleavage is present within all of the Krist Formation localities related to the D_2 regional deformation event (Bateman et al. 2004), and there is also a strong eastward-plunging stretching lineation of clasts (Photo 2.6E). The generation of deformation that resulted in this stretching of clasts is unknown (Bateman et al. 2004).

Geochemistry

Geochemical data for the Krist Formation samples are presented in Figures 2.11 to 2.15 and in Table 2.3.

Major and trace element Harker plots for the Krist Formation show no trends, most likely due to the small number of samples. Alteration plots for the Krist Formation indicate the fragmental unit has little to no alteration. The Krist Formation samples plot with fresh to weakly altered signatures (*see* Figures 2.12A to 2.12C).

Trace element ratios suggest that the Krist Formation is rhyodacite or dacite to trachyandesite in composition (*see* Figure 2.13A). The intrusions are subalkalic (*see* Figure 2.13B) displaying calc-alkaline trends (*see* Figures 2.13C and D) with Zr/Y ratios greater than 7 (*see* Figure 2.13D). Triangular CIPW normative plots of feldspars (*see* Figure 2.14A) suggests that the Krist Formation, like most of the porphyries, has a high-Al TTG affinity (*see* Figure 2.14B).

Extended primitive mantle normalized multi-element plots for the Krist Formation can be divided into 2 groups. The more common group (group G1) encompasses samples from the Porcupine and Kayorum synclines. These group G1 samples display strong HREE depletion and negative Nb and Ti anomalies, with positive Zr, Hf and Al anomalies (Figure 2.15G). The second Krist Formation REE grouping (group G2) includes the northern Deloro Township sample. The group G2 sample displays moderate fractionation (*see* Figure 2.15G) with more HREE depletion compared to group G1, and has more developed positive Zr, Hf and Al anomalies, and less developed negative Nb and Ti anomalies (*see* Figure 2.15G).

Geochronology

Previous U/Pb ages for the Krist Formation determined by Corfu et al. (1989) were interpreted to be older than the age of the porphyries of the Timmins camp (2698±4 Ma for the Krist Formation versus ca. 2689 Ma for the porphyries). However, recent work by Ayer et al. (2002) has yield new U/Pb ages for the crystallization of the Krist Formation: 2687.3±1.6 Ma within the Porcupine syncline and 2687.5±1.3 Ma within the Kayorum syncline. These ages are within error of many of the ages of the porphyries in the Timmins camp, and, combined with the chemical attributes of the Krist Formation described above, suggests the Krist Formation and the porphyries are coeval.

COMPARISON OF PORPHYRY TRENDS

The porphyry intrusions of the central and northern trends are spatially associated with the 2 largest gold deposits of the Timmins camp (the Hollinger–McIntyre and Dome mines) and, because of this association, they will be the datum to which the western, southern and eastern trends are compared. To begin, a comparison of the central and northern trends will be made so as to establish the datum to which all other trends will be compared.

Many similarities between the central and northern trends exist. Both trends exhibit similar field relationships, petrology, alteration, veining, deformation and geochronology as shown in Table 2.2. Gold mineralization is also similar within both of the trends, with the majority of enrichment being spatially related to porphyry intrusions that have undergone sericite alteration (sodium loss and/or potassium metasomatism). Copper mineralization is present only in the northern trend. The presence of hematite alteration accompanied by chalcopyrite and bornite sulphides is unique to the northern trend and was likely an important factor in copper enrichment (i.e., highly oxidized copper-bearing fluids).

The Bristol Township, Bristol Lake and South Bristol Lake porphyry intrusions of the western trend are similar to the central and northern trends, in terms of field relationships, petrology, copper mineralization, deformation, geochemistry and geochronology as shown in Table 2.2. These intrusions, however, do not have similar alteration (only minor sodium loss and/or potassium metasomatism) and veining (no quartz-tourmaline or quartz-ankerite) when compared to the central and northern trends, and this may explain why they do not have significant quantities of gold mineralization. The Holmer, Southwest Bristol and Thunder Creek porphyry and syenite intrusions of the western trend of intrusions are geochemically distinct from the gold-related intrusions of the northern and central trends; hence, it is not surprising that there is no significant quantities of gold or copper mineralization associated with these latter intrusions.

The southern trend of intrusions have many characteristics that are very similar to the gold-related intrusions of the northern and central trends. They have similar field relationships, petrology, deformation, geochemistry and ages (*see* Table 2.2). The southern trend intrusions, however, have weaker alteration (less sodium loss and/or potassium metasomatism) and the veins present are not quartz-tourmaline and quartz-ankerite veins, as are the veins in the main gold camp. Thus, this partly explains the dearth of gold associated with these intrusions south of the PDDZ. Furthermore, the southern trend intrusions also lack hematite alteration and associated copper sulphide mineralization and, thus, have minimal copper mineralization as well.

The eastern trend porphyries have some similarities in terms of their field relationships, petrology, alteration, veining, deformation, mineralization, deformation, geochemistry and geochronology relative to the gold-bearing intrusions of the northern and central trends (*see* Table 2.2). Notable, however, is that there are strong differences in alteration (little sodium loss and/or potassium metasomatism) and their primitive mantle normalized patterns are not entirely identical to the group A suite that are commonly associated with gold in the northern and central trends (*see* Figure 2.14A). Similarities in veining (quartz-ankerite) in the Aquarius Mine porphyry to veining observed in the gold-related intrusions of the northern and central trends is suspected to be an important factor in the fact that there is gold mineralization at the Aquarius Mine. Hematite alteration coupled with copper sulphide minerals is important in anomalous copper values within the Carr Township porphyry, which is similar to the relationships present in the gold-related intrusions of the northern and central trends.

COMPARISON OF THE KRIST FORMATION WITH PORPHYRY INTRUSIONS

The relationship between the porphyries and the Krist Formation has been a long-standing question in the Timmins camp. The results of this study illustrate that the Krist Formation and the porphyries are similar in terms of their petrography, geochemistry and geochronology (U/Pb ages). For example, the matrix of the volcaniclastic rocks and the lapilli tuffs of the Krist Formation, is identical to the mineralogy of the central and northern trend intrusions. The Krist Formation also contains similar secondary mineralogy and alteration as the porphyries. For example, the Krist Formation contains secondary white mica, chlorite and pyrite, and sericite, carbonate and chlorite alteration similar to the porphyries in the central and northern trends. Furthermore, the rounded porphyry and mafic volcanic fragments in the Krist Formation are similar to the marginal breccias observed in many of the main camp porphyry trends.

In addition to their field characteristics, the geochemical signatures of the Krist Formation are similar to the porphyry trends. For example, major and trace element abundances are similar to the porphyry trends (*see* Figure 2.11), as are their compositional and alteration trends (*see* Figures 2.12 and 2.13). Primitive mantle normalized plots of the Porcupine and Kayorum syncline samples display near identical signatures to the majority of porphyry intrusions examined in this study (*see* Figure 2.15A). Similarly, U/Pb geochronological results obtained from samples of the Krist Formation within the Porcupine and Kayorum synclines suggests the crystallization age (2687 Ma: Ayer et al. 2002) to be coeval with porphyry magmatism (2687–2691 Ma: Corfu et al. 1989; Ayer, Ketchum and Trowell 2002; Ayer et al. 2003). *In summary, the Krist Formation has field, geochemical, and temporal similarities to the porphyry* intrusions and these similarities would suggest that it is the extrusive equivalent to the porphyries of the central, northern, western (Bristol Township, Bristol Lake and South Bristol Lake porphyries) and southern trends. It is notable, however, that no parental vent, or vents, that may have been the source for the Krist Formation have been found; it is possible, however, that the elongate porphyry trends may mark the subvolcanic roots of fissures that have had their surface expressions eroded off.

DISCUSSION

Geochemical and Timing Relationships of Porphyries with Gold Mineralization

The porphyries of the Timmins camp associated with gold mineralization are associated with ages of 2687 to 2692 Ma (Corfu et al. 1989; Ayer, Ketchum and Trowell 2002; Ayer et al. 2003), have high-Al TTG signatures, and extended primitive mantle normalized multi-element signatures that display moderate fractionation with moderate depletion of HREE, negative Nb and Ti anomalies, and positive Zr, Hf and Al peaks (*see* Figure 2.15A). The porphyries associated with gold mineralization are also characterized by very low Y and Yb contents, with relative high Al_2O_3 contents. In contrast, intrusions not associated with gold mineralization are generally younger in age (2677.5 Ma: Pamour porphyry), and display a range of extended primitive mantle normalized multi-element signatures compared to the gold-bearing intrusions (*see* Figures 2.15B to 2.15F).

There are some exceptions to the above relationships. The Aquarius Mine porphyry has an age of emplacement (2705 Ma: Corfu et al. 1989) that differs from most of the gold mineralization associated porphyry intrusions, but its multi-element trend is the same as the other gold mineralization associated intrusions (*see* Figure 2.15A). The age of the Hoyle Pond porphyry is also younger than the main gold-mineralization associated porphyries (ca. 2683 Ma; Hamilton as cited *in* Dinel and Fowler 2004, p.46-3). Furthermore, the multi-element signature for this porphyry (*see* Figure 2.15E–Group E2) is also distinctive compared to the intrusions associated with gold mineralization. Further work is required to explain this difference between the Hoyle Pond mineralization and mineralization in the main camp.

Relationship of Porphyries to Gold and Copper Mineralization and Exploration Implications

Throughout the history of research in the Timmins camp, there has been significant controversy about whether the porphyries in the Timmins camp have played a passive (i.e., orogenic control on gold) or active (i.e., magmatic-hydrothermal control on gold) role in the generation of gold deposits (Davies and Luhta 1979; Mason and Melnik 1986; Wood et al. 1986; Burrows and Spooner 1986; Brisbin 2000; Gray and Hutchinson 2001). The results of this study, and that of others, clearly illustrate that gold mineralization is not genetically related to porphyry magmatism. Three lines of evidence can be used to negate a genetic role for these intrusions. Firstly, gold-bearing veins within the Timmins camp crosscut and are hosted within the porphyries, but also within surrounding wall rock, suggesting that the veins postdate porphyry formation. Secondly, the veins are in structurally controlled vein arrays (Wood et al. 1986; Burrows and Spooner 1986; Brisbin 2000; Gray and Hutchinson 2001), that, although spatially proximal to many intrusions, are independent of porphyry location, suggesting that the main controller on gold vein emplacement was structural, rather than magmatic. Finally, recent Re/Os isotope geochronological analyses of molybdenite at the McIntyre and Dome mines have yielded ages of 2661±13 Ma and 2670±10 Ma, respectively (Ayer et al. 2003), whereas porphyry magmatism occurred between 2691 and 2687 Ma (Corfu et al. 1989); this suggests that a gap of 17 to 30 million years exists between porphyry magmatism and gold emplacement. There is, however, a strong spatial association between porphyries and gold mineralization and this association may be a function of 1) that gold mineralization developed during regional deformation because of the competency difference between the porphyries and the surrounding mafic volcanic rocks (Burrows et al. 1993); and/or 2) that the porphyry intrusions and gold-bearing fluids utilized the same long-lived structure at different times.

Even though no genetic association exists between gold mineralization and porphyry magmatism, there are a number of empirical relationships between porphyries and gold that may aid exploration in the Timmins camp. Firstly, the intrusions associated with gold have high Al-TTG suite signatures, have Group A primitive mantle normalized signatures, and signatures akin to modern adakites. Secondly, gold mineralization shows a strong association to sericite- and carbonate-altered porphyry intrusions at the Hollinger–McIntyre and Dome deposits. Chemically, this alteration is characterized by sodium loss and potassium metasomatism. Secondly, there are clusters of numerous porphyry intrusions (5 or more) in an elongate east to west magmatic belt that show a strong association to gold mineralization at the Hollinger–McIntyre, Dome and Aquarius deposits. This clustering of intrusions helped nucleate structures large enough to form ore-grade deposits, whereas single intrusions were probably not of sufficient size to help nucleate structures. Finding similar clusters of porphyry intrusions associated with structures, with high Al-TTG signatures, and associated alteration may help identify prospective new ground to discover new gold occurrences.

Copper(-molybdenite) mineralization in the Timmins camp is also genetically unrelated to porphyry magmatism, as was previously suggested by Mason and Melnik (1986). New Re/Os geochronological analyses on molybdenite within the central copper zone of the Pearl Lake porphyry has yielded an age of 2672±7 Ma (Bateman et al. 2004), which is 15 to 19 million years younger than the actual porphyry ages in the Timmins camp. This suggests that copper-molybdenum mineralization, similar to gold mineralization, represents a distinctive pulse of mineralization unrelated to the porphyry intrusions. It is thus concluded that porphyry copper mineralization, similar to the Phanerozoic deposits in the western North and South American Cordillera, does not exist within the Archean porphyry intrusions of the Timmins camp. Nevertheless, a strong spatial association still exists between copper-molybdenum mineralization and the porphyry intrusions, and 2 observations may aid exploration for copper-molybdenum mineralization within the Archean porphyry intrusions of the Timmins camp. Firstly, only the largest intrusions have copper and molybdenum enrichment: the Pearl Lake, Bristol Township and Carr Township porphyries. Secondly, the association of hematite to copper enrichment is either the result of alteration caused by the oxidized copper-bearing fluids, or hematite-altered porphyry forms a chemically favourable zone for the deposition of copper from migrating metal-bearing fluids. Exploration for copper in Archean porphyry intrusions of the Timmins camp should be based on the size of the intrusion along with zones of hematite alteration.

SUMMARY

The main results of this intrusion subproject include

- The porphyry intrusions of the Timmins camp generally form east-trending belts ranging from 4 to 20 km long that are composed of multiple bodies. The sizes and shapes vary from intrusions to intrusions ranging from small dikes a few hundred metres long to oval bodies that are up to 11 km long. The porphyry intrusions generally intrude into the Vipond Formation of the Tisdale assemblage, but also at the Deloro–Tisdale and Tisdale–Porcupine assemblages contacts. The porphyry intrusions are generally semi-conformable to stratigraphy. The margins and/or contacts between the porphyry intrusions and host stratigraphy is generally sharp, although breccia zones do exist as do transition zones to a lesser extent.
- Petrographically, the intrusions are dominantly porphyritic in texture, but also occur as aphanitic and equigranular. Phenocrysts of plagioclase and quartz are typically 2 to 3 mm in diameter, but range up to 15 mm. These phenocrysts are hosted dominantly in a very fine-grained matrix, but do exist in fine- to medium-grained matrixes as well. Minor minerals present within the intrusions include apatite, tourmaline and leucoxene. Sulphide minerals include pyrite, chalcopyrite, pyrrhotite, bornite and arsenopyrite. Foreign clasts (green mica) are common in the northern and central trend intrusions and range up to 10 cm in length. Metamorphic minerals include stilpnomelane in the Edwards porphyry and biotite in the Pamour and Aquarius porphyries.
- The most dominant alteration facies observed was sericite and associated calcium-carbonate. Chlorite, iron-carbonate, hematite, leucoxene, silica and albite were all also observed in various intrusions.
- Most of the intrusions examined display structural fabrics associated with the D_1 and D_2 deformation events described by Bateman et al. (2004).
- Six geochemical groups of intrusions were identified using trace and REE chemistry.
- Timing of emplacement of porphyry intrusions occurred dominantly between 2687 and 2691 Ma (Corfu et al. 1989; Ayer et al. 2003), although the Aquarius porphyry was emplaced at 2705 Ma (Corfu et al. 1989), and the Pamour porphyry was emplaced at 2677.5 Ma.
- Although not genetically related, gold mineralization is associated spatially with porphyry intrusions that have undergone sericite alteration (sodium loss and potassium metasomatism) as well as clusters of intrusions.
- Copper mineralization is not genetically linked to porphyry magmatism, but is, however, associated spatially with large porphyry bodies that have undergone hematite alteration.
- Petrology, geochemistry and geochronology suggest that most of porphyry intrusions are related genetically to the Krist Formation. This is to say that the porphyry intrusions represent the subvolcanic equivalent of the Krist Formation.

REFERENCES

Arth, J.G. 1979. Some trace elements in trondhjemites—their implications to magma genesis and paleotectonic setting; *in* Trondhjemites, dacites and related rocks: Elsevier Scientific Publishing Co., New York, p.123-132.

Ayer, J., Amelin., Y., Corfu, F., Kamo, S., Ketchum, J.F., Kwok, K. and Trowell, H.F. 2002. Evolution of the Abitibi greenstone belt based on U-Pb geochronology: autochthonous volcanic construction followed by plutonism, regional deformation and sedimentation; Precambrian Research, v.115, p.63-95.

Ayer, J., Barr, E., Bleeker, W., Creaser, R., Hall, G., Ketchum, J., Powers, D., Salier, B., Still, A. and Trowell, N. 2003. Discover Abitibi. New geochronological results from the Timmins area: implications for the timing of late-tectonic stratigraphy, magmatism and gold mineralization; *in* Summary of Field Work and Other Activities 2003, Ontario Geological Survey, Open File Report 6120, p.33-1 to 33-11.

Ayer, J.A., Berger, B.R. and Trowell, N.F. 1999. Geological compilation of the Lake Abitibi area, Abitibi greenstone belt; Ontario Geological Survey, Preliminary Map P.3398, scale 1:100 000.

Ayer, J., Ketchum, J. and Trowell, N. 2002. New geochronological and Nd isotopic results from the Abitibi greenstone belt, with emphasis on timing and tectonic implications of Late Archean sedimentation and volcanism; *in* Summary of Field Work and Other Activities 2002, Ontario Geological Survey, Open File Report 6100, p.5-1 to 5-16.

Bateman, R., Ayer, J.A., Barr, E., Dubé, B. and Hamilton, M.A. 2004. Discover Abitibi. Gold Subproject 1. Protracted structural evolution of the Timmins–Porcupine gold camp and the Porcupine–Destor deformation zone; *in* Summary of Field Work and Other Activities 2004, Ontario Geological Survey, Open File Report 6145, p.41-1 to 41-10.

Brisbin, D.I. 1997. Geological setting of gold deposits in the Porcupine mining district, Timmins, Ontario; unpublished PhD thesis, Queen's University, Kingston, Ontario, 523p.

——— 2000. World class intrusion-related Archean vein gold deposits of the Porcupine gold camp, Timmins, Ontario; *in* Geology and Ore Deposits 2000: the Great Basin and beyond; Geological Society of Nevada, Symposium Proceedings, May 15-18, 2000, p.19-35.

Burrows, A.G. 1924. The Porcupine gold area, Cochrane District, Ontario; Ontario Department of Mines, Map 33a, scale 1:24 000.

——— 1925. The Porcupine gold area, Cochrane District, Ontario; Ontario Department of Mines, Annual Report, 1924, v.33, pt.2, 84p.

Burrows, D.R. and Spooner, E.T.C. 1986. The McIntyre Cu-Au deposit, Timmins, Ontario, Canada; *in* Proceedings of Gold '86: An international symposium on the geology of gold, Konsult International, Willowdale, Ontario, p.23-39.

Burrows, D.R., Spooner, E.T.C., Wood, P.C. and Jemielita, R.A. 1993. Structural controls on formation of the Hollinger–McIntyre Au-quartz vein system in the Hollinger shear zone, Timmins, southern Abitibi greenstone belt, Ontario; Economic Geology, v.88, p.1643-1663.

Corfu, F., Krogh, T.E., Kwok, Y.Y. and Jensen, L.S. 1989. U-Pb zircon geochronology in the southwestern Abitibi greenstone belt, Superior Province; Canadian Journal of Earth Sciences, v.26, p.1747-1763.

Date, J., Watanabe., Y. and Saeki, Y. 1983. Zonal alteration around the Fukazawa Kuroko deposits, Akita Prefecture, northern Japan; *in* Kuroko and related volcanogenic massive sulphide deposits, Economic Geology, Monograph 5, p.365-386.

Davies, J.F. 1977. Structural interpretation of the Timmins mining area; Canadian Journal of Earth Science, v.14, p.1046-1053.

Davies, J.F. and Luhta, L.E. 1978a. An Archean "porphyry-type" disseminated copper deposit, Timmins, Ontario; Economic Geology, v.73, p.383-396.

——— 1978b. An Archean "porphyry-type" disseminated copper deposit, Timmins, Ontario––A reply; Economic Geology, v.74, p.687.

Defant, M.J. and Drummond, M.S. 1993. Mount St. Helens: potential example of the partial melting of the subducted lithosphere in a volcanic arc; Geology, v.21, p.547-550.

Dinel, E. and Fowler, A.D. 2004. Discover Abitibi. Preliminary results of the geology and geochemistry of the volcanic rocks hosting the Hoyle Pond mine, Timmins, Ontario; *in* Summary of Field Work and Other Activities 2004, Ontario Geological Survey, Open File Report 6145, p.46-1 to 46-4.

Ferguson, S.A. 1966. Tisdale Township, District of Cochrane, Ontario Geological Survey, Map 2075, scale 1:12 000.

Gorman, B.E., Kerrich, R. and Fyfe, W.S. 1981. Geochemistry and field relations of lode gold deposits in felsic igneous intrusions—porphyries of the Timmins District; *in* Geoscience Research Grant Program: Summary of Research, 1980–1981 Ontario Geological Survey, Miscellaneous Paper 98, p.108-124.

Gray, M.D. and Hutchinson, R.W. 2001. New evidence for multiple periods of gold emplacement in the Porcupine mining district, Timmins area, Ontario, Canada; Economic Geology, v.96, p.453-475.

Griffis, A.T. 1962. A geological study of the McIntyre Mine; Canadian Institute of Mining and Metallurgy, Bulletin, v.55, no.598, p.76-83.

——— 1978. An Archean "porphyry-type" disseminated copper deposit, Timmins, Ontario—A discussion; Economic Geology, v.74, p.695-696.

Hall, L.A.F., Houlé, M.G. and Tremblay, E. 2004. Precambrian geology of Shaw Township; Ontario Geological Survey, Preliminary Map P.3541, scale 1:20 000.

Hall, L.A.F., MacDonald, C.A. and Dinel, E.R. 2003. Precambrian geology of Deloro Township; Ontario Geological Survey, Preliminary Map P.3528, scale 1:20 000.

Holmes, T.C. 1944. Some porphyry-sediment contacts at the Dome Mine, Ontario; Economic Geology, v.39, p.133-141.

Hughes, C.J. 1973. Spilites, keratophyres and igneous spectrum; Geological Magazine, v.109, no.6, p.513-527.

Hurst, M.E. 1936. Recent studies in the Porcupine area; Canadian Institute of Mining and Metallurgy, Transactions, v.45, p.379-386.

Irvine, T.N. and Baragar, W.R.A. 1971. A guide to the chemical classification of the common volcanic rocks; Canadian Journal of Earth Sciences, v.8, p.523-548.

Large, R.R., Gemmell, J.B., Paulick, H. and Huston, D.L. 2001. The alteration box plot: a simple approach to understanding the relationship between alteration mineralogy and lithogeochemistry associated with volcanic-hosted massive sulfide deposits; Economic Geology, v.96, p.957-971.

MacDonald, P.J. and Piercey, S.J. 2003. Discover Abitibi. Gold Subproject 3. Preliminary regional geological assessment of porphyry intrusions spatially associated with gold deposits in the western Abitibi Subprovince, Timmins, Ontario; *in* Summary of Field Work and Other Activities 2003, Ontario Geological Survey, Open File Report 6120, p.36-1 to 36-7.

MacDonald, P.J., Piercey, S.J. and Hamilton, M.A. 2004. Discover Abitibi. Gold Subproject 3. Regional geological assessment of porphyry intrusions spatially associated with gold deposits along the Porcupine–Destor deformation zone, western Abitibi Subprovince, Timmins, Ontario; *in* Summary of Field Work and Other Activities 2004, Ontario Geological Survey, Open File Report 6145, p.43-1 to 43-7.

Marmont, S. and Corfu, F. 1989. Timing of gold introduction in the Late Archean tectonic framework of the Canadian Shield: evidence from U-Pb zircon geochronology of the Abitibi Subprovince; *in* The geology of gold deposits: the perspective in 1988, Economic Geology, Monograph 6, p.101-111.

Mason, R. and Melnik, N. 1986. The anatomy of an Archean gold system—The McIntyre–Hollinger complex at Timmins, Ontario, Canada; *in* Proceedings of Gold '86: An international symposium on the geology of gold, Konsult International, Toronto, p.40-55.

Melnik-Proud, N. 1992. The geology and ore controls in and around the McIntyre Mine at Timmins, Ontario, Canada; unpublished PhD thesis, Queen's University, Kingston, Ontario, 353p.

O'Connor, J.T. 1965. A classification of quartz-rich igneous rocks based on feldspar ratio; *in* Geological Survey Research 1965, United States Geological Survey, Professional Paper 525B, p.79-84.

Piroshco, D.W. and Kettles, K. 1991. Structural geology of Tisdale and Whitney townships, Abitibi greenstone belt, District of Cochrane, northeastern Ontario; Ontario Geological Survey, Open File Report 5768, 115p.

Pyke, D.R. 1982. Geology of the Timmins area, District of Cochrane; Ontario Geological Survey, Report 219, 141p.

Saeki, Y. and Date, J. 1980. Computer application to the alteration data of the footwall dacite lava at the Ezuri Kuroko deposits, Akito Prefecture; Mining Geology, v.30, p.241-250.

Sun, S-s. and McDonough, W.F. 1989. Chemical and isotopic systematics of oceanic basalts: implications for mantle composition and processes; *in* Magmatism in the ocean basins, Geological Society, Special Publication No.42, p.313-345.

Thompson, P.H. 2003. Discover Abitibi. Metamorphic Subproject. Metamorphism and its relationship to gold deposits in the Timmins–Kirkland Lake area, western Abitibi greenstone belt, Ontario: Report 1; *in* Summary of Field Work and Other Activities 2003, Ontario Geological Survey, Open File Report 6120, p.37-1 to 37-8.

Vaillancourt, C., Pickett, C.L. and Dinel, E. 2001. Precambrian geology, Timmins west—Bristol and Ogden townships; Ontario Geological Survey, Preliminary Map P.3436, scale 1:20 000.

Wells, R.C. 2001. Petrographic, lithogeochemical and interpretative report on a porphyry sample suite, Dome Mine area; internal, unpublished report for Placer Dome Limited, 32p.

Winchester, J.A. and Floyd, P.A. 1977. Geochemical discrimination of different magma series and their differentiation products using immobile elements; Chemical Geology, v.20, p.325-343.

Wood, P.C., Burrows, D.R., Thomas, A.V. and Spooner, E.T.C. 1986. The Hollinger–McIntyre Au-quartz vein system, Timmins, Ontario, Canada: geologic characteristics, fluid properties and light stable isotope geochemistry; *in* Proceedings of Gold '86: An international symposium on the geology of gold, Konsult International, Toronto, p.56-80.

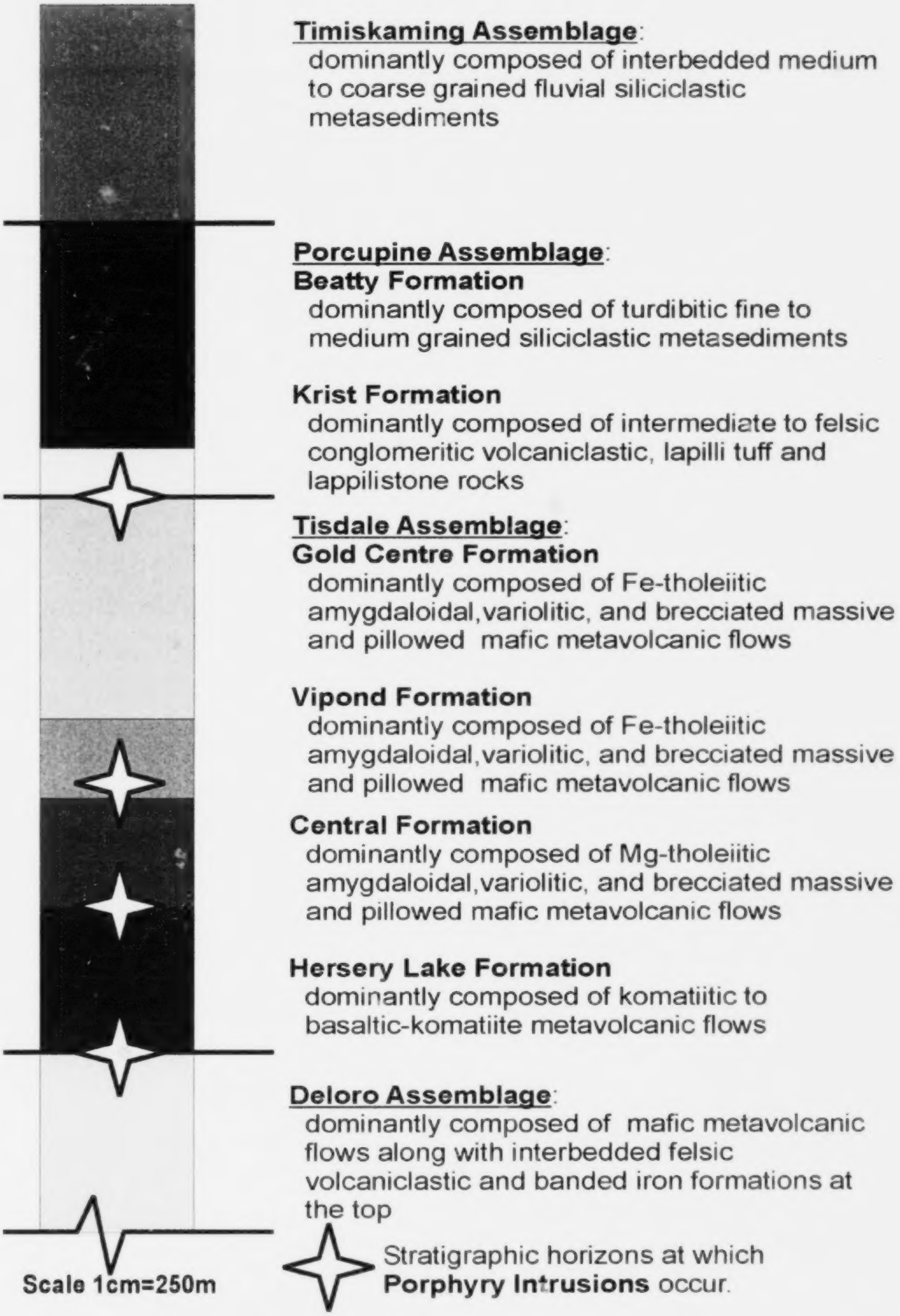
Timiskaming Assemblage:
dominantly composed of interbedded medium to coarse grained fluvial siliciclastic metasediments
Porcupine Assemblage:
Beatty Formation
dominantly composed of turdibitic fine to medium grained siliciclastic metasediments
Krist Formation
dominantly composed of intermediate to felsic conglomeritic volcaniclastic, lapilli tuff and lappilistone rocks
Tisdale Assemblage:
Gold Centre Formation
dominantly composed of Fe-tholeiitic amygdaloidal,variolitic, and brecciated massive and pillowed mafic metavolcanic flows
Vipond Formation
dominantly composed of Fe-tholeiitic amygdaloidal,variolitic, and brecciated massive and pillowed mafic metavolcanic flows
Central Formation
dominantly composed of Mg-tholeiitic amygdaloidal,variolitic, and brecciated massive and pillowed mafic metavolcanic flows
Hersery Lake Formation
dominantly composed of komatiitic to basaltic-komatiite metavolcanic flows
Deloro Assemblage:
dominantly composed of mafic metavolcanic flows along with interbedded felsic volcaniclastic and banded iron formations at the top
Scale 1cm=250m
Stratigraphic horizons at which Porphyry Intrusions occur.

Figure 2.1. Stratigraphic column of the Timmins area of the southern Abitibi greenstone belt including the Deloro, Tisdale, Porcupine and Timiskaming assemblages; stars indicate horizons of porphyry intrusions (*modified from* Ayer et al. 2002).

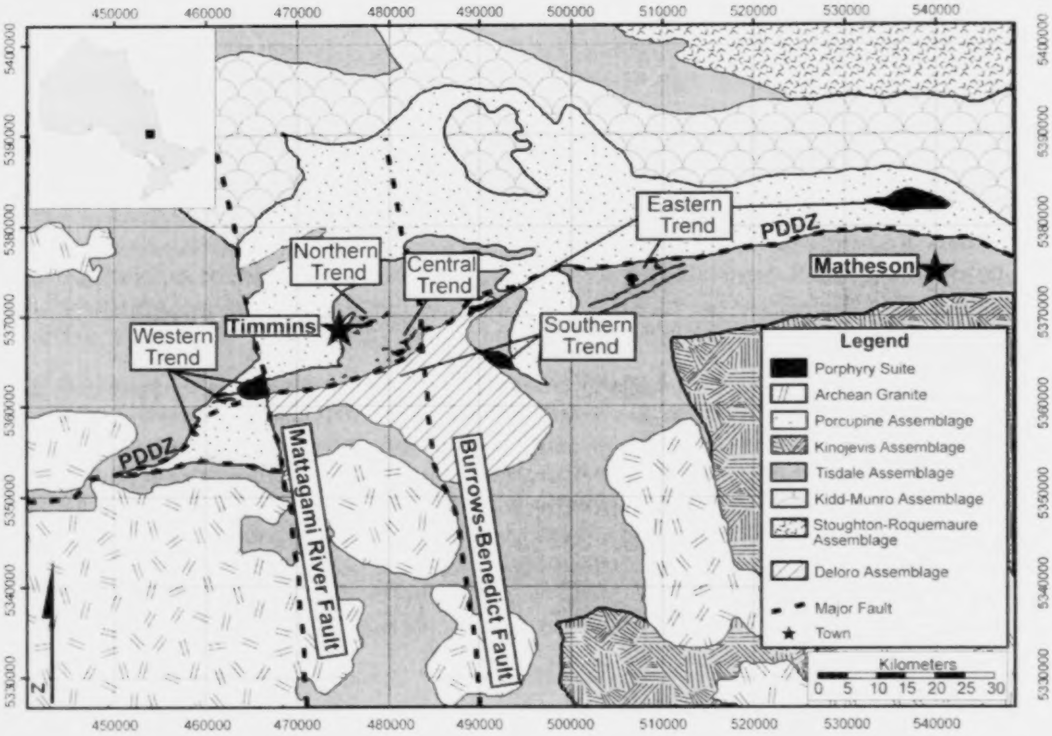
450000
460000
470000
480000
490000
500000
510000
520000
530000
540000
5400000
5390000
5380000
5370000
5360000
5350000
5340000
5330000
Eastern Trend
PDDZ
Matheson
Northern Trend
Central Trend
Timmins
Western Trend
Southern Trend
PDDZ
Mattagami River Fault
Burrows-Benedict Fault
Legend
Porphyry Suite
Archean Granite
Porcupine Assemblage
Kinojevis Assemblage
Tisdale Assemblage
Kidd-Munro Assemblage
Stoughton-Roquemaure Assemblage
Deloro Assemblage
Major Fault
Town
Kilometers
0 5 10 15 20 25 30
N

Figure 2.2. Simplified regional geology map of the Timmins portion of the southern Abitibi greenstone belt with the locations of the 5 geographical porphyry trends shown (*modified from* Ayer, Berger and Trowell 1999). Universal Transverse Mercator (UTM) co-ordinates are North American Datum 1927 (NAD27), Zone 17.

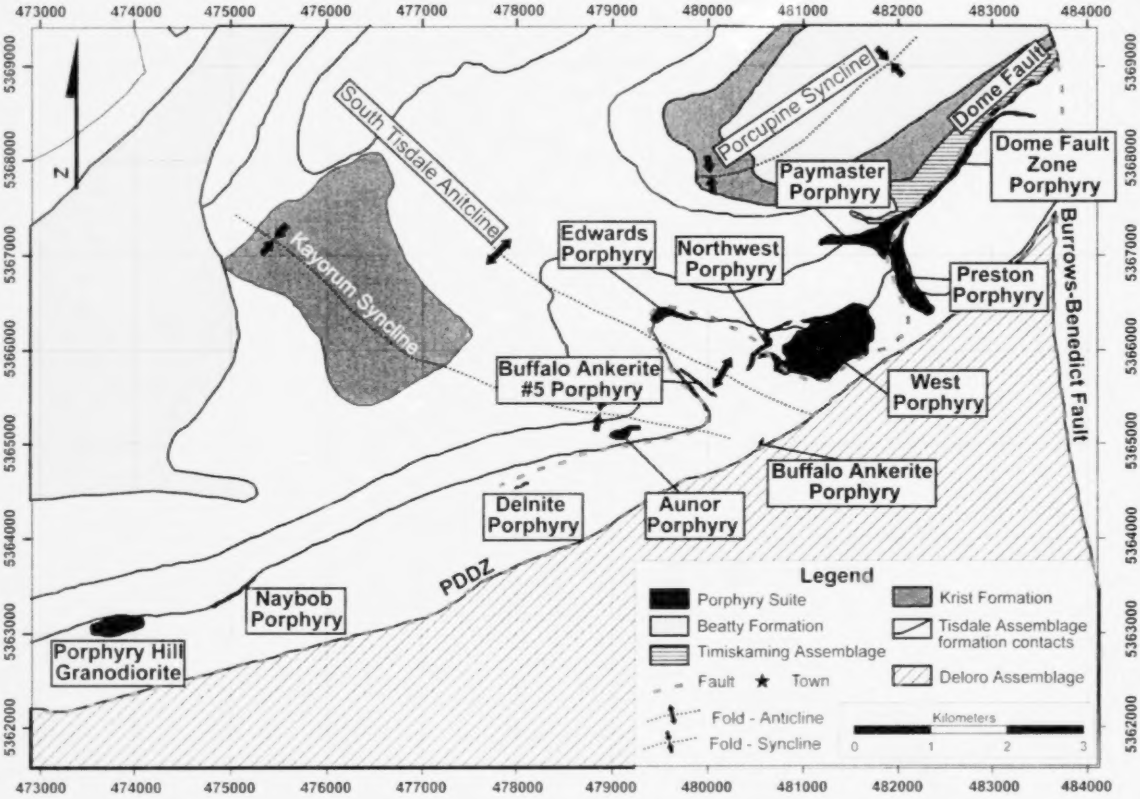
473000
474000
475000
476000
477000
478000
479000
480000
481000
482000
483000
484000
5369000
5368000
5367000
5366000
5365000
5364000
5363000
5362000
N
South Tisdale Anitcline
Kayorum Syncline
Porcupine Syncline
Dome Fault
Dome Fault Zone Porphyry
Paymaster Porphyry
Edwards Porphyry
Northwest Porphyry
Preston Porphyry
Burrows-Benedict Fault
Buffalo Ankerite #5 Porphyry
West Porphyry
Buffalo Ankerite Porphyry
Delnite Porphyry
Aunor Porphyry
PDDZ
Naybob Porphyry
Porphyry Hill Granodiorite
Legend
Porphyry Suite
Beatty Formation
Timiskaming Assemblage
Fault
Town
Fold - Anticline
Fold - Syncline
Krist Formation
Tisdale Assemblage formation contacts
Deloro Assemblage
Kilometers
0
1
2
3

Figure 2.3. Simplified surface geology map of the central trend showing the names and locations of the porphyry intrusions (*modified from* Ferguson 1966; Brisbin 1997; Vaillancourt, Pickett and Dinel 2001). UTM co-ordinates in NAD27, Zone 17.

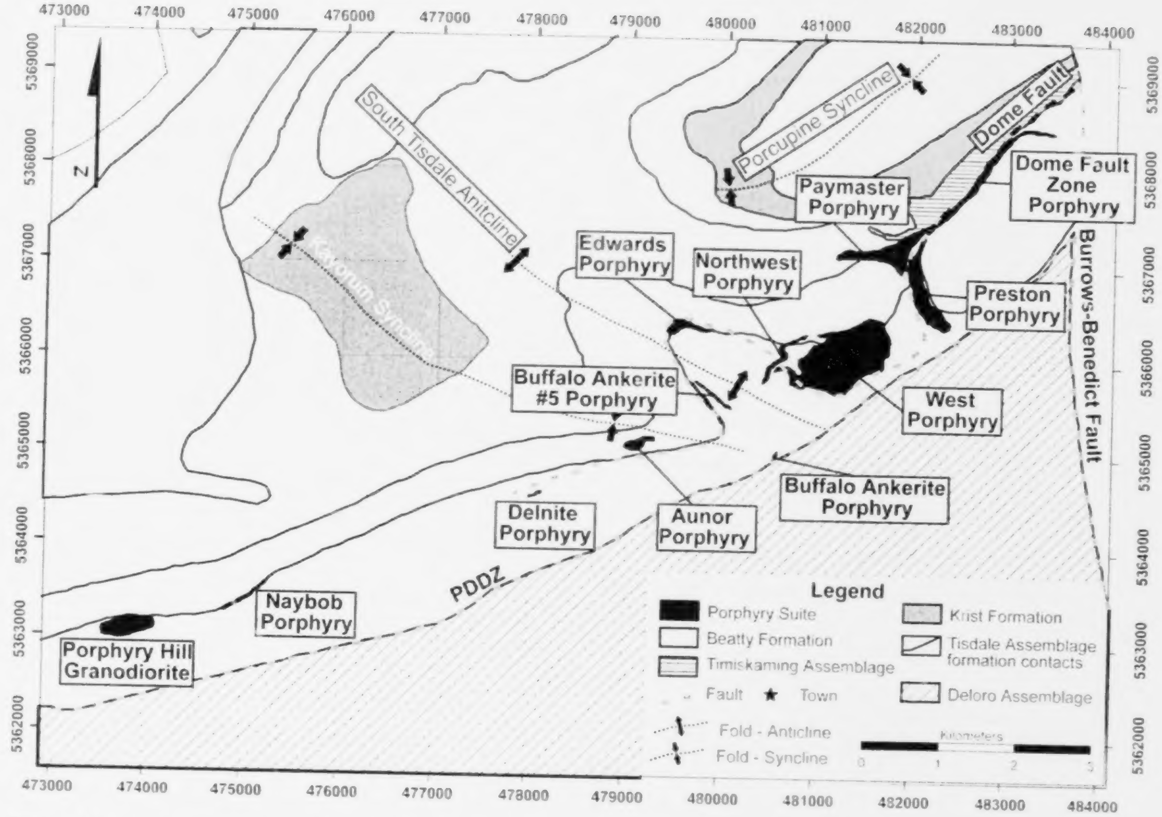
473000
474000
475000
476000
477000
478000
479000
480000
481000
482000
483000
484000
5369000
5368000
5367000
5366000
5365000
5364000
5363000
5362000
N
South Tisdale Anitcline
Porcupine Syncline
Dome Fault
Karorum Syncline
Dome Fault Zone Porphyry
Paymaster Porphyry
Edwards Porphyry
Northwest Porphyry
Preston Porphyry
Burrows-Benedict Fault
Buffalo Ankerite #5 Porphyry
West Porphyry
Buffalo Ankerite Porphyry
Delnite Porphyry
Aunor Porphyry
PDDZ
Naybob Porphyry
Porphyry Hill Granodiorite
Legend
Porphyry Suite
Beatty Formation
Timiskaming Assemblage
Fault
Town
Fold - Anticline
Fold - Syncline
Krist Formation
Tisdale Assemblage formation contacts
Deloro Assemblage
Kilometers
0
1
2
3

Figure 2.3. Simplified surface geology map of the central trend showing the names and locations of the porphyry intrusions (*modified from* Ferguson 1966; Brisbin 1997; Vaillancourt, Pickett and Dinel 2001). UTM co-ordinates in NAD27, Zone 17.

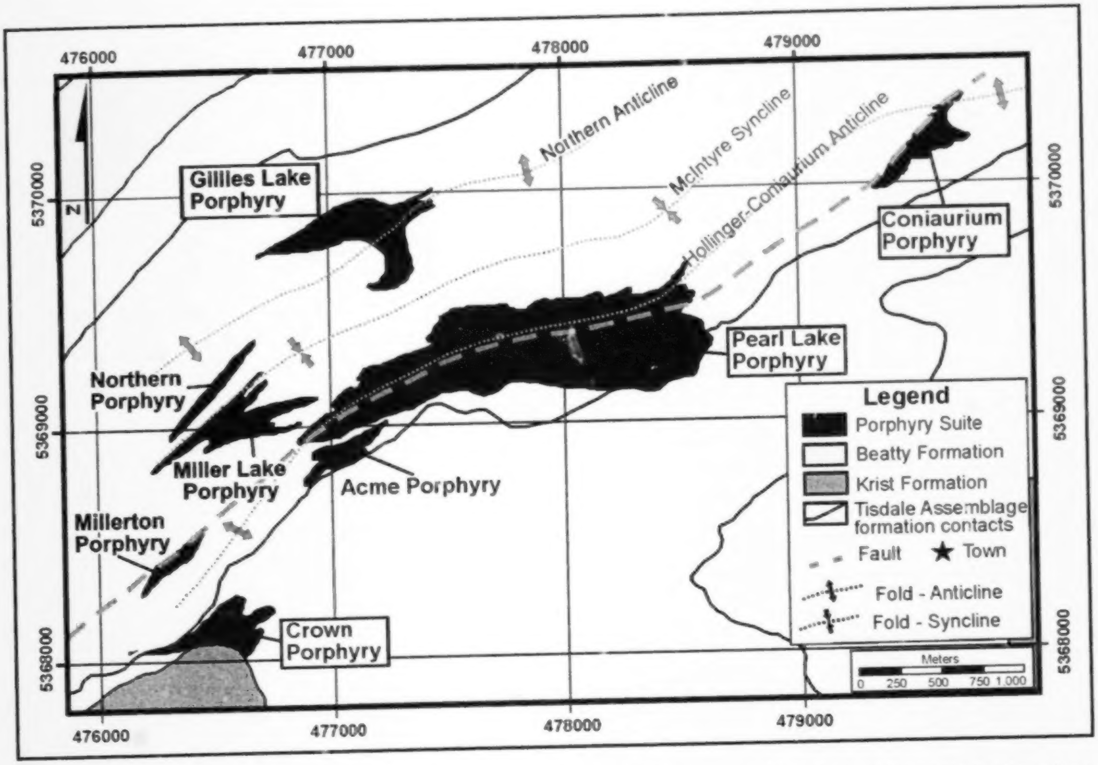
476000
477000
478000
479000
5370000
5369000
5368000
N
Northern Anticline
McIntyre Syncline
Hollinger-Coniaurium Anticline
Gillies Lake Porphyry
Coniaurium Porphyry
Pearl Lake Porphyry
Northern Porphyry
Miller Lake Porphyry
Acme Porphyry
Millerton Porphyry
Crown Porphyry
Legend
Porphyry Suite
Beatty Formation
Krist Formation
Tisdale Assemblage formation contacts
Fault
Town
Fold - Anticline
Fold - Syncline
Meters
0 250 500 750 1,000

Figure 2.4. Simplified surface geology map of the northern trend showing the names and locations of the porphyry intrusions (*modified from* Ferguson 1966; Brisbin 1997). Names of porphyry intrusions in boxes highlight those discussed within the report UTM co-ordinates in NAD27, Zone 17.

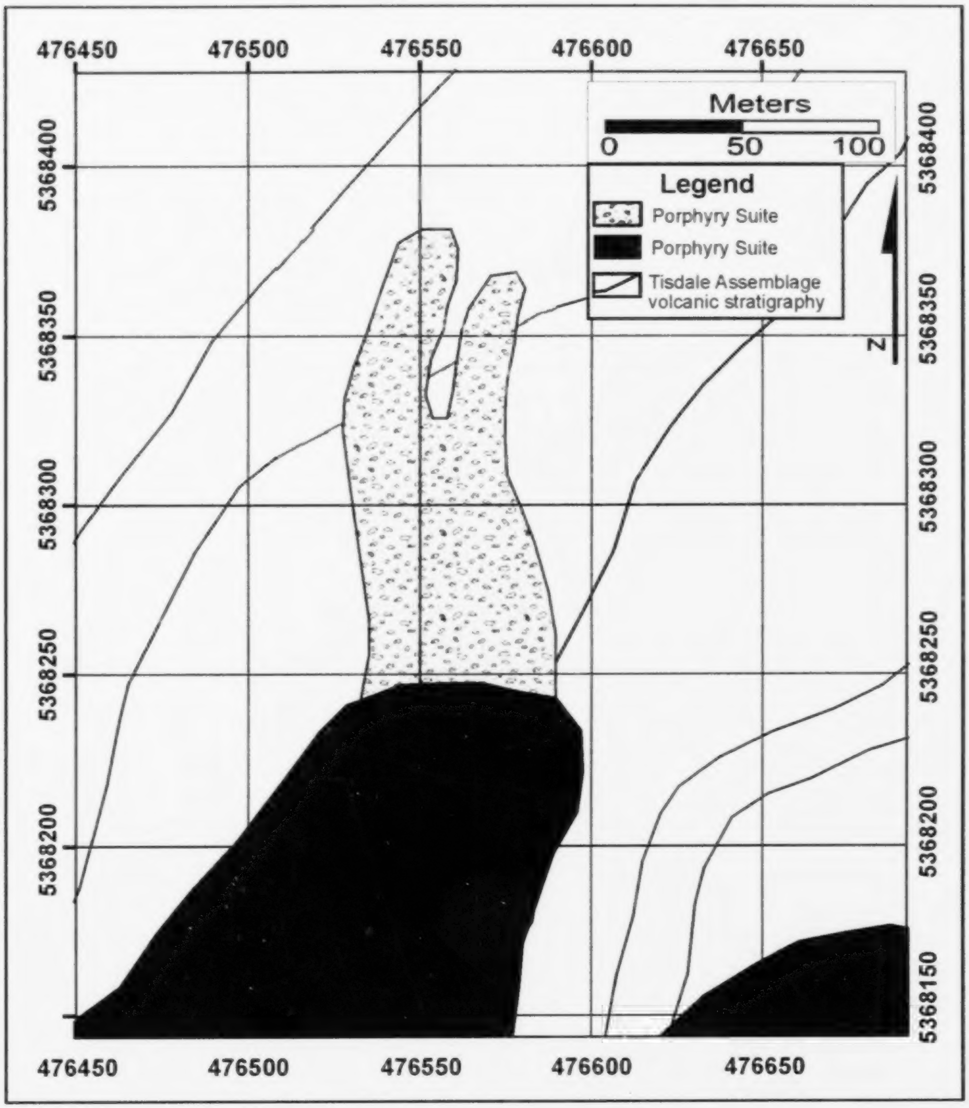
476450
476500
476550
476600
476650
5368400
5368350
5368300
5368250
5368200
5368150
Meters
0
50
100
Legend
Porphyry Suite
Porphyry Suite
Tisdale Assemblage volcanic stratigraphy
N

Figure 2.5. Surface geology map of the Crown porphyry breccia, Shania Twain Centre showing northward extension (*modified from* Ferguson 1966; Brisbin 1997). UTM co-ordinates in NAD27, Zone 17.

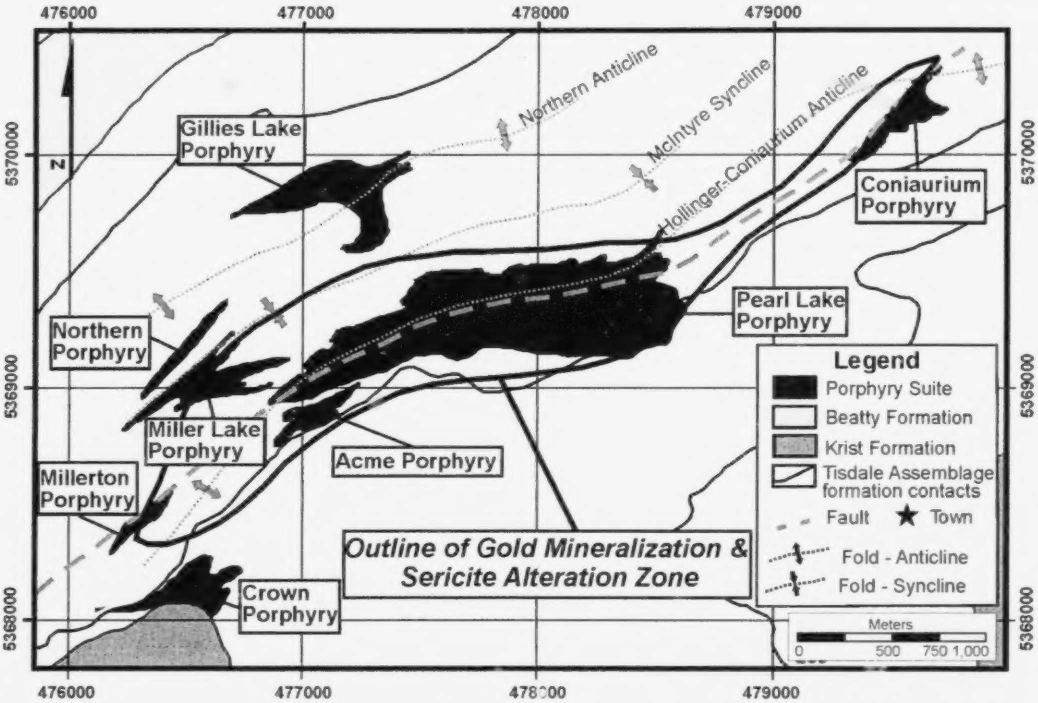
476000
477000
478000
479000
5370000
5369000
5368000
N
Gillies Lake Porphyry
Northern Anticline
McIntyre Syncline
Hollinger-Coniaurium Anticline
Coniaurium Porphyry
Pearl Lake Porphyry
Northern Porphyry
Miller Lake Porphyry
Millerton Porphyry
Acme Porphyry
Crown Porphyry
Outline of Gold Mineralization & Sericite Alteration Zone
Legend
Porphyry Suite
Beatty Formation
Krist Formation
Tisdale Assemblage formation contacts
Fault
Town
Fold - Anticline
Fold - Syncline
Meters
0
500
750 1,000

Figure 2.6. Map showing location relationship of Hollinger–McIntyre gold mineralization and sericite–calcium carbonate alteration to the northern trend porphyries (*modified from* Mason and Melnik 1986). UTM co-ordinates in NAD27, Zone 17.

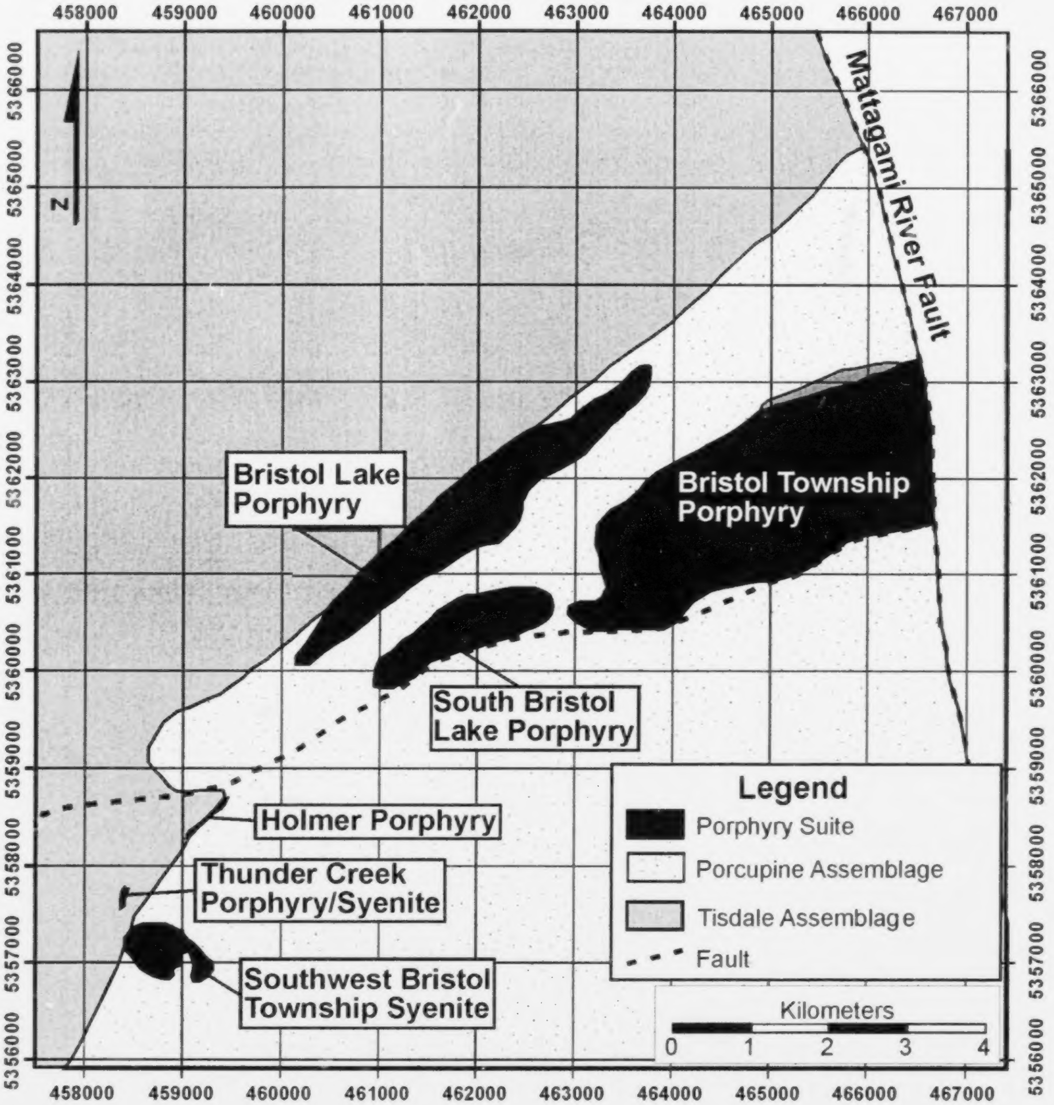
458000
459000
460000
461000
462000
463000
464000
465000
466000
467000
5356000
5357000
5358000
5359000
5360000
5361000
5362000
5363000
5364000
5365000
5366000
N
Mattagami River Fault
Bristol Lake Porphyry
Bristol Township Porphyry
South Bristol Lake Porphyry
Holmer Porphyry
Thunder Creek Porphyry/Syenite
Southwest Bristol Township Syenite
Legend
Porphyry Suite
Porcupine Assemblage
Tisdale Assemblage
Fault
Kilometers
0
1
2
3
4

Figure 2.7. Simplified surface geology map of the western trend showing the names and locations of the porphyry intrusions (*modified from* Ayer, Berger and Trowell 1999; Vaillancourt, Pickett and Dinel 2001). UTM co-ordinates in NAD27, Zone 17.

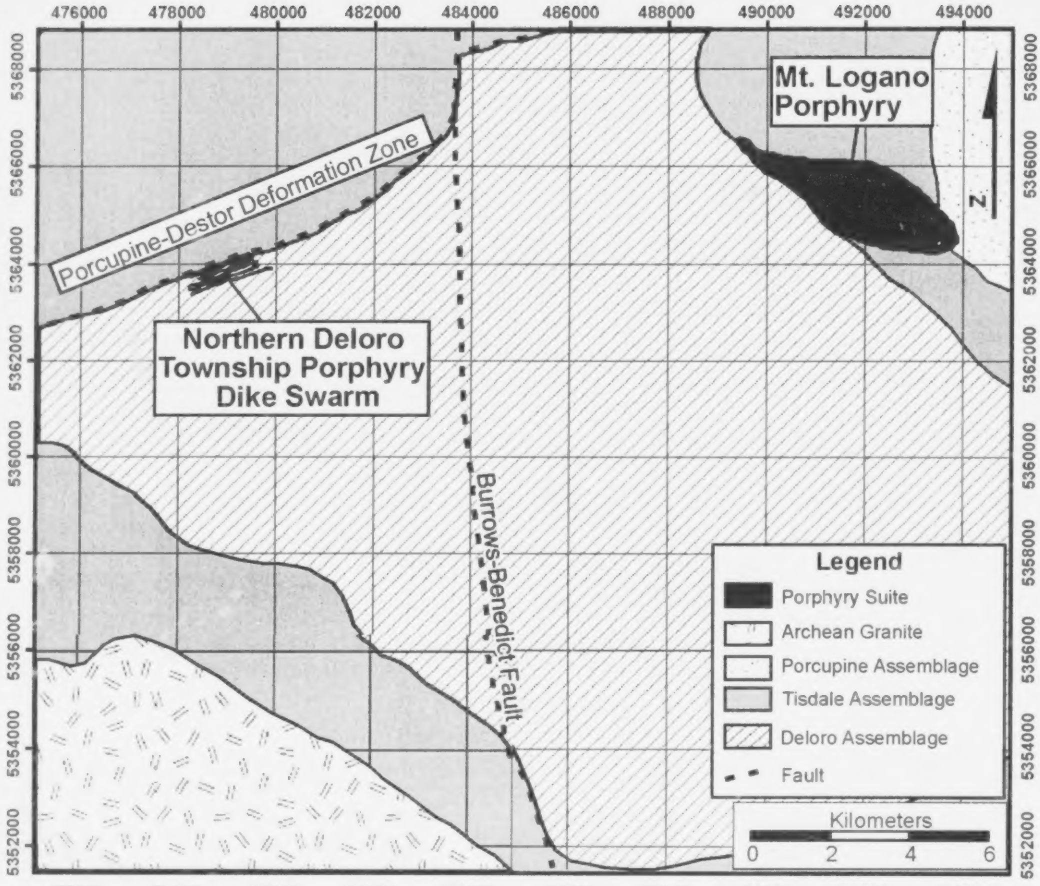
476000
478000
480000
482000
484000
486000
488000
490000
492000
494000
5368000
5366000
5364000
5362000
5360000
5358000
5356000
5354000
5352000
Mt. Logano Porphyry
Porcupine-Destor Deformation Zone
Northern Deloro Township Porphyry Dike Swarm
Burrows-Benedict Fault
N
Legend
Porphyry Suite
Archean Granite
Porcupine Assemblage
Tisdale Assemblage
Deloro Assemblage
Fault
Kilometers
0
2
4
6

Figure 2.8. Simplified surface geology map of the southern trend showing the names and locations of the porphyry intrusions (*modified from* Ayer, Berger and Trowell 1999; Hall, MacDonald and Dinel 2003; Hall, Houlé and Tremblay 2004). UTM coordinates in NAD27, Zone 17.

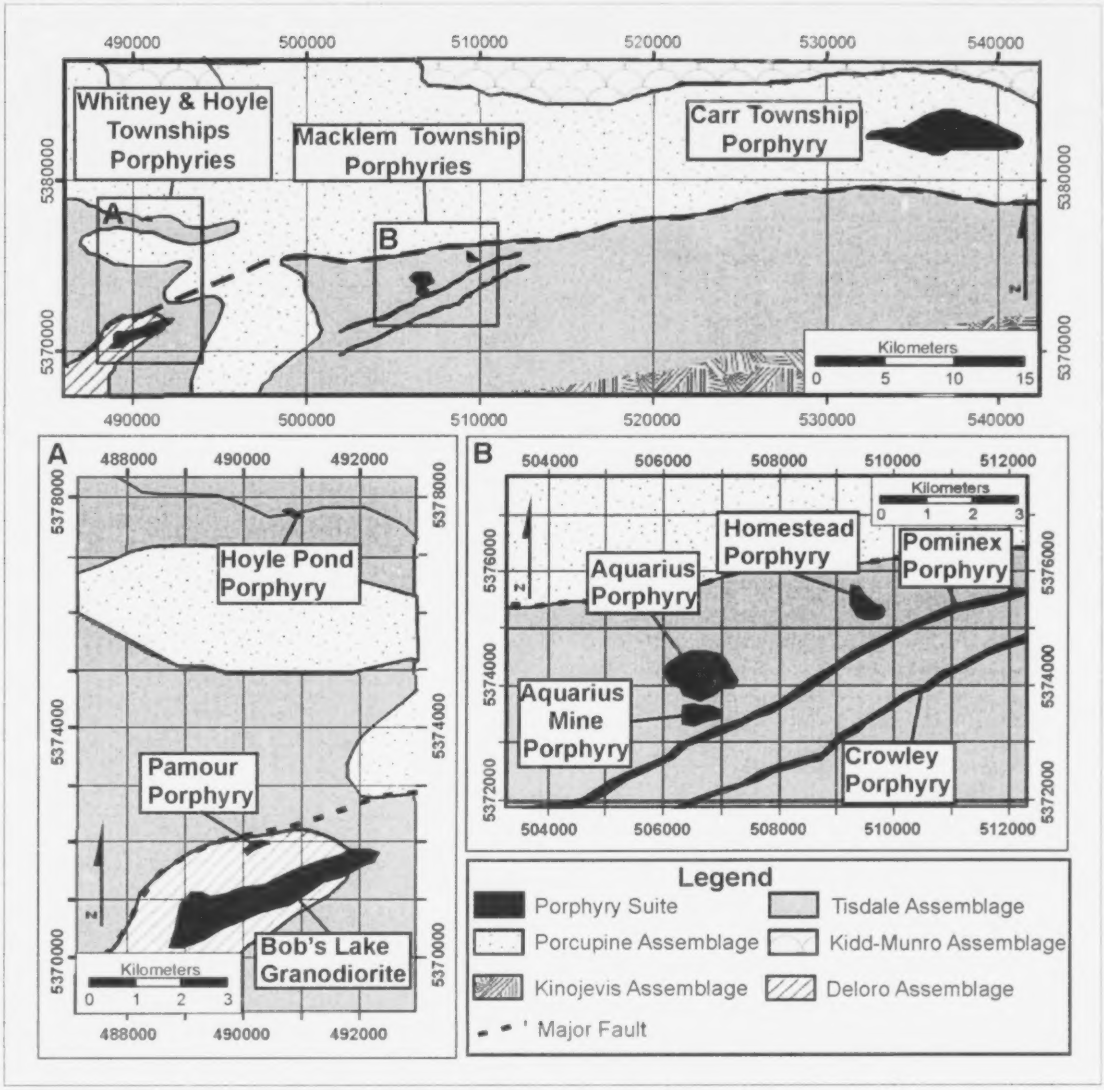
490000
500000
510000
520000
530000
540000
5380000
5370000
Whitney & Hoyle Townships Porphyries
Macklem Township Porphyries
Carr Township Porphyry
A
B
Kilometers
0
5
10
15
A
488000
490000
492000
5378000
5374000
5370000
Hoyle Pond Porphyry
Pamour Porphyry
Bob's Lake Granodiorite
Kilometers
0
1
2
3
B
504000
506000
508000
510000
512000
5376000
5374000
5372000
Kilometers
0
1
2
3
Homestead Porphyry
Pominex Porphyry
Aquarius Porphyry
Aquarius Mine Porphyry
Crowley Porphyry
Legend
Porphyry Suite
Tisdale Assemblage
Porcupine Assemblage
Kidd-Munro Assemblage
Kinojevis Assemblage
Deloro Assemblage
Major Fault
N

Figure 2.9. Simplified surface geology map of the eastern trend showing the names and locations of the porphyry intrusions (*modified from* Ayer, Berger and Trowell 1999; unpublished data courtesy of Kinross Gold Corp. (Echo Bay Mines Ltd.) 2004). UTM co-ordinates in NAD27, Zone 17.

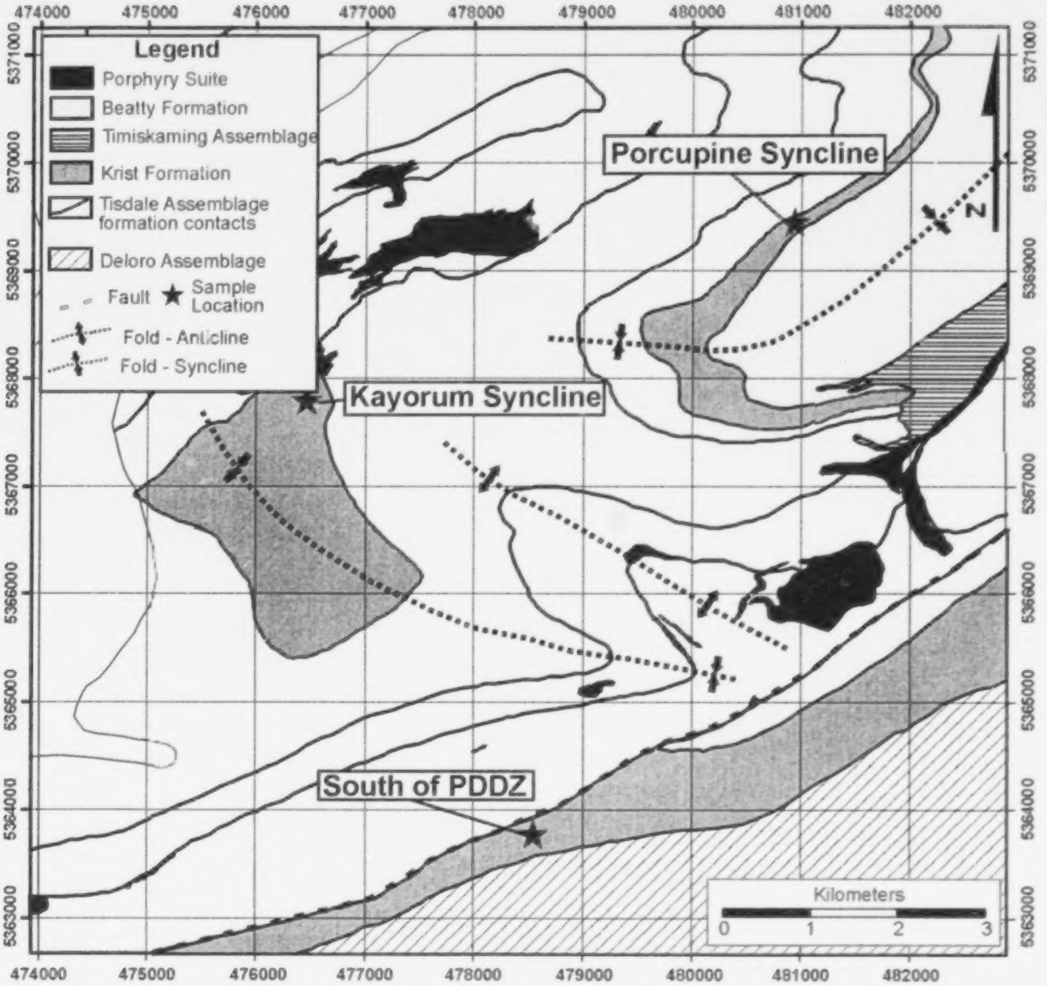
474000
475000
476000
477000
478000
479000
480000
481000
482000
5371000
5370000
5369000
5368000
5367000
5366000
5365000
5364000
5363000
Legend
Porphyry Suite
Beatty Formation
Timiskaming Assemblage
Krist Formation
Tisdale Assemblage formation contacts
Deloro Assemblage
Fault
Sample Location
Fold - Anticline
Fold - Syncline
Porcupine Syncline
Kayorum Syncline
South of PDDZ
N
Kilometers
0
1
2
3

Figure 2.10. Simplified surface geology map of the Krist Formation showing the locations of the samples collected (indicated by stars) (*modified from* Ferguson 1966; Brisbin 1997; Ayer, Berger and Trowell 1999; Hall, MacDonald and Dinel 2003). UTM co-ordinates in NAD27, Zone 17.

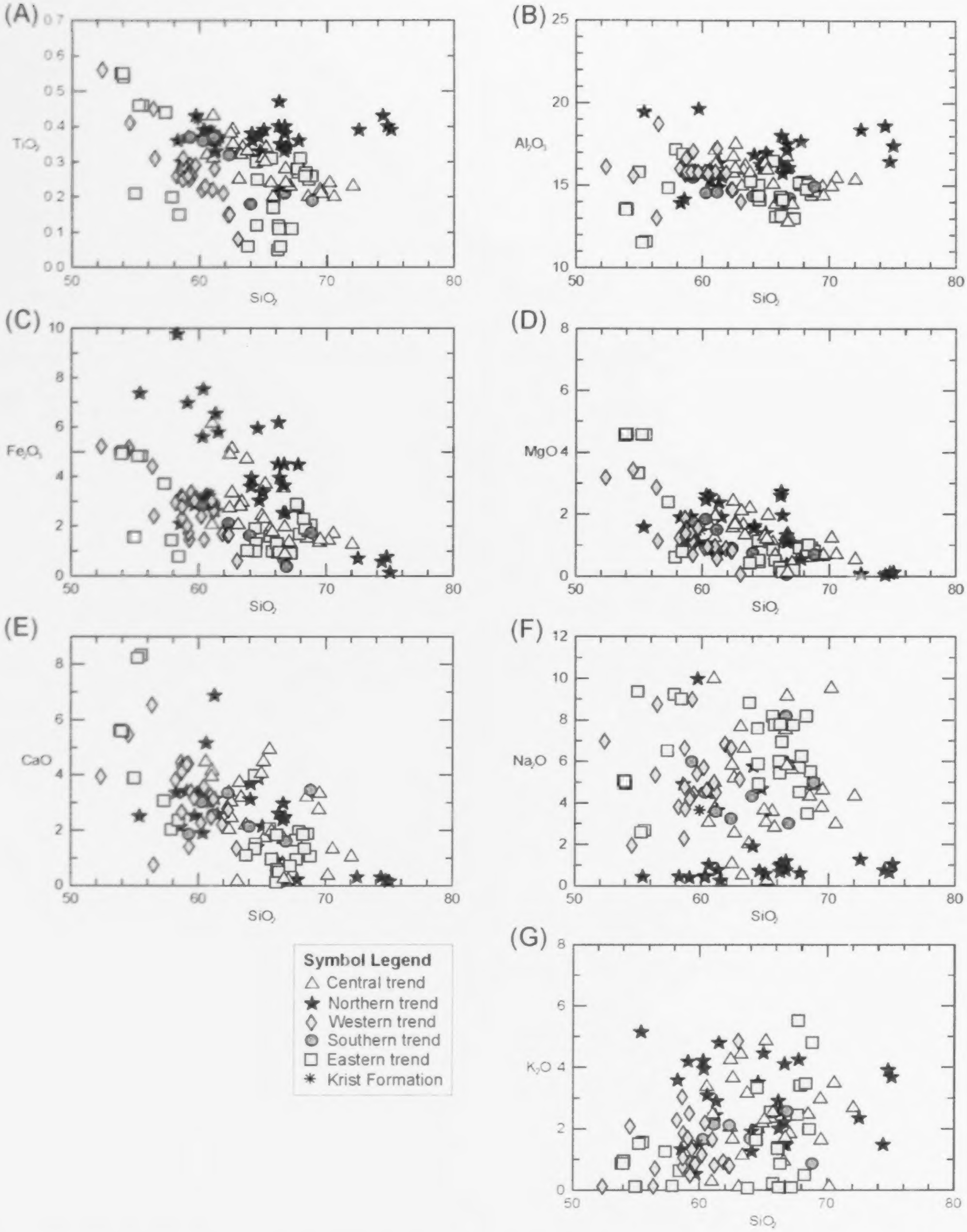

Figure 2.11. Standard Harker plots for the 5 geographical porphyry trends as well as the Krist Formation: A) TiO$_2$, B) Al$_2$O$_3$, C) Fe$_2$O$_3$T, D) MgO, E) CaO, F) Na$_2$O, and G) K$_2$O.

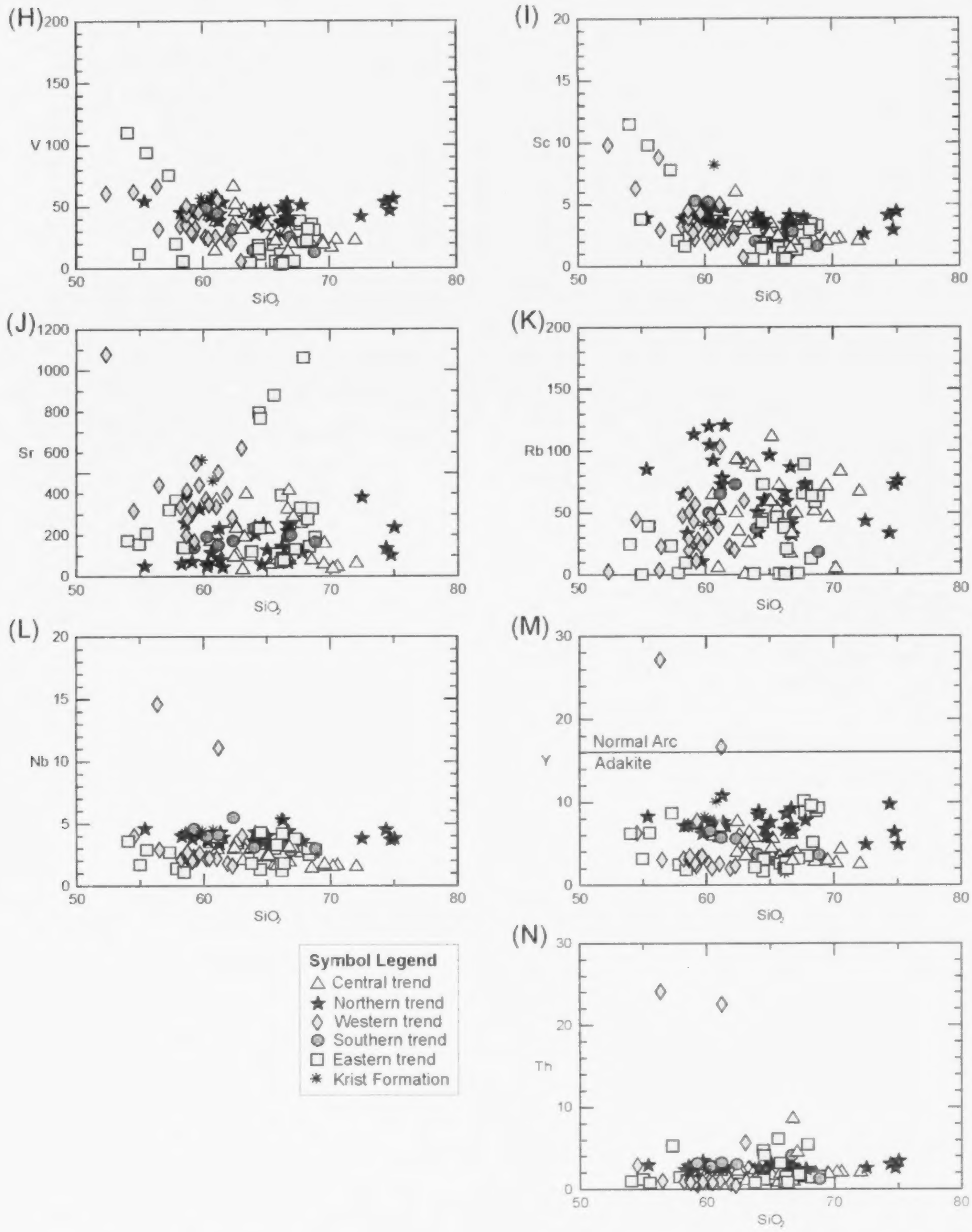

Figure 2.11, continued. Standard Harker plots for the 5 geographical porphyry trends as well as the Krist Formation: H) V, I) Sc, J) Sr, K) Rb, L) Nb, M) Y, and N) Th. The field for adakites in plot M *from* Defant and Drummond (1993).

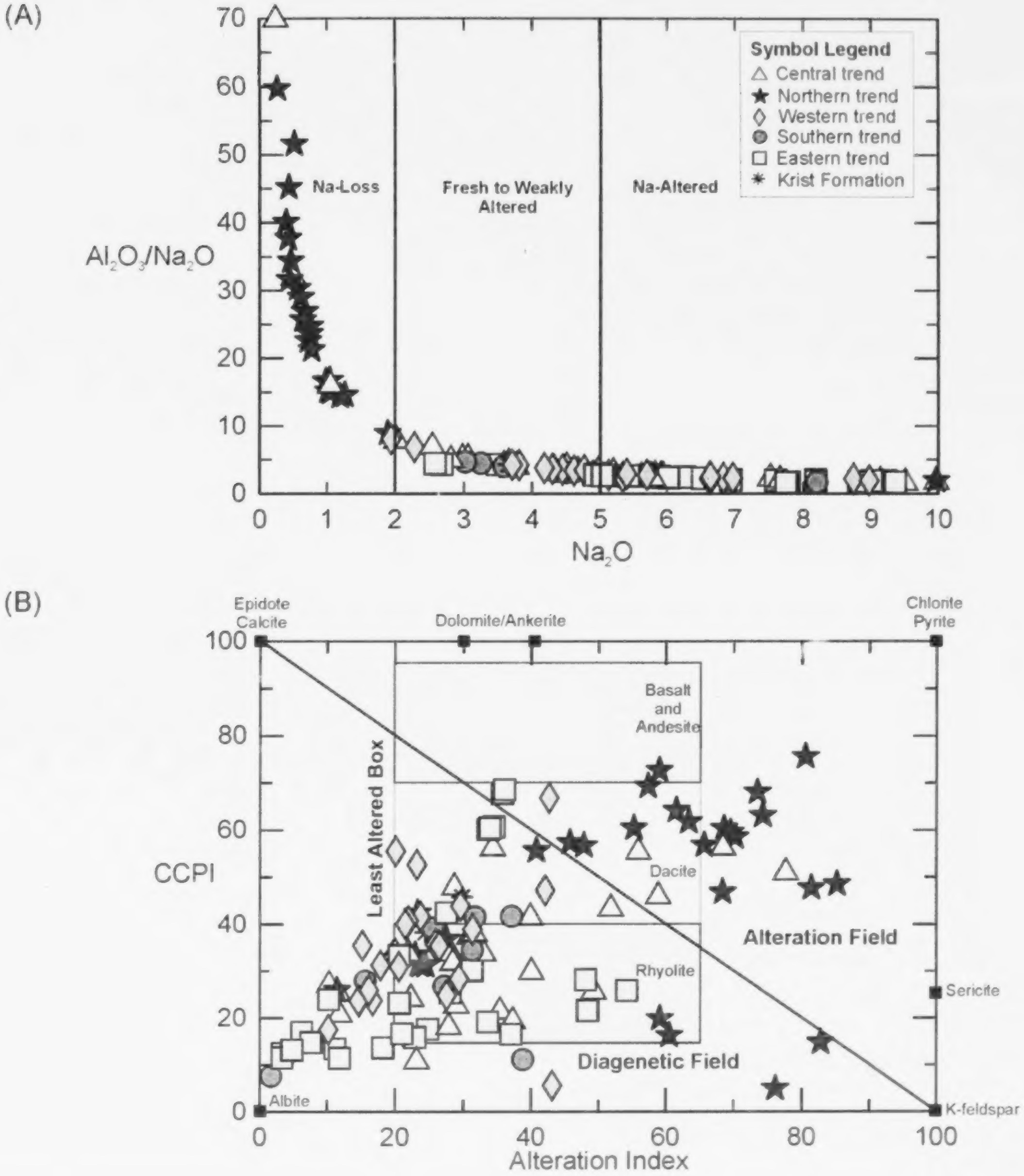

Figure 2.12. Major element alteration plots for the 5 geographical porphyry trends as well as the Krist Formation, including A) Na_2O versus Al_2O_3/Na_2O plot with designations for least-altered samples; and B) alteration box-plot (*from* Large et al. 2001) with Hashimoto alteration index ([$(MgO+K_2O)/(MgO+K_2O+Na_2O+CaO)$]; Date, Watanabe and Saeki 1983; Saeki and Date 1980) plotted against chlorite-carbonate-pyrite-index [CCPI: $(MgO+Fe_2O_3T)/(MgO+Fe_2O_3T+Na_2O+CaO)$].

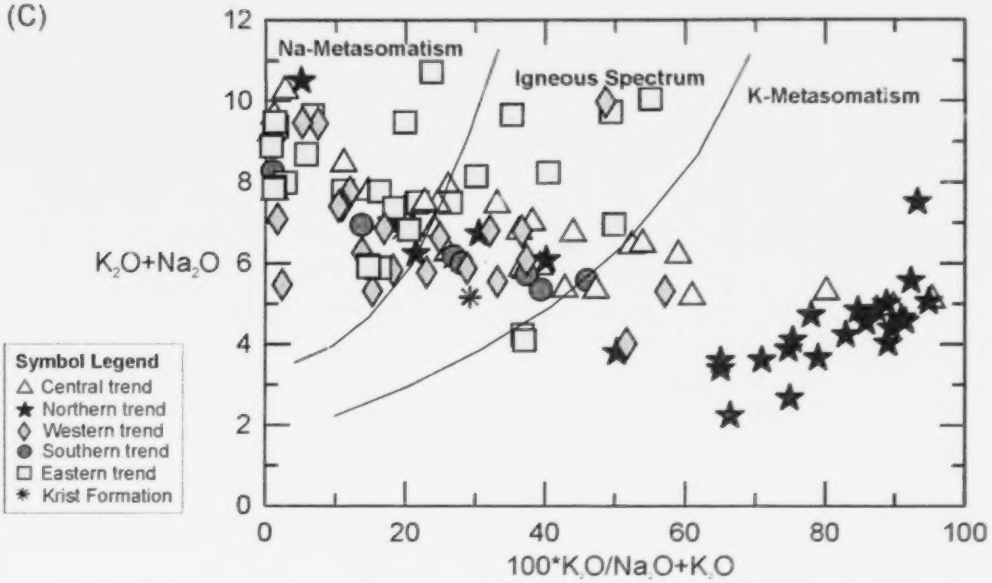

Figure 2.12, continued. Major element alteration plots for the 5 geographical porphyry trends as well as the Krist Formation: C) (100*K_2O/K_2O+Na_2O) versus (K_2O+Na_2O) Hughes plot (*from* Hughes 1973).

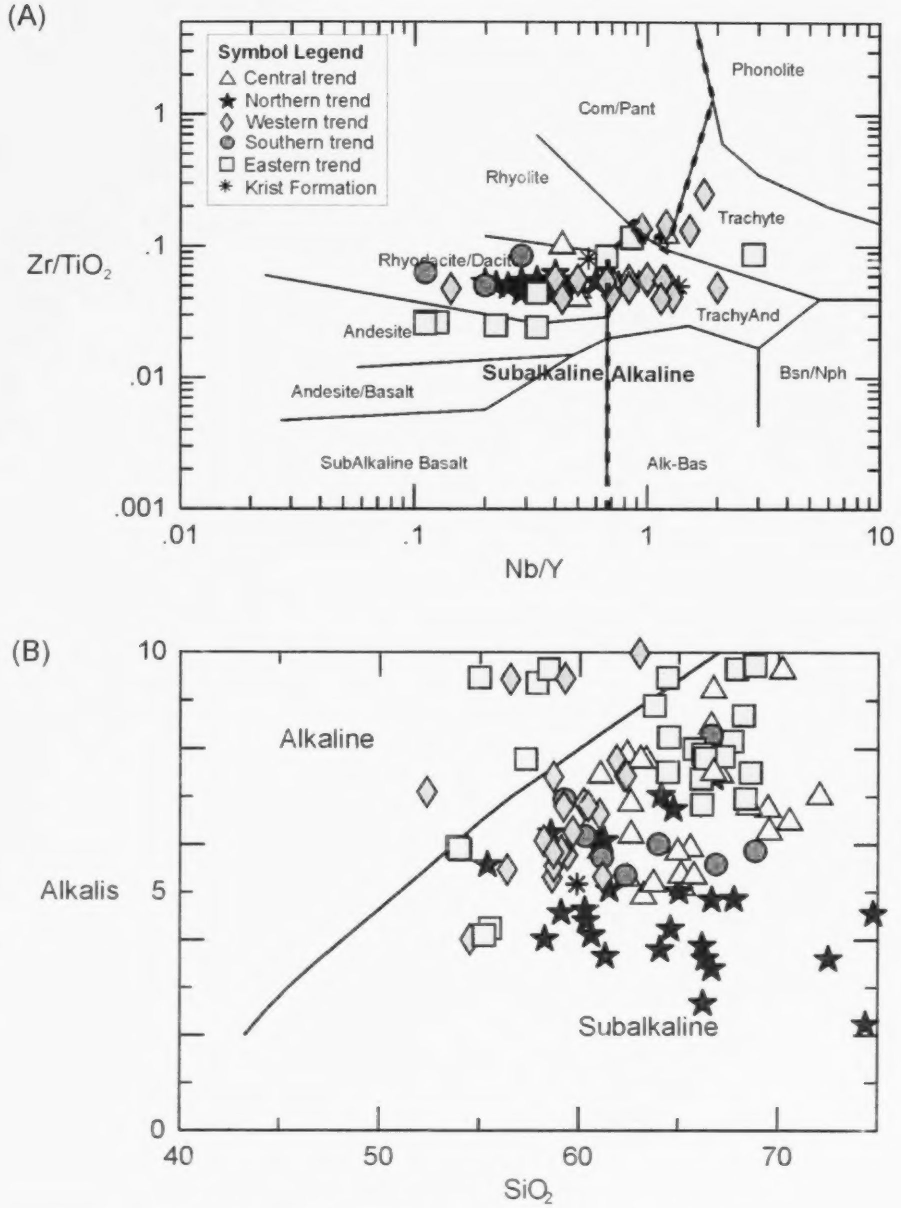

Figure 2.13. Classification plots for rocks of the 5 geographical porphyry trends as well as the Krist Formation: A) Nb/Y versus Zr/TiO_2 discrimination diagram of Winchester and Floyd (1977); and B) SiO_2 versus alkali plot showing alkaline versus subalkaline fields of Irvine and Baragar (1971). Abbreviations: Alk-Bas = alkali–basalt; Bsn/Nph = basanite–nephelinite; Com/Pant = comendite–pantellerite; TrachyAnd = trachyandesite.

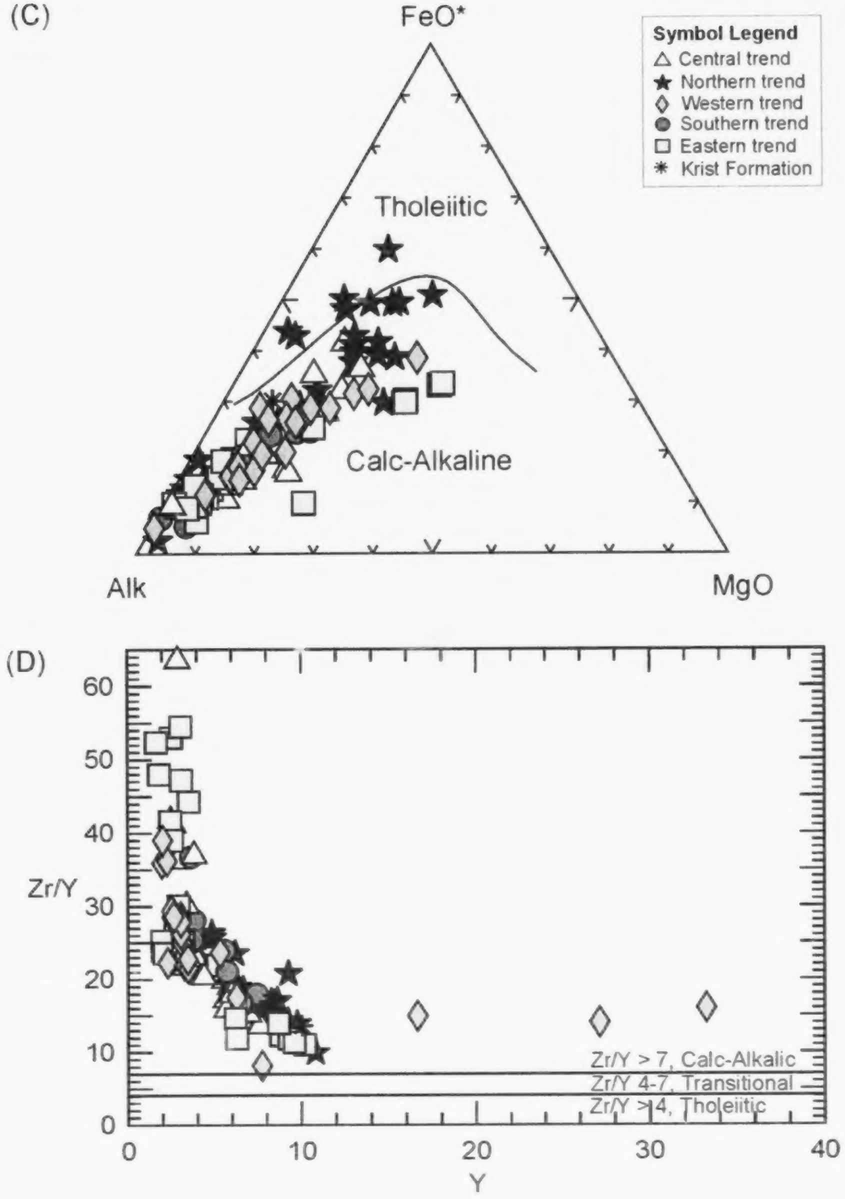

Figure 2.13, continued. Classification plots for rocks of the 5 geographical porphyry trends as well as the Krist Formation: C) alkali–FeO–MgO (AFM) plot *from* Irvine and Baragar (1971); and D) Y versus Zr/Y showing tholeiitic, transitional and calc-alkaline fields.

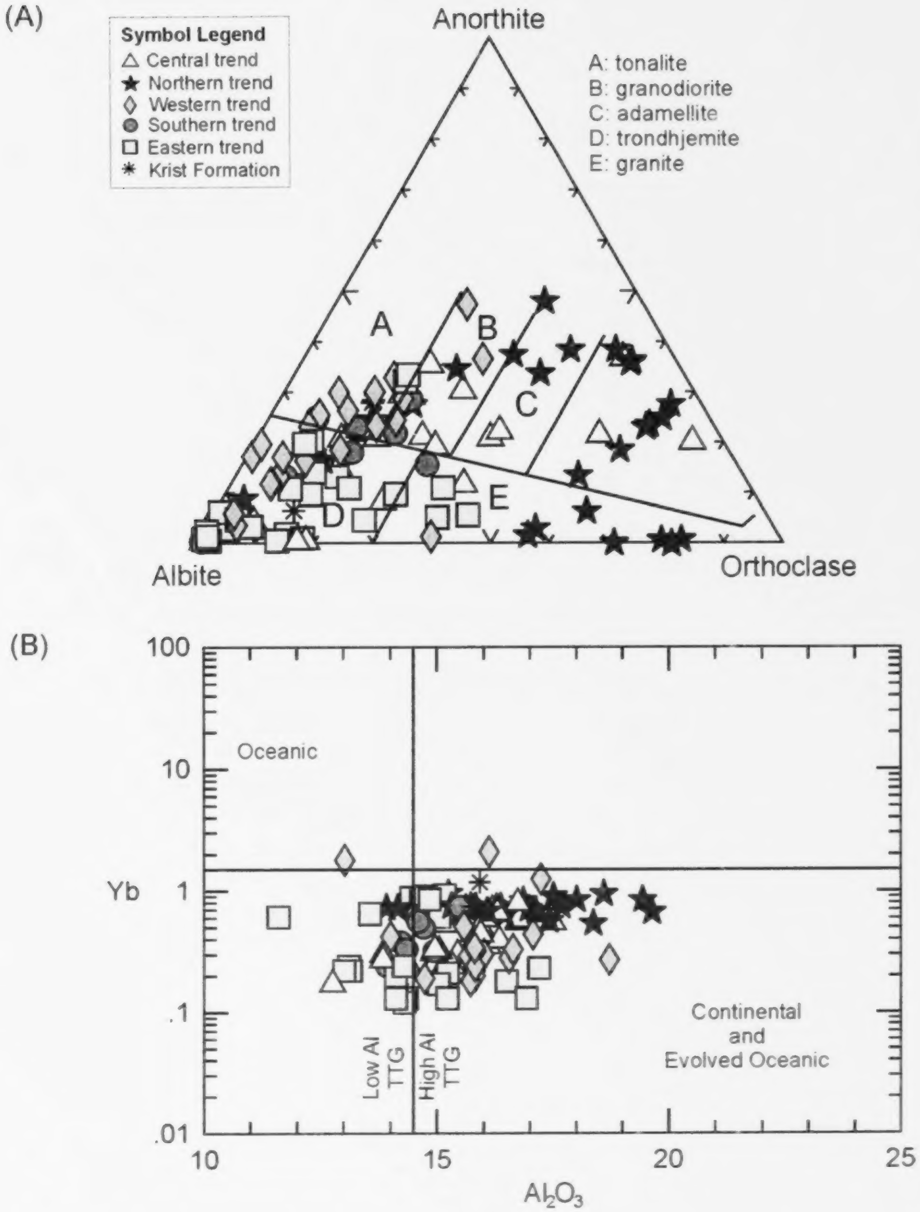

Figure 2.14. Classification plots for rocks of the 5 geographical porphyry trends as well as the Krist Formation: A) typical normative feldspar diagram *from* O'Connor (1965); and B) Al_2O_3 versus Yb diagram for classifying different types of tonalite-trondhjemite-granodiorite (TTG) *from* Arth (1979).

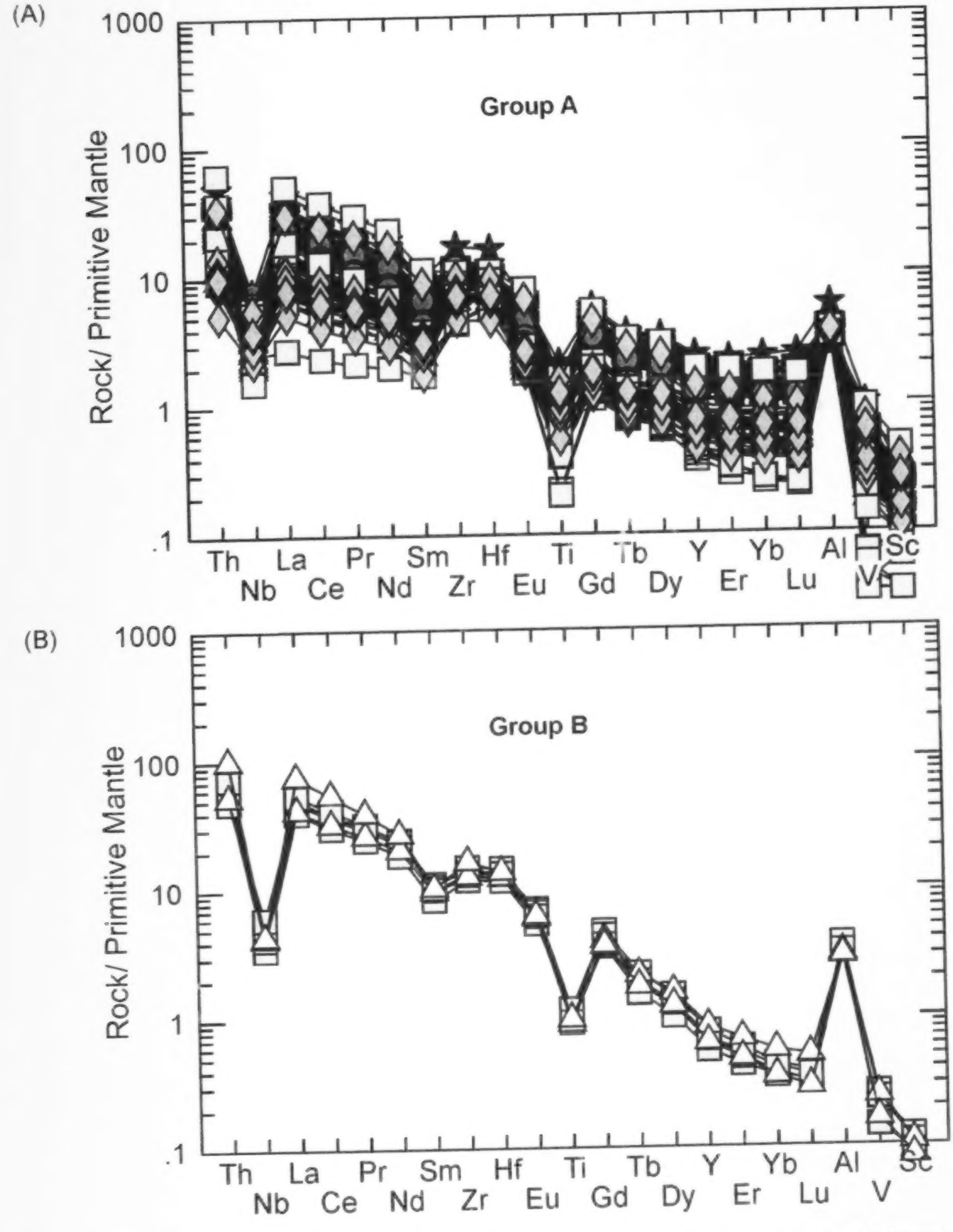

Figure 2.15. Primitive mantle normalized plots for rocks of the 5 geographical porphyry trends as well as the Krist Formation: A) Group A, porphyry intrusions; and B) Group B, porphyry intrusions. Primitive mantle values *from* Sun and McDonough (1989). *See* Figures 2.13 and 2.14 for the symbol legend.

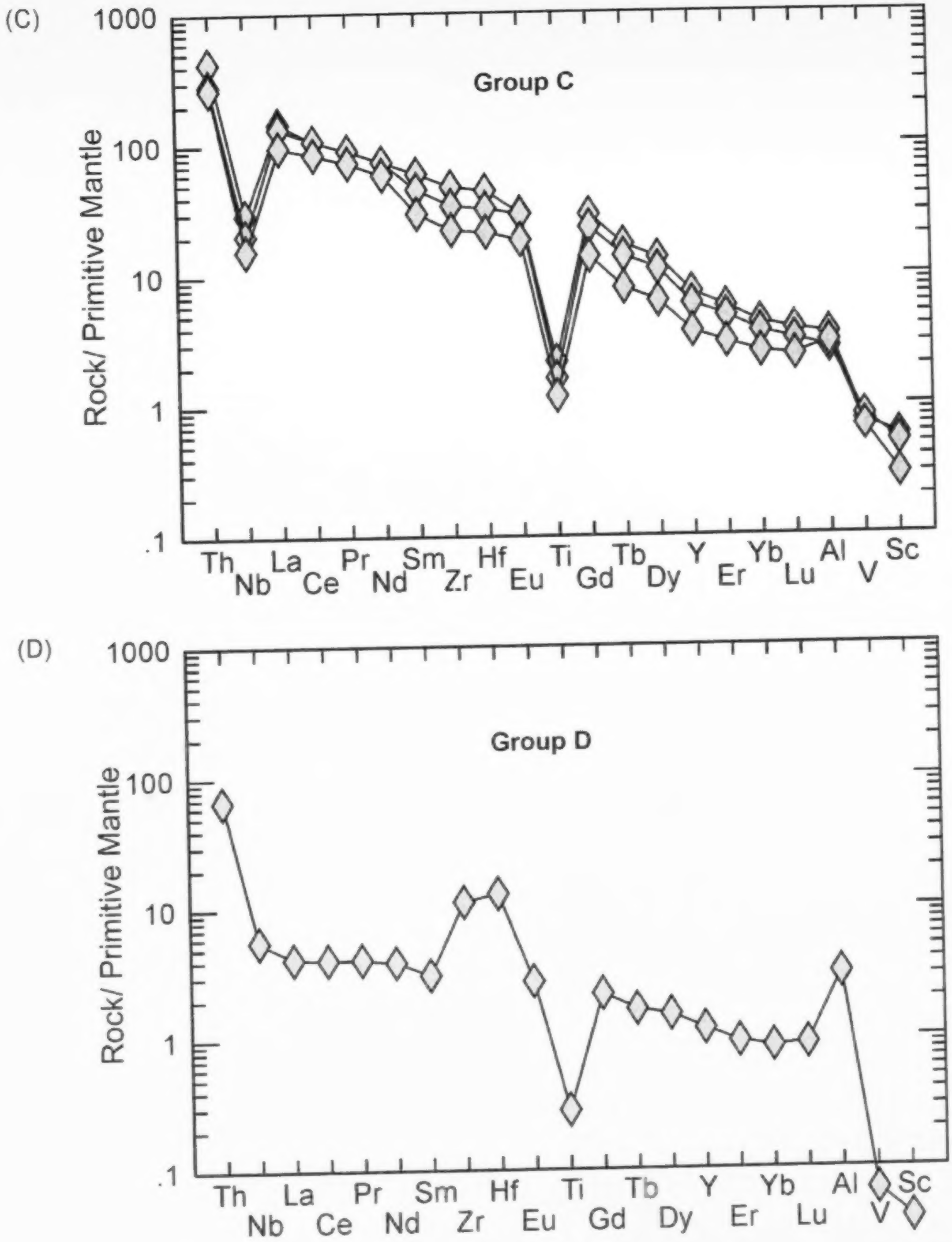

Figure 2.15, continued. Primitive mantle normalized plots for rocks of the 5 geographical porphyry trends as well as the Krist Formation: C) Group C, porphyry intrusions; and D) Group D, porphyry intrusions. Primitive mantle values *from* Sun and McDonough (1989). *See* Figures 2.13 and 2.14 for the symbol legend.

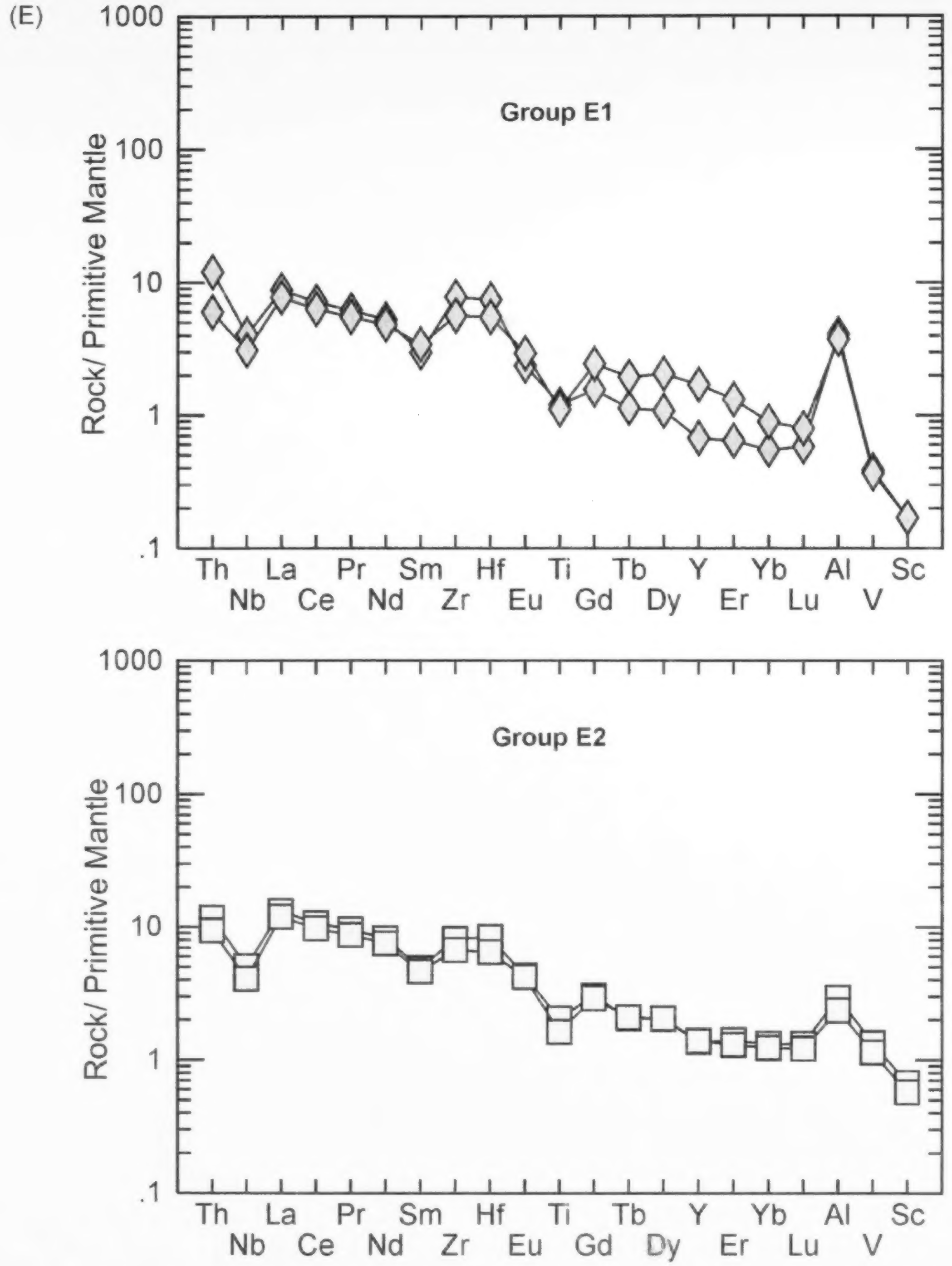

Figure 2.15, continued. Primitive mantle normalized plots for rocks of the 5 geographical porphyry trends as well as the Krist Formation: E) Groups E1 and E2, porphyry intrusions. Primitive mantle values *from* Sun and McDonough (1989). *See* Figures 2.13 and 2.14 for the symbol legend.

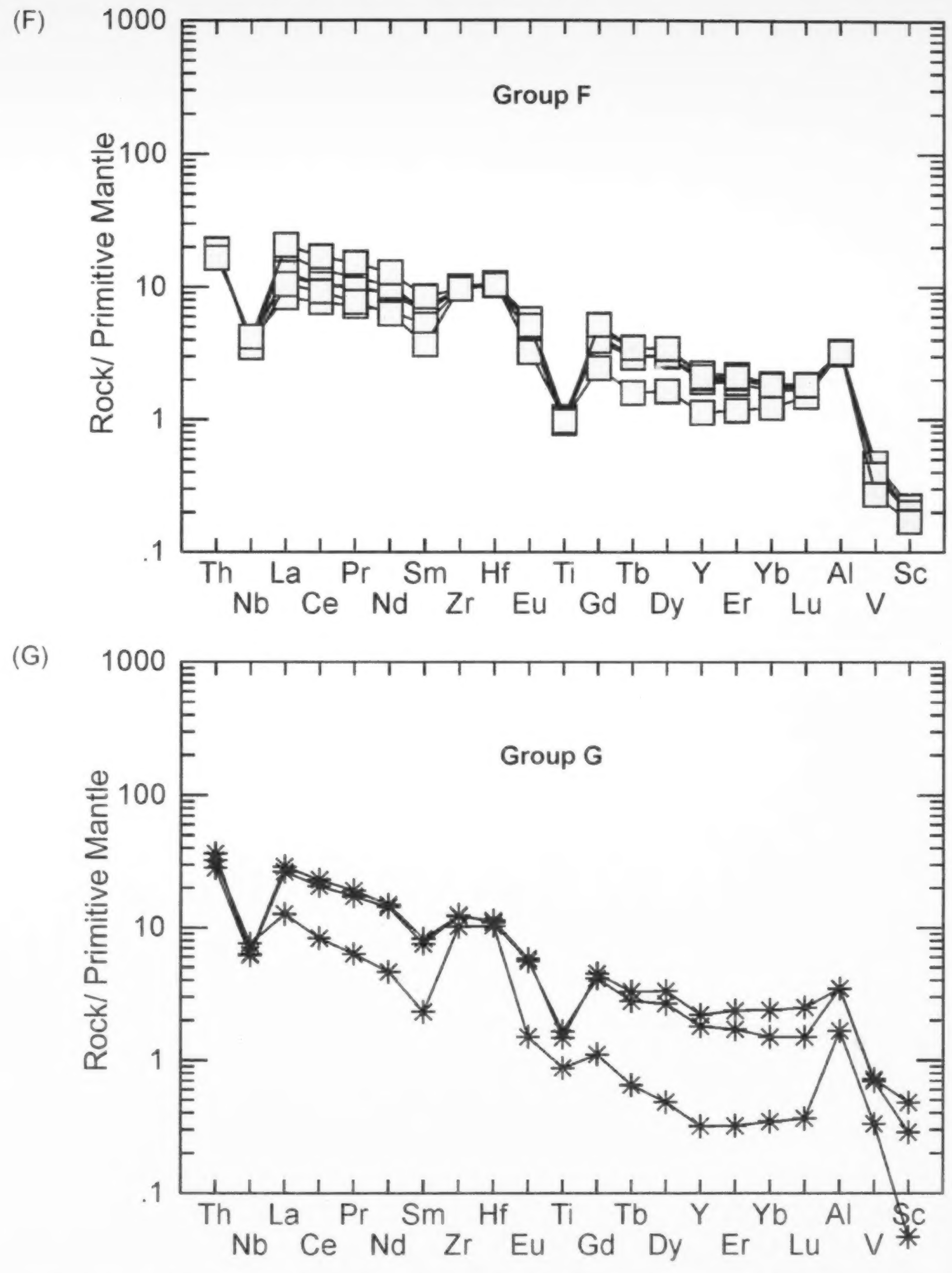

Figure 2.15, continued. Primitive mantle normalized plots for rocks of the 5 geographical porphyry trends as well as the Krist Formation: F) Group F, porphyry intrusions; and G) Group G, Krist Formation. Primitive mantle values *from* Sun and McDonough (1989). *See* Figures 2.13 and 2.14 for the symbol legend.

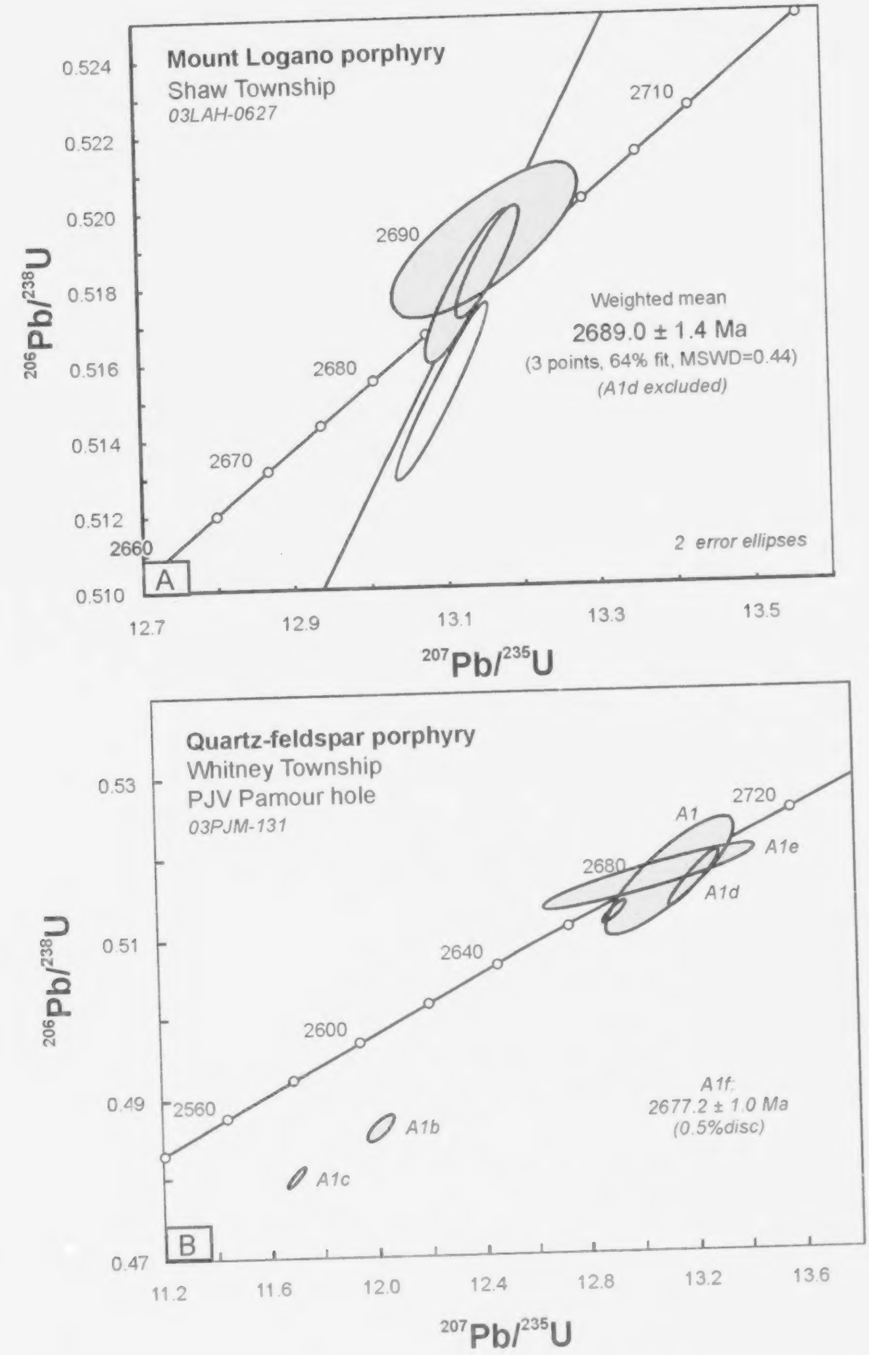

Figure 2.16. Concordia plots for porphyry U/Pb geochronology samples including: A) sample 03LAH-0627 (Mt. Logano porphyry (southern trend)); and B) sample 03PJM-131 (Pamour porphyry (eastern trend)).

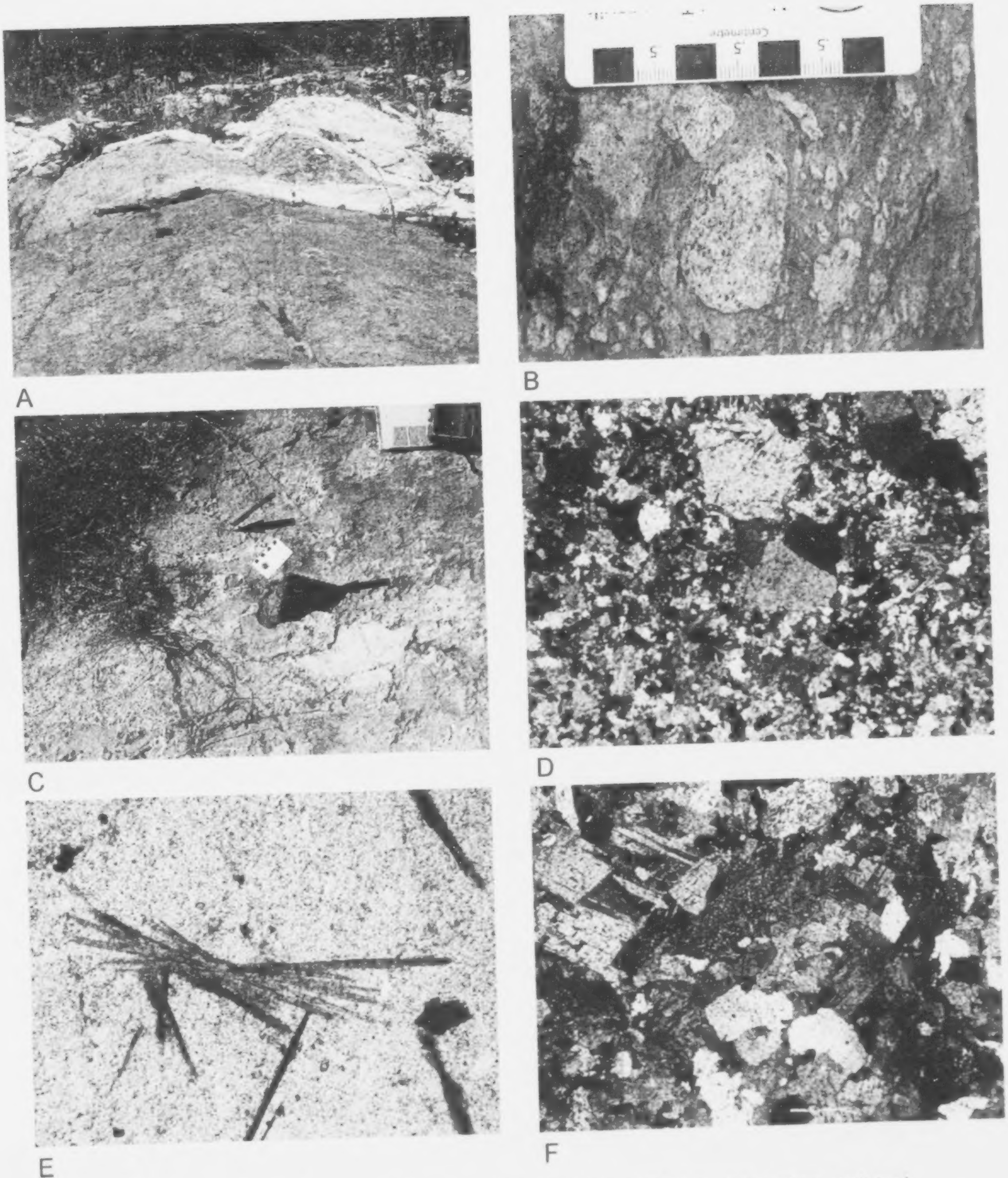

Photo 2.1. Selected photos and photomicrographs showing described features of the intrusions of the central trend: A) 2 m long transposed dike off of larger porphyry intrusions, near Vedron deposit; B) porphyry fragments within chloritic matrix, Edwards porphyry; C) mafic (white arrow) and porphyry (black arrow) fragments within chloritic matrix, Paymaster porphyry; D) porphyritic texture with quartz and feldspar phenocrysts within a quartzo-feldspathic matrix, Naybob porphyry, crossed polarized light (XPL), scale = 1 cm:2 mm; E) stilpnomelane blades within a aphanitic quartz-feldspathic matrix, Edwards porphyry, plane-polarized light (PPL), scale = 1.5 cm:1 mm; and F) equigranular texture of interlocking feldspars and quartz crystals, Porphyry Hill, XPL, scale = 1 cm:2 mm.

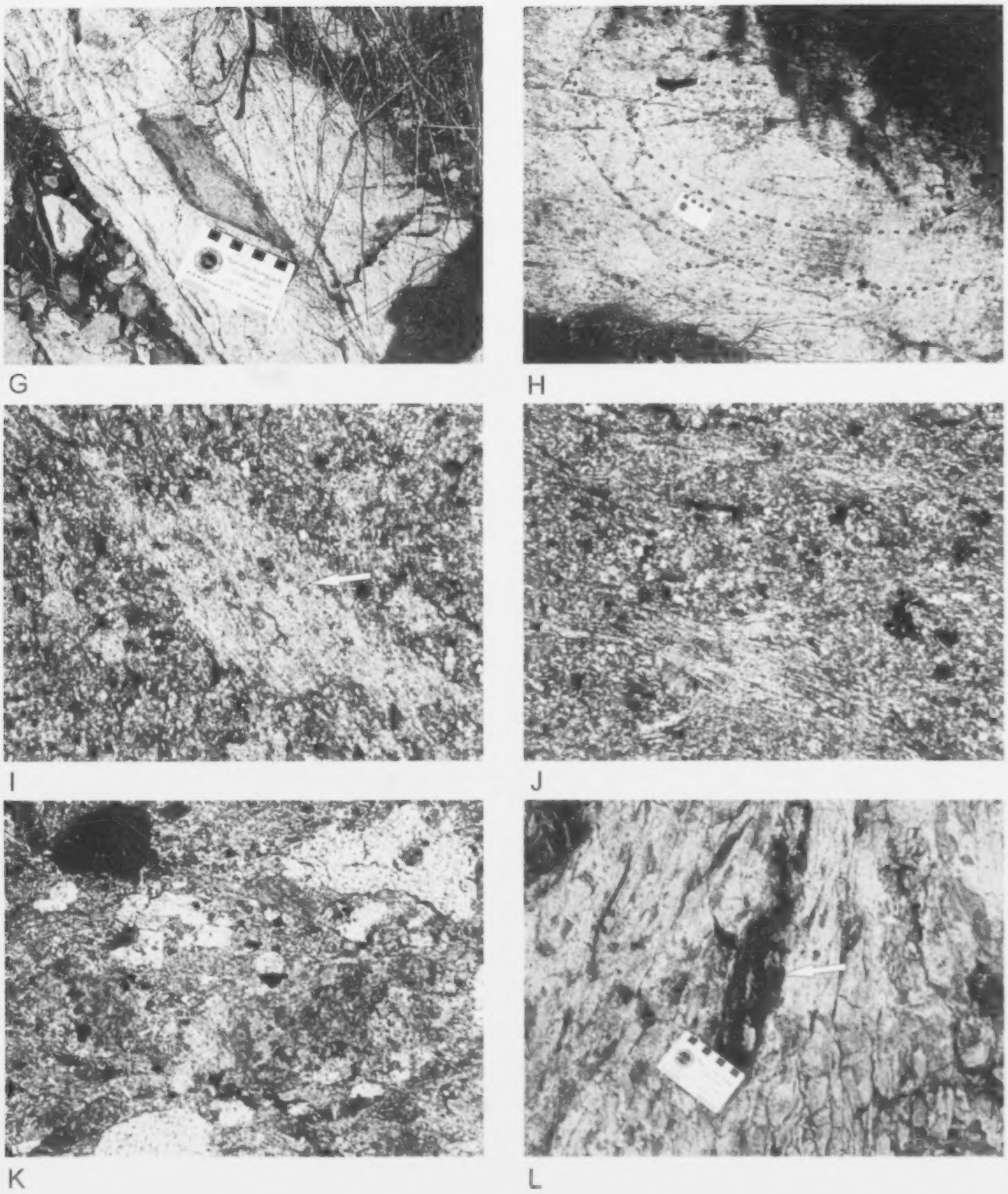

Photo 2.1, continued. Selected photos and photomicrographs showing described features of the intrusions of the central trend: G) large foreign (green mica) fragment within porphyry intrusion, Edwards porphyry; H) flow-banded lobe, Paymaster porphyry (dashed line highlights the lobe); I) relict feldspar phenocrysts that have undergone partial (near complete) sericite replacement (alteration), Preston porphyry, XPL, scale = 1 cm:1 mm; J) complete sericite replacement (alteration) of feldspar phenocrysts yielding quartz-sericite schist, Preston porphyry, XPL, scale =1 cm:1 mm; K) carbonate-altered porphyry displaying clouded grey appearance, Paymaster porphyry, XPL, scale = 1 cm:1.5 mm; and L) subhedral chlorite grain, Edwards porphyry, scale = 1 cm:1 mm.

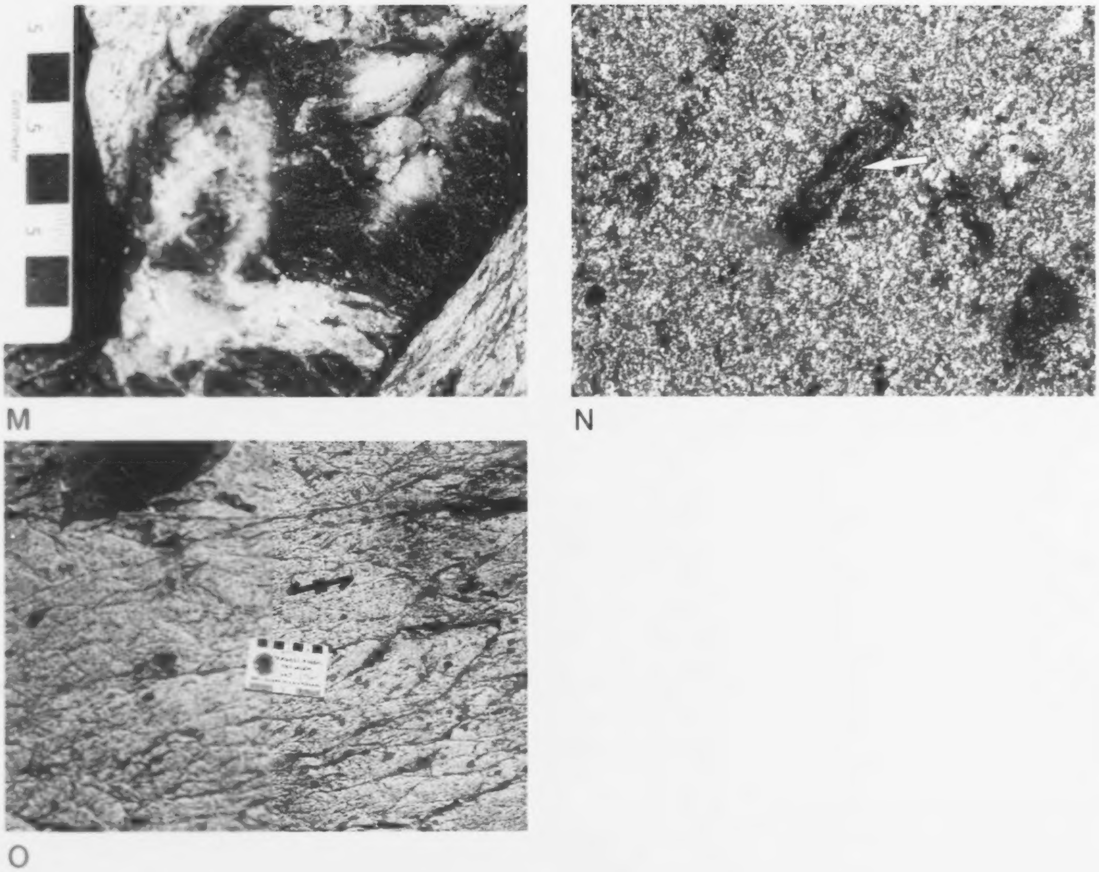

Photo 2.1, continued. Selected photos and photomicrographs showing described features of the intrusions of the central trend: M) iron-carbonate (ankerite) alteration of porphyry with a small ankerite veinlet, Buffalo Ankerite #5 porphyry; N) quartz-tourmaline vein (white arrow), Edwards porphyry; and O) well-developed D_2 spaced cleavage, Buffalo Ankerite #5 porphyry.

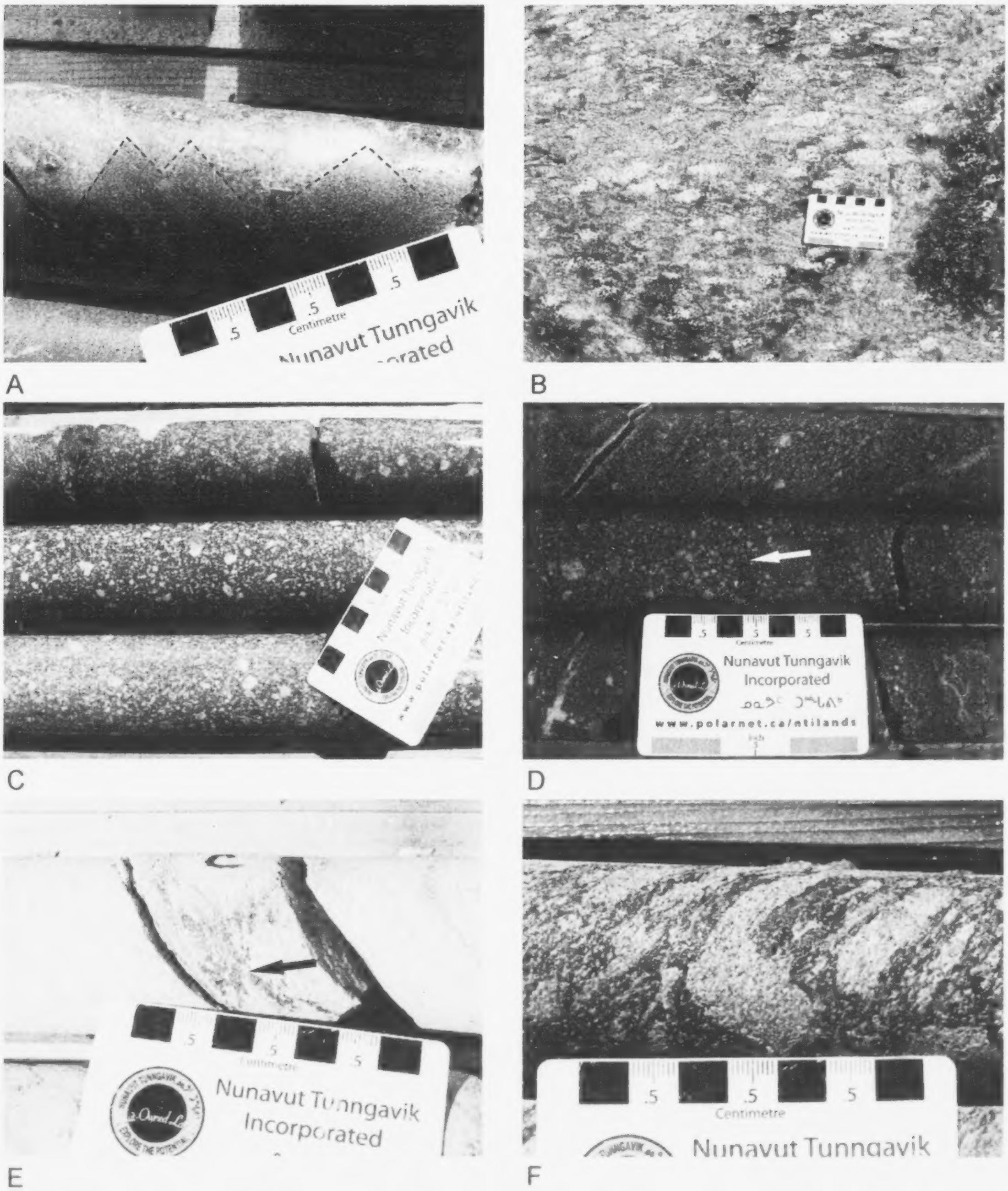
A
B
C
D
E
F
Nunavut Tunngavik Incorporated
Centimetre
www.polarnet.ca/ntilands

Photo 2.2. Selected photos and photomicrographs showing described features of the intrusions of the northern trend: A) sharp contact of porphyry intrusions and host mafic volcanic rocks, Gillies Lake porphyry (highlighted by dashed line); B) porphyry fragments within a chloritic matrix, Crown porphyry; C) porphyritic texture with feldspar and quartz phenocrysts within a quartzo-feldspathic matrix, Gillies Lake porphyry; D) black orthoclase phenocrysts (white arrow) within Gillies Lake porphyry; E) sulphide (pyrite and chalcopyrite) cluster (black arrow) within Pearl Lake porphyry; and F) sericite- and hematite-altered fragments of porphyry within a tourmaline-rich matrix, Pearl Lake porphyry.

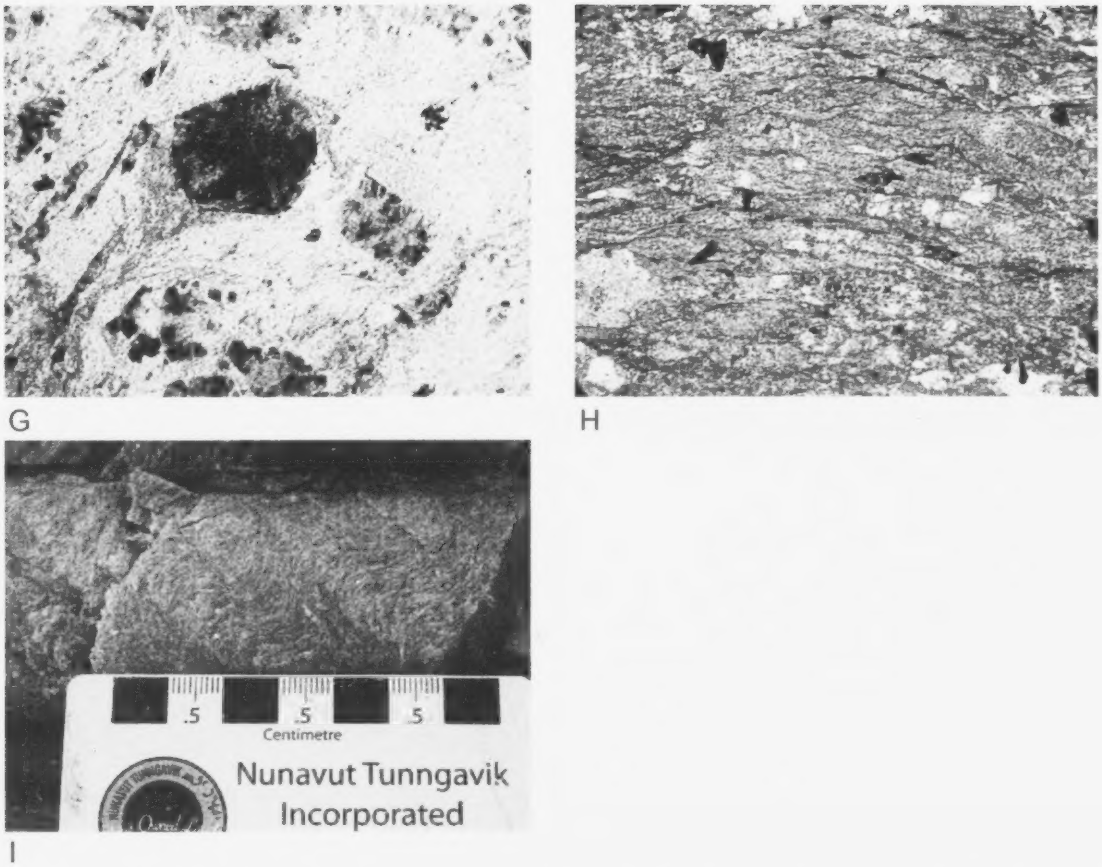

Photo 2.2, continued. Selected photos and photomicrographs showing described features of the intrusions of the northern trend: G) cloudy grey feldspar phenocrysts within weakly altered porphyry, Gillies Lake porphyry, PPL, scale = 1 cm:2 mm; H) strongly sericite-calcium carbonate ("dirty") altered porphyry with feldspar phenocrysts completely replaced, Pearl Lake porphyry, PPL, scale = 1 cm:1.5 mm; and I) highly deformed and calcium-carbonate (bleached) altered porphyry, Pearl Lake porphyry.

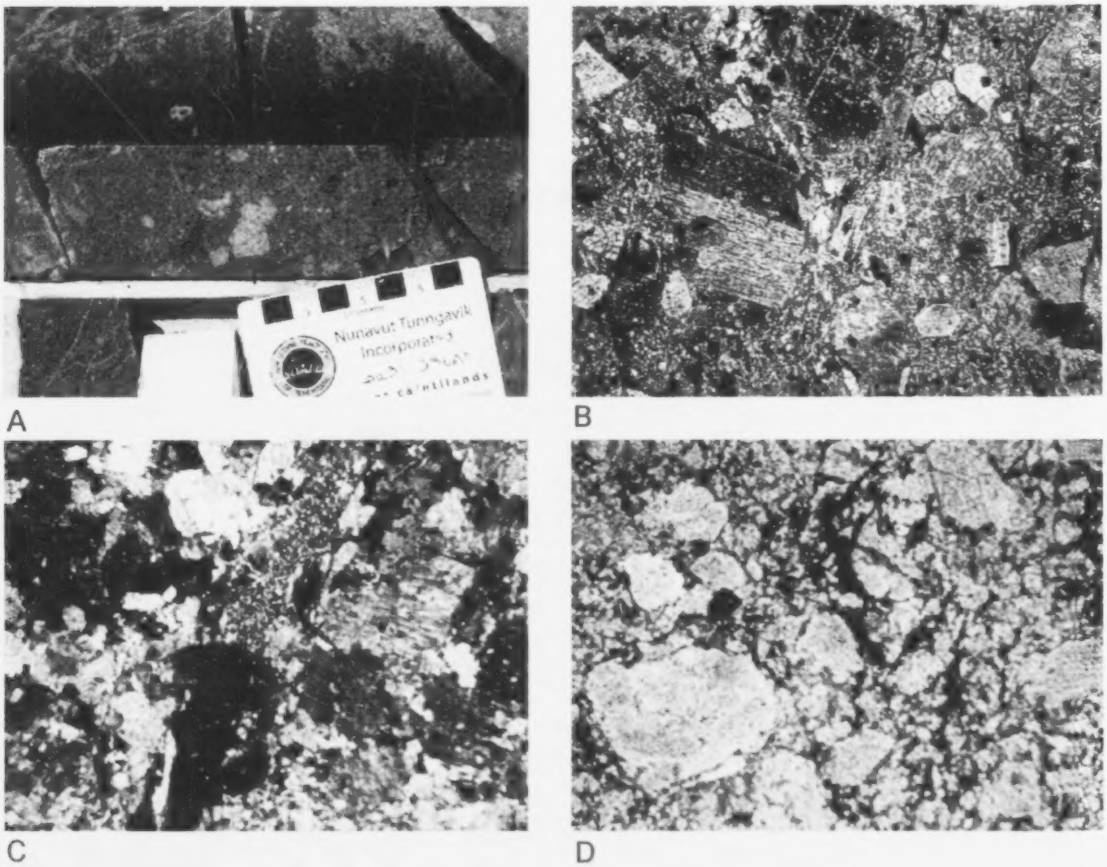

Photo 2.3. Selected photos and photomicrographs showing described features of the intrusions of the western trend:
A) heterolithic breccia including angular shaped, centimetre-size fragments of quartz-feldspar porphyry, mafic volcanic and siliciclastic mudstone sediments, Holmer porphyry; B) porphyritic texture with feldspar and quartz phenocrysts within a quaartzo-feldspathic matrix, Bristol Township porphyry, scale = 1 cm:2 mm; C) equigranular texture of interlocking feldspar crystals., Thunder Creek intrusion, scale = 1 cm:2 mm; D) calcium carbonate-altered (clouded grey appearance) feldspar phenocrysts., Holmer porphyry, scale = 1 cm:2 mm.

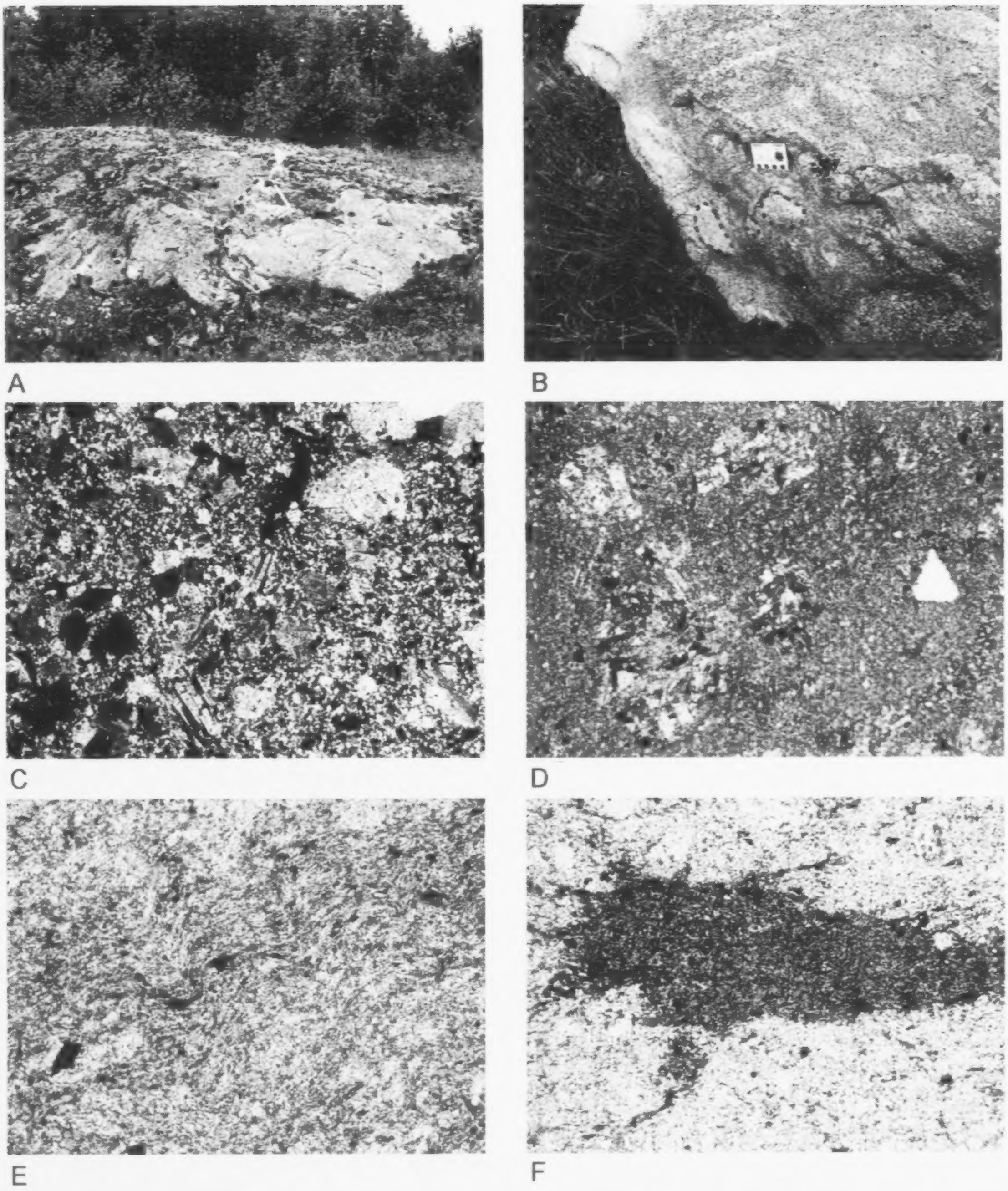

Photo 2.4. Selected photos and photomicrographs showing described features of the intrusions of the southern trend: A) sharp contact (indicated by dashed line) between porphyry dike and host mafic volcanic rocks, northern Deloro Township porphyry dike swarm, scale = 1 cm:2 m; B) subrounded porphyry fragments within a similar porphyry matrix, Mt. Logano porphyry (outlined by dashed line); C) porphyritic texture with feldspar and quartz phenocrysts within a quartzo-feldspathic matrix, northern Deloro Township porphyry dike swarm, XPL, scale = 1 cm:2 mm; D) moderately sericite-altered and replaced feldspar phenocrysts within a very fine-grained quartzo-feldspathic matrix, Mt. Logano porphyry, XPL, scale = 1.5 cm:1 mm; E) strongly sericite-altered porphyry exhibiting a well-developed crenulated D_2 foliation, northern Deloro Township porphyry dike swarm, XPL, scale = 1 cm:2 mm; F) anhedral chlorite lath, northern Deloro Township porphyry dike swarm, PPL, scale = 1 cm:2 mm.

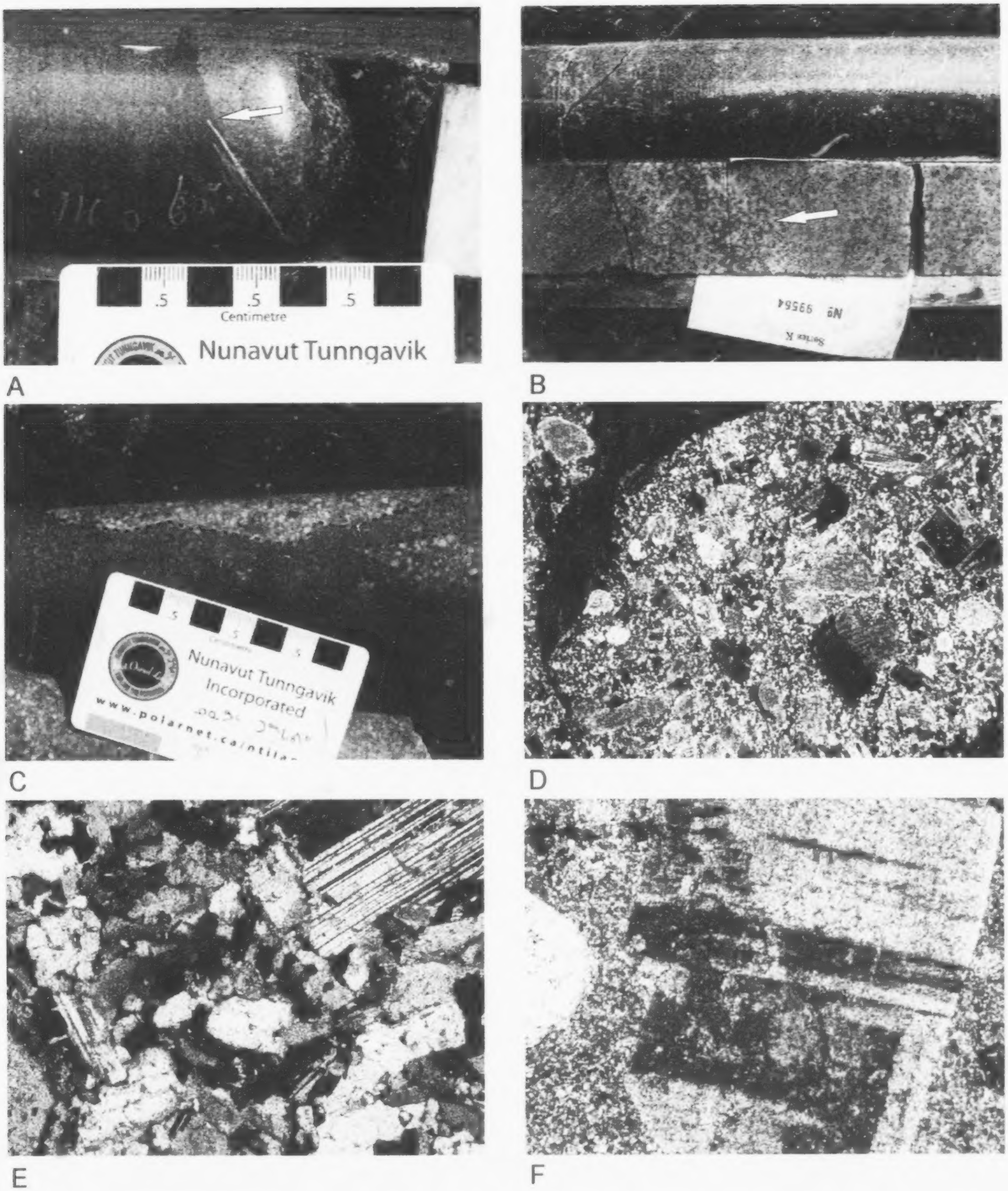
A
.5
.5
.5
Centimetre
Nunavut Tunngavik
B
N° 99564
Series K
C
Nunavut Tunngavik
Incorporated
www.polarnet.ca
D
E
F

Photo 2.5. Selected photos and photomicrographs showing described features of the intrusions of the eastern trend: A) sharp contact (arrow) between porphyry intrusion and host mafic volcanic rocks, Carr Township porphyry; B) transitional (gradational) contact (noted by arrow) between porphyry intrusions and mafic volcanic rocks, Aquarius porphyry, scale = 1 cm:5 cm; C) irregular, subrounded porphyry fragments (outlined by dashed lines) within chloritic mafic volcanic matrix, Carr Township porphyry; D) porphyritic texture with feldspar and quartz phenocrysts within a quartzo-feldspathic matrix, Pamour porphyry, XPL, scale = 1 cm:2 mm; E) equigranular texture of interlocking feldspar and quartz crystals, Bob's Lake granodiorite, XPL, scale = 1 cm:2 mm; and F) large feldspar phenocrysts, Carr Township porphyry, XPL, scale = 1 cm:3 mm.

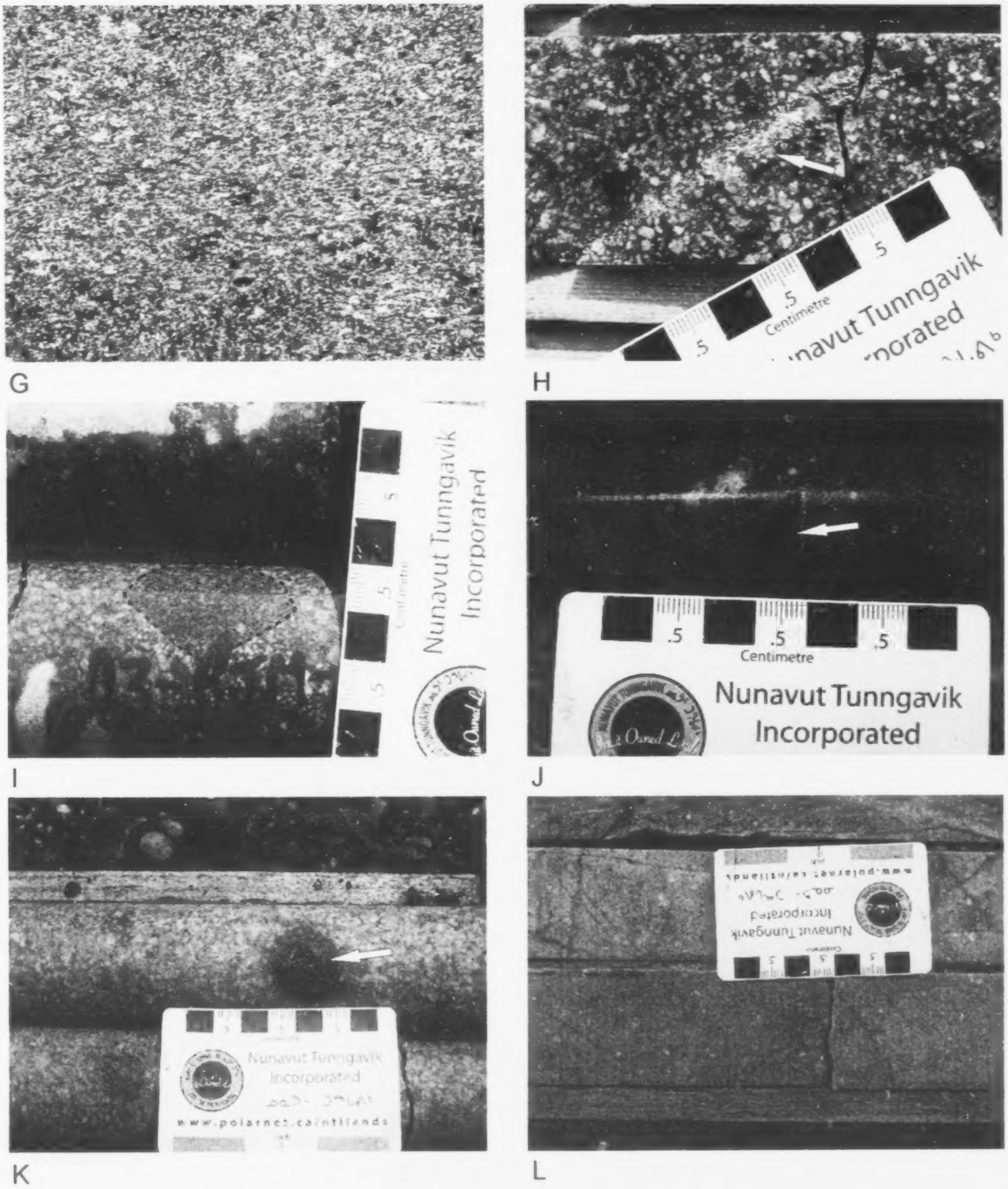

Photo 2.5, continued. Selected photos and photomicrographs showing described features of the intrusions of the eastern trend: G) strongly sericite-altered porphyry with feldspars and feldspathic matrix completely replaced by sericite. Carr Township porphyry. XPL, scale 1 cm:2 mm; H) large sulphide (pyrite) fragment (indicated by arrow). Carr Township porphyry; I) subrounded porphyry fragments within a porphyry matrix (outlined by dashed line). Carr Township porphyry; J) biotite cluster (noted by arrow) within the Pamour porphyry; K) rotated, large biotite-muscovite cluster. Aquarius porphyry; and L) silicified feldspar porphyry. Pominex porphyry.

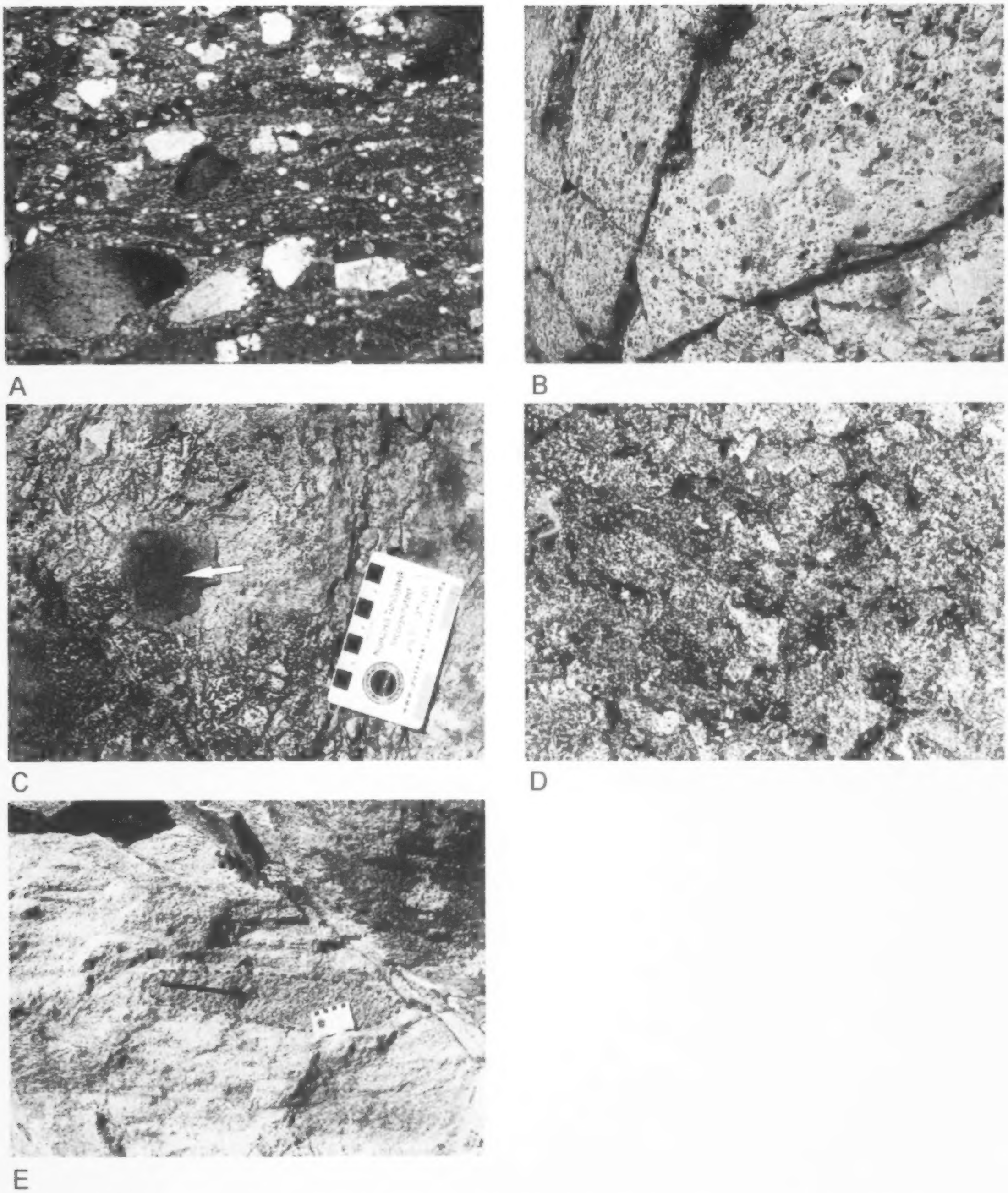

Photo 2.6. Selected photos and photomicrographs showing described features of the intrusions of the Krist Formation: A) quartz and feldspar-phyric lapilli tuff matrix of Krist Formation, Kayorum syncline, XPL, scale = 1 cm:2 mm; B) mafic clasts within conglomerate facies of Krist Formation, Kayorum syncline; C) large sulphide (pyrite) fragment (white arrow) within Krist Formation, Kayorum syncline; D) sericite- and calcium carbonate-altered (cloudy grey appearance) Krist Formation matrix, Porcupine syncline, XPL, scale = 1 cm:2 mm; E) elongate, stretched porphyry clasts (indicated by dashed outline) within Krist Formation, Kayorum syncline.

Table 2.1. The porphyry intrusions included in this study; information includes the porphyry name, geographical trend as explained in the report (central, northern, western, southern or eastern), age of emplacement (if known) and source for age.

Intrusion Name	Trend	Age (Ma)	Source
Dome Fault Zone porphyry	central	2688±2	Gray and Hutchinson (2001)
Preston porphyry	central	2690	Corfu et al. (1989)
Paymaster porphyry	central	2690±2	Corfu et al. (1989)
West porphyry	central		
Northwest porphyry	central		
Edwards porphyry	central		
Buffalo Ankerite #5 porphyry	central		
Buffalo Ankerite porphyry	central		
Aunor porphyry	central		
Delnite porphyry	central		
Naybob porphyry	central		
Porphyry Hill granodiorite	central		
Crown porphyry	northern	2688±2	Corfu et al. (1989)
Millerton porphyry	northern	2691±3	Corfu et al. (1989)
Miller Lake porphyry	northern		
Northern porphyry	northern		
Acme porphyry	northern		
Gillies Lake porphyry	northern		
Pearl Lake porphyry	northern	2689±1	Corfu et al. (1989)
Coniaurium porphyry	northern		
Bristol Twp. porphyry	western	2687.7±1.4	Ayer et al. (2003)
Bristol Lake porphyry	western		
South Bristol Lake porphyry	western		
Holmer porphyry	western		
Southwest Bristol syenite	western		
Thunder Creek porphyry	western		
northern Deloro Twp. porphyry dike swarm	southern		
Mt. Logano porphyry	southern	2689.0±1.4	This study
Pamour porphyry	eastern	2677.5±1	This study
Bob's Lake granodiorite	eastern		
Hoyle Pond porphyry	eastern		
Aquarius porphyry	eastern	2705±10	Corfu et al. (1989)
Aquarius Mine porphyry	eastern		
Homestead porphyry	eastern		
Crowley porphyry	eastern		
Pominex porphyry	eastern		
Carr Twp. porphyry	eastern		

Table 2.2. Summary of the field relationships, petrology, alteration, veining, mineralization, deformation, geochemistry and geochronology for quick comparison of the 5 geographical porphyry trends discussed in this chapter.

Category	Subcategory	Central trend	Northern trend	Western trend	Southern trend	Eastern trend
Field Relationships	Trend	west-southwest/ east-northeast	southwest-northeast	east-west	west-southwest/ east-northeast	east-west
	Size of trend?	11 x 2 km	4 x 1 km	13 km long	20+ km long	3 groups, each a few km long
	Join at depth?	yes	yes	???	???	???
	Plunge direction?	east	east	west and ???	???	???
	Stratigraphic level	1) northern margin of the PDDZ 2) Hersey Lake-Central Formation contact 3) Central and Vipond Formations (Tisdale Assemblage)	Central and Vipond Formations	contact of Tisdale and Porcupine Assemblages	Tisdale-Deloro Assemblage contact	1) Hersey Lake and Central Formations (Tisdale Assemblage) 2) contact of Tisdale Porcupine Assemblages
	Conformable with stratigraphy?	generally semi-conformable (all but Preston)	semi-conformable	semi-conformable	semi- to nonconformable	semi-conformable
	Other favourable zones for intrusion?	1) pillowed mafic flows of the Tisdale Assemblage 2) 'carb rock' alteration zones 3) fault zones (e.g., Dome Fault)	1) pillowed mafic flows of the Tisdale Assemblage 2) fault zones (Hollinger shear) 3) fold hinges	N/A	along the margins of the Shaw Dome	fault zones (PDDZ)
	Sizes & shapes	1) small dikes, sills and plugs (up to 500 x 300 m) 2) dikes and sills (up to 2 x 0.3 km) 3) large oval (~1.2 x 0.6 km)	1) small dikes and sills (up to ~400 x 100 m) 2) irregular shaped plugs (up to 1 x 0.5 km) 3) large elongate oval (2 x 0.5 km)	1) small sized dike and sills (up to 500 x 50 m) 2) medium sized dikes (up to 3 x 1 km) 3) large oval (5 x 3 km)	1) northern Deloro = swarm of small dikes (500 x 10 m) 2) Mt. Logano is a large elongate oval (6 x 1.5 km)	1) oval shaped plugs (100-300 m in diameter) 2) dikes (up to 1 x 0.1 km) 3) dikes (up to 3 x 0.1 km) 4) elongate oval plug (5 x 2 km) 5) large oval (12 x 5 km)
	Margins	generally straight and sharp with small apophyses lesser marked by breccias (Paymaster nose and Edwards)	generally straight and sharp (primary or tectonic) lesser marked by breccia (Crown)	generally straight and sharp (primary or tectonic) lesser marked by breccia (Bristol Township and Holmer)	generally straight and sharp (primary or tectonic) lesser marked by breccia (Mt. Logano)	generally straight and sharp (primary or tectonic) lesser marked by breccia (Carr Township) lesser marked by transitional zone (Aquarius)

Table 2.2. continued

Category	Subcategory	Central trend	Northern trend	Western trend	Southern trend	Eastern trend
Petrology	Texture	aphanitic, porphyritic and equigranular	porphyritic	porphyritic and equigranular	porphyritic	porphyritic and equigranular
	Phenocrysts	sub- to euhedral plagioclase and quartz up to 5 mm	sub- to euhedral feldspar and quartz up to 8mm	sub- to euhedral plagioclase and quartz up to 5mm	sub- to euhedral plagioclase and quartz up to 5mm	sub- to euhedral plagioclase and quartz up to 15mm
	Matrix	very fine to medium-fine grained	very fine grained	very fine to medium-fine grained	very fine grained	very fine to medium-fine grained
	Minor minerals	apatite and tourmaline	apatite and tourmaline	leucoxene	N/A	N/A
	Sulphides	dominantly pyrite, lesser pyrrhotite and chalcopyrite	pyrite, chalcopyrite, pyrrhotite, molybdenite and bornite	pyrite, chalcopyrite and arsenopyrite	pyrite	pyrite and chalcopyrite
	Foreign clasts	green mica fragments up to 10 cm	green mica fragments up to 10 cm	N/A	N/A	N/A
	Metamorphic minerals	stilpnomelane	N/A	N/A	N/A	biotite, chlorite and muscovite
Alteration, Veining and Mineralization	Alteration	white mica (sericite), calcium carbonate, chlorite and iron-carbonate (ankerite)	white mica (sericite), calcium carbonate, hematite, iron-carbonate (ankerite) and chlorite	sericite, chlorite, calcium-carbonate, hematite and iron-carbonate (ankerite)	sericite, chlorite and calcium-carbonate	sericite, calcium-carbonate, chlorite, hematite, iron-carbonate (ankerite), silicification and albite
	Veining	quartz-tourmaline, quartz-ankerite and quartz	quartz-tourmaline, quartz-ankerite, quartz-calcite and quartz	quartz-calcite and quartz sweats	quartz sweats and quartz-calcite	quartz sweats, quartz-calcite and quartz-ankerite
	Mineralization	gold mineralization	gold mineralization copper mineralization	anomalous gold anomalous copper	no gold known anomalous copper	gold mineralization anomalous copper
Deformation	Deformation	D1 foliation and D2 spaced cleavage	D1 foliation, D2 spaced cleavage, D? stretching lineation and D6 foliation	D1 foliation and D2 spaced cleavage	D1 foliation and D2 spaced cleavage	D? foliation

Table 2.2. continued

Category	Subcategory	Central trend	Northern trend	Western trend	Southern trend	Eastern trend
Geochemistry	Major Elements	Si = 60-72 wt %	Si = 55-76 wt %	Si = 52-63 wt %	Si = 59-69 wt %	Si = 53-69 wt %
		Ti, Al, Fe and Mg = compatible	Ti, Al, Fe, Mg and Ca = compatible	Ti, Al, Fe, Mg and Ca = compatible	Ti, Al, Fe and Mg = compatible	Ti, Al, Fe, Mg and Ca = compatible
		Ca, Na and K = incompatible/ mobile	Na and K = incompatible/ mobile	Na and K = incompatible/ mobile	Ca, Na and K = incompatible/ mobile	Na and K = incompatible/ mobile
	Trace Elements	V, Sc, Nb and Y = compatible	V, Sc, Nb and Y = compatible	V, Sc, Nb and Y = compatible	V, Sc, Nb, Y and Th = compatible	V and Sc = compatible
		Sr and Rb = incompatible/ mobile	Sr and Rb = incompatible/ mobile	Sr and Rb = incompatible/ mobile	Sr and Rb = incompatible/ mobile	Sr, Rb, Nb, Y and Th =incompatible/ mobile
		Th = incompatible	Th = incompatible	Th = incompatible		
	Alteration	mostly fresh to weakly altered	some fresh to weakly albite altered (Crown and Gillies Lake)	mostly fresh to weakly altered	mostly fresh to weakly altered	mostly albite alteration (Na altered/ metasomatized)
		sericite alteration (Na-loss and K-metasomatism) at Dome Mine	strong sericite alteration (Na-loss and K-metasomatism) in Pearl Lake	albite alteration (Na altered/ metasomatized) in Bristol Lake, South Bristol Lake and Holmer	albite alteration (Na altered/ metasomatized) in two northern Deloro Township dikes	some are fresh to weakly altered
		albite alteration (Na altered/ metasomatized) in Northwest, Edwards and Buffalo Ankerite #5		sericite alteration (Na-loss and K-metasomatism) in the Bristol Township		
	Composition	rhyodacite-dacite	rhyodacite-dacite	dacite (andesite-trachyandesite)	rhyodacite-dacite	dacite(-andesite)
		subalkalic, calc-alkaline	subalkalic, calc-alkaline	subalkalic, calc-alkaline to alkalic	subalkalic, calc-alkaline	subalkalic, calc-alkaline to alkalic
		mostly high-Al TTG, lesser low-Al TTG	mostly high-Al TTG	mostly high-Al TTG, lesser low-Al TTG	straddle the high-Al TTG/ low-Al TTG line	straddle the high-Al TTG/ low-Al TTG line
	REE (*see* Fig. 2.15)	mostly group A, lesser group B	all group A	groups A, C, D, and E	all group A	groups B, F, G, H and I
Geochronology	Geochronology	Preston = 2690 Ma*	Crown = 2688±2 Ma*	Bristol Township = 2687.7±1.4 Ma**	Mt. Logano = 2689.0±1.4 Ma	Pamour = 2677.5±1 Ma
		Paymaster = 2690±2 Ma*	Millerton = 2691±3 Ma*			Aquarius = 2705±10 Ma*
		Dome Fault Zone = 2688±2 Ma***	Pearl Lake = 2689±1 Ma*			

References: * = Corfu et al. (1989); ** = Ayer et al. (2003); *** = Gray and Hutchinson (2001)

Table 2.3. Geochemical data for rocks of the porphyry intrusion suite examined within this project.

Sample	03-PJM-148	03-PJM-005	03-PJM-006	03-PJM-007a	03-PJM-007c
UTME_nad27	482,392	482,221	482,187	482,130	482,130
UTMN_nad27	5,367,564	5,367,261	5,367,274	5,367,289	5,367,289
Hole Number	Dome Pit	Dome Pit	Dome Pit	Dome Pit	Dome Pit
Dip → Azimuth	-	-	-	-	-
Depth (m)	-	-	-	-	-
Rock Type	quartz-sericite schist	quartz-sericite schist	quartz-sericite schist	quartz-sericite schist	quartz-sericite schist
Trend	central	central	central	central	central
Unit	Dome Fault Zone Porphyry	Preston Porphyry	Preston Porphyry	Preston Porphyry	Paymaster Porphyry
SiO2	62.43	60.58	63.24	62.41	65.2
TiO2	0.38	0.32	0.32	0.32	0.34
Al2O3	16.74	15.92	15.93	15.74	16.76
Fe2O3	4.88	3.22	2.8	2.73	3.69
MnO	0.03	0.06	0.04	0.01	0.07
MgO	2.42	1.64	1.65	1.55	1.96
CaO	2.02	4.47	3.73	3.37	1.72
Na2O	1.05	3.06	0.5	5.82	0.24
K2O	4.24	3.36	4.41	2.05	4.85
P2O5	0.12	0.15	0.15	0.11	0.13
Cr	-	-	-	-	-
LOI	4.5	7.15	6.8	4.7	4.62
Total	98.82	99.92	99.57	98.81	99.59
Cr	-	-	-	-	-
Ni	-	-	-	-	-
V	-	-	-	-	-
Ni	25	12	15	18	23
Cr	-	-	-	-	-
Co	18	8	11	8	9
V	66.2	42.5	47.5	35.3	45.6
Sc	6	3.5	3.9	2.9	3.4
Cu	167	N.D.	N.D.	160	14
Zn	41	51	20	10	46
Cd	-	-	-	-	-
Mo	N.D.	N.D.	N.D.	N.D.	N.D.
W	10	5	N.D.	8	9
S	-	-	-	-	-
Be	0.88	0.46	0.63	0.57	0.63
Li	-	-	-	-	-
Cs	1.17	0.383	0.65	0.571	1.361
Rb	92.82	64.36	89.15	49.61	111.21
Ba	-	-	-	-	-
Sr	93.1	170.8	188.9	256.1	57.7
Nb	N.D.	2	2	N.D.	2
Y	8	6	5	4	6
Zr	95	100	99	88	93
Zr	103.5	111.8	100.7	91.8	110.1
Hf	2.8	3	2.7	2.6	3.1
Nb	3	3.4	2.9	2.9	3.1
Ta	0.2	0.23	0.2	0.22	0.24
Y	7.61	5.9	4.9	3.91	5.56
Th	2.16	2.44	2.49	1.74	2.47
U	0.799	0.809	0.787	0.712	0.841
La	13.15	16.23	15.95	9.95	13.88
Ce	27.62	33.12	31.44	23.35	28.75
Pr	3.4	3.99	3.839	2.815	3.528
Nd	13.63	15.82	15.14	10.86	13.38
Sm	2.5	2.64	2.48	1.8	2.35
Eu	0.703	0.716	0.637	0.536	0.679
Gd	2.125	1.978	1.807	1.357	1.814
Tb	0.268	0.222	0.204	0.156	0.207
Dy	1.414	1.142	1.021	0.798	1.112
Ho	0.277	0.212	0.188	0.149	0.211
Er	0.813	0.595	0.514	0.407	0.582
Tm	0.119	0.086	0.074	0.061	0.088
Yb	0.79	0.59	0.51	0.41	0.58
Lu	0.125	0.091	0.078	0.065	0.089

Table 2.3. Geochemical data for rocks of the porphyry intrusion suite examined within this project

Sample	03-PJM-008	03-PJM-009	03-PJM-010	03-PJM-152a	03-PJM-152b
UTME_nad27	482,039	482,084	481,913	481,257	481,257
UTMN_nad27	5,367,324	5,367,317	5,367,201	5,367,171	5,367,171
Hole Number	Dome Pit	Dome Pit	Dome Pit	outcrop	outcrop
Dip → Azimuth	-	-	-	-	-
Depth (m)	-	-	-	-	-
Rock Type	quartz-sericite schist	quartz-sericite schist	quartz-sericite schist	quartz-feldspar porphyry	quartz-feldspar porphyry
Trend	central	central	central	central	central
Unit	Paymaster Porphyry	Paymaster Porphyry	Paymaster Porphyry	Paymaster Porphyry	Paymaster Porphyry
SiO2	62.61	63.74	61.07	64.95	65.11
TiO2	0.35	0.33	0.31	0.31	0.3
Al2O3	17.5	15.77	15.19	16.34	15.94
Fe2O3	3.34	4.7	6.16	2.42	2.3
MnO	0.1	0.11	0.16	0.06	0.07
MgO	1.72	2.19	1.97	1.29	1.2
CaO	2.45	2.19	4.14	4.05	4.48
Na2O	2.54	2.02	3.72	3.66	3.06
K2O	3.65	3.15	2.15	2.17	2.29
P2O5	0.13	0.11	0.11	0.1	0.1
Cr	-	-	-	-	-
LOI	4.82	4.65	3.49	4.71	5.1
Total	99.2	98.97	98.48	100.04	99.95
Cr	-	-	-	-	-
Ni	-	-	-	-	-
V	-	-	-	-	-
Ni	18	26	21	24	19
Cr	-	-	-	-	-
Co	10	9	14	8	6
V	45.8	42.5	37.7	35.7	33.9
Sc	3.5	3.4	3.4	2.6	2.6
Cu	12	4	289	N.D.	N.D.
Zn	1223	89	91	53	54
Cd	-	-	-	-	-
Mo	N.D.	N.D.	N.D.	N.D.	N.D.
W	3	4	7	4	4
S	-	-	-	-	-
Be	0.63	0.49	0.44	0.53	0.56
Li	-	-	-	-	-
Cs	1.251	0.99	2.405	1.755	1.78
Rb	92.61	86.84	53.38	59.06	59.08
Ba	-	-	-	-	-
Sr	105.3	94.2	117.8	227.8	229
Nb	2	N.D.	2	N.D.	N.D.
Y	6	5	5	4	4
Zr	101	90	84	89	86
Zr	116.8	97.3	89.6	88.9	89.2
Hf	3.1	2.6	2.4	2.4	2.5
Nb	3.3	3	2.9	2.3	2.4
Ta	0.25	0.22	0.21	N.D.	0.2
Y	5.6	5.67	5.68	3.85	4.39
Th	2.45	2.3	2.13	1.64	1.64
U	0.856	0.672	0.773	0.627	0.576
La	15.15	16.02	12.41	10.18	9.78
Ce	31.11	32.12	25.62	20.77	20.19
Pr	3.787	3.958	3.15	2.479	2.404
Nd	14.94	15.29	12.61	9.6	9.36
Sm	2.54	2.69	2.22	1.77	1.62
Eu	0.696	0.778	0.738	0.478	0.482
Gd	1.906	1.982	1.713	1.281	1.256
Tb	0.213	0.226	0.2	0.15	0.155
Dy	1.117	1.144	1.077	0.757	0.827
Ho	0.204	0.203	0.197	0.139	0.154
Er	0.568	0.556	0.529	0.397	0.437
Tm	0.078	0.078	0.079	0.058	0.062
Yb	0.55	0.52	0.53	0.39	0.44
Lu	0.081	0.078	0.082	0.06	0.062

Table 2.3. Geochemical data for rocks of the porphyry intrusion suite examined within this project

Sample	03-PJM-146	03-PJM-149	03-PJM-001	03-PJM-002	03-PJM-004
UTME_nad27	481,616	481,277	480,487	480,466	480,486
UTMN_nad27	5,366,383	5,366,102	5,365,925	5,365,896	5,365,859
Hole Number	outcrop	outcrop	outcrop	outcrop	outcrop
Dip → Azimuth	-	-	-	-	-
Depth (m)	-	-	-	-	-
Rock Type	quartz-feldspar porphyry	quartz-feldspar porphyry	quartz-feldspar porphyry	quartz-feldspar porphyry	quartz-feldspar porphyry
Trend	central	central	central	central	central
Unit	West Porphyry	West Porphyry	Northwest Porphyry	Northwest Porphyry	Northwest Porphyry
SiO2	62.59	61.05	63.37	60.98	66.63
TiO2	0.39	0.43	0.34	0.38	0.36
Al2O3	16.03	16.3	16.19	17.14	16.75
Fe2O3	5.13	2.06	2.97	2.83	3.53
MnO	0.03	0.03	0.03	0.04	N.D
MgO	1.66	1.93	1.32	1.24	1.15
CaO	3.02	3.94	3.19	3.25	0.8
Na2O	5.2	4.98	6.62	9.97	7.52
K2O	1.65	2.46	1.13	0.28	0.94
P2O5	0.15	0.18	0.14	0.2	0.15
Cr	-	-	-	-	-
LOI	3.39	5.77	3.87	3.23	1.68
Total	99.24	99.14	99.17	99.54	99.52
Cr	-	-	-	-	-
Ni	-	-	-	-	-
V	-	-	-	-	-
Ni	15	14	13	12	10
Cr	-	-	-	-	-
Co	5	9	7	11	6
V	51.7	58.4	44.4	14.1	37.3
Sc	3.9	4.4	3.5	2.8	2.8
Cu	7	10	N.D	34	154
Zn	32	15	45	9	18
Cd	-	-	-	-	-
Mo	N.D	N.D	N.D	N.D	N.D
W	6	8	7	12	8
S	-	-	-	-	-
Be	0.5	0.61	0.66	0.39	0.5
Li	-	-	-	-	-
Cs	0.189	0.263	0.156	0.044	0.104
Rb	34.77	51.44	25.62	5.41	17.11
Ba	-	-	-	-	-
Sr	232.8	370.2	397.4	199.6	324.4
Nb	2	3	2	3	2
Y	6	6	6	6	5
Zr	101	103	100	106	109
Zr	107	105.3	108.4	109.2	117.8
Hf	2.8	2.8	2.9	3	3.1
Nb	3.5	3.8	3.3	3.6	3.5
Ta	0.22	0.23	0.24	0.25	0.25
Y	5.99	6.95	6.32	6.64	6.06
Th	2.48	2.91	2.53	2.43	2.25
U	0.842	0.558	0.801	0.749	0.771
La	14.11	16.4	15.94	18.83	14.45
Ce	29.24	37.83	32.64	35.88	30.18
Pr	3.528	4.956	3.987	4.328	3.72
Nd	13.83	20.2	16.11	17.44	15.01
Sm	2.24	3.42	2.84	2.9	2.6
Eu	0.694	0.88	0.739	0.784	0.69
Gd	1.769	2.39	2.091	2.133	1.935
Tb	0.199	0.272	0.249	0.244	0.231
Dy	1.07	1.436	1.279	1.305	1.17
Ho	0.205	0.256	0.235	0.24	0.213
Er	0.575	0.685	0.653	0.69	0.587
Tm	0.088	0.101	0.094	0.096	0.086
Yb	0.59	0.66	0.69	0.64	0.55
Lu	0.098	0.1	0.097	0.098	0.084

Table 2.3. Geochemical data for rocks of the porphyry intrusion suite examined within this project

Sample	03-PJM-011	03-PJM-015	03-PJM-022	03-PJM-028	03-PJM-037
UTME_nad27	479,424	479,453	479,413	479,458	479,513
UTMN_nad27	5,366,297	5,366,278	5,366,339	5,366,358	5,366,261
Hole Number	outcrop	outcrop	outcrop	outcrop	outcrop
Dip → Azimuth	-	-	-	-	-
Depth (m)	-	-	-	-	-
Rock Type	quartz-feldspar porphyry	quartz-feldspar porphyry	quartz-feldspar porphyry	quartz-feldspar porphyry	quartz-feldspar porphyry
Trend	central	central	central	central	central
Unit	Edwards Porphyry	Edwards Porphyry	Edwards Porphyry	Edwards Porphyry	Edwards Porphyry
SiO2	69.47	68.52	70.56	72.05	70.19
TiO2	0.22	0.2	0.2	0.23	0.24
Al2O3	14.93	15.19	15.45	15.33	14.94
Fe2O3	1.34	1.52	1.7	1.26	1.42
MnO	0.03	0.03	0.06	0.01	0.03
MgO	0.62	0.61	0.69	0.53	1.22
CaO	2.75	3.2	1.31	1.04	0.36
Na2O	3.77	4.32	2.98	4.33	9.51
K2O	2.96	2.46	3.48	2.67	0.11
P2O5	0.07	0.08	0.08	0.08	0.08
Cr	-	-	-	-	-
LOI	3.37	3.71	2.77	1.98	0.83
Total	99.52	99.82	99.28	99.5	98.91
Cr	-	-	-	-	-
Ni	-	-	-	-	-
V	-	-	-	-	-
Ni	11	8	20	12	13
Cr	-	-	-	-	-
Co	4	4	7	5	5
V	21.4	21	22.6	22.3	16.4
Sc	2.1	2.1	2.2	2	2.1
Cu	N.D.	3	N.D.	N.D.	8
Zn	23	21	22	12	28
Cd	-	-	-	-	-
Mo	N.D.	N.D.	N.D.	N.D.	N.D.
W	11	6	9	8	5
S	-	-	-	-	-
Be	0.52	0.51	0.57	0.49	0.22
Li	-	-	-	-	-
Cs	0.444	0.23	0.55	0.354	4.346
Rb	71.16	51.24	82.9	66.68	4.83
Ba	-	-	-	-	-
Sr	57.7	76.6	45.2	61.4	36.3
Nb	N.D.	N.D.	N.D.	N.D.	N.D.
Y	3	2	4	2	2
Zr	96	93	97	95	100
Zr	105.3	103.9	107.8	103.4	107.6
Hf	2.8	2.9	2.9	2.8	2.9
Nb	1.5	1.4	1.6	1.5	1.5
Ta	N.D.	N.D.	N.D.	N.D.	N.D.
Y	2.86	2.79	4.25	2.48	2.62
Th	1.88	1.87	2.04	2.02	1.99
U	0.642	0.668	0.505	0.656	0.654
La	9.92	10.12	11.44	10.34	7.29
Ce	19.16	19.06	20.6	19.62	15.19
Pr	2.19	2.211	2.46	2.261	1.901
Nd	8.36	8.23	9.24	8.43	7.5
Sm	1.54	1.55	1.66	1.46	1.41
Eu	0.404	0.424	0.456	0.373	0.354
Gd	1.181	1.208	1.355	1.036	1.028
Tb	0.125	0.129	0.142	0.11	0.118
Dy	0.588	0.586	0.709	0.533	0.574
Ho	0.102	0.099	0.131	0.092	0.098
Er	0.263	0.266	0.346	0.248	0.276
Tm	0.036	0.038	0.048	0.035	0.038
Yb	0.24	0.25	0.3	0.24	0.31
Lu	0.037	0.037	0.045	0.036	0.038

Table 2.3. Geochemical data for rocks of the porphyry intrusion suite examined within this project.

Sample	03-PJM-045	03-PJM-084	03-PJM-105	04-PJM-230	04-PJM-231
UTME_nad27	479,537	479,624	479,700	479,929	479,861
UTMN_nad27	5,366,340	5,366,539	5,366,480	5,365,581	5,365,544
Hole Number	outcrop	outcrop	outcrop	outcrop	outcrop
Dip → Azimuth	-	-	-	-	-
Depth (m)	-	-	-	-	-
Rock Type	quartz-feldspar porphyry	quartz-feldspar porphyry	quartz-feldspar porphyry	quartz-feldspar porphyry	quartz-feldspar porphyry
Trend	central	central	central	central	central
Unit	Edwards Porphyry	Edwards Porphyry	Edwards Porphyry	Buffalo Ankerite #5 Porphyry	Buffalo Ankerite #5 Porphyry
SiO2	66.74	69.53	65.59	63.09	65.77
TiO2	0.28	0.21	0.24	0.25	0.2
Al2O3	16.1	14.37	15.05	14.96	13.85
Fe2O3	1.96	1.46	1.86	2.05	1.76
MnO	0.05	0.03	0.09	0.029	0.058
MgO	1.35	0.67	1.07	2.1	0.67
CaO	1.67	3.34	4.92	0.15	1.96
Na2O	9.14	4.63	3.59	7.66	2.81
K2O	0.07	1.63	2.32	0.1	2.52
P2O5	0.08	0.07	0.07	0.08	0.09
Cr	-	-	-	N.D.	N.D.
LOI	1.8	3.74	5.11	9.8935	10.6592
Total	99.22	99.68	99.92	100.3525	100.3372
Cr	-	-	-	N.D.	35
Ni	-	-	-	N.D.	19
V	-	-	-	37	23
Ni	8	9	6	10	24
Cr	-	-	-	9.67	34.18
Co	10	5	4	8	6
V	30	19.2	27	31.7	22
Sc	2.7	2	2.3	2.9	2.4
Cu	5	N.D.	N.D.	N.D.	N.D.
Zn	68	43	51	5	N.D.
Cd	-	-	-	N.D.	N.D.
Mo	N.D.	N.D.	N.D.	N.D.	N.D.
W	6	4	2	N.D.	N.D.
S	-	-	-	>400	N.D.
Be	0.4	0.42	0.4	0.28	0.48
Li	-	-	-	15	3
Cs	0.028	1.149	1.35	0.041	2.22
Rb	0.8	45.87	53.66	0.28	71.85
Ba	-	-	-	26	677
Sr	78.7	158.5	84.7	30.9	79.6
Nb	N.D.	N.D.	N.D.	N.D.	N.D.
Y	2	2	3	7	7
Zr	73	92	66	80	98
Zr	79.3	104.5	71.8	79.1	102
Hf	2.2	2.9	2	2.2	2.7
Nb	1.9	1.7	1.7	2	1.6
Ta	0.17	N.D.	N.D.	N.D.	N.D.
Y	3.48	2.89	3.32	3.48	3.39
Th	0.95	1.82	0.83	0.98	1.86
U	0.349	0.594	0.305	0.335	0.564
La	6.16	9	4.54	6.06	9.52
Ce	12.96	17.05	9.68	12.96	17.82
Pr	1.617	2.01	1.22	1.616	2.076
Nd	6.72	7.67	5.22	6.44	8.15
Sm	1.35	1.42	1.06	1.32	1.47
Eu	0.338	0.375	0.306	0.366	0.415
Gd	1.085	1.109	0.901	1.101	1.119
Tb	0.136	0.122	0.114	0.14	0.133
Dy	0.718	0.613	0.63	0.696	0.659
Ho	0.133	0.109	0.126	0.131	0.116
Er	0.364	0.277	0.349	0.354	0.314
Tm	0.049	0.039	0.05	0.05	0.043
Yb	0.35	0.25	0.32	0.33	0.3
Lu	0.049	0.038	0.047	0.049	0.041

Table 2.3. Geochemical data for rocks of the porphyry intrusion suite examined within this project.

Sample	04-PJM-233	04-PJM-253	03-PJM-133a	03-PJM-133f	03-PJM-134d
UTME_nad27	474,544	473,806	477,733	477,733	477,495
UTMN_nad27	5,363,207	5,363,103	5,369,696	5,369,696	5,369,818
Hole Number	outcrop	outcrop	PJV # MC02-24	PJV # MC02-24	PJV # MC02-23
Dip → Azimuth	-	-	62 → 335	62 → 335	62 → 335
Depth (m)	-	-	512	663	233
Rock Type	quartz-feldspar porphyry	granodiorite	quartz-feldspar porphyry	quartz-feldspar porphyry	quartz-feldspar porphyry
Trend	central	central	northern	northern	northern
Unit	Naybob Porphyry	Porphyry Hill Granodiorite	Gillies Lake Porphyry	Gillies Lake Porphyry	Gillies Lake Porphyry
SiO2	67.09	66.75	64.73	64.11	59.7
TiO2	0.23	0.24	0.33	0.36	0.43
Al2O3	13.84	12.77	16.06	15.25	19.64
Fe2O3	1.35	0.87	3.03	3.95	2.86
MnO	0.006	0.008	0.06	0.07	0.05
MgO	0.42	0.12	1.2	1.62	1.09
CaO	0.2	0.23	3.87	3.69	2.53
Na2O	5.62	5.79	4.68	5.76	9.97
K2O	1.83	1.7	2.05	1.26	0.53
P2O5	0.12	0.15	0.14	0.14	0.21
Cr	N.D.	0.01	-	-	-
LOI	9.5788	11.2975	3.73	3.58	2.07
Total	100.2748	99.9355	99.87	99.79	99.08
Cr	9	88	-	-	-
Ni	N.D.	4	-	-	-
V	21	19	-	-	-
Ni	5	11	15	15	19
Cr	9.31	97.52	-	-	-
Co	4	6	10	10	12
V	19.7	13.2	39.9	36.3	47.6
Sc	1.8	1.4	3.3	4.2	3.7
Cu	6	37	N.D.	N.D.	N.D.
Zn	N.D.	N.D.	310	49	41
Cd	N.D.	N.D.	-	-	-
Mo	N.D.	N.D.	N.D.	N.D.	N.D.
W	N.D.	5	3	4	N.D.
S	231	109	-	-	-
Be	1.04	0.75	0.59	0.6	0.46
Li	6	3	-	-	-
Cs	1.013	0.364	1.13	0.515	0.151
Rb	49.21	33.18	59.5	33.68	10.73
Ba	506	584	-	-	-
Sr	286.7	415.1	253.6	202.5	326.1
Nb	3	6	2	2	3
Y	7	5	6	8	5
Zr	139	175	107	107	139
Zr	141.4	183.5	112.3	114	145.8
Hf	3.8	4.2	3	3	3.8
Nb	3	3.1	3.5	3.6	4.1
Ta	N.D.	N.D.	0.26	0.24	0.28
Y	3.83	2.89	5.83	8.87	6.2
Th	4.45	8.52	2.5	2.47	3.42
U	1.499	1.467	0.838	0.835	0.958
La	28.49	51.55	14.35	15.87	14.94
Ce	60.53	101.85	29.36	32.05	32.51
Pr	7.269	10.755	3.58	4.009	4.034
Nd	27.5	36.31	14.18	16.5	16.04
Sm	4.29	4.58	2.42	3.08	2.86
Eu	1	1.039	0.618	0.792	0.814
Gd	2.371	2.145	1.837	2.627	2.187
Tb	0.231	0.188	0.203	0.314	0.251
Dy	0.926	0.734	1.065	1.659	1.262
Ho	0.142	0.102	0.212	0.324	0.23
Er	0.325	0.228	0.593	0.931	0.647
Tm	0.043	0.026	0.092	0.136	0.093
Yb	0.27	0.17	0.63	0.95	0.67
Lu	0.037	0.021	0.099	0.151	0.112

Table 2.3. Geochemical data for rocks of the porphyry intrusion suite examined within this project

Sample	03-PJM-134e	03-PJM-132e	03-PJM-132f	03-PJM-132g	03-PJM-132n
UTME_nad27	477,495	478,103	478,103	478,103	478,103
UTMN_nad27	5,369,818	5,369,503	5,369,503	5,369,503	5,369,503
Hole Number	PJV # MC02-23	PJV # MC03-39	PJV # MC03-39	PJV # MC03-39	PJV # MC03-39
Dip → Azimuth	62 → 335	45 → 160	45 → 160	45 → 160	45 → 160
Depth (m)	241	155	77	175	310
Rock Type	quartz-feldspar porphyry	quartz-sericite schist	quartz-sericite schist	quartz-sericite schist	quartz-sericite schist
Trend	northern	northern	northern	northern	northern
Unit	Gillies Lake Porphyry	Pearl Lake Porphyry	Pearl Lake Porphyry	Pearl Lake Porphyry	Pearl Lake Porphyry
SiO2	61.26	65.02	66.19	38.86	66.33
TiO2	0.33	0.39	0.4	0.56	0.35
Al2O3	14.88	16.98	16.28	26.3	15.73
Fe2O3	2.62	3.36	4.51	7.65	3.95
MnO	0.07	0.03	0.03	0.06	0.06
MgO	0.7	1.39	2.59	3.01	1.96
CaO	6.87	2.14	0.92	4.72	2.61
Na2O	3.64	0.56	0.98	0.51	1.05
K2O	2.44	4.45	2.9	7	2.56
P2O5	0.14	0.21	0.1	0.2	0.12
Cr	-	-	-	-	-
LOI	5.64	4.47	4.6	7.29	5.46
Total	98.57	99.01	99.49	96.16	100.17
Cr	-	-	-	-	-
Ni	-	-	-	-	-
V	-	-	-	-	-
Ni	18	26	13	31	18
Cr	-	-	-	-	-
Co	11	21	13	14	9
V	38.3	33.8	36.6	79.6	37.9
Sc	3.4	2.5	2.4	4.7	3.4
Cu	14	5	53	219	32
Zn	2668	21	87	43	58
Cd	-	-	-	-	-
Mo	N.D.	N.D.	N.D.	8	N.D.
W	N.D.	N.D.	3	11	N.D.
S	-	-	-	-	-
Be	0.55	0.57	0.59	1.35	0.49
Li	-	-	-	-	-
Cs	1.141	1.652	2.56	2.075	1.63
Rb	72.76	96.4	66.14	107.42	59.33
Ba	-	-	-	-	-
Sr	232.9	127.7	143.2	92.6	84.7
Nb	2	3	3	4	2
Y	10	8	7	10	9
Zr	105	114	108	186	107
Zr	107.4	125	124	192.1	122.4
Hf	2.8	3.3	3.2	5	3.2
Nb	3.4	4	3.6	5.5	3.5
Ta	0.26	0.26	0.25	0.41	0.25
Y	10.81	7.61	6.66	9.25	8.62
Th	2.66	3.21	2.6	4.16	2.51
U	0.887	1.941	1.014	1.714	1.041
La	21.92	18.51	19.89	30.36	12.4
Ce	45.54	39.98	40.82	61.62	26.01
Pr	5.699	4.885	4.95	7.151	3.202
Nd	23.23	19.69	19.48	26.05	13.02
Sm	4.21	3.37	3.27	4.29	2.4
Eu	0.938	0.985	0.962	1.108	0.713
Gd	3.394	2.546	2.266	3.188	2.234
Tb	0.383	0.293	0.257	0.365	0.299
Dy	1.979	1.462	1.322	1.884	1.663
Ho	0.373	0.286	0.244	0.362	0.309
Er	0.969	0.775	0.713	1.048	0.85
Tm	0.135	0.108	0.101	0.161	0.119
Yb	0.84	0.71	0.7	1.13	0.75
Lu	0.125	0.111	0.107	0.179	0.112

Table 2.3. Geochemical data for rocks of the porphyry intrusion suite examined within this project.

Sample	03 -JM-139d	03-PJM-139e	03-PJM-139h	03-PJM-139i	03-PJM-139j
UTME_nad27	478,435	478,435	478,435	478,435	478,435
UTMN_nad27	5,369,481	5,369,481	5,369,481	5,369,481	5,369,481
Hole Number	PJV # MC03-41	PJV # MC03-41	PJV # MC03-41	PJV # MC03-41	PJV # MC03-41
Dip → Azimuth	45 → 160	45 → 160	45 → 160	45 → 160	45 → 160
Depth (m)	85	89	234	248	253
Rock Type	quartz-sericite schist	quartz-sericite schist	quartz-sericite schist	quartz-sericite schist	quartz-sericite schist
Trend	northern	northern	northern	northern	northern
Unit	Pearl Lake Porphyry	Pearl Lake Porphyry	Pearl Lake Porphyry	Pearl Lake Porphyry	Pearl Lake Porphyry
SiO2	64.59	66.67	66.67	66.24	74.39
TiO2	0.37	0.4	0.38	0.47	0.43
Al2O3	16.28	17.51	17.13	18.01	18.6
Fe2O3	5.95	4.5	3.64	6.18	0.57
MnO	0.02	N.D.	0.07	0.07	N.D.
MgO	1.1	0.37	1.31	2.72	0.04
CaO	1.39	0.28	2.98	0.47	0.3
Na2O	0.72	0.74	1.19	0.67	0.75
K2O	3.51	4.1	2.21	2	1.48
P2O5	0.13	0.19	0.15	0.18	0.16
Cr	-	-	-	-	-
LOI	4.93	4.43	4.77	3.63	3.37
Total	98.99	99.19	100.51	100.64	100.09
Cr	-	-	-	-	-
Ni	-	-	-	-	-
V	-	-	-	-	-
Ni	22	18	18	26	7
Cr	-	-	-	-	-
Co	22	16	12	16	8
V	47.4	53.1	45.4	49.4	53.5
Sc	3.7	4.1	3.6	2.5	4.1
Cu	114	9	3	17	N.D.
Zn	29	16	144	238	3
Cd	-	-	-	-	-
Mo	N.D.	N.D.	N.D.	N.D.	N.D.
W	N.D.	4	2	5	N.D.
S	-	-	-	-	-
Be	0.52	0.57	0.62	0.45	0.25
Li	-	-	-	-	-
Cs	1.603	1.728	2.346	1.503	1.8
Rb	60.26	86.78	40.44	38.44	33.48
Ba	-	-	-	-	-
Sr	56.6	66.4	217.4	131.6	134.8
Nb	3	3	2	3	3
Y	7	9	7	9	9
Zr	109	123	117	130	124
Zr	118	131.6	125.9	147.2	135.3
Hf	3	3.4	3.3	3.8	3.5
Nb	4.1	4.4	3.8	5.3	4.5
Ta	0.26	0.28	0.25	0.32	0.29
Y	6.8	9.22	7.18	8.61	9.75
Th	2.42	2.89	2.61	2.72	3.04
U	1.01	1.003	0.919	1.389	0.935
La	13.26	23.66	15.77	17.11	24.71
Ce	28.32	48.48	34	37.14	49.48
Pr	3.529	5.86	4.267	4.614	5.886
Nd	13.74	22.8	16.86	18.55	22.78
Sm	2.47	3.87	3.08	3.28	3.84
Eu	0.738	1.023	0.869	0.868	1.037
Gd	2.056	2.775	2.262	2.538	2.958
Tb	0.253	0.327	0.275	0.305	0.372
Dy	1.359	1.781	1.389	1.703	1.946
Ho	0.249	0.334	0.257	0.324	0.352
Er	0.735	0.932	0.722	0.882	0.986
Tm	0.107	0.134	0.105	0.131	0.144
Yb	0.73	0.9	0.68	0.84	0.94
Lu	0.115	0.134	0.107	0.129	0.146

Table 2.3. Geochemical data for rocks of the porphyry intrusion suite examined within this project.

Sample	03-PJM-140a	03-PJM-140b	03-PJM-140c	03-PJM-140h	03-PJM-140i
UTME_nad27	478,283	478,283	478,283	478,283	478,283
UTMN_nad27	5,369,546	5,369,546	5,369,546	5,369,546	5,369,546
Hole Number	PJV # MC03-02	PJV # MC03-02	PJV # MC03-02	PJV # MC03-02	PJV # MC03-02
Dip → Azimuth	50 → 160	50 → 160	50 → 160	50 → 160	50 → 160
Depth (m)	45	67	125	92	98
Rock Type	quartz-sericite schist	quartz-sericite schist	quartz-sericite schist	quartz-sericite schist	quartz-sericite schist
Trend	northern	northern	northern	northern	northern
Unit	Pearl Lake Porphyry	Pearl Lake Porphyry	Pearl Lake Porphyry	Pearl Lake Porphyry	Pearl Lake Porphyry
SiO2	59.1	60.34	61.52	58.27	55.38
TiO2	0.37	0.39	0.37	0.36	0.46
Al2O3	15.62	15.81	15.52	13.92	19.44
Fe2O3	6.98	7.53	5.8	9.77	7.37
MnO	0.1	0.13	0.05	0.04	0.04
MgO	1.93	2.61	1.91	1.9	1.58
CaO	3.42	1.9	2.58	3.36	2.51
Na2O	0.39	0.46	0.26	0.44	0.43
K2O	4.18	3.94	4.79	3.58	5.14
P2O5	0.17	0.17	0.19	0.18	0.19
Cr	-	-	-	-	-
LOI	6.44	7.06	6.88	6.83	6.22
Total	98.7	100.34	99.87	98.67	98.75
Cr	-	-	-	-	-
Ni	-	-	-	-	-
V	-	-	-	-	-
Ni	23	27	28	19	22
Cr	-	-	-	-	-
Co	18	14	14	47	25
V	44.8	52.7	53.3	45.1	54.4
Sc	4.1	4.5	4.5	3.8	3.9
Cu	314	114	5	160	1185
Zn	123	181	60	52	44
Cd	-	-	-	-	-
Mo	N.D.	N.D.	N.D.	N.D.	9
W	4	N.D.	7	14	25
S	-	-	-	-	-
Be	0.5	0.56	0.54	0.54	0.65
Li	-	-	-	-	-
Cs	2.42	2.322	2.511	1.688	1.909
Rb	113.28	104.72	120.64	64.9	85.11
Ba	-	-	-	-	-
Sr	70.7	64	44	61.2	49.1
Nb	3	2	3	2	3
Y	7	7	7	6	9
Zr	103	104	102	100	130
Zr	114.7	110.1	111.6	108.2	140.2
Hf	2.9	2.9	2.8	2.8	3.5
Nb	3.8	3.6	3.9	4	4.6
Ta	0.23	0.23	0.23	0.23	0.28
Y	7.38	7.48	7.12	7.14	8.27
Th	2.5	2.6	2.53	2.39	2.94
U	1.274	1.299	0.99	2.532	2.446
La	16.5	17.46	13.99	14.37	18.29
Ce	34.42	36.66	29.73	30.85	38.57
Pr	4.278	4.498	3.807	3.88	4.781
Nd	16.62	17.98	15.17	15.55	18.78
Sm	2.78	3.15	2.81	2.79	3.15
Eu	0.684	0.736	0.814	0.746	0.791
Gd	2.16	2.385	2.259	2.187	2.34
Tb	0.249	0.274	0.269	0.258	0.283
Dy	1.349	1.435	1.412	1.432	1.549
Ho	0.256	0.265	0.254	0.268	0.3
Er	0.733	0.756	0.715	0.722	0.827
Tm	0.107	0.111	0.102	0.107	0.127
Yb	0.72	0.72	0.69	0.73	0.84
Lu	0.116	0.116	0.11	0.112	0.138

Table 2.3. Geochemical data for rocks of the porphyry intrusion suite examined within this project.

Sample	03-PJM-143c	03-PJM-143e	03-PJM-143h	03-PJM-143i	03-PJM-144b
UTME_nad27	477,464	477,464	477,464	477,464	478,347
UTMN_nad27	5,369,367	5,369,367	5,369,367	5,369,367	5,369,610
Hole Number	PJV # MC02-21	PJV # MC02-21	PJV # MC02-21	PJV # MC02-21	PJV # MC03-01
Dip → Azimuth	50 → 180	50 → 180	50 → 180	50 → 180	50 → 160
Depth (m)	76	127	239	383	424
Rock Type	quartz-sericite schist	quartz-sericite schist	quartz-sericite schist	quartz-sericite schist	Internal porphyry breccia
Trend	northern	northern	northern	northern	northern
Unit	Pearl Lake Porphyry	Pearl Lake Porphyry	Pearl Lake Porphyry	Pearl Lake Porphyry	Pearl Lake Porphyry
SiO2	67.78	72.5	74.77	75.04	64.07
TiO2	0.36	0.39	0.4	0.39	0.38
Al2O3	17.68	18.37	16.46	17.42	16.86
Fe2O3	4.48	0.7	0.76	0.14	3.59
MnO	N.D.	N.D.	N.D.	N.D.	0.03
MgO	0.54	0.07	0.1	0.12	1.54
CaO	0.22	0.31	0.19	0.15	3.12
Na2O	0.61	1.26	0.64	1.04	1.89
K2O	4.24	2.34	3.9	3.68	1.91
P2O5	0.14	0.18	0.16	0.12	0.16
Cr	-	-	-	-	-
LOI	4.42	3.48	2.55	2.35	5.38
Total	100.47	99.6	99.93	100.47	98.94
Cr	-	-	-	-	-
Ni	-	-	-	-	-
V	-	-	-	-	-
Ni	19	N.D.	4	N.D.	15
Cr	-	-	-	-	-
Co	10	1	4	1	27
V	51.1	42	46.6	56.2	46
Sc	3.9	2.6	2.9	4.4	3.6
Cu	13	N.D.	3	N.D.	138
Zn	30	7	1439	8	38
Cd	-	-	-	-	-
Mo	N.D.	N.D.	N.D.	N.D.	N.D.
W	3	2	N.D.	7	3
S	-	-	-	-	-
Be	0.42	0.37	0.39	0.57	0.58
Li	-	-	-	-	-
Cs	1.395	2.863	1.731	1.964	2.381
Rb	72.31	43.19	72.38	76.29	50.38
Ba	-	-	-	-	-
Sr	114.2	382.8	102.8	235.7	240
Nb	3	2	3	3	2
Y	7	5	6	4	7
Zr	109	119	106	119	123
Zr	121.3	125.6	120.1	127.7	141.4
Hf	3.2	3.3	3.1	3.3	3.5
Nb	3.6	3.8	3.7	3.8	4.3
Ta	0.23	0.24	0.23	0.24	0.28
Y	7.8	4.89	6.35	4.85	8.45
Th	2.44	2.58	2.58	3.42	2.61
U	0.864	0.743	0.747	0.674	0.772
La	15.7	15.33	10.56	11.51	16.03
Ce	33.49	32.72	24.03	21.77	34.11
Pr	4.048	3.989	3.173	2.563	4.261
Nd	15.94	15.94	13.47	10.05	16.78
Sm	2.78	3.05	2.92	1.88	3.09
Eu	1.152	1.074	0.89	0.811	0.949
Gd	2.082	2.13	2.21	1.455	2.371
Tb	0.286	0.21	0.252	0.154	0.291
Dy	1.582	1.031	1.25	0.8	1.592
Ho	0.293	0.18	0.221	0.156	0.295
Er	0.8	0.512	0.618	0.485	0.814
Tm	0.115	0.076	0.091	0.074	0.12
Yb	0.75	0.54	0.64	0.57	0.83
Lu	0.111	0.09	0.1	0.093	0.121

Table 2.3. Geochemical data for rocks of the porphyry intrusion suite examined within this project.

Sample	03-PJM-144f	03-PJM-144g	03-PJM-144i	03-PJM-150a	03-PJM-150b
UTME_nad27	478,347	478,347	478,347	476,559	476,559
UTMN_nad27	5,369,610	5,369,610	5,369,610	5,368,255	5,368,255
Hole Number	PJV # MC03-01	PJV # MC03-01	PJV # MC03-01	outcrop	outcrop
Dip → Azimuth	50 → 160	50 → 160	50 → 160	-	-
Depth (m)	312	261	214	-	-
Rock Type	quartz-sericite schist	quartz-sericite schist	quartz-sericite schist	quartz-feldspar porphyry	quartz-feldspar porphyry
Trend	northern	northern	northern	northern	northern
Unit	Pearl Lake Porphyry	Pearl Lake Porphyry	Pearl Lake Porphyry	Crown Porphyry	Crown Porphyry
SiO2	61.32	60.62	60.29	66.79	66.63
TiO2	0.36	0.36	0.37	0.34	0.33
Al2O3	16.37	15.32	15.83	16.09	16.08
Fe2O3	6.54	3.12	5.61	2.54	2.53
MnO	0.09	0.06	0.05	0.03	0.03
MgO	2.38	2.57	2.46	1.1	1.1
CaO	3.15	5.16	3.43	2.48	2.38
Na2O	0.77	1.01	0.42	5.91	5.94
K2O	2.89	3.09	4.21	1.48	1.49
P2O5	0.15	0.14	0.19	0.14	0.14
Cr	-	-	-	-	-
LOI	6.71	8.79	8.61	3.04	3
Total	100.74	100.23	101.48	99.94	99.65
Cr	-	-	-	-	-
Ni	-	-	-	-	-
V	-	-	-	-	-
Ni	17	14	18	11	12
Cr	-	-	-	-	-
Co	10	7	12	5	5
V	44	42.4	50.5	38.8	40.9
Sc	3.6	3.4	4	3.5	3.6
Cu	72	14	N.D.	N.D.	N.D.
Zn	123	51	89	49	50
Cd	-	-	-	-	-
Mo	8	N.D.	N.D.	N.D.	N.D.
W	N.D.	3	6	4	3
S	-	-	-	-	-
Be	0.49	0.37	0.49	0.51	0.51
Li	-	-	-	-	-
Cs	1.336	2.444	2.593	0.873	0.889
Rb	78.08	92.12	119.75	31.85	33.18
Ba	-	-	-	-	-
Sr	78.9	114	48.7	248.6	253.6
Nb	3	3	3	2	2
Y	7	8	8	5	6
Zr	112	114	99	108	110
Zr	130	120.5	122	115.4	117.2
Hf	3.3	3.1	3.1	3.1	3.1
Nb	4.3	4	3.7	3.6	3.8
Ta	0.28	0.26	0.23	0.24	0.24
Y	7.59	7.59	7.53	6.44	6.68
Th	2.7	2.62	2.58	2.68	2.72
U	1.132	0.966	1.491	0.796	0.791
La	22.85	21.36	16.47	16.3	16.59
Ce	46.28	44.34	34.53	33.8	34.75
Pr	5.393	5.207	4.276	4.116	4.237
Nd	20.38	20.28	16.3	15.95	15.98
Sm	3.31	3.48	2.73	2.73	2.8
Eu	0.94	0.966	0.797	0.708	0.727
Gd	2.39	2.575	2.091	1.984	2.078
Tb	0.274	0.297	0.25	0.232	0.241
Dy	1.462	1.525	1.385	1.251	1.28
Ho	0.262	0.274	0.265	0.235	0.236
Er	0.729	0.786	0.77	0.664	0.668
Tm	0.108	0.112	0.111	0.097	0.101
Yb	0.74	0.75	0.74	0.68	0.68
Lu	0.113	0.116	0.117	0.106	0.111

Table 2.3. Geochemical data for rocks of the porphyry intrusion suite examined within this project.

Sample	04-PJM-200	04-PJM-256	04-PJM-257	04-PJM-257 Pulp Duplicate	04-PJM-258
UTME_nad27	476,563	461,657	462,033	462,033	459,491
UTMN_nad27	5,368,243	5,361,212	5,360,669	5,360,669	5,358,728
Hole Number	outcrop	outcrop	outcrop	outcrop	LSG # TG03-10
Dip → Azimuth	-	-	-	-	45 → 180
Depth (m)	-	-	-	-	217
Rock Type	quartz-feldspar porphyry	quartz-feldspar porphyry	quartz-feldspar porphyry	quartz-feldspar porphyry	quartz-feldspar porphyry
Trend	northern	western	western	western	western
Unit	Crown Porphyry	Bristol Lake Porphyry	South Bristol Lake Porphyry	South Bristol Lake Porphyry	Holmer Porphyry
SiO2	58.57	61.87	62.26	62.37	52.35
TiO2	0.3	0.21	0.15	0.15	0.56
Al2O3	14.16	15.75	14.74	14.74	16.12
Fe2O3	2.1	1.69	1.64	1.65	5.22
MnO	0.042	0.026	0.023	0.025	0.087
MgO	0.94	0.89	0.81	0.82	3.18
CaO	2.13	2.21	2.78	2.74	3.94
Na2O	4.9	6.83	6.62	6.64	6.97
K2O	1.34	0.93	0.81	0.79	0.12
P2O5	0.14	0.08	0.05	0.05	0.69
Cr	0.01	N.D.	N.D.	N.D.	0.02
LOI	14.955	9.8745	10.1546	10.5413	11.0938
Total	99.587	100.3505	100.0276	100.5063	100.3508
Cr	31	31	23	15	151
Ni	6	4	N.D.	N.D.	81
V	47	33	21	22	77
Ni	13	11	8	-	82
Cr	32.7	36.29	18.9	-	123.99
Co	9	7	5	-	19
V	41.4	23.8	20.2	-	60.8
Sc	4	2.2	2.3	-	9.8
Cu	11	66	9	-	11
Zn	N.D.	4	N.D.	-	64
Cd	N.D.	N.D.	N.D.	-	N.D.
Mo	N.D.	N.D.	N.D.	-	N.D.
W	N.D.	N.D.	N.D.	-	5
S	172	366	76	-	>400
Be	0.58	0.57	0.42	-	1.48
Li	11	9	9	-	44
Cs	0.881	0.615	0.662	-	0.2
Rb	33.5	22.92	20.05	-	2.49
Ba	408	1165	205	-	267
Sr	257.6	398.3	284	-	1078.6
Nb	4	6	3	2	42
Y	10	5	6	5	35
Zr	112	69	50	51	486
Zr	117.5	71.1	51.4	-	532.8
Hf	3.1	2	1.4	-	13.7
Nb	4.2	1.8	1.6	-	20.9
Ta	0.24	N.D.	N.D.	-	0.9
Y	7.17	1.98	2.31	-	33.24
Th	2.8	0.71	0.43	-	35.81
U	0.735	0.252	0.176	-	9.086
La	17.34	5.03	3.52	-	>100.00
Ce	35.72	10.84	7.5	-	>200.00
Pr	4.27	1.357	0.951	-	>25.000
Nd	16.69	5.56	3.92	-	>100.00
Sm	2.88	1.01	0.77	-	26.64
Eu	0.722	0.297	0.309	-	>5.000
Gd	1.977	0.694	0.71	-	17.201
Tb	0.253	0.079	0.09	-	1.839
Dy	1.329	0.399	0.457	-	7.999
Ho	0.25	0.072	0.082	-	1.214
Er	0.737	0.194	0.211	-	2.704
Tm	0.105	0.027	0.031	-	0.342
Yb	0.72	0.19	0.19	-	2.1
Lu	0.115	0.027	0.029	-	0.28

Table 2.3. Geochemical data for rocks of the porphyry intrusion suite examined within this project.

Sample	04-PJM-259	04-PJM-261a	04-PJM-262	04-PJM-263	04-PJM-265
UTME_nad27	459,491	458,526	459,049	459,049	458,680
UTMN_nad27	5,358,728	5,358,056	5,359,313	5,359,313	5,357,015
Hole Number	LSG # TG03-10	LSG # TC03-06	LSG # TG04-48	LSG # TG04-48	outcrop
Dip → Azimuth	45 → 180	45 → 125	55 → 180	55 → 180	-
Depth (m)	221	334	69	79	-
Rock Type	quartz-feldspar porphyry	quartz-feldspar porphyry	quartz-feldspar porphyry	quartz-feldspar porphyry	syenite
Trend	western	western	western	western	western
Unit	Holmer Porphyry	Thunder Creek Syenite Dyke	Holmer Porphyry	Holmer Porphyry	Southwest Bristol Syenite
SiO2	56.37	63.02	56.5	59.27	61.18
TiO2	0.45	0.08	0.31	0.29	0.28
Al2O3	13.03	14.01	18.72	17.07	17.24
Fe2O3	4.41	0.59	2.41	1.46	2.62
MnO	0.113	0.014	0.033	0.021	0.051
MgO	2.86	0.06	1.13	0.69	0.56
CaO	6.53	1.34	0.75	1.4	3.12
Na2O	5.34	5.13	8.74	8.97	4.51
K2O	0.13	4.85	0.7	0.49	0.81
P2O5	0.54	0.03	0.14	0.12	0.13
Cr	0.01	N.D.	N.D.	N.D.	N.D.
LOI	10.4202	11.0817	10.724	10.5739	10.0276
Total	100.2032	100.1957	100.147	100.3449	100.5186
Cr	127	40	22	44	24
Ni	73	N.D.	15	16	15
V	88	13	37	36	65
Ni	70	N.D.	22	19	21
Cr	96.71	45.82	29.12	44.18	28.88
Co	15	3	8	3	8
V	66.4	5.5	31.6	30	55.3
Sc	8.8	0.7	2.9	2.9	5
Cu	15	4	3	N.D.	N.D.
Zn	45	N.D.	N.D.	N.D	N.D.
Cd	N.D.	N.D.	N.D.	N.D.	N.D.
Mo	N.D.	N.D.	N.D.	N.D.	N.D.
W	N.D	6	N.D.	N.D.	50
S	383	>400	66	58	>400
Be	1.48	0.98	0.54	0.4	0.48
Li	34	N.D.	21	15	8
Cs	0.221	0.749	0.562	0.406	0.549
Rb	3.41	59.51	22.85	11.02	103.32
Ba	361	>1400	168	107	>1400
Sr	>1200.0	621.6	442.3	169.3	504.3
Nb	44	14	9	N.D	18
Y	29	8	7	10	19
Zr	357	120	83	65	228
Zr	381.3	125.7	87	63.1	248.7
Hf	10	4	2.3	1.7	6.6
Nb	14.6	4	2.9	2.2	11.1
Ta	0.67	0.2	0.17	N.D.	0.48
Y	27.12	5.32	3.05	7.74	16.64
Th	24.1	5.65	1.02	0.51	22.55
U	4.71	2.93	0.289	0.172	4.24
La	91.43	2.85	6.02	5.3	65.77
Ce	>200.00	7.64	13.39	11.84	158.2
Pr	>25.000	1.13	1.702	1.521	20.134
Nd	>100.00	5.25	7.12	6.52	79.55
Sm	20.22	1.38	1.32	1.52	13.22
Eu	4.918	0.462	0.398	0.494	3.12
Gd	13.744	1.304	0.929	1.458	8.217
Tb	1.499	0.179	0.122	0.21	0.855
Dy	6.561	0.902	0.642	1.223	3.737
Ho	1.016	0.163	0.116	0.244	0.59
Er	2.302	0.446	0.308	0.632	1.443
Tm	0.287	0.064	0.041	0.077	0.192
Yb	1.79	0.42	0.27	0.44	1.25
Lu	0.234	0.066	0.043	0.059	0.177

Table 2.3. Geochemical data for rocks of the porphyry intrusion suite examined within this project.

Sample	04-PJM-275	04-PJM-276	04-PJM-277	04-PJM-278	04-PJM-283
UTME_nad27	464,871	464,871	464,871	464,871	464,871
UTMN_nad27	5,361,827	5,361,827	5,361,827	5,361,827	5,361,827
Hole Number	TX # BRS04-24	TX # BRS04-24	TX # BRS04-24	TX # BRS04-24	TX # BRS04-24
Dip → Azimuth	58.7 → 188.8	58.7 → 188.8	58.7 → 188.8	58.7 → 188.8	58.7 → 188.8
Depth (m)	44	65	89	98	248
Rock Type	quartz-feldspar porphyry	quartz-feldspar porphyry	quartz-feldspar porphyry	quartz-feldspar porphyry	quartz-feldspar porphyry
Trend	western	western	western	western	western
Unit	Bristol Twp. Porphyry	Bristol Twp. Porphyry	Bristol Twp. Porphyry	Bristol Twp. Porphyry	Bristol Twp. Porphyry
SiO2	59.41	58.21	61.02	60.21	54.53
TiO2	0.26	0.26	0.22	0.22	0.41
Al2O3	15.83	16.01	15.82	15.81	15.58
Fe2O3	3.34	2.94	3.02	2.4	5.17
MnO	0.041	0.045	0.036	0.033	0.113
MgO	1.12	1.22	0.96	0.91	3.43
CaO	3.4	3.82	2.47	2.27	5.45
Na2O	4.45	3.81	4.98	5.7	1.94
K2O	1.33	2.27	1.65	1.16	2.07
P2O5	0.1	0.1	0.08	0.08	0.2
Cr	N.D.	N.D.	N.D.	N.D.	0.01
LOI	10.8505	11.7139	10.0862	11.2924	11.459
Total	100.1215	100.3889	100.3322	100.0754	100.362
Cr	44	22	38	N.D.	112
Ni	6	8	N.D.	N.D.	90
V	36	39	31	28	76
Ni	15	15	9	8	82
Cr	44.39	19.42	28.44	9.91	85.75
Co	10	7	13	5	14
V	32.7	34.1	25.4	25.3	62
Sc	3.1	3.2	2.2	2.3	6.3
Cu	109	N.D.	16	N.D.	N.D.
Zn	N.D.	N.D.	N.D.	N.D.	20
Cd	N.D.	N.D.	N.D.	N.D.	N.D.
Mo	N.D.	N.D.	N.D.	N.D.	N.D.
W	3	N.D.	N.D.	N.D.	N.D.
S	>400	>400	>400	>400	69
Be	0.51	0.51	0.62	0.55	0.61
Li	11	9	9	9	19
Cs	0.469	0.879	0.835	0.928	1.084
Rb	27.83	47.45	38.32	29.64	44.69
Ba	242	407	444	324	531
Sr	548	335.8	336.4	373	317.6
Nb	12	5	5	6	7
Y	6	7	6	6	10
Zr	76	79	73	73	105
Zr	79.9	78.3	72.4	74.3	110
Hf	2.1	2.1	2	2	2.9
Nb	2.2	2.1	2.2	2.2	4
Ta	N.D.	N.D.	N.D.	N.D.	0.25
Y	3.2	3.15	2.54	2.53	6.28
Th	0.93	0.89	0.93	0.97	2.89
U	0.284	0.282	0.367	0.354	0.762
La	6.85	7.07	6.34	6.95	20.58
Ce	15.36	15.75	14.37	15.13	45.28
Pr	2.005	2.044	1.822	1.927	5.702
Nd	8.1	8.36	7.55	7.85	23.16
Sm	1.44	1.55	1.41	1.41	3.92
Eu	0.429	0.454	0.439	0.421	1.099
Gd	1.042	1.102	0.954	0.988	2.628
Tb	0.122	0.126	0.111	0.112	0.298
Dy	0.65	0.637	0.522	0.55	1.416
Ho	0.111	0.117	0.09	0.092	0.236
Er	0.304	0.303	0.24	0.244	0.601
Tm	0.044	0.043	0.032	0.033	0.079
Yb	0.3	0.3	0.22	0.23	0.51
Lu	0.043	0.043	0.032	0.032	0.072

Table 2.3. Geochemical data for rocks of the porphyry intrusion suite examined within this project

Sample	04-PJM-286	04-PJM-287	04-PJM-288	04-PJM-292	04-PJM-293
UTME_nad27	464,871	464,871	464,871	464,871	464,871
UTMN_nad27	5,361,827	5,361,827	5,361,827	5,361,827	5,361,827
Hole Number	TX # BRS04-24	TX # BRS04-24	TX # BRS04-24	TX # BRS04-24	TX # BRS04-24
Dip → Azimuth	58.7 → 188.8	58.7 → 188.8	58.7 → 188.8	58.7 → 188.8	58.7 → 188.8
Depth (m)	309	354	375	566	604
Rock Type	quartz-sericite schist	quartz-feldspar porphyry	quartz-feldspar porphyry	quartz-feldspar porphyry	quartz-feldspar porphyry
Trend	western	western	western	western	western
Unit	Bristol Twp. Porphyry	Bristol Twp. Porphyry	Bristol Twp. Porphyry	Bristol Twp. Porphyry	Bristol Twp. Porphyry
SiO2	58.64	59.21	60.44	58.69	58.73
TiO2	0.27	0.25	0.23	0.25	0.29
Al2O3	15.67	15.82	15.72	16.55	15.83
Fe2O3	3.2	1.72	1.45	2.33	3.14
MnO	0.088	0.071	0.06	0.055	0.094
MgO	1.87	1.13	0.94	1.26	1.52
CaO	4.46	4.4	3.57	2.66	4.28
Na2O	2.28	4.3	4.62	6.64	3.71
K2O	3.03	2.49	2.18	0.77	1.84
P2O5	0.11	0.1	0.11	0.11	0.09
Cr	N.D.	N.D.	N.D.	N.D.	N.D.
LOI	10.1548	10.9706	10.7838	11.0806	10.5769
Total	99.7628	100.4516	100.0938	100.3856	100.0909
Cr	32	28	N.D.	49	19
Ni	20	7	4	8	12
V	47	39	30	39	48
Ni	26	11	7	15	19
Cr	27.94	31.56	10.26	46.96	23.51
Co	10	4	4	6	11
V	35.8	27.2	24	34.8	43.5
Sc	3.5	2.2	1.9	3.2	3.9
Cu	8	N.D.	16	10	N.D.
Zn	N.D.	N.D.	N.D.	10	26
Cd	N.D.	N.D.	N.D.	N.D.	N.D.
Mo	N.D.	N.D.	N.D.	N.D.	N.D.
W	2	N.D.	N.D.	N.D.	N.D.
S	>400	>400	>400	>400	>400
Be	0.52	0.51	0.45	0.45	0.62
Li	11	3	4	12	12
Cs	1.537	1.465	1.723	0.675	1.768
Rb	65.1	56.67	47.24	19.69	50.2
Ba	822	693	548	121	304
Sr	198.2	316.3	347	398.3	279.5
Nb	1	4	6	7	3
Y	7	6	6	6	7
Zr	77	81	79	83	70
Zr	80.1	82.2	78.8	85.2	71.8
Hf	2.1	2.2	2.1	2.2	2
Nb	2.5	2.3	2.2	2.3	2.4
Ta	N.D.	N.D.	N.D.	N.D.	0.24
Y	3.06	2.27	2.02	3.06	3.27
Th	1.17	0.89	0.78	0.94	0.82
U	0.384	0.324	0.29	0.314	0.395
La	7.79	6.97	5.91	7.59	5.77
Ce	16.89	14.97	12.86	17.4	12.64
Pr	2.137	1.88	1.672	2.174	1.605
Nd	8.69	7.62	6.62	8.62	6.72
Sm	1.54	1.35	1.11	1.51	1.35
Eu	0.444	0.404	0.319	0.461	0.426
Gd	1.045	0.901	0.723	1.062	1
Tb	0.119	0.095	0.088	0.122	0.123
Dy	0.61	0.476	0.424	0.619	0.661
Ho	0.113	0.083	0.074	0.106	0.119
Er	0.327	0.227	0.185	0.307	0.314
Tm	0.045	0.03	0.027	0.043	0.047
Yb	0.29	0.2	0.18	0.28	0.32
Lu	0.045	0.031	0.027	0.044	0.046

Table 2.3. Geochemical data for rocks of the porphyry intrusion suite examined within this project

Sample	04-PJM-294	04-PJM-296	04-PJM-297	04-PJM-221	04-PJM-222
UTME_nad27	464,871	464,871	464,871	478,500	478,506
UTMN_nad27	5,361,827	5,361,827	5,361,827	5,363,889	5,363,513
Hole Number	TX # BRS04-24	TX # BRS04-24	TX # BRS04-24	outcrop	outcrop
Dip → Azimuth	58.7 → 188.8	58.7 → 188.8	58.7 → 188.8	-	-
Depth (m)	653	717	732	-	-
Rock Type	quartz-feldspar porphyry	quartz-feldspar porphyry	quartz-feldspar porphyry	quartz-feldspar porphyry	quartz-feldspar porphyry
Trend	western	western	western	southern	southern
Unit	Bristol Twp. Porphyry	Bristol Twp. Porphyry	Bristol Twp. Porphyry	Deloro Twp. Porphyry Dyke	Deloro Twp. Porphyry Dyke
SiO2	59.09	59.67	58.7	66.65	62.33
TiO2	0.26	0.29	0.31	0.21	0.32
Al2O3	15.82	15.81	16.64	13.93	14.72
Fe2O3	2.01	3.04	2.79	0.69	2.12
MnO	0.1	0.069	0.068	0.01	0.037
MgO	1.4	1.56	1.38	0.06	0.91
CaO	4.39	3.18	4.11	0.16	3.36
Na2O	4.18	5.4	4.77	8.2	3.25
K2O	1.69	0.86	1.06	0.08	2.11
P2O5	0.1	0.08	0.09	0.09	0.11
Cr	N.D.	N.D.	N.D.	N.D.	N.D.
LOI	11.0087	10.3259	10.0915	10.4649	11.0683
Total	100.0387	100.2749	99.9995	100.5349	100.3253
Cr	42	23	61	N.D.	38
Ni	7	10	15	4	9
V	36	50	52	8	39
Ni	14	19	19	9	15
Cr	37.29	29.08	54.72	13.82	27.6
Co	7	11	7	5	8
V	29.3	45.2	50.6	8.6	31.6
Sc	2.7	4.3	4.5	1	2.8
Cu	7	N.D.	N.D.	12	10
Zn	2	41	17	N.D.	13
Cd	N.D.	N.D.	N.D.	N.D.	N.D.
Mo	N.D.	N.D.	N.D.	N.D.	N.D.
W	N.D.	N.D.	N.D.	14	N.D.
S	>400	>400	>400	120	N.D.
Be	0.55	0.77	0.73	0.5	0.71
Li	11	13	15	1	28
Cs	1.63	0.91	1.16	0.053	2.47
Rb	43.04	22.7	28.99	0.47	73.01
Ba	319	162	229	132	593
Sr	322.8	442.3	415.7	193.1	172.4
Nb	5	9	8	N.D.	1
Y	6	7	7	7	9
Zr	75	72	74	135	121
Zr	75.7	75	78.6	133.4	134
Hf	2	2.1	2.2	3.7	3.7
Nb	2	2.6	2.7	3.2	5.5
Ta	N.D.	0.24	0.26	N.D.	0.45
Y	2.65	3.48	3.46	3.63	5.59
Th	0.79	0.86	0.84	4.1	3.04
U	0.265	0.367	0.432	1.521	1.259
La	6.59	5.24	5.42	26.93	17.26
Ce	14.02	11.34	11.73	56.84	34.96
Pr	1.737	1.489	1.569	6.888	4.228
Nd	7.06	6.29	6.54	26.09	15.86
Sm	1.26	1.26	1.37	4.15	2.78
Eu	0.347	0.404	0.435	0.92	0.742
Gd	0.875	1.003	1.065	2.31	1.93
Tb	0.103	0.128	0.133	0.218	0.244
Dy	0.532	0.699	0.7	0.903	1.137
Ho	0.099	0.13	0.133	0.132	0.194
Er	0.253	0.368	0.359	0.311	0.539
Tm	0.037	0.051	0.051	0.039	0.075
Yb	0.24	0.34	0.33	0.24	0.5
Lu	0.037	0.05	0.05	0.033	0.073

Table 2.3. Geochemical data for rocks of the porphyry intrusion suite examined within this project

Sample	04-PJM-223	04-PJM-224	04-PJM-225	03-PJM-153	04-PJM-227
UTME_nad27	478,567	478,574	478,628	492,142	490,744
UTMN_nad27	5,363,333	5,363,112	5,362,883	5,364,796	5,365,416
Hole Number	outcrop	outcrop	outcrop	outcrop	outcrop
Dip → Azimuth	-	-	-	-	-
Depth (m)	-	-	-	-	-
Rock Type	quartz-feldspar porphyry	quartz-feldspar porphyry	quartz-feldspar porphyry	quartz-feldspar porphyry	quartz-feldspar porphyry
Trend	southern	southern	southern	southern	southern
Unit	Deloro Twp. Porphyry Dyke	Deloro Twp. Porphyry Dyke	Deloro Twp. Porphyry Dyke	Mt. Logano Porphyry	Mt. Logano Porphyry
SiO2	59.24	60.27	61.15	68.83	66.87
TiO2	0.37	0.36	0.37	0.19	0.23
Al2O3	15.49	14.56	14.6	14.95	14.23
Fe2O3	3.04	2.84	2.89	1.74	0.38
MnO	0.054	0.044	0.077	0.04	0.014
MgO	1.75	1.85	1.5	0.7	0.36
CaO	1.87	3.03	2.57	3.47	1.6
Na2O	6	4.52	3.59	5	3.02
K2O	0.95	1.66	2.14	0.87	2.57
P2O5	0.11	0.11	0.12	0.07	0.07
Cr	N.D.	N.D.	N.D.	-	N.D.
LOI	11.305	10.9908	11.4366	3.85	10.9965
Total	100.169	100.2248	100.4336	99.72	100.3305
Cr	63	54	40	-	36
Ni	40	34	25	-	6
V	57	57	64	-	31
Ni	47	41	32	6	13
Cr	52.17	47.18	34.39	-	25.84
Co	14	13	8	4	8
V	47.3	48.8	44.9	12.9	25.3
Sc	5.3	5.2	4.8	1.6	2.8
Cu	N.D.	28	7	N.D.	N.D.
Zn	39	4	134	50	784
Cd	N.D.	N.D.	N.D.	-	N.D.
Mo	N.D.	N.D.	N.D.	N.D.	N.D.
W	N.D.	N.D.	N.D.	3	N.D.
S	N.D.	48	54	-	>400
Be	0.63	0.67	0.68	0.45	0.52
Li	45	25	16	-	9
Cs	2.393	2.985	2.782	0.203	0.963
Rb	25.36	50.08	65.18	18.28	48.39
Ba	464	612	769	-	552
Sr	139.6	192	150.4	166	198
Nb	N.D.	2	N.D.	2	N.D.
Y	10	10	9	3	7
Zr	129	109	118	88	107
Zr	133.4	109.8	120.9	91.4	108.1
Hf	3.6	3	3.3	2.7	3.1
Nb	4.6	4	4.1	3	2.8
Ta	0.34	0.29	0.31	0.24	0.21
Y	7.42	6.54	5.73	3.65	3.85
Th	3.16	2.78	3.24	1.26	1.79
U	1.043	0.908	1.127	0.49	0.793
La	17.46	15.81	16.39	19.33	13.65
Ce	35.84	32.09	34.58	2.252	27.15
Pr	4.313	3.781	4.185	8.66	3.131
Nd	16.63	14.97	16.23	1.56	11.88
Sm	3.07	2.77	2.93	0.385	2.03
Eu	0.843	0.746	0.759	1.175	0.562
Gd	2.253	2.042	2.026	N.D.	1.339
Tb	0.288	0.247	0.235	0.141	0.164
Dy	1.507	1.296	1.185	0.131	0.792
Ho	0.273	0.241	0.216	0.348	0.144
Er	0.774	0.663	0.585	N.D.	0.381
Tm	0.111	0.095	0.087	0.048	0.056
Yb	0.74	0.62	0.56	0.32	0.38
Lu	0.114	0.099	0.085	N.D.	0.056

Table 2.3. Geochemical data for rocks of the porphyry intrusion suite examined within this project

Sample	04-PJM-228	03-PJM-141a	03-PJM-131g	03-PJM-141b	03-PJM-141f
UTME_nad27	490,678	489,964	490,035	489,964	489,964
UTMN_nad27	5,365,748	5,373,248	5,373,031	5,373,248	5,373,248
Hole Number	outcrop	PJV # 18986	PJV # 18985	PJV # 18986	PJV # 18986
Dip → Azimuth	-	50 → 162	50 → 162	50 → 162	50 → 162
Depth (m)	-	217	137	344	353
Rock Type	quartz-feldspar porphyry	lamprophyry	quartz-feldspar porphyry	quartz-feldspar porphyry	quartz-feldspar porphyry
Trend	southern	eastern	eastern	eastern	eastern
Unit	Mt. Logano Porphyry	Pamour Lamprophyre	Pamour Porphyry	Pamour Porphyry	Pamour Porphyry
SiO2	63.98	44.28	67.9	64.42	65.59
TiO2	0.18	0.64	0.31	0.3	0.31
Al2O3	14.35	10.29	15.24	15.04	16.5
Fe2O3	1.62	9.69	1.69	1.91	1.59
MnO	0.021	0.17	0.02	0.03	0.02
MgO	0.74	12.01	0.77	1.14	0.85
CaO	2.14	8.93	1.97	3.99	2.07
Na2O	4.33	3.28	6.26	7.6	8.18
K2O	1.68	3.92	3.4	1.88	2.54
P2O5	0.06	0.35	0.13	0.11	0.12
Cr	N.D.	-	-	-	-
LOI	10.6621	6.96	1.01	2.93	1.47
Total	99.7531	100.52	98.69	99.36	99.24
Cr	12	-	-	-	-
Ni	N.D.	-	-	-	-
V	15	-	-	-	-
Ni	7	163	12	22	22
Cr	10.99	-	-	-	-
Co	5	48	4	5	5
V	14.7	148.2	20.9	18.6	18.8
Sc	2	25.2	1.8	2	1.8
Cu	N.D.	N.D.	N.D.	N.D.	N.D.
Zn	N.D.	83	56	71	60
Cd	N.D.	-	-	-	-
Mo	N.D.	N.D.	N.D.	N.D.	N.D.
W	N.D.	7	N.D.	N.D.	2
S	N.D.	-	-	-	-
Be	0.61	0.83	1.17	1.14	1.12
Li	18	-	-	-	-
Cs	0.968	4.173	0.427	0.501	0.415
Rb	37.24	>150.00	71.28	44.85	46.58
Ba	470	-	-	-	-
Sr	232.6	213.2	1061.3	793.9	879.1
Nb	2	2	N.D.	N.D.	N.D.
Y	7	18	2	1	2
Zr	92	100	161	142	174
Zr	95	103.6	155.8	133	167.3
Hf	2.8	2.8	4.2	3.6	4.5
Nb	3.1	3.4	2.9	2.5	3
Ta	0.24	0.19	0.21	N.D.	0.2
Y	3.74	18.23	3.52	2.51	3.07
Th	1.34	3.17	5.46	4.76	6.14
U	0.47	0.941	1.749	1.395	1.895
La	12.38	25.5	34.81	27.54	33.05
Ce	25.41	57.86	71.54	57.03	68.01
Pr	3.013	7.706	8.613	6.753	8.113
Nd	11.17	32.8	32.76	24.97	30.84
Sm	1.92	6.33	4.94	3.69	4.7
Eu	0.506	1.242	1.178	0.903	1.118
Gd	1.336	5.301	2.79	2.098	2.583
Tb	0.158	0.688	0.235	0.166	0.202
Dy	0.774	3.65	0.882	0.605	0.78
Ho	0.138	0.708	0.124	0.086	0.107
Er	0.346	1.904	0.28	0.204	0.232
Tm	0.05	0.272	0.035	0.024	0.029
Yb	0.33	1.76	0.21	0.17	0.18
Lu	0.048	0.256	0.028	0.024	0.023

Table 2.3. Geochemical data for rocks of the porphyry intrusion suite examined within this project

Sample	04-PJM-229	04-PJM-299	04-PJM-299 Prep Duplicate (1)	04-PJM-299 Prep Duplicate (2)
UTME_nad27	489,709	???	???	???
UTMN_nad27	5,370,755	???	???	???
Hole Number	outcrop	Hoyle Pond Mine	Hoyle Pond Mine	Hoyle Pond Mine
Dip → Azimuth	-	-	-	-
Depth (m)	-	720m level	720m level	720m level
Rock Type	granodiorite	quartz-sericite schist	quartz-sericite schist	quartz-sericite schist
Trend	eastern	eastern	eastern	eastern
Unit	Bob's Lake Granodiorite	Hoyle Pond Porphyry	Hoyle Pond Porphyry	Hoyle Pond Porphyry
SiO2	64.5	54.03	53.87	53.96
TiO2	0.25	0.54	0.55	0.55
Al2O3	14.12	13.57	13.6	13.54
Fe2O3	1.31	5.01	4.93	4.93
MnO	0.024	0.091	0.095	0.093
MgO	0.45	4.59	4.56	4.6
CaO	1.51	5.58	5.63	5.6
Na2O	4.91	4.93	5.08	5.04
K2O	3.33	0.96	0.87	0.87
P2O5	0.15	0.15	0.15	0.14
Cr	0.01	0.03	0.04	0.03
LOI	9.2539	10.8124	10.866	10.866
Total	99.8179	100.2934	100.241	100.219
Cr	22	274	295	293
Ni	N.D.	106	107	106
V	15	134	134	135
Ni	5	106	-	-
Cr	33.54	226.25	-	-
Co	4	24	-	-
V	11.6	110.1	-	-
Sc	1.5	11.5	-	-
Cu	6	7	-	-
Zn	16	50	-	-
Cd	N.D.	N.D.	-	-
Mo	N.D.	N.D.	-	-
W	N.D.	5	-	-
S	>400	>400	-	-
Be	1.19	0.65	-	-
Li	32	22	-	-
Cs	1.055	0.877	-	-
Rb	72.89	24.65	-	-
Ba	>1400	698	-	-
Sr	767.3	173.7	-	-
Nb	20	1	1	1
Y	7	9	8	9
Zr	131	86	87	85
Zr	145.9	90.7	-	-
Hf	4.1	2.6	-	-
Nb	4.3	3.6	-	-
Ta	0.26	0.21	-	-
Y	3.09	6.21	-	-
Th	4.12	1	-	-
U	2.29	0.424	-	-
La	36.93	9.08	-	-
Ce	78.27	20	-	-
Pr	8.881	2.648	-	-
Nd	32.25	11.08	-	-
Sm	4.45	2.18	-	-
Eu	1.031	0.722	-	-
Gd	2.174	1.81	-	-
Tb	0.204	0.222	-	-
Dy	0.759	1.21	-	-
Ho	0.106	0.24	-	-
Er	0.251	0.673	-	-
Tm	0.031	0.099	-	-
Yb	0.2	0.65	-	-
Lu	0.026	0.098	-	-

Table 2.3. Geochemical data for rocks of the porphyry intrusion suite examined within this project

Sample	04-PJM-300	04-PJM-300 Pulp Duplicate	04-PJM-234	04-PJM-235	04-PJM-252
UTME_nad27	???	???	???	???	???
UTMN_nad27	???	???	???	???	???
Hole Number	Hoyle Pond Mine	Hoyle Pond Mine	EBM # A96-414	EBM # A96-414	EBM # 96-42
Dip → Azimuth	-	-	55 → 344	55 → 344	60 → 270
Depth (m)	720m level	720m level	66.5	117	81
Rock Type	quartz-sericite schist	quartz-sericite schist	feldspar porphyry	feldspar porphyry	feldspar porphyry
Trend	eastern	eastern	eastern	eastern	eastern
Unit	Hoyle Pond Porphyry	Hoyle Pond Porphyry	Aquarius Poprhyry	Aquarius Poprhyry	Aquarius Mine Porphyry
SiO2	55.52	55.22	66.17	57.85	54.96
TiO2	0.46	0.46	0.12	0.2	0.21
Al2O3	11.61	11.54	14.29	17.2	15.82
Fe2O3	4.84	4.84	0.95	1.44	1.56
MnO	0.106	0.106	0.016	0.019	0.03
MgO	4.57	4.58	0.22	0.61	3.33
CaO	8.34	8.24	1.83	2.04	3.9
Na2O	2.68	2.58	5.43	9.22	9.36
K2O	1.56	1.52	1.4	0.14	0.12
P2O5	0.1	0.11	0.05	0.05	0.05
Cr	0.03	0.03	0.01	N.D.	N.D.
LOI	10.1988	10.8066	9.9895	10.9623	10.7801
Total	100.0148	100.0326	100.4755	99.7213	100.1101
Cr	274	276	68	N.D.	23
Ni	83	86	N.D.	N.D.	41
V	129	126	13	18	12
Ni	91	-	N.D.	4	46
Cr	184.93	-	50	8.25	29.33
Co	19	-	3	5	8
V	93.7	-	11.8	19.8	11.8
Sc	9.8	-	1.6	2.1	3.8
Cu	8	-	N.D.	N.D.	20
Zn	71	-	177	N.D.	N.D.
Cd	4	-	N.D.	N.D.	N.D.
Mo	N.D.	-	N.D.	N.D.	N.D.
W	3	-	N.D.	N.D.	N.D.
S	>400	-	N.D.	85	>400
Be	0.52	-	0.59	0.29	0.15
Li	14	-	5	1	N.D.
Cs	1.277	-	0.629	0.072	0.032
Rb	39.24	-	40.57	1.55	0.31
Ba	1088	-	440	65	57
Sr	207	-	393.4	368.1	155.8
Nb	2	3	6	4	N.D.
Y	9	9	7	6	6
Zr	69	67	84	101	72
Zr	75	-	88.4	102.4	80
Hf	2	-	2.6	2.9	2.1
Nb	2.9	-	1.2	1.4	1.7
Ta	N.D.	-	N.D.	N.D.	N.D.
Y	6.31	-	2.94	2.46	3.18
Th	0.8	-	1.32	1.5	1.2
U	0.357	-	0.567	0.585	0.367
La	8.2	-	8.86	7.53	7.07
Ce	18.25	-	14.96	16.05	14.21
Pr	2.399	-	2.165	1.948	1.695
Nd	10.18	-	8.79	7.62	6.51
Sm	2.05	-	1.68	1.51	1.17
Eu	0.705	-	0.465	0.479	0.326
Gd	1.738	-	1.288	1.155	0.871
Tb	0.225	-	0.142	0.125	0.114
Dy	1.221	-	0.64	0.537	0.61
Ho	0.233	-	0.103	0.091	0.116
Er	0.626	-	0.288	0.24	0.319
Tm	0.092	-	0.039	0.034	0.044
Yb	0.61	-	0.24	0.23	0.29
Lu	0.09	-	0.035	0.035	0.044

Table 2.3. Geochemical data for rocks of the porphyry intrusion suite examined within this project.

Sample	04-PJM-243	04-PJM-244	04-PJM-245	04-PJM-238	04-PJM-239
UTME_nad27	???	???	???	???	???
UTMN_nad27	???	???	???	???	???
Hole Number	EBM # 97-68	EBM # 97-68	EBM # 97-68	EBM # 97-78	EBM # 97-78
Dip → Azimuth	55 → 344	55 → 344	55 → 344	55 → 344	55 → 344
Depth (m)	75.5	102.5	190	244.9	252.5
Rock Type	feldspar porphyry	feldspar porphyry	feldspar porphyry	feldspar porphyry	feldspar porphyry
Trend	eastern	eastern	eastern	eastern	eastern
Unit	Homestead Porphyry	Homestead Porphyry	Homestead Porphyry	Crowley Porphyry	Crowley Porphyry
SiO2	65.77	66.22	67.23	64.45	58.42
TiO2	0.17	0.11	0.11	0.12	0.15
Al2O3	13.12	13.16	13.02	14.36	16.93
Fe2O3	0.98	1.03	0.91	0.99	0.78
MnO	0.019	0.019	0.018	0.011	0.047
MgO	0.5	0.19	0.2	0.52	0.79
CaO	0.96	0.59	0.72	1.33	2.37
Na2O	7.77	7.79	7.75	5.88	9.01
K2O	0.22	0.1	0.09	1.63	0.64
P2O5	0.04	0.03	0.06	0.04	0.12
Cr	N.D.	N.D.	N.D.	N.D.	N.D.
LOI	10.8255	11.1111	10.2245	10.931	11.1214
Total	100.3645	100.3401	100.3225	100.252	100.3684
Cr	16	39	N.D.	50	12
Ni	N.D.	N.D.	N.D.	N.D.	N.D.
V	N.D.	N.D.	N.D.	17	5
Ni	4	N.D.	N.D.	7	5
Cr	12.9	41.2	10.32	31.95	11.31
Co	3	3	2	4	4
V	5.8	3.3	5.7	15.7	5.7
Sc	1.5	1.1	1.3	1.4	1.6
Cu	7	6	8	N.D.	N.D.
Zn	N.D.	16	N.D.	N.D.	N.D.
Cd	N.D.	N.D.	12	N.D.	N.D.
Mo	N.D.	N.D.	N.D.	N.D.	N.D.
W	N.D.	N.D.	N.D.	N.D.	7
S	>400	>400	>400	>400	>400
Be	0.63	0.67	0.54	0.84	0.44
Li	N.D.	N.D.	N.D.	4	N.D.
Cs	0.036	0.041	0.606	0.69	0.087
Rb	0.96	0.33	1.08	42.11	9.58
Ba	108	91	60	629	461
Sr	110.5	88.9	130.9	233.4	139.5
Nb	N.D.	N.D.	N.D.	N.D.	N.D.
Y	6	6	6	5	5
Zr	98	71	71	83	85
Zr	99.8	73.8	72.3	86.4	87.8
Hf	2.9	2.5	2.4	2.9	3
Nb	3.3	4.2	3.8	1.3	1.1
Ta	0.25	0.33	0.32	N.D.	N.D.
Y	2.56	2.74	3.17	1.65	1.83
Th	3.16	1.54	1.76	1.16	1.1
U	1.931	1.745	1.817	1.13	0.871
La	12.78	5.69	6.52	6.78	7.07
Ce	24.64	11.42	13.33	14.59	14.89
Pr	2.723	1.326	1.54	1.753	1.794
Nd	9.48	4.98	5.67	7.23	7.14
Sm	1.5	0.96	1.12	1.36	1.43
Eu	0.392	0.297	0.345	0.381	0.399
Gd	0.943	0.769	0.929	0.856	0.94
Tb	0.113	0.102	0.125	0.091	0.106
Dy	0.52	0.522	0.634	0.37	0.444
Ho	0.092	0.093	0.106	0.057	0.067
Er	0.237	0.238	0.259	0.135	0.152
Tm	0.036	0.033	0.037	0.019	0.019
Yb	0.24	0.22	0.22	0.13	0.13
Lu	0.034	0.028	0.03	0.018	0.017

Table 2.3. Geochemical data for rocks of the porphyry intrusion suite examined within this project.

Sample	04-PJM-241	04-PJM-248	04-PJM-249	04-PJM-251	03-PJM-142a
UTME_nad27	???	???	???	???	535.691
UTMN_nad27	???	???	???	???	5,383,412
Hole Number	EBM # C-02-2	EBM # P-00-2	EBM # P-00-2	EBM # P-00-2	PJV # CR02-1
Dip → Azimuth	50 → 342	60 → 344	60 → 344	60 → 344	50 → 180
Depth (m)	198	117.7	141.5	183	60
Rock Type	feldspar porphyry	feldspar porphyry	feldspar porphyry	feldspar porphyry	quartz-feldspar porphyry
Trend	eastern	eastern	eastern	eastern	eastern
Unit	Crowley Porphyry	Pominex Porphyry	Pominex Porphyry	Pominex Porphyry	Carr Twp. Porphyry
SiO2	57.29	66.13	66.33	63.78	68.59
TiO2	0.44	0.05	0.06	0.06	0.25
Al2O3	14.85	14.31	14.12	15.23	14.45
Fe2O3	3.72	1.31	0.96	1.01	1.82
MnO	0.059	0.003	0.01	0.014	N.D.
MgO	2.39	0.29	0.14	0.43	0.91
CaO	3.08	0.12	0.5	1.1	1.88
Na2O	6.52	6.02	6.94	8.82	5.52
K2O	1.26	1.35	0.86	0.07	1.98
P2O5	0.17	0.05	0.06	0.05	0.07
Cr	0.01	0.03	N.D.	N.D.	-
LOI	10.5294	10.6514	10.3734	9.8208	3.21
Total	100.3184	100.3144	100.3434	100.3748	98.7
Cr	62	58	11	49	-
Ni	34	N.D.	N.D.	N.D.	-
V	97	N.D.	N.D.	N.D.	-
Ni	43	N.D.	N.D.	6	13
Cr	52.84	41.11	7.37	64	-
Co	16	2	2	4	11
V	75.5	2.9	4	4.6	35.7
Sc	7.8	0.6	0.6	0.6	3.1
Cu	14	N.D.	N.D.	37	244
Zn	N.D.	N.D.	N.D.	N.D.	14
Cd	N.D.	N.D.	N.D.	N.D.	-
Mo	N.D.	N.D.	N.D.	N.D.	N.D.
W	N.D.	N.D.	N.D.	N.D.	8
S	>400	>400	>400	>400	-
Be	0.98	0.7	0.46	0.37	0.75
Li	5	2	1	2	-
Cs	0.216	0.327	0.275	0.055	0.889
Rb	23.35	37.77	20.8	0.82	58.36
Ba	>1400	473	373	67	-
Sr	322	68.9	78.9	120.6	328.3
Nb	4	N.D.	N.D.	N.D.	N.D.
Y	12	5	5	5	8
Zr	117	53	54	50	108
Zr	121.4	48.5	49.7	49.7	110.4
Hf	3.4	1.9	1.9	1.8	3.3
Nb	2.7	1.8	1.8	1.8	2.7
Ta	N.D.	N.D.	N.D.	N.D.	0.19
Y	8.69	2.02	1.97	2.11	8.89
Th	5.28	0.84	0.82	0.81	1.57
U	1.659	0.88	0.885	0.882	0.736
La	34.54	1.9	4.7	4.56	12.11
Ce	70.37	4.38	9.65	9.06	25.27
Pr	8.269	0.589	1.164	1.112	3.266
Nd	31.24	2.68	4.48	4.49	13.78
Sm	5.04	0.76	0.97	1	2.92
Eu	1.331	0.3	0.311	0.296	0.864
Gd	3.165	0.653	0.738	0.765	2.52
Tb	0.35	0.082	0.085	0.089	0.327
Dy	1.769	0.386	0.411	0.403	1.799
Ho	0.315	0.063	0.069	0.066	0.337
Er	0.886	0.165	0.155	0.156	0.97
Tm	0.128	0.021	0.021	0.021	0.136
Yb	0.85	0.12	0.13	0.13	0.88
Lu	0.124	0.017	0.018	0.018	0.136

Table 2.3. Geochemical data for rocks of the porphyry intrusion suite examined within this project

Sample	03-PJM-142f	03-PJM-142h	03-PJM-142i	03-PJM-142j	03-PJM-142x
UTME_nad27	535,691	535,691	535,691	535,691	535,691
UTMN_nad27	5,383,412	5,383,412	5,383,412	5,383,412	5,383,412
Hole Number	PJV # CR02-1	PJV # CR02-1	PJV # CR02-1	PJV # CR02-1	PJV # CR02-1
Dip → Azimuth	50 → 180	50 → 180	50 → 180	50 → 180	50 → 180
Depth (m)	100	120	134	143	250
Rock Type	quartz-feldspar porphyry	quartz-feldspar porphyry	quartz-feldspar porphyry	quartz-feldspar porphyry	quartz-feldspar porphyry
Trend	eastern	eastern	eastern	eastern	eastern
Unit	Carr Twp. Porphyry	Carr Twp. Porphyry	Carr Twp. Porphyry	Carr Twp. Porphyry	Carr Twp. Porphyry
SiO2	67.72	67.66	68.8	68.34	68.24
TiO2	0.27	0.28	0.26	0.27	0.26
Al2O3	15.04	15.17	14.67	15.06	14.76
Fe2O3	2.81	2.9	2.06	1.91	2.31
MnO	N.D.	0.01	N.D.	N.D.	N.D.
MgO	0.97	0.9	0.82	1.01	0.65
CaO	0.95	1.65	1.06	1.34	1.85
Na2O	4.53	5.7	4.93	3.49	8.19
K2O	5.52	2.45	4.8	3.47	0.5
P2O5	0.09	0.08	0.08	0.08	0.08
Cr	-	-	-	-	-
LOI	1.55	2.83	1.59	4.42	1.89
Total	99.45	99.66	99.09	99.4	98.74
Cr	-	-	-	-	-
Ni	-	-	-	-	-
V	-	-	-	-	-
Ni	16	13	11	13	9
Cr	-	-	-	-	-
Co	13	10	6	5	6
V	35.7	38.5	31	31.9	22.3
Sc	3.4	3.8	3.3	3.4	2.9
Cu	463	163	2187	595	293
Zn	19	15	12	12	9
Cd	-	-	-	-	-
Mo	N.D.	N.D.	N.D.	N.D.	58
W	N.D.	6	3	4	N.D.
S	-	-	-	-	-
Be	0.63	0.84	0.61	0.64	0.62
Li	-	-	-	-	-
Cs	1.874	1.179	0.707	0.775	0.265
Rb	89.23	65.35	63.33	63.52	12.87
Ba	-	-	-	-	-
Sr	263.7	332.1	190.1	144.7	276.4
Nb	N.D.	N.D.	N.D.	N.D.	N.D.
Y	8	9	9	5	9
Zr	105	106	98	103	106
Zr	108.3	112.5	110.1	113	108.9
Hf	3.2	3.3	3.2	3.3	3.2
Nb	2.8	2.8	2.9	2.5	3
Ta	0.19	0.19	0.19	0.18	0.19
Y	8.8	10.19	9.31	5.16	9.59
Th	1.58	1.62	1.55	1.63	1.41
U	1.079	0.804	1.084	1.083	1.059
La	8.28	8.79	5.74	7.22	14.16
Ce	19.63	19.63	14.4	17.32	31.67
Pr	2.787	2.692	1.99	2.134	4.174
Nd	12.04	12.12	8.96	8.53	17.34
Sm	2.88	3.08	2.32	1.64	3.77
Eu	0.732	0.964	0.72	0.544	0.862
Gd	2.595	2.814	2.339	1.459	3.088
Tb	0.321	0.377	0.318	0.172	0.375
Dy	1.792	2.032	1.821	0.98	2.046
Ho	0.324	0.375	0.342	0.191	0.37
Er	0.907	1.045	0.982	0.564	1.01
Tm	0.129	0.146	0.14	0.088	0.14
Yb	0.82	0.92	0.88	0.61	0.9
Lu	0.125	0.137	0.13	0.111	0.135

Table 2.3. Geochemical data for rocks of the porphyry intrusion suite examined within this project.

Sample	04-PJM-217 (1)	04-PJM-217 (2)	04-PJM-218	04-PJM-255 (1)	04-PJM-255 (2)
UTME_nad27	476,572	476,572	479,421	480,743	480,743
UTMN_nad27	5,368,066	5,368,066	5,364,094	5,369,297	5,369,297
Hole Number	outcrop	outcrop	outcrop	outcrop	outcrop
Dip → Azimuth	-	-	-	-	-
Depth (m)	-	-	-	-	-
Rock Type	felsic crystal tuff	felsic crystal tuff	felsic crystal tuff	felsic crystal tuff	felsic crystal tuff
Trend	Krist Fm.	Krist Fm.	Krist Fm.	Krist Fm.	Krist Fm.
Unit	Krist Formation (Kayorum Syncline)	Krist Formation (Kayorum Syncline)	Krist Formation (Deloro Twp.)	Krist Formation (Porcupine Syncline)	Krist Formation (Porcupine Syncline)
SiO2	60.74	60.92	66.11	59.87	59.89
TiO2	0.39	0.39	0.22	0.42	0.42
Al2O3	15.92	15.85	14.16	15.76	15.82
Fe2O3	3.29	3.29	1.03	3.21	3.21
MnO	0.063	0.062	0.016	0.059	0.06
MgO	0.8	0.82	0.38	1.49	1.48
CaO	2.99	3.02	0.81	3.41	3.35
Na2O	4.47	4.46	5.48	3.65	3.67
K2O	1.62	1.62	1.31	1.51	1.51
P2O5	0.17	0.17	0.05	0.18	0.18
Cr	N.D.	N.D.	N.D.	N.D.	N.D.
LOI	9.9118	9.9118	10.6218	10.836	10.836
Total	100.3548	100.5038	100.1778	100.365	100.416
Cr	25	25	36	9	9
Ni	16	18	N.D.	10	9
V	74	76	33	68	68
Ni	24	-	6	15	-
Cr	16.38	-	37.08	13.13	-
Co	22	-	2	9	-
V	59.1	-	27.2	56.9	-
Sc	8.2	-	0.8	4.9	-
Cu	8	-	6	5	-
Zn	N.D.	-	N.D.	15	-
Cd	N.D.	-	N.D.	N.D.	-
Mo	N.D.	-	N.D.	N.D.	-
W	N.D.	-	N.D.	N.D.	-
S	68	-	138	99	-
Be	0.71	-	0.84	0.61	-
Li	15	-	5	20	-
Cs	1.009	-	0.61	1.312	-
Rb	42.46	-	41.48	39.81	-
Ba	580	-	377	331	-
Sr	464	-	106.3	565.7	-
Nb	11	11	5	15	14
Y	13	12	9	11	11
Zr	128	128	107	126	128
Zr	136.7	-	114.2	139.5	-
Hf	3.5	-	3.2	3.4	-
Nb	4.5	-	5.4	4.4	-
Ta	0.28	-	0.42	0.24	-
Y	10.04	-	1.45	8.22	-
Th	3.09	-	2.75	2.4	-
U	0.71	-	1.547	0.747	-
La	19.87	-	8.71	18.18	-
Ce	43.11	-	15.58	38.67	-
Pr	5.273	-	1.745	4.767	-
Nd	20.15	-	6.25	19.26	-
Sm	3.67	-	1.03	3.35	-
Eu	0.979	-	0.252	0.938	-
Gd	2.692	-	0.659	2.474	-
Tb	0.356	-	0.07	0.302	-
Dy	1.982	-	0.288	1.593	-
Ho	0.394	-	0.05	0.3	-
Er	1.139	-	0.154	0.822	-
Tm	0.17	-	0.023	0.112	-
Yb	1.18	-	0.17	0.74	-
Lu	0.185	-	0.027	0.111	-

Chapter 3: The Setting and Importance of Subvolcanic Intrusions in the Blake River Group of Ontario

INTRODUCTION

The role of subvolcanic intrusive rocks in the generation of volcanogenic massive sulphide (VMS) deposits has been known for some time (e.g., Campbell et al. 1981; Galley 2003, and references therein). Many researchers have argued that these intrusions provide the critical heat engine that drives the VMS hydrothermal systems, and some workers have also suggested that they may be potential metal contributors to VMS deposits (e.g., Campbell et al. 1981; Galley 1996, 2003; Large et al. 1996). In the Abitibi greenstone belt, the role of subvolcanic intrusions in the genesis of VMS deposits has been fairly well established, with much of the seminal work coming from the Flavrian–Powell intrusive complex in the Noranda camp in Quebec (Galley 1996, 2003; Goldie 1978, 1979; Paradis, Ludden and Gélinas 1988). In the Ontario portion of the Abitibi, however, there has been very little detailed work undertaken on subvolcanic intrusive rocks of the Blake River Group, and whether or not they have features (e.g., geology, geochemistry, alteration, timing) similar to VMS-related intrusions in the Blake River Group in Quebec.

The Blake River Group in Ontario is located primarily in northeastern Ontario on the Quebec–Ontario border (Figure 3.1), primarily in Pontiac, Ossian, Ben Nevis and Clifford townships (Figure 1.2). This component of the intrusion subproject is located within Clifford Township approximately 50 km east of the town of Noranda, Quebec. In this chapter, we report on the regional geological setting of the Blake River Group and Clifford stock in Clifford Township, document the different styles of mineralization and alteration in Clifford Township, and provide an interpretation of new U/Pb geochronological and lithogeochemical data for the rocks of Clifford Township. Finally, exploration suggestions and implications of the data herein will be provided at the end of this chapter.

REGIONAL GEOLOGIC AND TECTONIC SETTING

The rocks of Clifford Township are part of the Abitibi Subprovince of the Superior Province (e.g., Card and Poulsen 1998). The area is part of the southern volcanic zone of the Abitibi greenstone belt (Dimroth et al. 1982; Ludden and Hubert 1986), is located near the Ontario–Quebec border, approximately 50 km west of the Noranda mining camp, and consists predominantly of rocks from the Blake River Group, and associated younger intrusive rocks of the Clifford stock and equivalents (Jensen 1974, 1975). The Blake River Group, of which the bulk of Clifford Township outcrops is comprised, consists of an approximately 10 km thick sequence of basaltic through rhyolitic volcanic rocks (Dimroth et al. 1982; Gibson and Watkinson 1990; Péloquin 1999; Péloquin et al. 1990) and associated synvolcanic plutons (e.g., Flavrian–Powell: Galley 2003; Goldie 1978, 1979; Goldie and Goodwin 1977), that extends from Cadillac Township in Quebec to Clifford Township in Ontario (*see* Figure 3.1). In Quebec, the Blake River Group has produced over 3 million ounces of copper and zinc from volcanogenic massive sulphide (VMS) deposits (Racicot 1990) from 17 past-producing deposits (Gibson and Watkinson 1990). The Blake River Group in Ontario is located south of the Porcupine–Destor fault, and lies north of the Larder–Cadillac deformation zone primarily in Pontiac, Ossian, Ben Nevis and Clifford townships (e.g., Hogg 1964a, 1964b; Jensen 1974, 1975). It lies in unconformable contact with the underlying tholeiitic rocks of the

Kinojevis assemblage (Ayer et al. 2002; Dimroth et al. 1982; Fowler and Jensen 1989; Jensen 1985; Jensen and Langford 1985) and, in a regional sense, is overlain by rocks of the younger Porcupine and Timiskaming assemblages (Ayer et al. 2002). Uranium–lead ages for igneous rocks of the Blake River Group in both Quebec and Ontario range from 2701 to 2696 Ma (Ayer et al. 2002; Corfu 1993; Corfu et al. 1989, and references therein; Mortensen 1993; Piercey et al. 2004). The entire Blake River Group is intruded by synvolcanic plutons (e.g., Flavrian: Galley and van Breeman 2002; Galley 2003; Goldie 1978, 1979; Goldie and Goodwin 1977), and numerous syntectonic to posttectonic tonalite-trondhjemite-granodiorite (TTG) suite intrusions (e.g., Lac Dufault, Lac Clarice: Chown, Harrap and Moukhsil 2002; Feng and Kerrich 1992; Sutcliffe et al. 1993) of similar age (ca. 2.69 Ma: Corfu 1993; Corfu and Noble 1992; Mortensen 1993).

The deformation and metamorphic history of the Blake River Group has been studied by numerous workers (e.g., Dimroth et al. 1983a, 1983b; Hubert, Trudell and Gélinas 1984; Jensen 1974, 1975). In Ben Nevis and Clifford townships in Ontario, the Blake River Group has been folded into domal-shaped patterns with stratigraphy facing outwards from the Clifford stock (*see* Figure 3.2; Jensen 1974, 1975; Péloquin and Piercey 2003; Piercey et al. 2004). The Blake River Group is also cut by the later Larder–Cadillac deformation zone and Porcupine–Destor fault (*see* Figure 3.1), and, in Clifford and Ben Nevis townships, the Blake River Group and Clifford stock are cut by high-angle north-northwest-trending, and east-northeast-trending strike-slip faults of uncertain kinematics (*see* Figure 3.2). The metamorphic grade of the Blake River Group is quite low and predominantly greenschist to subgreenschist facies in Quebec, whereas in Ontario, the rocks are predominantly at prehnite-pumpellyite facies (Hannington et al. 2003; Jensen 1975; Jolly 1980; Powell, Carmichael and Hodgson 1993, 1995). Locally, around the intrusive rocks, there are zones of contact metamorphism in the Blake River Group to albite-epidote-magnetite facies (Goldie 1979; Jensen 1975; Piercey et al. 2004).

The combination of field, geological, and geochemical attributes have led to various interpretations for the tectonic setting of the Blake River Group and the later post-Blake River Group intrusions (e.g., Clifford stock). In recent years, most workers have suggested that the Blake River Group represents an arc to back-arc basinal geodynamic setting (Lafleche, Dupuy and Dostal 1992; Ludden and Péloquin 1996; Péloquin 1999; Wyman 2003; Wyman, Kerrich and Polat 2002), with potential for plume–arc interaction (Wyman 2003; Wyman, Kerrich and Polat 2002). The later TTG suite magmatism (at ca. 2.69 Ga) that postdates the Blake River Group is interpreted to reflect TTG generation via slab melting, potentially due to melting of mafic to ultramafic slab material due to flat subduction (Drummond and Defant 1990; Drummond, Defant and Kepezhinskas 1996; Feng and Kerrich 1992; Gutscher et al. 2000; Smithies, Champion and Cassidy 2003; Wyman 2003; Wyman, Kerrich and Polat 2002).

PREVIOUS WORK

The Clifford stock and the Blake River Group in Clifford Township have been the focus of study for numerous years. The most modern regional mapping investigation of Clifford Township was undertaken by Jensen (1974, 1975), which updated the previous vintage mapping studies of Wilson (1901), Knight (1920a, 1920b) and Gledhill (1928, 1929). Jensen's (1974, 1975) study provided a regional stratigraphic framework for the Blake River Group and Clifford stock, upon which most of the mapping in this project is built.

Wolfe (1977) conducted a volcanic lithogeochemical and soil and till geochemical study of rocks and soils in Ben Nevis Township and illustrated that the results of zinc and copper analyses in volcanic rocks can be used to outline mineralization, and other elements (e.g., As, Sb, Pb, Li, Sn and Hg) could be used to outline alteration zones much larger than mineralization zones.

Grunsky (1986) undertook a regional alteration lithogeochemical study of the volcanic rocks in Clifford and Ben Nevis Townships. His research employed multivariate statistical techniques to outline various alteration zones and how to separate rock type (e.g., basalt versus rhyolite) chemical variations from variations induced by hydrothermal alteration. Grunsky (1986) also illustrated the importance CO_2 and S alteration zones in outlining mineralized zones in Ben Nevis and Clifford townships. This work was built upon by Grunsky and Agterberg (1988) and by Grunsky (1988).

In the 1990s, rocks of the Blake River Group in Clifford and Ben Nevis townships were part of the Canadian Mining Industry Research Organization (CAMIRO) study on regional hydrothermal alteration systems and subvolcanic intrusions (Bailes et al. 1998). Initial results of this project were presented as a CAMIRO report in 1998 (Bailes et al. 1998), with subsequent results published by the Geological Survey of Canada as research articles (e.g., Galley and van Breeman 2002; Hannington, Santaguida and Kjarsgaard 2001), and peer-reviewed journal articles (e.g., Hannington et al. 2003). Within the initial phase of the project, there were 3 main themes of research that concentrated on the Clifford stock and surrounding Blake River Group rocks, including 1) studies of the Clifford stock as a subvolcanic intrusive system (Galley 1998); 2) regional stable isotope studies of hydrothermal alteration (Taylor and Timbal 1998); and 3) regional mineral chemical studies of hydrothermal alteration (Hannington and Kjarsgaard 1998). Galley (1998) briefly discussed the Clifford stock in light of other subvolcanic intrusive complexes (e.g., Flavrian, Sneath Lake, etc.) that were part of the CAMIRO project. He illustrated that the intrusion was calc-alkalic in nature and small in comparison to most VMS camp-related subvolcanic intrusive systems. Taylor and Timbal (1998) illustrated that there were zones of $\delta^{18}O$ depletion surrounding the Clifford stock and other discrete areas (e.g., near the Croxall occurrence), suggesting that there was high-temperature hydrothermal activity associated with the emplacement of the Clifford stock. In contrast to the Noranda camp, however, the lateral extent of the high-temperature alteration zones was much smaller suggesting the potential for large VMS deposits to have formed was quite low. The mineral chemical work of Hannington and Kjarsgaard (1998), Hannington, Santaguida and Kjarsgaard (2001) and Hannington et al. (2003) echoed the results of Taylor and Timbal (1998) and illustrated that although there were pockets of high-temperature alteration, most alteration minerals and assemblages in the Ben Nevis–Clifford area (e.g., Mg-rich chlorite, high-Fe epidote, absence of siderite) were not indicative of high-temperature water–rock interaction, suggesting the potential for large VMS deposits was low.

Ioannou et al. (2004) studied the cathodoluminescence characteristics of quartz-epidote veins, quartz-veins, interstitial and vein quartz, and breccia pipe quartz from areas in Ben Nevis Township, with the latter focussed on breccia pipe quartz from the Canagau mines occurrences (*see* Jensen 1974, 1975). Their results illustrated that the quartz was of hydrothermal origin, that the breccia pipe quartz had multiple generations, was strongly zoned, and suggested that it formed in a fluctuating hydrothermal environment. They further suggested that some of the quartz may have originated as non-crystalline quartz (e.g., chalcedony or opal). Coincident with this cathodoluminescence study were fluid inclusion studies were undertaken by Weiershaeuser and Spooner (2002, 2003). They used the same quartz media as above and demonstrated that most of the fluid inclusions were liquid rich, with some vapour rich, had low temperatures (120–160°C), and had salinities higher than modern seawater (6–16 CaCl wt %). Both the cathodoluminescence and fluid inclusion studies interpreted all quartz, epidote and carbonate to be related to semi-conformable alteration in a VMS environment; however, in light of new overprinting mineralization relationships outlined below, it is uncertain what the significance of these data are, due to poor field and paragenetic control on the sample suite.

Recent work as part of the Discover Abitibi Initiative involved regional studies of the volcanic stratigraphy of Ben Nevis Township (Péloquin and Piercey 2003), and studies of the Clifford stock and related mineralization (Piercey et al. 2004). This research involved new thematic mapping of key localities of the Blake River Group in Ben Nevis and Clifford townships, detailed petrological studies of the Clifford stock and Blake River Group (this study; Péloquin and Piercey 2005), and new documentation of mineralization styles due to new drilling by Wallbridge Mining Company Ltd. in both Clifford and Ben Nevis townships. Details of these results are presented in this chapter and in Péloquin and Piercey (2005).

GEOLOGY AND STRATIGRAPHIC RELATIONSHIPS

The geological and stratigraphic relationships between the Blake River Group and Clifford stock and related rocks in Clifford Township were determined by geological mapping in 2003 and augmented by drill core studies in 2004 (Figures 3.2 and 3.3). Clifford Township is dominated by volcanic and subvolcanic rocks of the Blake River Group, felsic intrusive rocks of the Clifford stock and associated dikes, and Paleoproterozoic dikes of the Matachewan dike swarm (*see* Figures 3.2 and 3.3).

In Clifford Township, the Blake River Group consists of a succession of basaltic-andesite, andesite, and felsic volcaniclastic rocks that young outward from the Clifford stock, and are interpreted to record 2 cycles of volcanism and comprise 5 volcanic to volcaniclastic units, and associated synvolcanic diabase or gabbro intrusions (*see* Figures 3.2 and 3.3). The lowermost packages consist of pillowed to massive, basaltic andesite to andesite (Photo 3.1A) that is amygdaloidal and variably plagioclase porphyritic; porphyritic plagioclase crystals are 2 to 3 mm long and relatively euhedral. Conformably overlying the amygdaloidal basaltic andesite is a package of andesitic volcaniclastic rocks (*see* Figures 3.2 and 3.3). Péloquin and Piercey (2003) interpreted this package as a series of andesitic flows, but recent investigations of drill core from Wallbridge Mining Company Ltd. illustrate that these rocks are best described as andesitic tuffs, lapilli tuffs, and tuff breccias (Photo 3.1B). These volcaniclastic rocks are matrix supported and consist mainly of fine-grained grey to grey-black andesitic tuff with varying amounts of feldspar lapilli and black andesitic fragments (*see* Photo 3.1B). Feldspar grains range from less than 1 to 5 mm in size and are euhedral to subhedral; in places, they comprise 30 to 40% of the rock. Black andesitic fragments are not easily discernable on surface, but, in drill core, they are typically subrounded to subangular, range from less than 1 cm up to 10 cm in size and, in places, comprise 20 to 30% of the rock (*see* Photo 3.1B). Overlying this andesitic tuff unit is the first of 2 felsic volcaniclastic units consisting of a matrix-supported felsic tuff breccia (nomenclature from Fisher 1966)(Figures 3.2 and 3.3). On surface, these tuff breccias appear monolithic to weakly polylithic (Photo 3.1C); however, in drill core, these samples are clearly polylithic and contain clasts of andesite, basaltic-andesite, dacite, and rhyolite, and are angular to subrounded and range in size from 1 to 30 cm; all the clasts are within a matrix of fine siliceous ash material (Photo 3.1D). Overlying the latter is a second unit of amygdaloidal and variably plagioclase porphyritic basaltic-andesite to andesitic tuff (*see* Figures 3.2 and 3.3) with small plagioclase feldspars: less than 1 mm and up to 2–3 mm. The uppermost stratigraphic unit consists of a second tuff breccia to lapilli tuff (*see* Figures 3.2 and 3.3), very similar to the underlying tuff breccia, consisting of a matrix-supported breccia with angular clasts of predominantly dacite to rhyolite. There appears to be a southward younging of the tuff breccia into a lapilli tuff on a regional scale, suggesting normal grading outward from the Clifford stock (Jensen 1974, 1975).

Minor felsic flows and cryptodomes occur within the study area. In southern Clifford Township, there are felsic flows associated with a primarily felsic volcaniclastic package. These flows are white, aphyric rhyolitic rocks that are relatively massive in nature. In eastern Clifford Township, there are flow-banded rhyolitic volcaniclastic rocks (Photo 3.1E) spatially associated with synvolcanic rhyolitic dikes (Photo 3.1F), interpreted to be part of a cryptodome. The rhyolitic volcaniclastic rocks are different than most felsic volcaniclastic rocks in the area in that they are clast supported, monolithic, and consist of polygonally jointed rhyolite fragments that have flow banding (*see* Photo 3.1E). Rhyolitic intrusive rocks that intrude these felsic volcaniclastic rocks have irregular margins, are fine grained, and are synvolcanic in nature (see "Uranium–Lead Geochronology"; *see* Photo 3.1F).

Mafic intrusive units cutting the Blake River Group stratigraphy are metamorphosed (*see* Figures 3.2 and 3.3) and are hard to distinguish from more mafic to intermediate volcanic rocks of the Blake River Group itself. These rocks intrude all stratigraphic units of the Blake River Group, but have similar chemical attributes as the volcanic rocks (see below) suggesting that it is a synvolcanic intrusive complex related to the overlying basaltic-andesitic to andesitic volcanic rocks of the Blake River Group. The intrusions form sheet-like and dike-like intrusions of mostly diabase to diorite and locally gabbro. In some places, the dike-like intrusions have amygdules (Photo 3.1G) suggesting emplacement at high levels, also supporting a synvolcanic origin (e.g., Gibson, Morton and Hudak 1999).

The Blake River Group is intruded by granitoids of the Clifford stock, by east-northeast-trending dikes interpreted to be equivalent to the Clifford stock, and by gabbroic rocks of the Paleoproterozoic Matachewan dike swarm (*see* Figures 3.2 and 3.3). The Clifford stock is located in the core of the Blake River Group in Clifford Township and consists of a relatively equigranular tonalite to granodiorite, commonly hornblende bearing and locally hornblende-biotite bearing (Photos 3.2A and 3.2B). The intrusion does not appear to be polyphase and contains xenoliths of the surrounding wall rock in only a few localities. Southeast of the Clifford stock, numerous east- to northeast-striking dike- to sill-like intrusions cut the Blake River Group. These dikes are fine to medium grained, variably feldspar porphyritic, locally pyrite bearing, siliceous, and dacitic to rhyolitic in composition (Photo 3.2C); these dikes crosscut stratigraphy. They have very straight walls in most places, suggesting emplacement into solidified host rock material, but are irregular in some localities as a result of emplacement into dilatent zones or when associated with hydrothermal brecciation. The dikes are locally associated with xenoliths of very angular fragments of wall rock and the breccias are interpreted to be due to forceful emplacement of the dikes into their hosts (Photo 3.2D). Furthermore, they are also spatially associated with breccia-pipes (e.g., Croxall occurrence) and stockworks of pyrite-quartz-gold-molybdenite veins.

Also present are north-northwest-trending dikes of the Matachewan swarm (2.47–2.45 Ga: Heaman 1997). Unlike the synvolcanic Archean gabbro-diabase sheets within the Blake River Group, these gabbroic dikes are coarse grained, have no recrystallization of primary igneous mineralogy, and are highly magnetic.

The rocks of the Blake River Group and Clifford stock (and equivalents) are interpreted to represent 2 cycles of volcanism and synvolcanic gabbro or diabase magmatism, followed by a younger felsic intrusive event (*see* Figure 3.3), all of which are affected by a younger Paleoproterozoic mafic dike event.

ALTERATION AND MINERALIZATION STYLES

Alteration and mineralization within Clifford Township include 1) contact metamorphic alteration around the Clifford stock with minor pyrite mineralization; 2) VMS-style alteration and mineralization; and 3) intrusion-related or porphyry-style alteration and copper-molybdenum-gold (Cu-Mo-Au) mineralization.

Metamorphism-related alteration is dominated by low-grade regional prehnite-pumpellyite facies mineral assemblages (Hannington et al. 2003; Jensen 1975), and, in the immediate vicinity of the Clifford stock, contact metamorphism. Near the Clifford stock, a well-defined contact aureole surrounds the intrusion for 200 to 300 m (*see* Figure 3.2). In the aureole, the basaltic-andesitic to andesitic rocks exhibit a distinctive dark colouration and contain ubiquitous magnetite, lath-like needles of plagioclase (albite?), epidote patches, and, in some cases, a fibrous or needle-like amphibole of probable actinolitic composition (Photo 3.3A). Minor disseminated pyrite is present in the metamorphic aureole.

Volcanogenic massive sulphide (VMS)-style alteration is observed on surface and in drill core. In both cases, amygdule filling by chlorite-quartz-epidote-pyrite assemblages is commonly observed to varying degrees (Photo 3.3B), which is interpreted to represent semi-conformable-style alteration (e.g., Galley 1993). Most common are quartz-pyrite fillings, but there are also epidote-quartz-pyrite, chlorite-quartz, and chlorite-pyrite infillings. These mineral assemblages are also present in some rocks, commonly the more mafic members of the Blake River Group, as patches, typically near permeable zones in the rocks (i.e., near hyaloclastite or in volcanic breccia). Silicification and chlorite alteration are present in some drill cores and are associated with sulphide mineralization and are interpreted to be more indicative of proximal, high-temperature alteration (e.g., Franklin 1993). This style of alteration and mineralization has been observed only in drill core and occurs associated with the lowermost basaltic-andesite pillow lava sequence. The mineralization is generally restricted to hyaloclastite along pillow margins (Photo 3.3C). Along these margins, chalcopyrite, pyrite, and quartz are found interstitial to angular hyaloclastite; sulphides comprise a maximum of approximately 10% of the rock (*see* Photo 3.3C). Hyaloclastite fragments are either bleached to a white-pink colour and silicified or are completely altered to chlorite with or without epidote (*see* Photo 3.3C). Finer grained ash-sized material in between the hyaloclastite is often completely replaced by chlorite.

Porphyry Cu-Mo-Au-style alteration is present overprinting, and thus younger than, the VMS-style alteration. The porphyry-style alteration is visible both on surface and in drill core, and is associated with numerous breccia-pipe-style occurrences on surface (e.g., Brett–Trethway (Croxall) prospect). On surface, the mineralization is not easily visible and occurs within breccia pipes, like the Croxall prospect. These pipes are broadly radial in nature and spatially associated with rhyolite porphyry and brecciated porphyry; in between the brecciated porphyry, there is abundant quartz±sulphide mineralization forming the interstices between porphyry clasts (Photos 3.3D and 3.3E; E. Chaloux, personal communication, 2004). Alteration associated with this style of mineralization is commonly silicification and pyrite alteration near the breccia pipes, whereas, outside of the breccia pipes, the regional wall rocks have a randomly oriented network of millimetre- to centimetre-scale veins consisting of quartz, epidote, potassium feldspar, hematite and calcite (±sericite). In drill core, mineralization and alteration are associated primarily with a randomly oriented vein network that exhibits a complex paragenesis. The veinlets form a stockwork 1 mm up to several centimetres in width. The paragenesis appears to be, from oldest to youngest: 1) epidote, chlorite and sericite (Photo 3.3F); 2) quartz-pyrite; 3) dark grey quartz-pyrite-chalcopyrite-molybdenum (and gold?) (Photo 3.3G); and 4) hematite-calcite-±potassium feldspar (Photo 3.3H). This paragenesis is not always present and some events appear to be synchronous and overlap in some areas (as observed in drill cores). Nonetheless, there seems to be an intermediate Cu-Mo-Au event associated with dark grey quartz veins, and all alteration styles are cut by late hematite-calcite±potassium feldspar veins. The veins that host mineralization are widespread across all rock types, but most molybdenum- (and gold-?) rich zones are also hosted by dikes of rhyolitic feldspar porphyry similar to the Clifford stock. This relationship provides compelling evidence that the porphyry-style mineralization is a distinctly younger hydrothermal event in Clifford Township and is directly related to the emplacement of the Clifford stock.

LITHOGEOCHEMISTRY: PETROGENETIC ASPECTS

The lithogeochemistry for the Blake River Group and Clifford stock and associated rocks are presented in Tables 3.1 and 3.2. The samples were collected from outcrop and drill core and were prepared and analyzed according to the methods outlined in Appendix A; quality control and quality assurance data are also presented in Appendix A. In this section, the data will be described in 2 subsections, one for the Blake River Group and synvolcanic intrusions, and one for the Clifford stock.

Alteration and Metamorphism: Constraints on Elemental Utility

Samples for this study were acquired to understand first-order petrogenetic and chemostratigraphic trends. Notable, however, is that even though most samples of the Blake River Group, and the Clifford stock and associated rocks, show some degree of alteration, their mobile element systematics are remarkably well behaved, most samples lie between 2 and 5% Na_2O, have Al_2O_3/Na_2O less than 10, lie proximal to the least-altered compositions on an alteration box plot (Large et al. 2001), and lie primarily in the igneous spectrum on a Hughes plot (Hughes 1973) (e.g., Figure 3.4). These features suggest that the rocks are at worst weakly altered and that the mobile major and trace elements in these rocks provide crude first-order petrogenetic trends. In contrast, the immobile elements including the major elements Al_2O_3 and TiO_2 ($\pm P_2O_5$), the low field strength element (LFSE) Th, the high field strength elements (HFSE: Zr, Hf, Nb, Ta, Y), some transition elements (Sc, Ni, Cr, V), and the rare earth elements (REE; except Eu), are more reliably interpreted to reflect primary abundances, with a few exceptions, and when discussing petrogenetic aspects of these rocks these elements will be concentrated upon.

Results: Blake River Group

Geochemical data for the Blake River Group volcanic rocks and the synvolcanic diabase and gabbros from Clifford Township are presented in Figures 3.4 to 3.6 and in Tables 3.1 and 3.2. As stated above, most of the volcanic and intrusive rocks are least-altered samples with $Al_2O_3/Na_2O < 10$, Na_2O between 2 and 5%, and lie within the least-altered fields on the alteration box plot and a Hughes plot (*see* Figures 3.4A, 3.4B and 3.4C, respectively). All of the rocks have subalkaline Nb/Y ratios (<0.7), and Zr/TiO_2 values (*see* Figure 3.5A) consistent with their SiO_2 designations (*see* Tables 3.1 and 3.2) as basaltic andesites to andesites. They plot predominantly in the calc-alkalic field on the AFM plot, except for 2 basaltic samples (cycle 1, unit 2) that are more tholeiitic in nature (*see* Figure 3.5B). However, the bulk of the samples have Zr/Y ratios between 4 and 7 and have affinities transitional between tholeiitic and calc-alkalic (*see* Figure 3.5C; *see* Table 3.2). On standard Harker diagrams (*see* Figures 3.6A to 3.6P), the rocks form arrays with decreasing TiO_2, Al_2O_3, Fe_2O_3T, MgO, CaO, Ni, Cr, V, Sc, and to a lesser extent Sr, with increasing SiO_2, consistent with fractionation of olivine, clinopyroxene, plagioclase, and possibly spinel (or some other oxide). There is scatter in the Na_2O, K_2O and Rb data, but all these elements suggest that these were incompatible and that potassium feldspar was not a fractionating phase (*see* Figure 3.6); similarly, the increasing Nb, Th and Y with increasing SiO_2 also suggest that these elements behaved incompatibly during magmatic differentiation of these rocks.

The primitive mantle normalized patterns of the different cycles and units of the Blake River Group and associated synvolcanic gabbros and diabase are presented in Figures 3.7A to 3.7J. With the exception of the rhyolitic rocks, and 2 samples from cycle 1, unit 2, all of the rocks from the Blake River Group can be separated into 2 broad geochemical groupings: 1) samples that have signatures like modern enriched-mid-ocean ridge basalt (E-MORB) and oceanic plateau basalts (e.g., Lassiter and DePaolo 1997; Sun and McDonough 1989); and 2) those that are similar to the former but are crustally contaminated. The E-MORB-like samples are characterized by relatively flat, to slightly LREE-enriched primitive mantle normalized patterns, which have flat Th and Nb relative to La, flat to weakly positive Zr and Hf anomalies, and flat to weakly negative Ti anomalies, and depletions in the compatible elements (Al, V, Sc; *see* Figure 3.7); these rocks are called E-MORB-like based on their primitive mantle normalized pattern and the name does not imply that they formed at a mid-ocean ridge. The second geochemical group is similar to the first with similar crustally insensitive incompatible element contents (e.g., Nb, Y, heavy-REE (HREE); *see* Figure 3.7; *see* Table 3.1), but they have marked differences including distinctive negative Nb anomalies relative to Th and La on primitive mantle normalized plots (Nb/Th_{pmN} and $Nb/La_{pmN} < 1$; pmN = primitive mantle normalized), are more LREE-enriched, and have more strongly developed negative Ti anomalies (*see* Figure 3.7). These types of primitive mantle patterns, and in particular the negative Nb anomalies, are often heralded as the subduction zone signature typical of arc magmatic rocks (Pearce and Peate 1995). It is notable, however, that the greater magnitude of the negative Nb anomalies (as measured by the Nb/Th_{pmN} values) are correlated with increased LREE-enrichment (e.g., lower Nb/La_{pmN} and higher La/Sm values), higher SiO_2 contents, and lower Nb/U ratios (Figures 3.8A to 3.8D)—features all consistent with the negative Nb anomalies having been produced in parallel with Th, SiO_2, and LREE-enrichment due to crustal contamination, rather than being a true "arc" signature. It is uncertain at this point, however, whether this contamination was due to contamination by a pre-existing arc substrate or continental crustal basement.

Results: Clifford Stock and Equivalents

Geochemical data for the Clifford stock and equivalents (CSE) are presented in Figures 3.9 to 3.12 and Tables 3.1 and 3.2. The CSE are characterized by SiO_2 values of approximately 60 to 70%, and, for the most part, have Na_2O values 2 to 5%, and Al_2O_3/Na_2O values less than 10 (*see* Figure 3.9A; *see* Table 3.1). Most samples have LOI values less than 4, and there is an antipathetic relationship between Na_2O and LOI (*see* Table 3.1), suggesting that the lower Na_2O values are due to alteration. In any case, the samples have major element compositions which appear to deviate little from pristine igneous compositions (*see* Figures 3.9B and 3.9C), suggesting that most are only weakly altered. The normative mineralogy for the CSE illustrate that these rocks are primarily tonalite, trondhjemite, and granodiorite (TTG), typical of Archean TTG suites (*see* Figure 3.10A). The CSE have broadly calc-alkalic affinities on a standard AFM plot (*see* Figure 3.10B), and straddle near the subalkaline–alkaline boundary (Nb/Y ~0.7) on a Winchester and Floyd (1977; modified by Pearce 1996) plot (*see* Figure3.10C), suggesting that they are broadly subalkalic, calc-alkalic rocks. The rocks do have relatively high Al_2O_3 contents (>13%), and low Yb (≤2 ppm) and are consistent with being part of a high-Al TTG suite (*see* Figure3.10D). The low Yb values in CSE samples are echoed by very low Y values (typically <10 ppm; *see* Table 3.1), both of which are distinctly lower than in Blake River Group units. Moreover, these lead to very high calc-alkalic Zr/Y ratios (>7) that are characteristic of Lesher et al.'s (1986) FI rhyolites (*see* Figure 3.11A).

The primitive mantle normalized plots for these rocks have LREE-enriched patterns with HREE-depletions, distinctive negative Nb, Ti and Eu anomalies, relative positive Zr, Hf and Al anomalies, and depletions in compatible elements (*see* Figure 3.11B). The low HREE contents (i.e., Yb) and Y in these rocks is consistent with them having been derived from a source in which garnet (and/or hornblende) were both stable in the residue. Furthermore, the high Sc and low Y leads to the CSE to have Sc/Y ratios ~0.5 to 1.0 (*see* Figure 3.11C) which are consistent with garnet and hornblende (e.g., Feng and Kerrich 1992) residing in the source from which the CSE were partially melted (i.e., generation at high pressures).

On standard Harker diagrams (*see* Figures 3.12A to 3.12O), the CSE exhibit broadly negative trends in TiO_2, Al_2O_3, Fe_2O_3T, MgO and CaO with increasing SiO_2, which suggests the involvement of plagioclase, hornblende and oxide minerals as fractionating phases; this is further supported by the downward trends in Ni, Cr, V, Sc and Sr (*see* Figure 3.12). There is considerable scatter in the Na_2O, K_2O and Rb data suggesting that these elements have been significantly mobilized during alteration; nonetheless, they do exhibit an increase with SiO_2 (*see* Figure 3.12) suggesting that they behaved incompatibly during fractional crystallization. The scatter in the so-called incompatible Nb and Y values with changing SiO_2 (*see* Figure 3.12) may reflect the influence of oxide and hornblende fractionation, respectively, as both these phases have high partition coefficients for these elements (e.g., Green 1994; Green and Pearson 1987; Rollinson 1993).

URANIUM–LEAD GEOCHRONOLOGY

Preliminary U/Pb geochronological results from Clifford Township include a sample from the Clifford stock, and a felsic dike interpreted to be related to the Clifford stock. Samples were analyzed at the Jack Satterly Geochronology Laboratory at the University of Toronto following the methods outlined in Appendix B.

Age of Clifford Stock

Sample 03SJP-115 (Universal Transverse Mercator (UTM) North American Datum 1983 (NAD83), Zone 17, 591133E, 5351000N) was collected in order to determine the primary crystallization age of the Clifford stock and to assess its potential age similarity to the surrounding Blake River Group and to ages of other subvolcanic intrusive rocks within the Blake River Group stratigraphy (ca. 2700 Ma: Mortensen 1993). This sample is tonalitic to granodioritic in composition, and is texturally equigranular to weakly porphyritic with some larger (0.5 cm) potassium feldspar phenocrysts to megacrysts. Hornblende is the dominant mafic phase and there are some rounded epidote patches within the sample. The sample yielded abundant zircon, dominated by a population of elongate (up to 6:1) cylindrical euhedral grains as well as subordinate, larger, 'glassy' fragments. Results from 3 analyzed single-grain fractions all overlap, straddling concordia, and a simple weighted mean ^{207}Pb/^{206}Pb age for all 3 fractions yields a result of 2686.9±1.2 Ma (Figure 3.13A).

This age of 2686.9 Ma is interpreted to represent the best estimate of the timing of magmatic crystallization of the Clifford stock, and is similar to that determined for the Clarice Lake pluton (Corfu and Noble 1992), which also intruded the Blake River Group near the Ontario–Quebec border. Emplacement of the Clifford stock also coincided in time with intrusion of the Lac Dufault pluton in the eastern Abitibi of Quebec and a late, potassium feldspar porphyritic phase of the Lac Abitibi batholith (Mortensen 1993, and references therein), the potassium feldspar porphyritic Adams stock south of Timmins (2686±3 Ma: Frarey and Krogh 1986), and several gold-related intrusive rocks in the Porcupine camp (Corfu et al. 1989).

Age of Felsic Dikes

Sample 03SJP-059-1 (UTM NAD83, Zone 17, 590369E, 5349181N) was collected from a representative felsic dike intruding andesitic volcaniclastic rocks and was initially interpreted to be synvolcanic with the surrounding andesites. Further examination of stripped outcrops in 2004 revealed that these dikes have straight margins and are not synvolcanic with the surrounding Blake River Group rocks. In drill core, porphyry dikes (interpreted to be the same as those sampled here), exhibit razor-sharp contacts with surrounding rocks, and add supportive evidence for a post-volcanic origin. Abundant, high-quality zircons were recovered from this sample, comprising populations of colourless to pale brown, water-clear, euhedral long prisms, and stubbier or lozenge-shaped, sharp, doubly terminated grains. Small fluid, melt or apatite inclusions were few in any given zircon grain, but were nearly ubiquitous. Four representative single grains were abraded and analyzed. All analyses are overlapping, and most straddle concordia. Precise analyses obtained for 3 grains (A1, A3, A4) yield a weighted mean ^{207}Pb/^{206}Pb age of 2688.5±2.3 Ma (Figure 3.13B). The fourth fraction (A2) has a high proportion of common lead and commensurate large errors, yields a slightly higher ^{207}Pb/^{206}Pb age (2694±5 Ma), and may reflect minor inheritance.

We regard the age of 2688.5±2.3 Ma as the best estimate of the timing of emplacement and crystallization of the felsic dike. This age is similar to the Clifford stock and suggests that the dikes are coeval with the stock, consistent with chemical results above. Moreover, these ages are synchronous with late-tectonic magmatic activity throughout the eastern Abitibi greenstone belt (Corfu et al. 1989; Corfu and Noble 1992; Mortensen 1993).

EXPLORATION IMPLICATIONS AND RECOMMENDATIONS

The results of this study illustrate that Clifford Township has different styles of mineralization and alteration and, hence, has numerous potential target commodities for explorationists. In the past, early workers in the area considered many of the targets in both Clifford and Ben Nevis townships to be gold targets (*see* summaries in Jensen 1975) and, more recently, workers have viewed the rocks of this area to be primarily VMS-related base metal targets (e.g., Hannington and Kjarsgaard 1998; Ioannou et al. 2004; Taylor and Timbal 1998; Weiershaeuser and Spooner 2002, 2003). The results of this study clearly illustrate that both of the above ideas are correct, but there is clearly an early VMS-related event coeval with the Blake River Group that is overprinted by a younger porphyry Cu-Mo-Au event associated with the emplacement of the Clifford stock (*see also* Piercey et al. 2004).

The occurrence of 2 different styles of mineralization provides opportunities and challenges for exploration, and will require different exploration strategies for the different styles and commodities. When searching for VMS-related mineralization, one should concentrate on rocks of the Blake River Group, as they are host to significant VMS mineralization in the Noranda camp just 50 km east (e.g., Gibson and Watkinson 1990). In Clifford Township, VMS-related mineralization and alteration is sporadic but is present. When trying to vector into potential areas, it is important to distinguish between VMS-related semi-conformable and pipe-like alteration, versus later porphyry-style mineralization. Semi-conformable, or lateral fluid flow related, VMS alteration is manifested in epidote-quartz-chlorite-pyrite assemblages in permeable areas in the Blake River Group volcanic rocks. For example, they commonly occur as infillings in amygdules (e.g., *see* Photo 3.3B), and as patches along pillow margins and pillow rinds, and in interpillow areas associated with hyaloclastites. Identification of these zones will outline zones of lateral fluid flow and help one identify that they are in the VMS system and in a zone of lateral seawater–rock interaction. The association of pipe-like, or discordant, chlorite-chalcopyrite-pyrite-quartz-rich alteration (e.g., *see* Photo 3.3C) can be used to identify zones of potential high-temperature discharge and environments most conducive to the formation of significant quantities of VMS mineralization. In addition, the combination of the above alteration types, the association with synvolcanic intrusions (e.g., *see* Photos 3.1F and 3.1G), and association with highly altered volcanic rocks (e.g., $Al_2O_3/Na_2O > 10$, $Na_2O < 2\%$) can point to potentially prospective VMS stratigraphy.

The younger age of the Clifford stock and related dikes suggests that they represent a distinctly younger pulse of magmatism that is temporally, and petrologically, distinct from the VMS-associated Flavrian intrusion (e.g., Mortensen 1993) in Noranda. Thus, one implication of the results of the current project is that previous work which considered the Clifford stock as the subvolcanic heat engine for VMS-related alteration and/or mineralization in this region (Galley 1998; Hannington and Kjarsgaard 1998; Hannington et al. 2003; Taylor and Timbal 1998) may not be entirely valid. Nonetheless, this stock does have a hydrothermal system associated with it, but represents a porphyry Cu-Mo-Au target, rather than a VMS-related target. Future exploration programs for porphyry Cu-Mo-Au style mineralization in the region should consider late plutons, such as the Clifford stock and related east-northeast-trending felsic dikes, as potential targets. As summarized earlier, several other age-equivalent intrusive units in the Abitibi greenstone belt are known to exist (see also below).

A key problem explorationists may encounter is delineating TTG intrusions younger than the Blake River Group from synvolcanic felsic intrusive rocks of the Blake River Group. The post-volcanic intrusions of the Clifford stock and associated dikes typically have sharp margins in drill core, crosscut stratigraphy, and are primarily tonalitic to granodioritic or quartz-feldspar porphyries. In contrast, the synvolcanic Blake River Group intrusions, like that in eastern Clifford Township, typically have irregular margins, and are associated polygonally jointed and flow-banded rhyolite clasts. Further field criteria for the Blake River Group synvolcanic felsic intrusive rocks are provided in Péloquin and Piercey (2005). In addition to field criteria, the Clifford stock and related rocks have younger U/Pb zircon ages (ca. 2690 Ma and younger), and have very distinctive lithogeochemical features. In particular, they have very low HREE and Y contents (i.e., Y <10 ppm, Yb <2 ppm with most <1 ppm), and very high Zr/Y (>7), Nb/Y (>0.4), Al_2O_3/Yb (>10), and La/Yb (>10) ratios, when compared to rocks of the Blake River Group (Figure 3.14).

A regional consideration of the U/Pb geochronological and geochemical results from the Clifford stock and associated dikes reveals that there are numerous intrusions in the Abitibi Subprovince of Quebec and Ontario that are temporally (and compositionally?) equivalent. For example, the Clarice Lake intrusion (2689±1 Ma: Corfu and Noble 1992) near the Ontario–Quebec border has a similar age to the Clifford stock. Similarly, syntectonic to posttectonic intrusions such as the Lac Dufault pluton in Quebec and younger, porphyritic phases of the Lac Abitibi batholith also have ages near 2690 Ma (Mortensen 1993). The results found herein also suggest that these plutons may be hosts to potential porphyry Cu-Mo-Au-style mineralization. It is also notable that porphyry-style mineralization has been also observed in the Blake River Group in the Noranda camp (Galley and van Breeman 2002). In the Noranda camp, the later phases of the Flavrian–Powell subvolcanic intrusive complex host crosscutting, intrusion-related porphyry Cu-Mo-Au occurrences that have an age of 2697±2 Ma (Galley and van Breeman 2002). Unlike Clifford Township, however, this mineralization is only slightly younger than the volcanic-hosted VMS-style mineralization (2701–2698 Ma; Mortensen 1993). The results of this study extend the ages of porphyry Cu-Mo-Au mineralization to circa 2690 Ma and suggest that there were multiple pulses of overprinting porphyry-style mineralization in the Blake River Group during its evolution. It remains to be seen, however, if there will be sufficient tonnages associated with these intrusions to make them economic porphyry Cu-Mo-Au targets. Nonetheless, they represent a potentially underexplored Cu-Mo-Au target within the Blake River Group of Ontario.

SUMMARY

- Rocks of the Blake River Group in Clifford Township, Ontario, consist predominantly of basalt to andesite with lesser rhyolite. These volcanic rocks are associated with synvolcanic, high level rhyolitic intrusive rocks, and synvolcanic gabbros and diabase. Collectively, these rocks have lithogeochemical signatures similar to modern enriched mid-ocean ridge basalt (E-MORB) and many have evidence for crustal contamination (contaminated E-MORB). It is uncertain at this point whether this contamination was due to contamination by an underlying arc substrate or due to contamination by true continental crust.

- The Clifford stock and age equivalent east-northeast-trending dikes from Clifford Township represent a distinctively younger pulse of magmatic activity within northeastern Ontario. The Clifford stock has yielded a U/Pb zircon age of 2686.9±1.2 Ma, and an age-equivalent east-northeast-trending dike has yielded an age of 2688.5±2.3 Ma. These ages are younger than the Blake River Group magmatism in this area (ca. 2700–2696 Ma; Péloquin and Piercey 2005), but are similar to other late tectonic tonalite-trondhjemite-granodiorite (TTG) plutons in the southeastern Abitibi greenstone belt (e.g., Clarice Lake, Lac Dufault: Corfu and Noble 1992; Mortensen 1993). The Clifford stock has very distinctive signatures typical of high-Al TTG suites, and have very distinctively low Y (<10 ppm) and Yb (<2 ppm), and high Zr/Y (>7), Nb/Y (>0.4), Al_2O_3/Yb (>10) and La/Yb (>10) ratios, as compared to the older Blake River Group rocks; these features can be used to geochemically discriminate felsic magmatism associated with the Blake River Group from younger TTG-related magmatism associated with the Clifford stock and other TTG magmatism circa 2690 Ma.

- Mineralization in Clifford Township consists of an older VMS-related style of mineralization, and a younger, overprinting porphyry Cu-Mo-Au style of mineralization. The VMS-related mineralization consists of epidote-quartz-pyrite-chlorite assemblages, typical of semi-conformable-style alteration associated with permeable zones (e.g., amygdules, pillow margins and interpillow regions) in the volcanic rocks of the Blake River Group. There are also some zones of higher temperature chlorite-quartz-chalcopyrite-pyrite assemblages typical of pipe-like alteration. The younger porphyry Cu-Mo-Au style mineralization occurs as a series of breccia pipes and stockwork vein systems. This latter style of mineralization is associated with a complex array of veinlet and vein-styles of alteration that is quite distinct from VMS mineralization. The fact that this mineralization is hosted in the Clifford stock and associated dikes, which have an age circa 2690 Ma, suggests that this mineralization represents a discrete younger magmatic-hydrothermal event, separate from the early VMS-related event.

REFERENCES

Arth, J.G. 1979. Some trace elements in trondhjemites—their implications to magma genesis and paleotectonic setting; *in* Trondhjemites, dacites and related rocks: Elsevier Scientific Publishing Co., New York, p.123-132.

Ayer, J., Amelin., Y., Corfu, F., Kamo, S., Ketchum, J.F., Kwok, K. and Trowell, H.F. 2002. Evolution of the Abitibi greenstone belt based on U-Pb geochronology: autochthonous volcanic construction followed by plutonism, regional deformation and sedimentation; Precambrian Research, v.115, p.63-95.

Bailes, A., Galley, A.G., Hannington, M.D., Holk, G., Katsube, J., Paquette, F., Paradis, S., Santaguida, F. and Taylor, B.E. 1998. Project 94OE7: The use of regional-scale alteration zones and subvolcanic intrusions in the exploration for volcanic-associated massive sulphide deposits; unpublished report for Canadian Mining Industry Research Organization Report, 369p.

Barrett, T.J. and MacLean, W.H. 1999. Volcanic sequences, lithogeochemistry, and hydrothermal alteration in some bimodal volcanic-associated massive sulfide systems; *in* Volcanic-associated massive sulfide deposits: processes and examples in modern and ancient environments, Society of Economic Geologists, Reviews of Economic Geology, v.8, p.101-131.

Campbell, I.H., Franklin, J.M., Gorton, M.P., Hart, T.R. and Scott, S.D. 1981. The role of subvolcanic sills in the generation of massive sulfide deposits; Economic Geology, v.76, p.2248-2253.

Card, K.D. and Poulsen, K.H. 1998. Archean and Paleoproterozoic geology and metallogeny of the southern Canadian Shield; Exploration and Mining Geology, v.7, no.3, p.181-215.

Chown, E.H., Harrap, R. and Moukhsil, A. 2002. The role of granitic intrusions in the evolution of the Abitibi belt, Canada; Precambrian Research, v.115, p.291-310.

Corfu, F. 1993. The evolution of the southern Abitibi greenstone belt in light of precise U-Pb geochronology; Economic Geology, v.88, p.1323-1340.

Corfu, F., Krogh, T.E., Kwok, Y.Y. and Jensen, L.S. 1989. U-Pb zircon geochronology in the southwestern Abitibi greenstone belt, Superior Province; Canadian Journal of Earth Sciences, v.26, p.1747-1763.

Corfu, F. and Noble, S.R. 1992. Genesis of the southern Abitibi greenstone belt, Superior Province, Canada: evidence from zircon Hf isotope analyses using a single filament technique; Geochimica et Cosmochimica Acta, v.56, p.2081-2097.

Date, J., Watanabe., Y. and Saeki, Y. 1983. Zonal alteration around the Fukazawa Kuroko deposits. Akita Prefecture, northern Japan; *in* Kuroko and related volcanogenic massive sulphide deposits, Economic Geology, Monograph 5, p.365-386.

Dimroth, E., Imreh, L., Goulet, N. and Rocheleau, M. 1983a. Evolution of the south-central segment of Archean Abitibi belt, Quebec: Part II. Tectonic evolution and geomechanical model; Canadian Journal of Earth Sciences, v.20, p.1355-1373.

——— 1983b. Evolution of the south-central segment of the Archean Abitibi belt, Quebec: Part III. Plutonic and metamorphic evolution and geotectonic model; Canadian Journal of Earth Sciences, v.20, p.1374-1388.

Dimroth, E., Imreh, L., Rocheleau, M. and Goulet, N. 1982. Evolution of the south-central part of the Archean Abitibi belt, Quebec: Part I. Stratigraphy and paleogeographic model; Canadian Journal of Earth Sciences, v.19, p.1729-1758.

Drummond, M.S. and Defant, M.J. 1990. A model for trondhjemite-tonalite-dacite genesis and crustal growth via slab melting: Archean to modern comparisons: Journal of Geophysical Research, Solid Earth and Planets, v.95, p.B21,503-B21,521.

Drummond, M.S., Defant, M.J. and Kepezhinskas, P.K. 1996. Petrogenesis of slab-derived trondhjemite-tonalite-dacite/adakite magmas; *in* The Third Hutton Symposium on the Origin of Granites and Related Rocks, Geological Society of America, Special Paper 315, p.205-215.

Feng, R. and Kerrich, R. 1992. Geochemical evolution of granitoids from the Archean Abitibi Southern Volcanic Zone and the Pontiac Subprovince, Superior Province, Canada: implications for tectonic history and source regions; Chemical Geology, v.98, July, p.23-70.

Fowler, A.D. and Jensen, L.S. 1989. Quantitative trace-element modelling of the crystallization history of the Kinojévis and Blake River groups, Abitibi greenstone belt, Ontario; Canadian Journal of Earth Sciences, v.26, p.1356-1367.

Franklin, J.M. 1993. Volcanic-associated massive sulphide deposits; *in* Mineral deposit modeling, Geological Association of Canada, Special Paper 40, p.315-334.

Frarey, M.J. and Krogh, T.E. 1986. U-Pb zircon ages of late internal plutons of the Abitibi and eastern Wawa subprovinces, Ontario and Quebec; *in* Current Research Part A, Geological Survey of Canada, Paper 86-1A, p.43-48.

Galley, A.G. 1993. Characteristics of semi-conformable alteration zones associated with volcanogenic massive sulphide districts; Journal of Geochemical Exploration, v.48, p.175-200.

——— 1996. Geochemical characteristics of subvolcanic intrusions associated with Precambrian massive sulphide deposits; *in* Trace element geochemistry of volcanic rocks: applications for massive sulphide exploration, Geological Association of Canada, Short Course Notes, v.12, p.239-278.

——— 1998. Characteristics of composite subvolcanic intrusive complexes associated with Precambrian VMS districts; *in* Project 94OE7: The use of regional-scale alteration zones and subvolcanic intrusions in the exploration for volcanic-associated massive sulphide deposits, unpublished report for Canadian Mining Industry Research Organization, p.1-40.

——— 2003. Composite synvolcanic intrusions associated with Precambrian VMS-related hydrothermal systems; Mineralium Deposita, v.38, p.443-473.

Galley, A. and van Breeman, O. 2002. Timing of synvolcanic magmatism in relation to base-metal mineralization, Rouyn–Noranda, Abitibi volcanic belt, Quebec; *in* Radiogenic Age and Isotopic Studies, Report 15, Geological Survey of Canada, 9p. [electronic access only]

Gibson, H.L., Morton, R.L. and Hudak, G.J. 1999. Submarine volcanic processes, deposits, and environments favorable for the location of volcanic-associated massive sulfide deposits; *in* Volcanic-associated massive sulfide deposits: processes and examples in modern and ancient environments, Society of Economic Geologists, Reviews of Economic Geology, v.8, p.13-51.

Gibson, H.L. and Watkinson, D.H. 1990. Volcanogenic massive sulphide deposits of the Noranda cauldron and shield volcano, Quebec; *in* The northwestern Quebec polymetallic belt: a summary of 60 years of mining exploration, Canadian Institute of Mining and Metallurgy, Special Volume 43, p.119-132.

Gledhill, T.L. 1928. Ben Nevis, Munro, Kamiskotia, and other base metal areas, districts of Cochrane and Timiskaming; Ontario Department of Mines, Map 37g, scale 1:63 360.

——— 1929. Ben Nevis, Munro, Kamiskotia, and other base metal areas, districts of Cochrane and Timiskaming; Ontario Department of Mines, Annual Report, 1928, v.37, pt.3, p.1-52.

Goldie, R.J. 1978. Magma mixing in the Flavrian pluton, Noranda area, Quebec; Canadian Journal of Earth Sciences, v.15, p.132-144.

——— 1979. Metamorphism of the Flavrian and Powell plutons, Noranda area, Quebec; Journal of Petrology, v.20, p.227-238.

Goldie, R.J. and Goodwin, A.M. 1977. The Flavrian and Powell plutons, Noranda area, Quebec: Archean volcanism in Superior Province, Canadian Shield; *in* Volcanic regimes in Canada, Geological Association of Canada, Special Paper 16, p.205-241.

Green, T.H. 1994. Experimental studies of trace-element partitioning applicable to igneous petrogenesis; Sedona 16 years later; Chemical Geology, v.117, November, p.1-36.

Green, T.H. and Pearson, N.J. 1987. An experimental study of Nb and Ta partitioning between Ti-rich minerals and silicate liquids at high pressure and temperature; Geochimica et Cosmochimica Acta, v.51, p.55-62.

Grunsky, E.C. 1986. Recognition of alteration in volcanic rocks using statistical analysis of lithogeochemical data: Journal of Geochemical Exploration, v.25, March, p.157-183.

——— 1988. Multivariate and spatial analysis of lithogeochemical data from metavolcanics with zones of alteration and mineralization in Ben Nevis Township, Ontario; unpublished PhD thesis, University of Ottawa, Ottawa, Ontario, 710p.

Grunsky, E.C. and Agterberg, F.P. 1988. Spatial and multivariate analysis of geochemical data from metavolcanic rocks in the Ben Nevis area, Ontario; Mathematical Geology, v.20, p.825-861.

Gutscher, M.-A., Maury, R., Eissen, J.-P. and Bourdon, E. 2000. Can slab melting be caused by flat subduction?; Geology, v.28, p.535-538.

Hannington, M.D. and Kjarsgaard, I.M. 1998. Mineral chemical studies of regional-scale hydrothermal alteration in the central Blake River Group, western Abitibi Subprovince: Part II. The Ben Nevis Volcanic Complex; *in* Project 94OE7: The use of regional-scale alteration zones and subvolcanic intrusions in the exploration for volcanic-associated massive sulphide deposits, unpublished report for Canadian Mining Industry Research Organization, p.77-122.

Hannington, M.D., Santaguida, F. and Kjarsgaard, I.M. 2001. Mineral-chemical database of regional greenschist facies assemblages in the central Blake River Group, western Abitibi Subprovince (NTS 32D); Geological Survey of Canada, Open File D3560.

Hannington, M.D., Santaguida, F., Kjarsgaard, I.M. and Cathles, L.M. 2003. Regional-scale hydrothermal alteration in the central Blake River Group, western Abitibi Subprovince, Canada: implications for VMS prospectivity; Mineralium Deposita, v.38, p.393-422.

Heaman, L.M. 1997. Global mafic magmatism at 2.45 Ga: remnants of an ancient large igneous province?; Geology, v.25, p.299-302.

Hofmann, A.W., Jochum, K.P., Suefert, M. and White, W.M. 1986. Nb and Pb in oceanic basalts: new constraints on mantle evolution; Earth and Planetary Science Letters, v.79, p.33-45.

Hogg, W.A. 1964a. Arnold and Katrine townships, District of Timiskaming, Ontario: Ontario Department of Mines, Report 29, 15p.

——— 1964b. Arnold and Katrine townships, District of Timiskaming, Ontario: Ontario Department of Mines, Map 2061, scale 1:31 680.

Hubert, C., Trudel, P. and Gélinas, L. 1984. Archean wrench fault tectonics and structural evolution of the Blake River Group, Abitibi belt, Quebec; Canadian Journal of Earth Sciences, v.21, p.1024-1032.

Hughes, C.J. 1973. Spilites, keratophyres and igneous spectrum; Geological Magazine, v.109, no.6, p.513-527.

Ioannou, S.E., Gotze, J., Weiershaeuser, L., Zubowski, S.M. and Spooner, E.T.C. 2004. Cathodoluminescence characteristics of Archean volcanogenic massive sulfide related quartz: Noranda, Ben Nevis, and Mattagami districts, Abitibi Subprovince, Canada; Geochemistry, Geophysics, Geosystems, v.5, DOI: 10.1029/2003GC000613 (24 pages).

Irvine, T.N. and Baragar, W.R.A. 1971. A guide to the chemical classification of the common volcanic rocks; Canadian Journal of Earth Sciences, v.8, p.523-548.

Jensen, L.S. 1974. Precambrian geology, Clifford and Ben Nevis townships, Timiskaming District, Ontario; Ontario Division of Mines, Map 2283, scale 1:31 680.

——— 1975. Geology of Clifford and Ben Nevis townships, District of Cochrane, Ontario; Ontario Division of Mines, Report 132, 55p.

——— 1985. Stratigraphy and petrogenesis of Archean metavolcanic sequences, southwestern Abitibi Subprovince, Ontario; *in* Evolution of Archean supracrustal sequences, Geological Association of Canada, Special Paper 28, p.65-87.

Jensen, L.S. and Langford, F.F. 1985. Geology and petrogenesis of the Archean Abitibi belt in the Kirkland Lake area, Ontario; Ontario Geological Survey, Miscellaneous Paper 123, 130p.

Jolly, W.T. 1980. The development and degradation of Archean lavas, Abitibi area, Canada; Journal of Petrology, v.21, p.323-363.

Knight, C.W. 1920a. Ben Nevis gold area, Cochrane and Timiskaming districts, Ontario; Ontario Department of Mines, Annual Report, 1920, v.29, pt.3, p.1-27.

——— 1920b. Ben Nevis gold area, Timiskaming and Cochrane districts, Ontario; Ontario Department of Mines, Map 29e, scale 1:63 360.

Lafleche, M.R., Dupuy, C. and Dostal, J. 1992. Tholeiitic volcanic rocks of the Late Archean Blake River Group, southern Abitibi greenstone belt: origin and geodynamic implications; Canadian Journal of Earth Sciences, v.29, p.1448-1458.

Large, R.R., Doyle, M., Raymond, O., Cooke, D., Jones, A. and Heasman, L. 1996. Evaluation of the role of Cambrian granites in the genesis of world class VHMS deposits in Tasmania; Ore Geology Reviews, v.10, p.215-230.

Large, R.R., Gemmell, J.B., Paulick, H. and Huston, D.L. 2001. The alteration box plot: a simple approach to understanding the relationship between alteration mineralogy and lithogeochemistry associated with volcanic-hosted massive sulfide deposits; Economic Geology, v.96, p.957-971.

Lassiter, J.C. and DePaolo, D.J. 1997. Plume/lithosphere interaction in the generation of continental and oceanic flood basalts: chemical and isotopic constraints; *in* Large igneous provinces: continental, oceanic and planetary flood volcanism, American Geophysical Union, Geophysical Monograph 100, p.335-355.

Lentz, D.R. 1998. Petrogenetic evolution of felsic volcanic sequences associated with Phanerozoic volcanic-hosted massive sulfide systems: the role of extensional geodynamics; Ore Geology Reviews, v.12, p.289-327.

Lesher, C.M., Goodwin, A.M., Campbell, I.H. and Gorton, M.P. 1986. Trace element geochemistry of ore-associated and barren felsic metavolcanic rocks in the Superior Province, Canada; Canadian Journal of Earth Sciences, v.23, p.222-237.

Ludden, J.N. and Hubert, C. 1986. Geological evolution of the Late Archean Abitibi greenstone belt in Canada; Geology, v.14, p.707-711.

Ludden, J.N. and Péloquin, A.S. 1996. A geodynamic model for the evolution of the Abitibi belt: implications for the origins of volcanic massive sulphide (VMS) deposits; *in* Trace element geochemistry of volcanic rocks: applications for massive sulfide exploration, Geological Association of Canada, Short Course Notes, v.12, p.205-237.

McLennan, S.M. 2001. Relationships between the trace element composition of sedimentary rocks and upper continental crust; Geochemistry, Geophysics, Geosystems, v.2, doi:10.1029/2000GC000109, 2001.

Mortensen, J.K. 1993. U–Pb geochronology of the eastern Abitibi Subprovince. Part 2: Noranda–Kirkland Lake area; Canadian Journal of Earth Sciences, v.30, p.29-41.

O'Connor, J.T. 1965. A classification for quartz-rich igneous rocks based on feldspar ratio; *in* Geological Survey Research 1965, United States Geological Survey, Professional Paper 525B, p.79-84.

Paradis, S., Ludden, J.N. and Gélinas, L. 1988. Evidence for contrasting compositional spectra in comagmatic intrusive and extrusive rocks of the Late Archean Blake River Group, Abitibi, Quebec; Canadian Journal of Earth Sciences, v.25, p.134-144.

Pearce, J.A. 1996. A user's guide to basalt discrimination diagrams; *in* Trace element geochemistry of volcanic rocks: applications for massive sulphide exploration, Geological Association of Canada, Short Course Notes, v.12, p.79-113.

Pearce, J.A. and Peate, D.W. 1995. Tectonic implications of the composition of volcanic arc magmas; Annual Reviews of Earth and Planetary Science, v.23, p.251-285.

Péloquin, A.S. 1999. Reappraisal of the Blake River Group stratigraphy and its place in the Archean volcanic record; Thèse de doctorat [unpublished PhD thesis], Université de Montréal, Montreal, Quebec, 189p.

Péloquin, A.S. and Piercey, S.J. 2003. Discover Abitibi. Base Metal Subproject 3: Geology and base metal mineralization in Ben Nevis, Katrine and Clifford townships; *in* Summary of Field Work and Other Activities 2003, Ontario Geological Survey, Open File Report 6120, p.41-1 to 41-8.

——— 2005. Geology and base metal mineralization in Ben Nevis, Katrine and Clifford townships: Discover Abitibi; Ontario Geological Survey, Open File Report 6161.

Péloquin, A.S., Potvin, R., Paradis, S., Laflèche, M.R., Verpaelst, P. and Gibson, H.L. 1990. The Blake River Group, Rouyn–Noranda area, Quebec: a stratigraphic synthesis; *in* The northwestern Quebec polymetallic belt: a summary of 60 years of mining exploration, Canadian Institute of Mining and Metallurgy, Special Volume 43, p.107-118.

Piercey, S.J., Hamilton, M.A., Péloquin, A.S. and Chaloux, E. 2004. Discover Abitibi. Intrusion Subproject. Updates on studies of the Clifford stock and Blake River Group, Clifford Township; *in* Summary of Field Work and Other Activities 2004, Ontario Geological Survey, Open File Report 6145, p.44-1 to 44-14.

Powell, W.G., Carmichael, D.M. and Hodgson, C.J. 1993. Thermobarometry in a subgreenschist to greenschist transition in metabasites of the Abitibi greenstone belt, Superior Province, Canada; Journal of Metamorphic Geology, v.11, p.165-178.

——— 1995. Conditions and timing of metamorphism in the southern Abitibi greenstone belt, Quebec; Canadian Journal of Earth Sciences, v.32, p.787-805.

Racicot, D. 1990. La production minière dans la partie Québécoise de la Sous-province d'Abitibi: 1927–1988; *in* The northwestern Quebec polymetallic belt: a summary of 60 years of mining exploration, Canadian Institute of Mining and Metallurgy, Special Volume 43, p.33-42.

Rollinson, H.R. 1993. Using geochemical data: evaluation, presentation, interpretation, John Wiley and Sons, New York, 352p.

Saeki, Y. and Date, J. 1980. Computer application to the alteration data of the footwall dacite lava at the Ezuri Kuroko deposits, Akito Prefecture; Mining Geology, v.30, p.241-250.

Smithies, R.H., Champion, D.C. and Cassidy, K.F. 2003. Formation of Earth's early Archaean continental crust; Precambrian Research, v.127, p.89-101.

Sun, S-s. and McDonough, W.F. 1989. Chemical and isotopic systematics of oceanic basalts: implications for mantle composition and processes; *in* Magmatism in the ocean basins, Geological Society, Special Publication No.42, p.313-345.

Sutcliffe, R.H., Barrie, C.T., Burrows, D.R. and Beakhouse, G.P. 1993. Plutonism in the southern Abitibi Subprovince: a tectonic and petrogenetic framework; Economic Geology, v.88, p.1359-1375.

Taylor, B.E. and Timbal, A. 1998. Regional stable isotope studies in the Clifford–Ben Nevis area; *in* Project 94OE7: The use of regional-scale alteration zones and subvolcanic intrusions in the exploration for volcanic-associated massive sulphide deposits, unpublished report for Canadian Mining Industry Research Organization, p.123-130.

Weiershaeuser, L. and Spooner, E. 2002. Constraints on Archean (2.7 Ga) seawater salinity from fluid inclusion data, Ben Nevis area, Abitibi greenstone belt, Ontario, Canada; Geological Society of America, Abstracts with Programs, v.34, no.6, p.271.

———2003. Archean (2.7 Ga) seawater salinity; constraints from fluid inclusion microthermometry, Ben Nevis area, Abitibi greenstone belt, Ontario, Canada; Geological Society of America, Abstracts with Programs, v.35, no.6, p.594.

Wilson, W.J. 1901. Western part of the Abitibi region; Summary Report A, Geological Survey of Canada, XIV, p.117A-130A.

Winchester, J.A. and Floyd, P.A. 1977. Geochemical discrimination of different magma series and their differentiation products using immobile elements; Chemical Geology, v.20, p.325-343.

Wolfe, W.J. 1977. Geochemical exploration of Early Precambrian volcanogenic massive sulphide mineralization in Ben Nevis Township, District of Cochrane; Ontario Geological Survey, Study 19, 39p.

Wyman, D.A. 2003. Upper mantle processes beneath the 2.7 Ga Abitibi belt, Canada: a trace element perspective; Precambrian Research, v.127, p.143-165.

Wyman, D.A., Kerrich, R. and Polat, A. 2002. Assembly of Archean cratonic mantle lithosphere and crust; plume-arc interaction in the Abitibi–Wawa subduction-accretion complex; Precambrian Research, v.115, p.37-62.

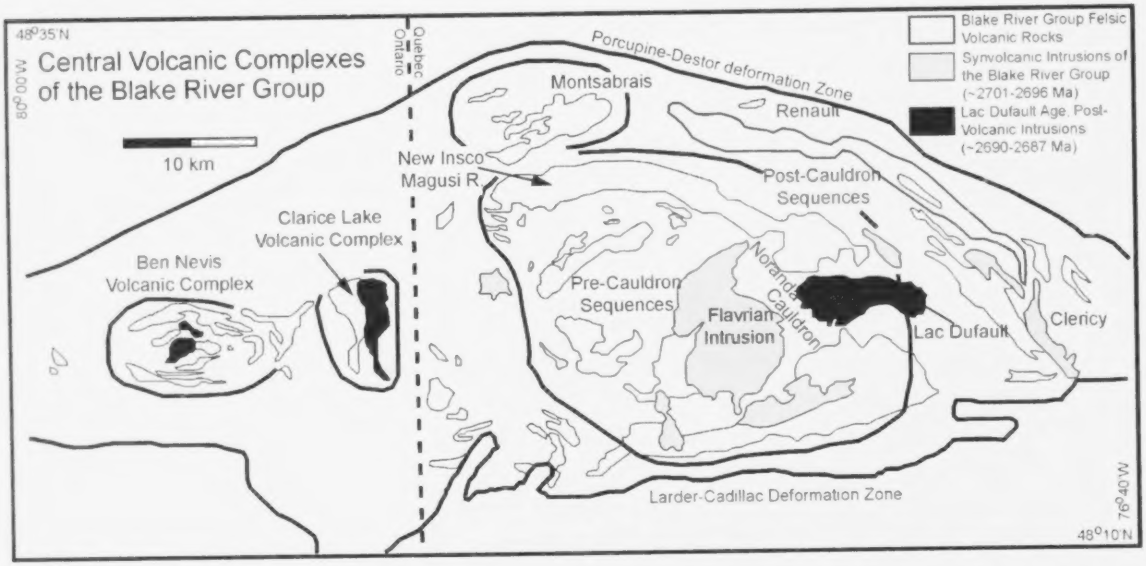
48°35'N
80°00'W
Central Volcanic Complexes of the Blake River Group
10 km
Quebec
Ontario
Porcupine-Destor deformation Zone
Montsabrais
Renault
New Insco
Magusi R.
Post-Cauldron Sequences
Clarice Lake Volcanic Complex
Ben Nevis Volcanic Complex
Noranda Cauldron
Pre-Cauldron Sequences
Flavrian Intrusion
Lac Dufault
Clericy
Larder-Cadillac Deformation Zone
76°40'W
48°10'N
Blake River Group Felsic Volcanic Rocks
Synvolcanic Intrusions of the Blake River Group (~2701-2696 Ma)
Lac Dufault Age, Post-Volcanic Intrusions (~2690-2687 Ma)

Figure 3.1. Regional distribution of the Blake River Group (upper and lower bounds between the Porcupine–Destor fault and the Larder–Cadillac deformation zone), with locations of major felsic volcanic complexes of the central Blake River Group, synvolcanic intrusions of the Blake River Group, and younger, Lac Dufault age intrusions. Figure *modified from* Hannington et al. (2003).

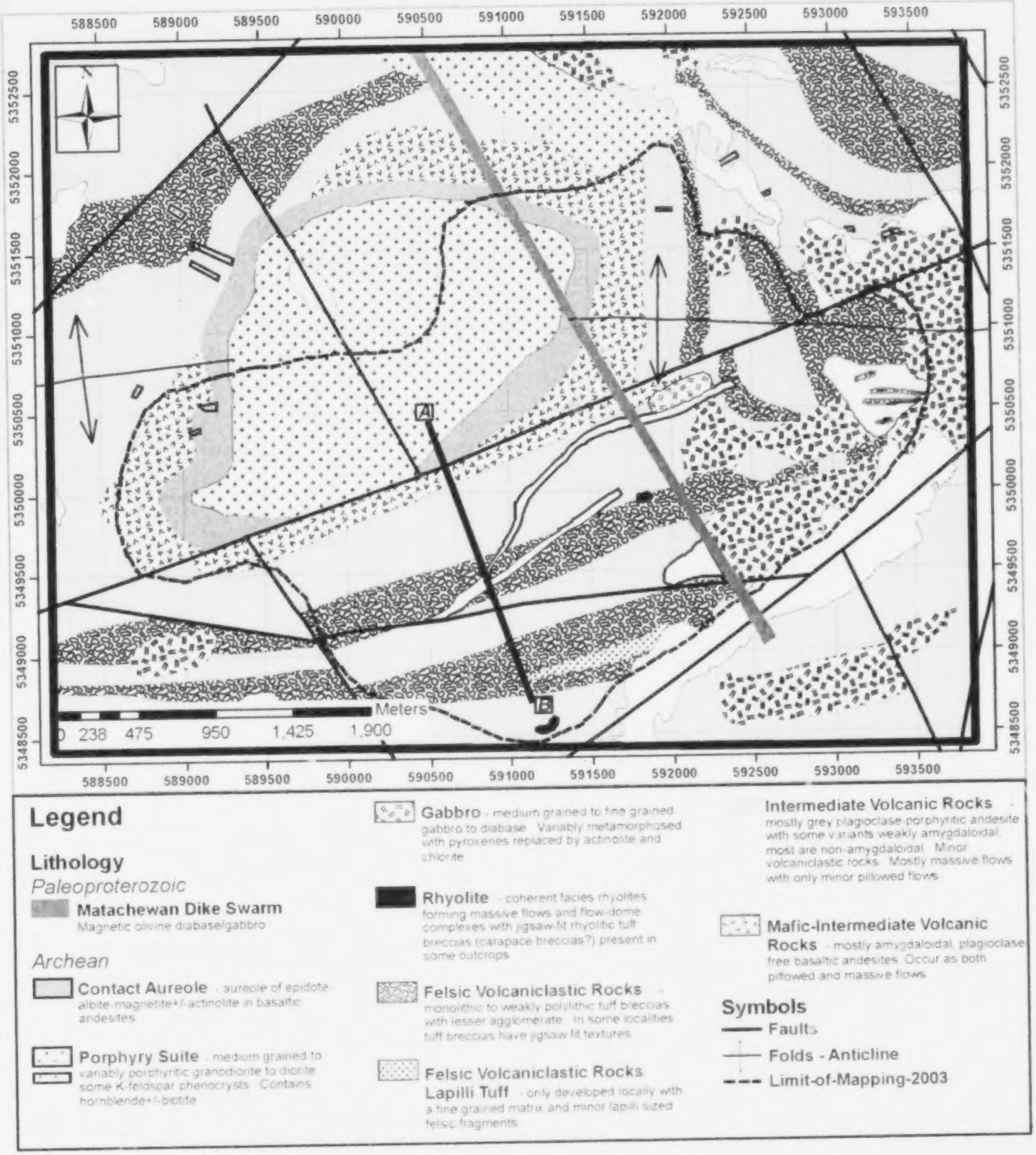

588500
589000
589500
590000
590500
591000
591500
592000
592500
593000
593500
5352500
5352000
5351500
5351000
5350500
5350000
5349500
5349000
5348500
A
B
Meters
0 238 475 950 1,425 1,900
Legend
Lithology
Paleoproterozoic
Matachewan Dike Swarm
Magnetic olivine diabase/gabbro
Archean
Contact Aureole - aureole of epidote albite-magnetite+/-actinolite in basaltic andesites
Porphyry Suite - medium grained to variably porphyritic granodiorite to diorite some K-feldspar phenocrysts. Contains hornblende+/-biotite
Gabbro - medium grained to fine grained gabbro to diabase. Variably metamorphosed with pyroxenes replaced by actinolite and chlorite
Rhyolite - coherent facies rhyolites forming massive flows and flow-dome complexes with jigsaw-fit rhyolitic tuff breccias (carapace breccias?) present in some outcrops
Felsic Volcaniclastic Rocks - monolithic to weakly polylithic tuff breccias with lesser agglomerate. In some localities tuff breccias have jigsaw fit textures
Felsic Volcaniclastic Rocks Lapilli Tuff - only developed locally with a fine grained matrix and minor lapilli sized felsic fragments
Intermediate Volcanic Rocks - mostly grey plagioclase-porphyritic andesite with some variants weakly amygdaloidal, most are non-amygdaloidal. Minor volcaniclastic rocks. Mostly massive flows with only minor pillowed flows
Mafic-Intermediate Volcanic Rocks - mostly amygdaloidal, plagioclase-free basaltic andesites. Occur as both pillowed and massive flows
Symbols
Faults
Folds - Anticline
Limit-of-Mapping-2003

Figure 3.2. Geological map of the Clifford stock and Blake River Group, Clifford Township. Geology based on the mapping of Piercey et al. (2004), Péloquin and Piercey (2003) and Jensen (1975). Line A–B is the line of section for the schematic section outlined in Figure 3.3.

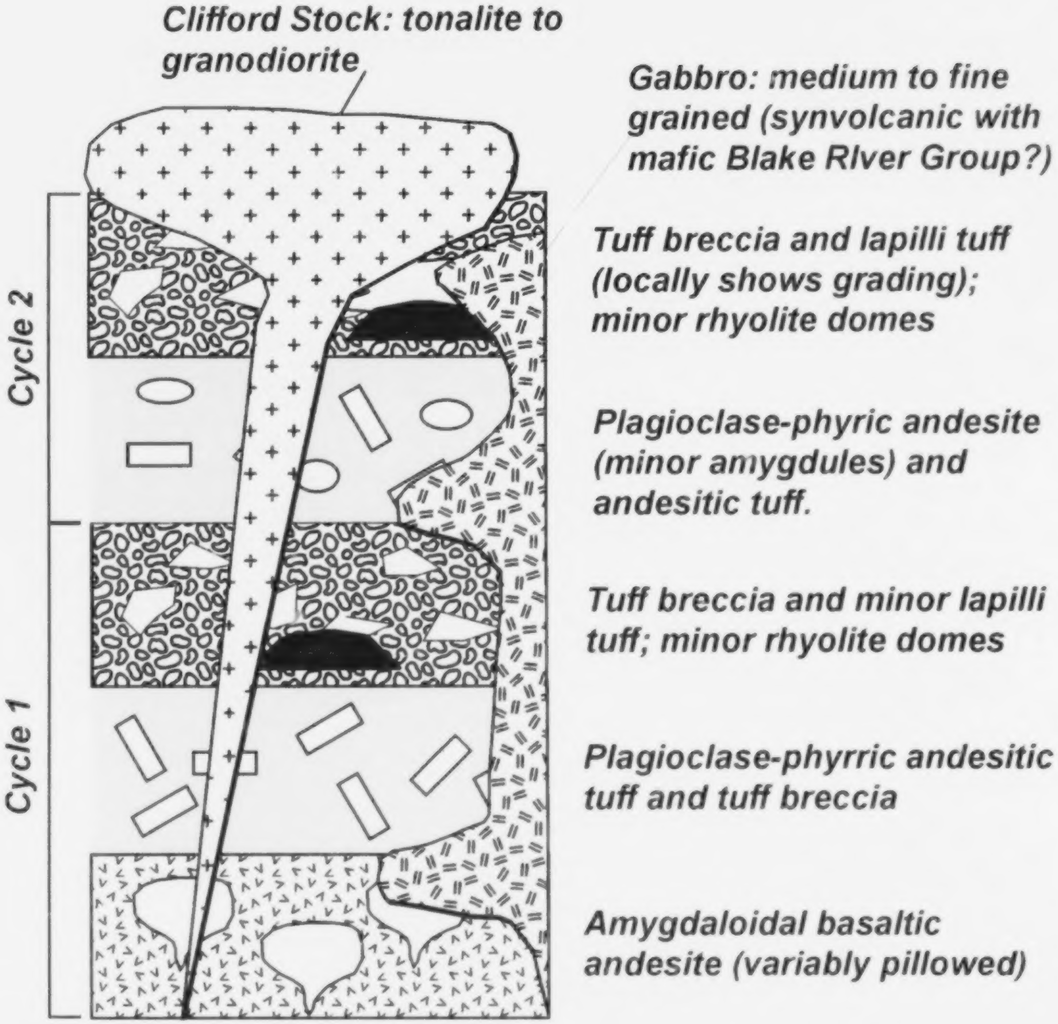
Clifford Stock: tonalite to granodiorite
Gabbro: medium to fine grained (synvolcanic with mafic Blake RIver Group?)
Tuff breccia and lapilli tuff (locally shows grading); minor rhyolite domes
Plagioclase-phyric andesite (minor amygdules) and andesitic tuff.
Tuff breccia and minor lapilli tuff; minor rhyolite domes
Plagioclase-phyrric andesitic tuff and tuff breccia
Amygdaloidal basaltic andesite (variably pillowed)
Cycle 2
Cycle 1

Figure 3.3. Schematic stratigraphic column for rocks of the Blake River Group in Clifford Township. Location of the section shown in Figure 3.2.

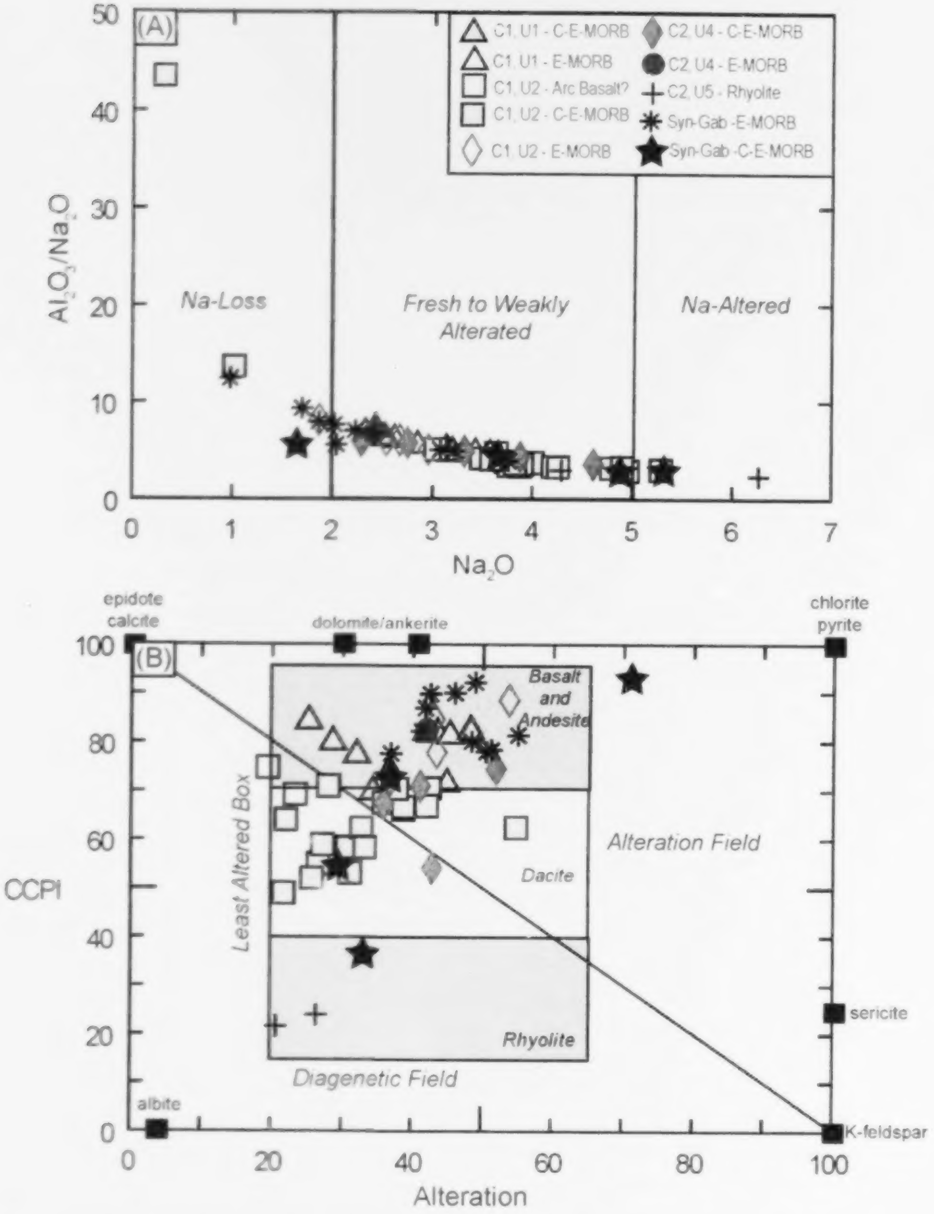

Figure 3.4. Major element alteration plots for the Blake River Group Rocks in Clifford Township, including A) Na_2O versus Al_2O_3/Na_2O plot with designations for least-altered samples; and B) alteration box-plot (*from* Large et al. 2001) with Hashimoto alteration index ([$(MgO+K_2O)/(MgO+K_2O+Na_2O+CaO)$]; Date, Watanabe and Saeki 1983; Saeki and Date 1980) plotted against chlorite-carbonate-pyrite-index [CCPI: $(MgO+Fe_2O_3T)/(MgO+Fe_2O_3T+Na_2O+CaO)$]. Abbreviations in legend: C = cycle, U = unit (e.g., C1, U1 = cycle 1, unit 1), E-MORB = E-MORB-like signatures; C-E-MORB = contaminated E-MORB-like signatures; Syn-Gab = synvolcanic gabbro and diabase.

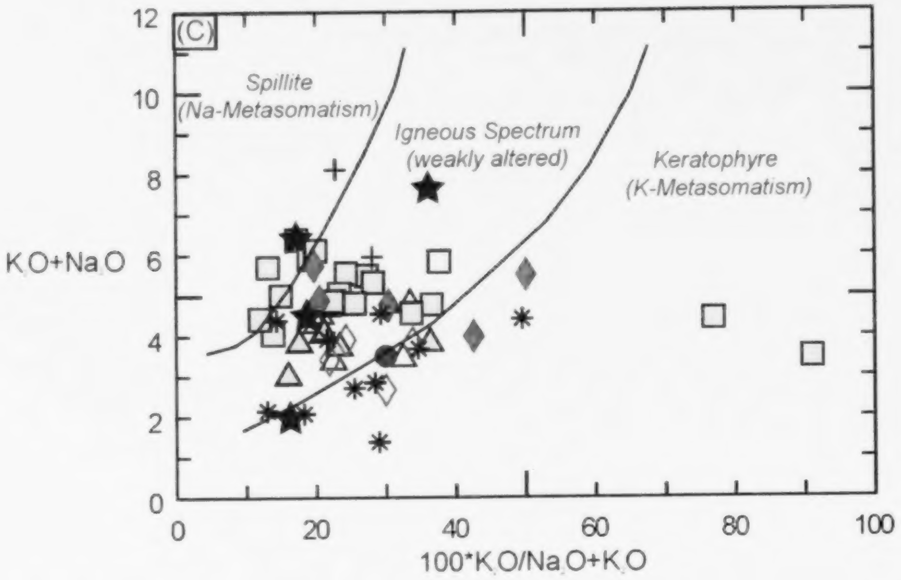

Figure 3.4, continued. Major element alteration plots for the Blake River Group Rocks in Clifford Township: C) ($100*K_2O/K_2O+Na_2O$) versus (K_2O+Na_2O) Hughes plot (*from* Hughes 1973). Abbreviations in legend: C = cycle, U = unit (e.g., C1, U1 = cycle 1, unit 1). E-MORB = E-MORB-like signatures; C-E-MORB = contaminated E-MORB-like signatures; Syn-Gab = synvolcanic gabbro and diabase.

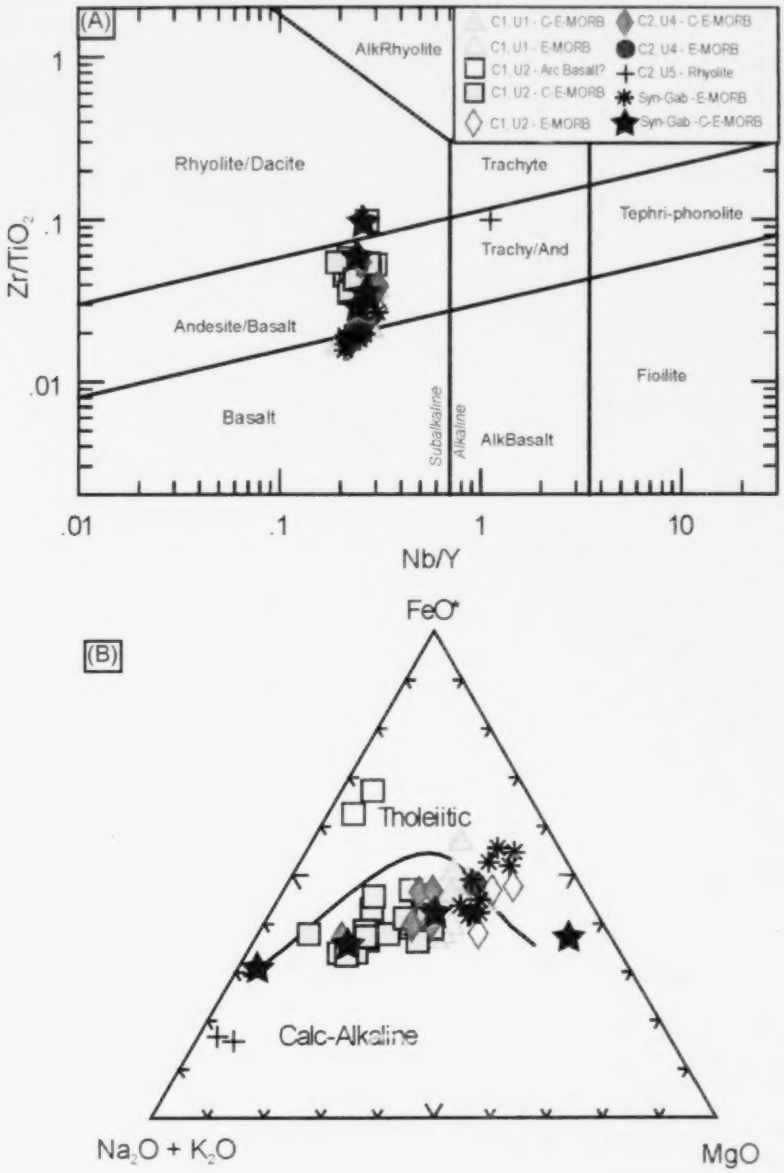

Figure 3.5. Geochemical classification diagrams for the Blake River Group rocks. A) Modified Winchester and Floyd (1977) Nb/Y versus Zr/TiO$_2$ diagram (Pearce 1996); and B) standard AFM diagram (Irvine and Baragar 1971).

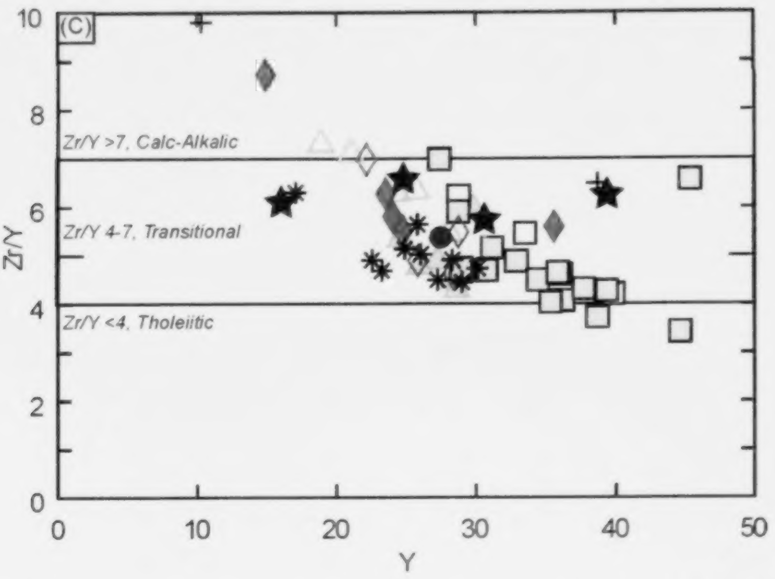

Figure 3.5, continued. Geochemical classification diagrams for the Blake River Group rocks. C) Y versus Zr/Y diagram using Zr/Y ratios as measure of tholeiitic versus calc-alkalic, based on Zr/Y classification concept of Barrett and MacLean (1999).

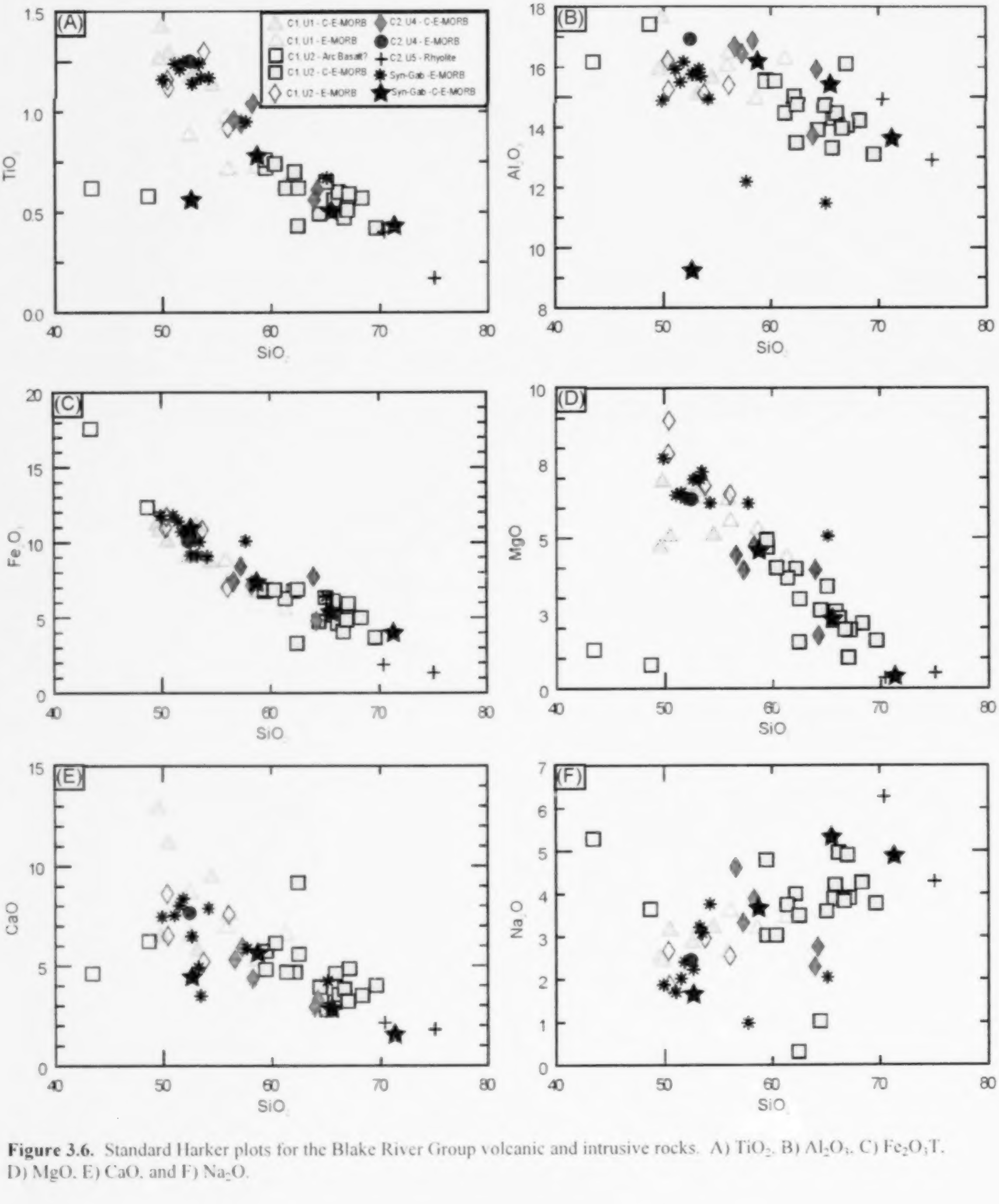

Figure 3.6. Standard Harker plots for the Blake River Group volcanic and intrusive rocks. A) TiO_2, B) Al_2O_3, C) Fe_2O_3T, D) MgO, E) CaO, and F) Na_2O.

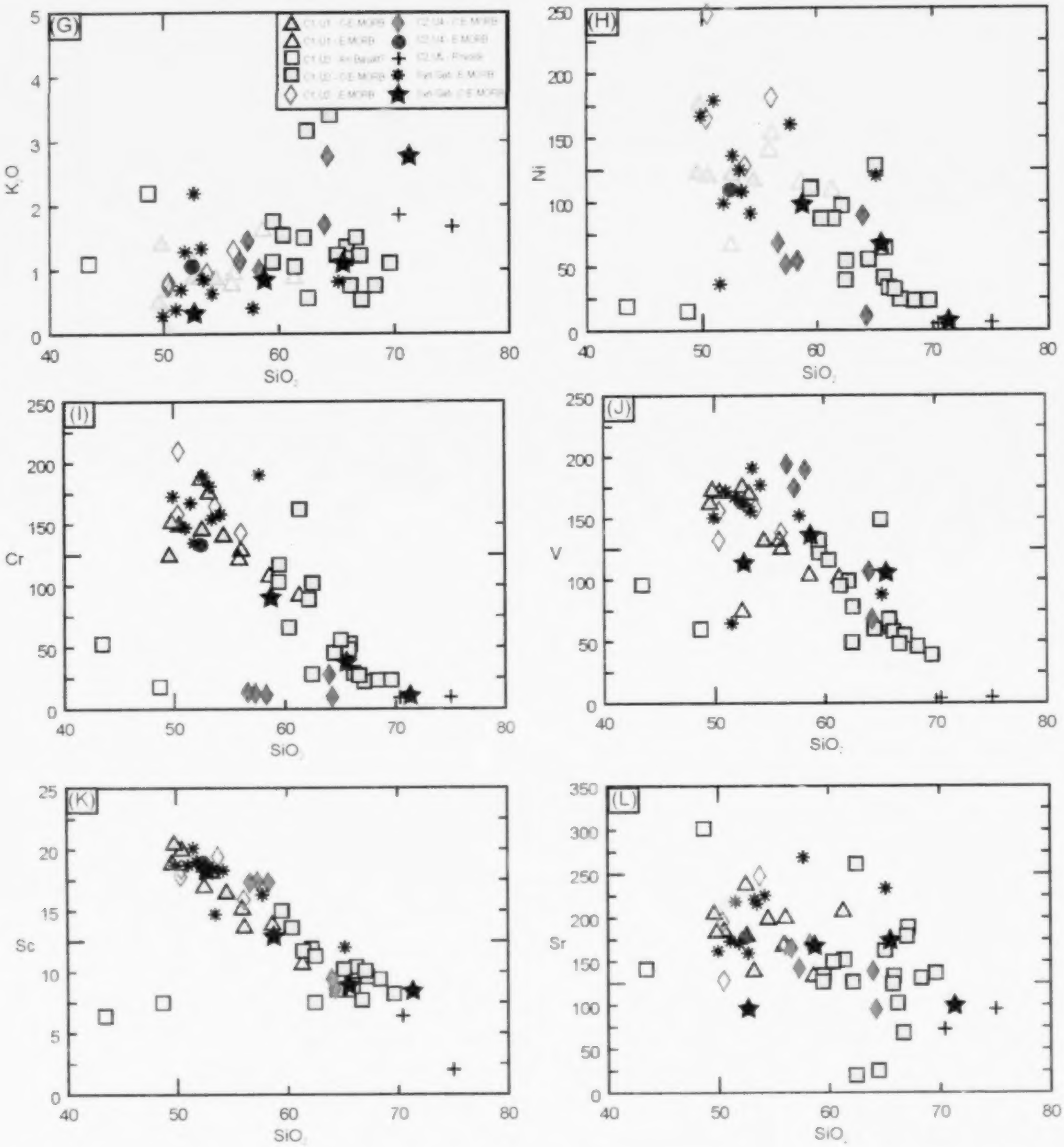

Figure 3.6, continued. Standard Harker plots for the Blake River Group volcanic and intrusive rocks. G) K_2O, H) Ni, I) Cr, J) V, K) Sc, and L) Sr.

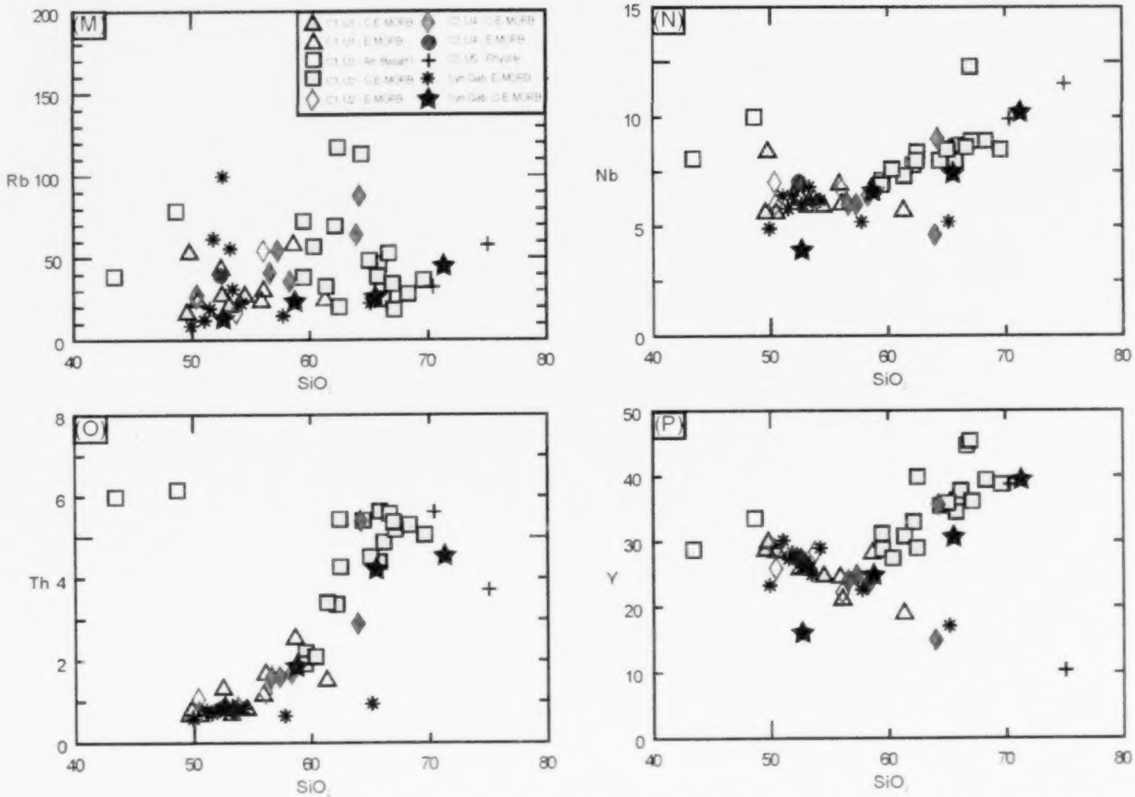

Figure 3.6, continued. Standard Harker plots for the Blake River Group volcanic and intrusive rocks. M) Rb, N) Nb, O) Th, and P) Y.

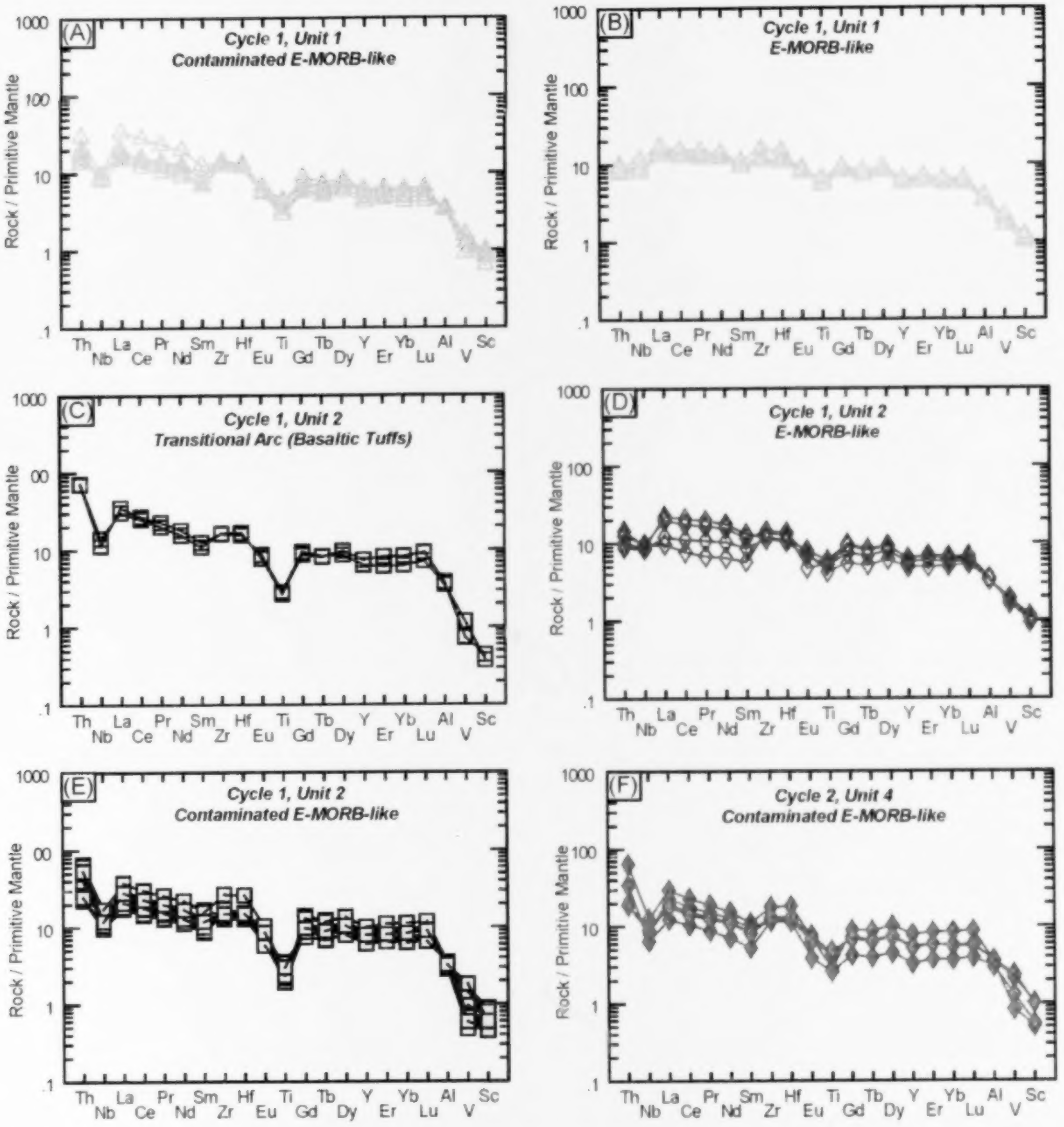

Figure 3.7. Primitive mantle normalized plots for rocks of the Blake River Group: A) cycle 1, unit 1, contaminated E-MORB-like; B) cycle 1, unit 1, E-MORB-like; C) cycle 1, unit 2, transitional arc (basaltic tuffs); D) cycle 1, unit 2, E-MORB-like; E) cycle 1, unit 2, contaminated E-MORB-like; and F) cycle 2, unit 4, contaminated E-MORB-like. Primitive mantle values *from* Sun and McDonough (1989).

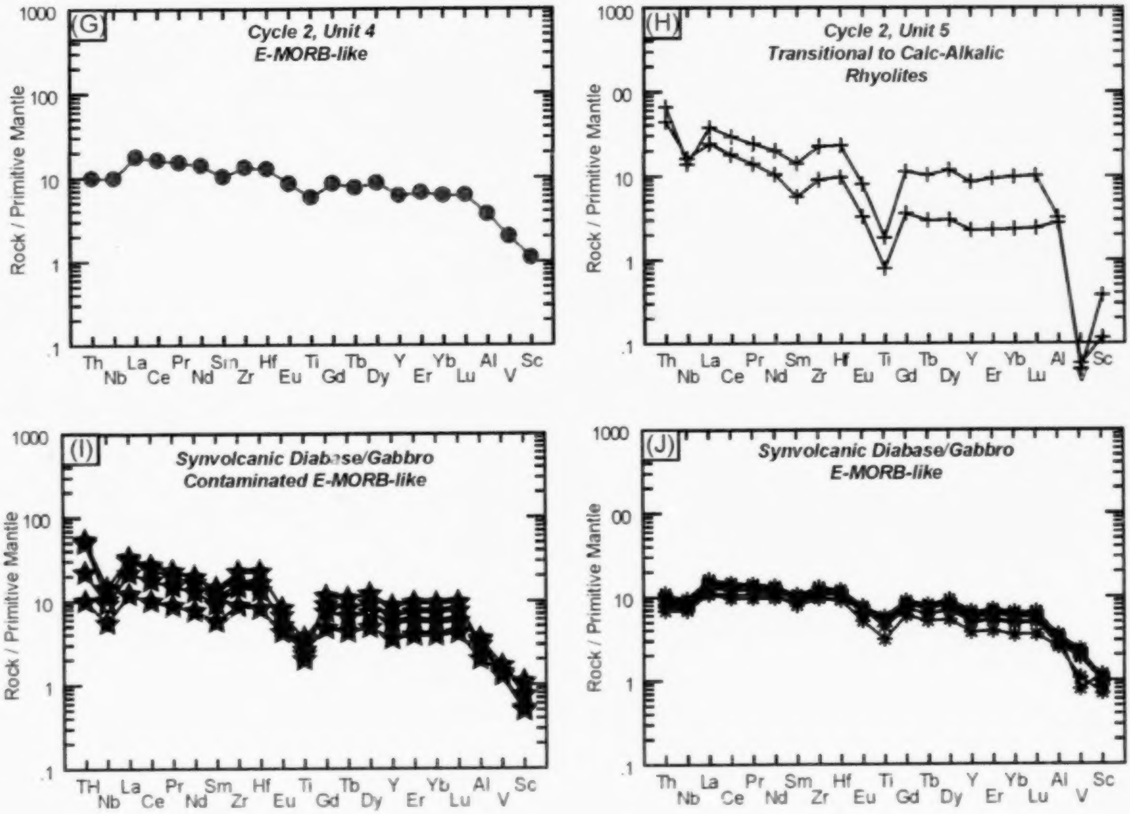

Figure 3.7, continued. Primitive mantle normalized plots for rocks of the Blake River Group: G) cycle 2, unit 4, E-MORB-like; H) cycle 2, unit 5, transitional to calc-alkalic rhyolites; I) synvolcanic gabbro and diabase, contaminated E-MORB like; and J) synvolcanic gabbro and diabase, E-MORB like. Primitive mantle values *from* Sun and McDonough (1989).

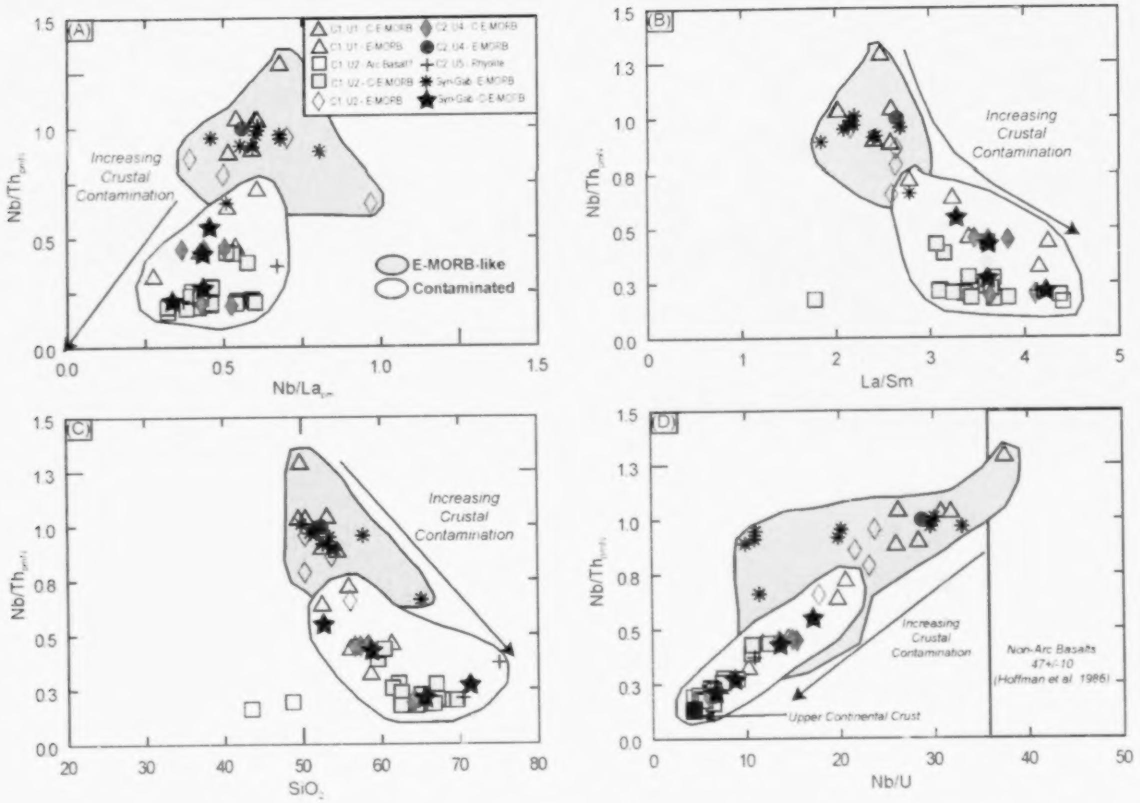

Figure 3.8. Trace element plots illustrating relationship of the size of the negative Nb anomaly (Nb/Th_{pmN}) to contamination sensitive elements and element ratios: A) Nb/La_{pmN} versus Nb/Th_{pmN}; B) La/Sm versus Nb/Th_{pmN}; C) SiO_2 versus Nb/Th_{pmN}; and D) Nb/U versus Nb/Th_{pmN}. Values for oceanic basalts of Nb/U = 47±10, and for the upper continental crust (D) are *from* Hofmann et al. (1986) and McLennan (2001).

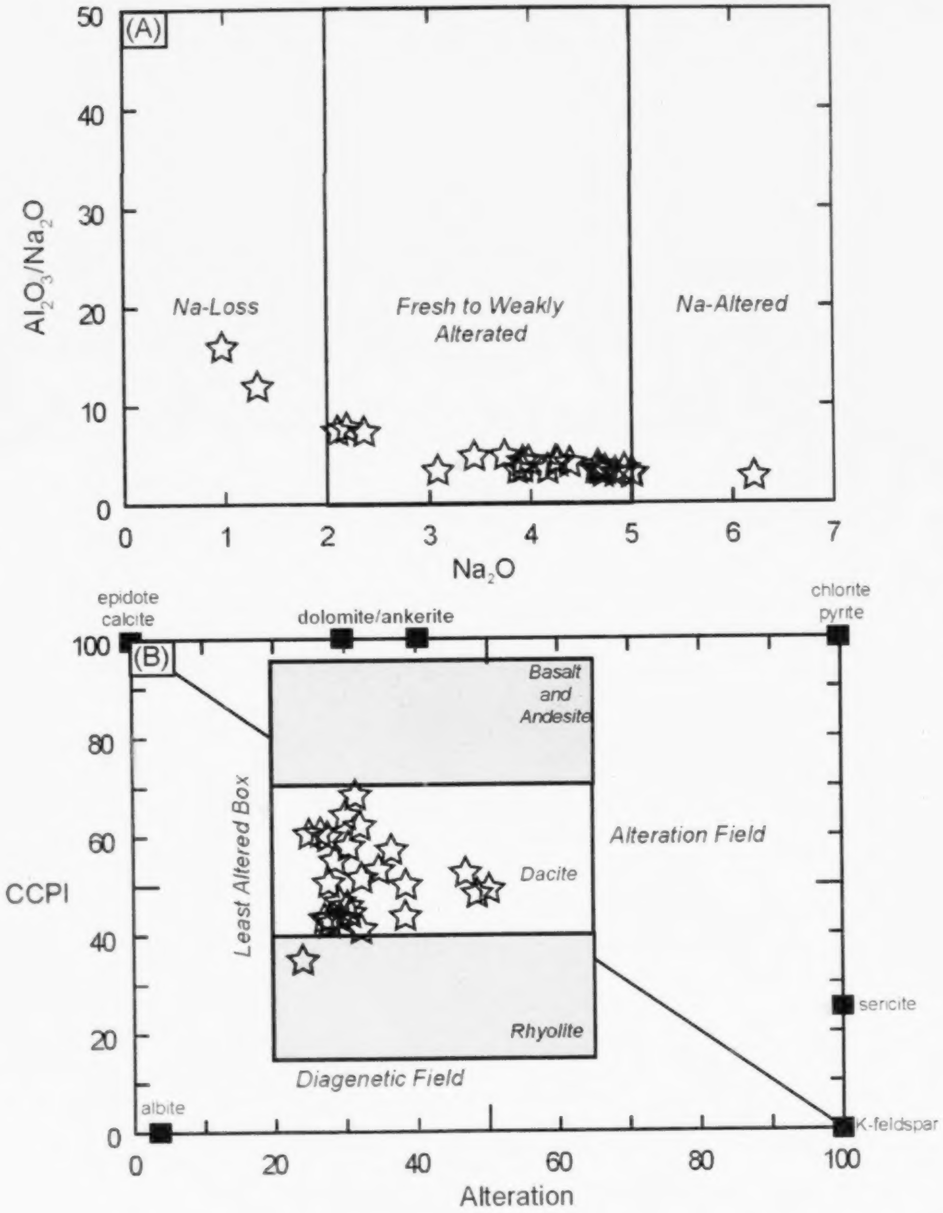

Figure 3.9. Major element alteration plots for the Clifford stock and equivalent rocks from Clifford Township, including: A) Na_2O versus Al_2O_3/Na_2O plot with designations for least-altered samples: and B) alteration box-plot (*from* Large et al. 2001) with Hashimoto alteration index ([$(MgO+K_2O)/(MgO+K_2O+Na_2O+CaO)$]: Date, Watanabe and Saeki 1983: Saeki and Date 1980) plotted against chlorite-carbonate-pyrite-index [CCPI: $(MgO+Fe_2O_3T)/(MgO+Fe_2O_3T+Na_2O+CaO)$].

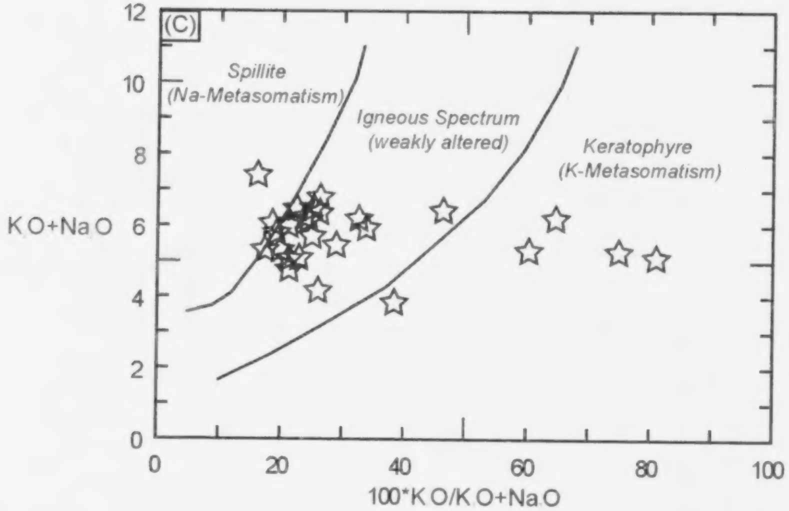

Figure 3.9, continued. Major element alteration plots for the Clifford stock and equivalent rocks from Clifford Township: C) (100*K_2O/K_2O+Na_2O) versus (K_2O+Na_2O) Hughes plot (*from* Hughes 1973).

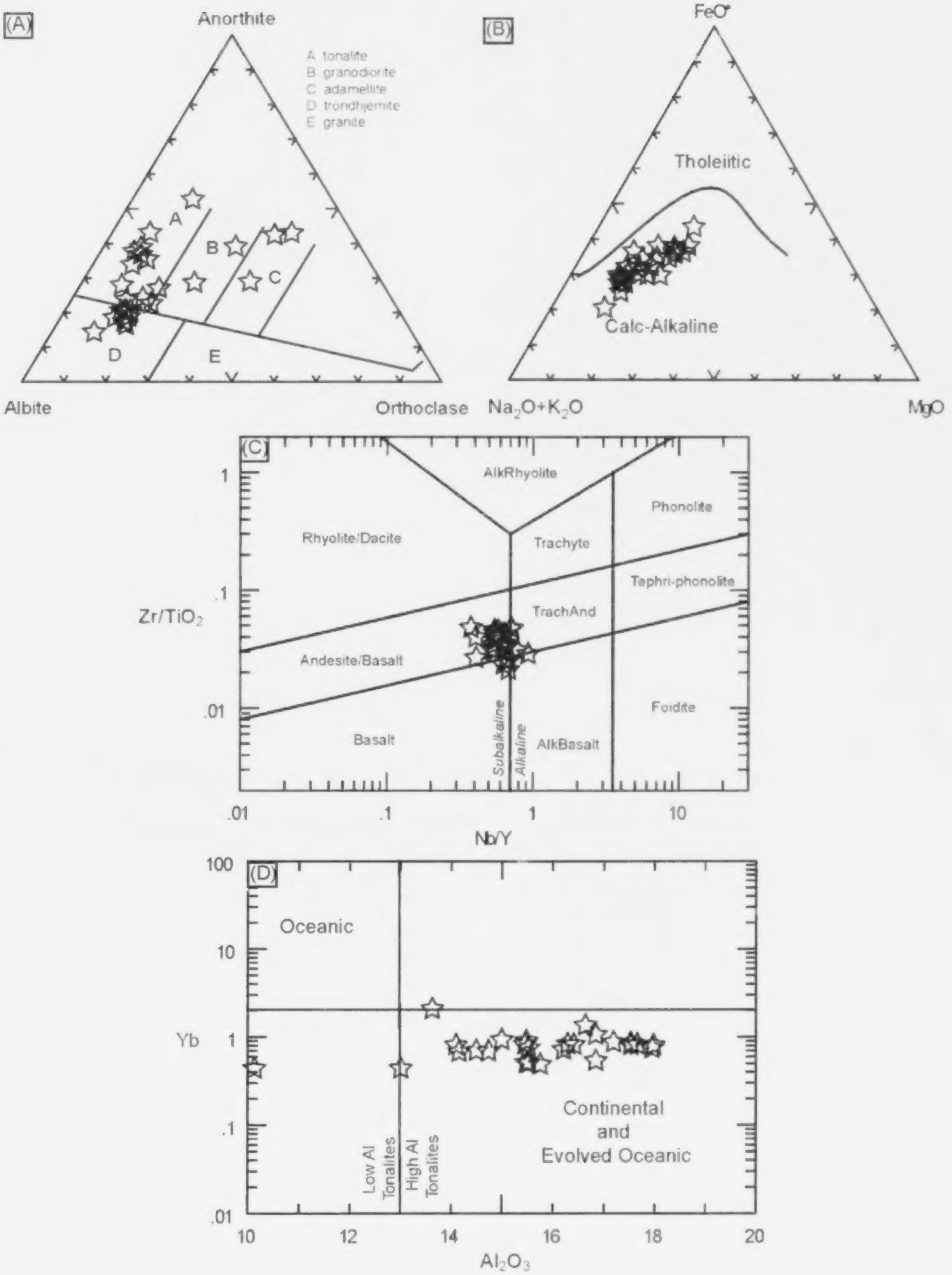

Figure 3.10. Classification plots for the rocks of the Clifford stock and equivalents. A) typical normative feldspar diagram *from* O'Connor (1965); B) alkali–FeO–MgO (AFM) plot *from* Irvine and Baragar (1971); C) Nb/Y versus Zr/TiO$_2$ discrimination diagram of Winchester and Floyd (1977); modification *from* Pearce (1996); and D) Al$_2$O$_3$ versus Yb diagram for classifying different types of TTG *from* Arth (1979).

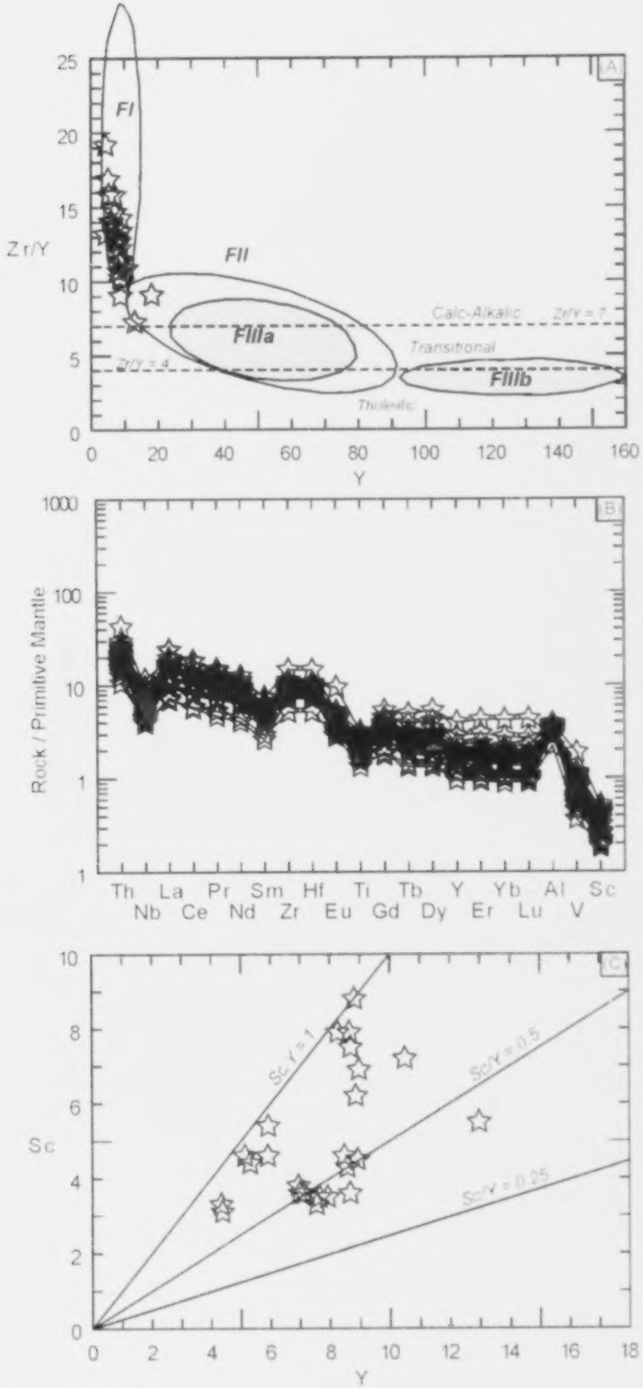

Figure 3.11. Trace element plots for rocks of the Clifford stock and equivalents: A) Y versus Zr/Y diagram of Lesher et al. (1986) as modified by Lentz (1998), with magmatic affinities based on Zr/Y ratios from the concepts of Barrett and MacLean (1999); B) primitive mantle normalized plot (primitive mantle values *from* Sun and McDonough 1989); and C) Y versus Sc plot of Feng and Kerrich (1992).

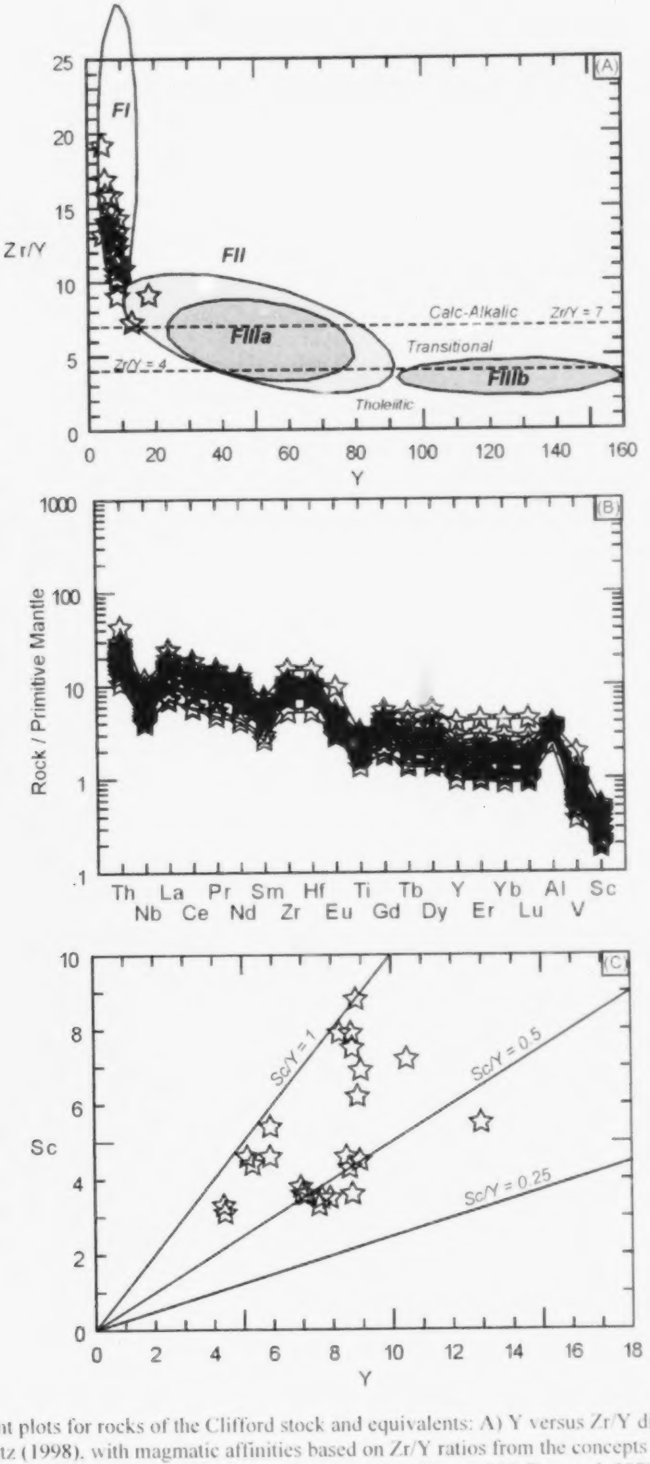

Figure 3.11. Trace element plots for rocks of the Clifford stock and equivalents: A) Y versus Zr/Y diagram of Lesher et al. (1986) as modified by Lentz (1998), with magmatic affinities based on Zr/Y ratios from the concepts of Barrett and MacLean (1999); B) primitive mantle normalized plot (primitive mantle values *from* Sun and McDonough 1989); and C) Y versus Sc plot of Feng and Kerrich (1992).

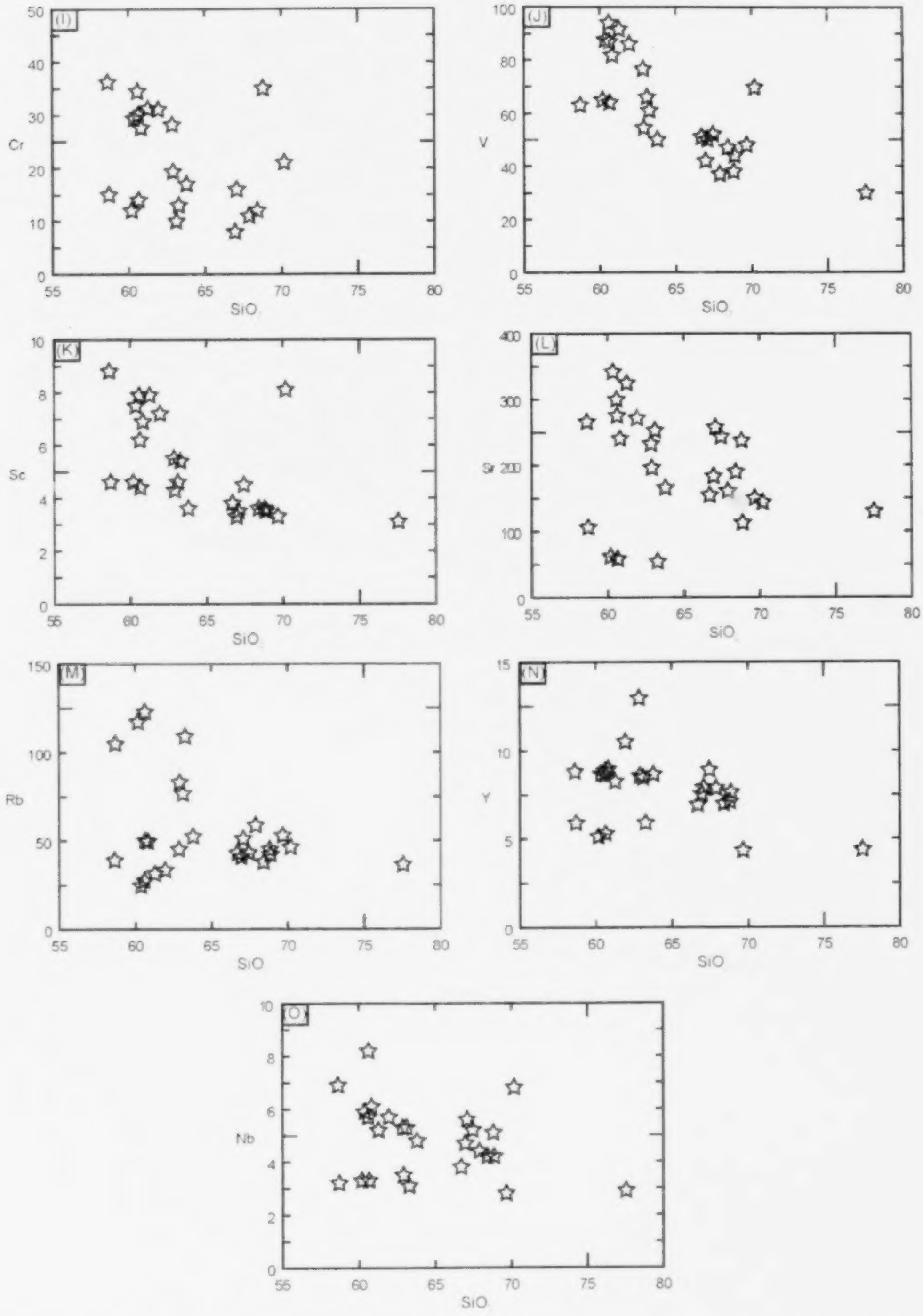

Figure 3.12. Standard Harker plots for rocks of the Clifford stock and equivalents. A) TiO_2; B) Al_2O_3; C) Fe_2O_3T; D) MgO; E) CaO; F) Na_2O; G) K_2O; and H) Ni.

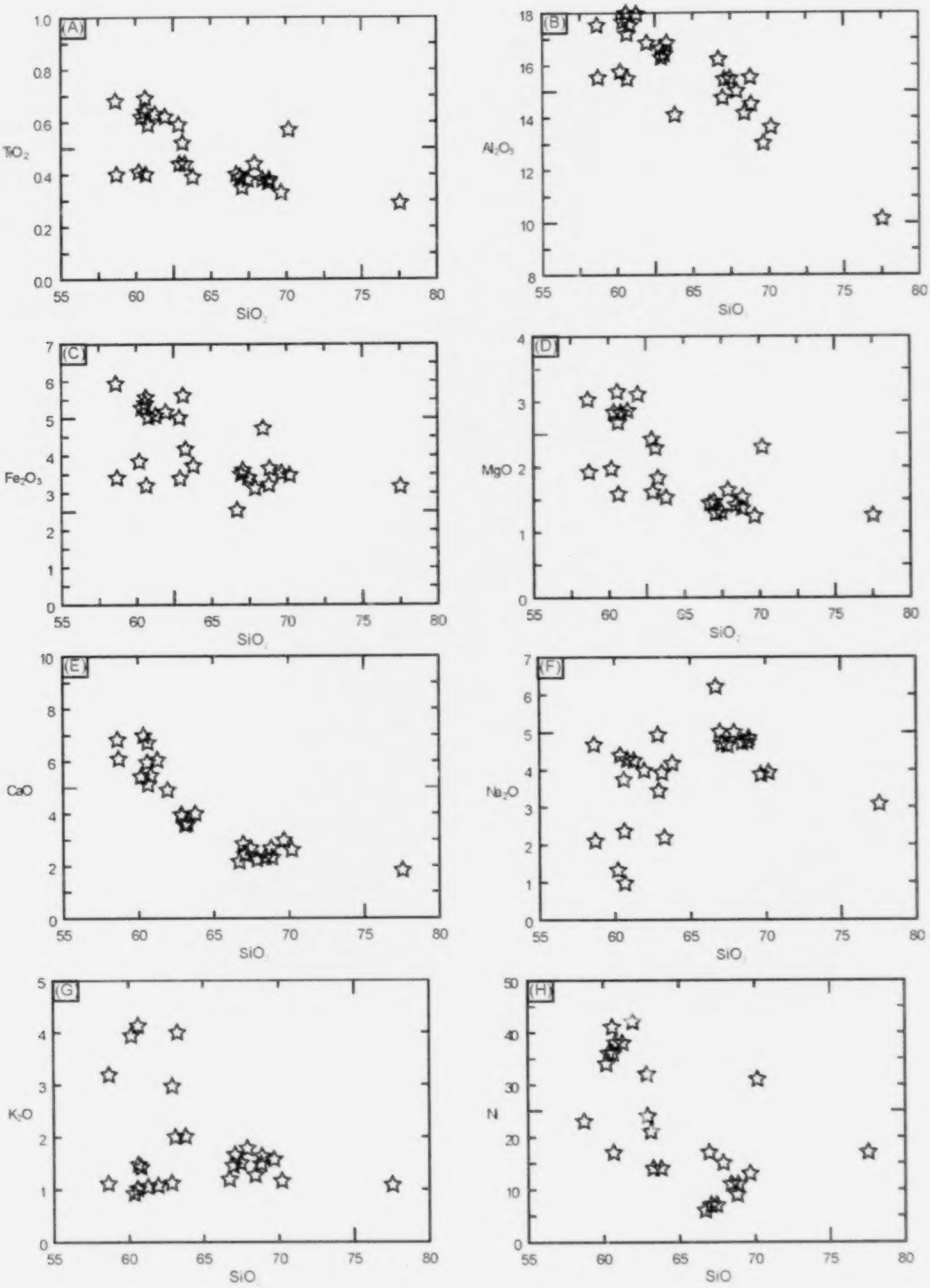

Figure 3.12, continued. Standard Harker plots for rocks of the Clifford stock and equivalents. I) Cr; J) V; K) Sc; L) Sr; M) Rb; N) Y; and O) Nb.

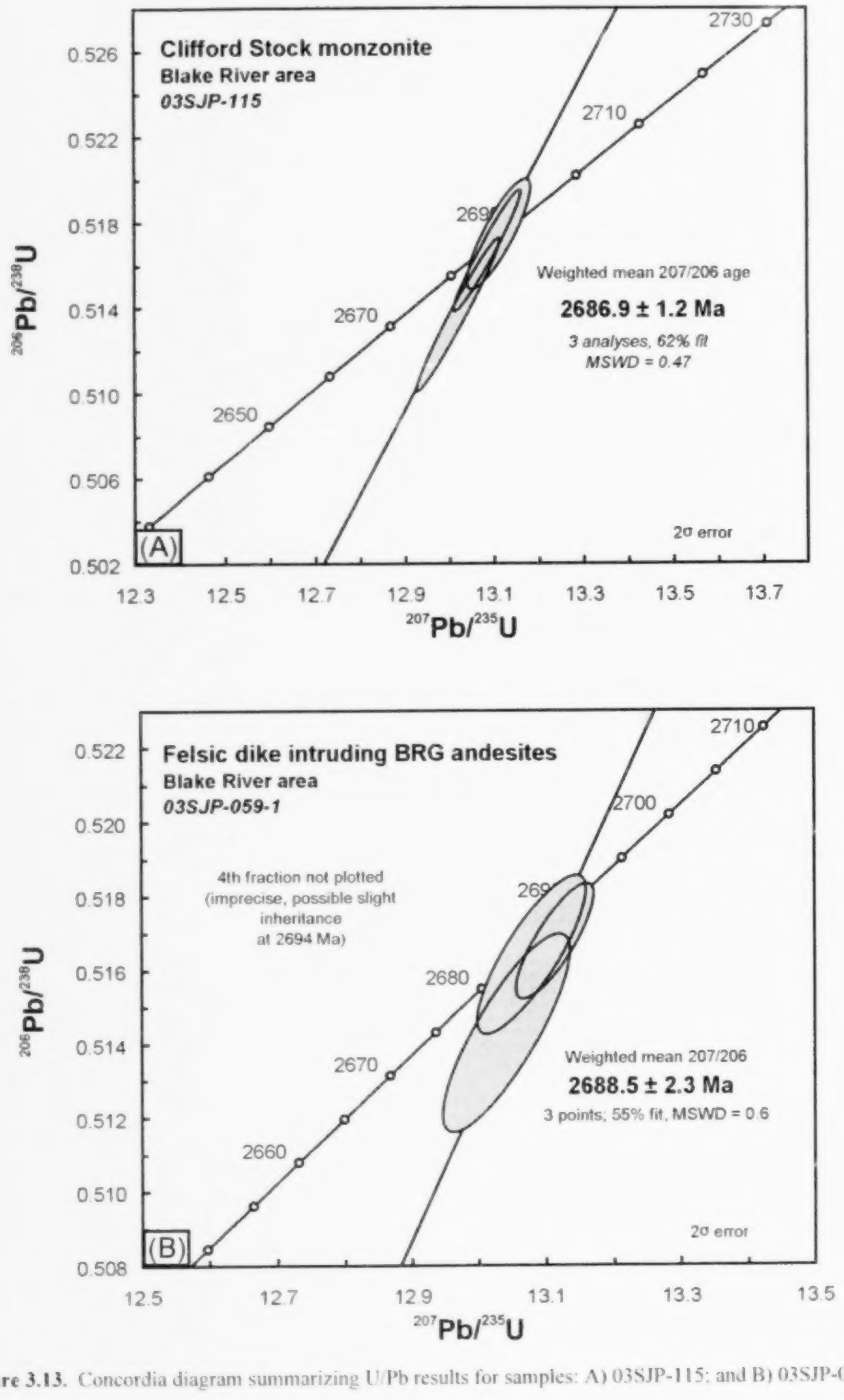

Figure 3.13. Concordia diagram summarizing U/Pb results for samples: A) 03SJP-115; and B) 03SJP-059-1.

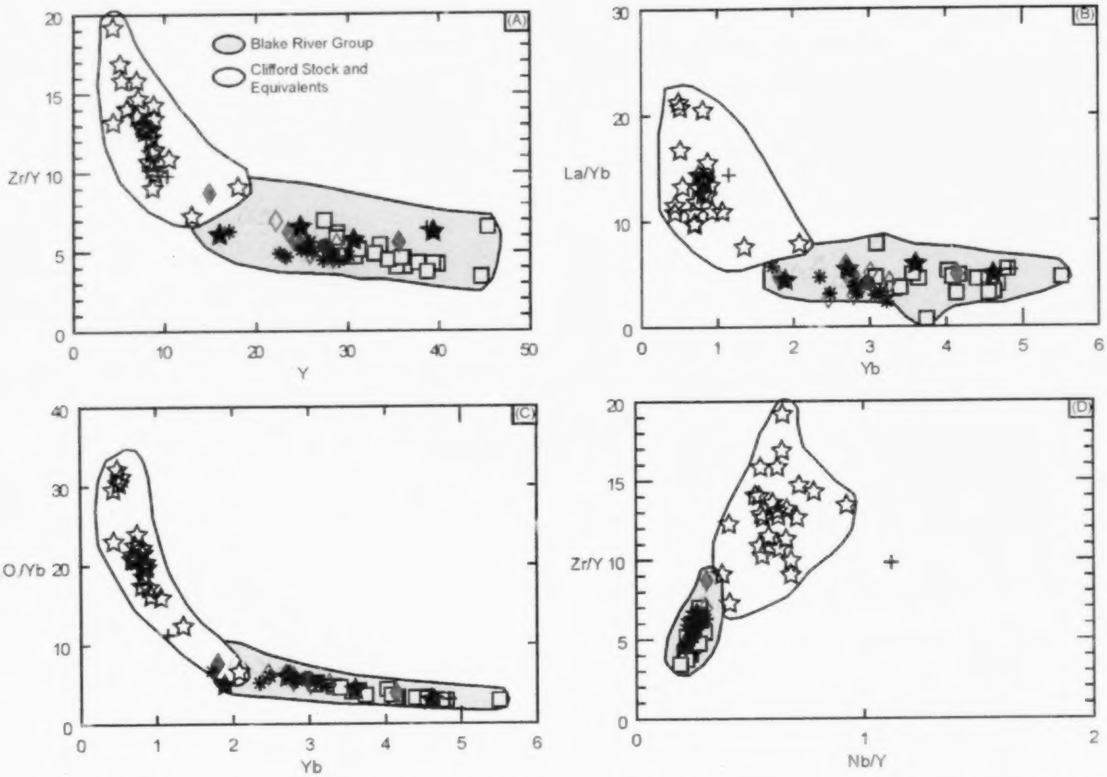

Figure 3.14. Geochemical diagrams that effectively discriminate the Clifford stock from the older Blake River Group rocks. including: A) Y versus Zr/Y; B) Yb versus La/Yb; C) Yb versus Al_2O_3/Yb; and D) Nb/Y versus Zr/Y. Symbols as in Figure 3.5; open stars are the Clifford stock and equivalents.

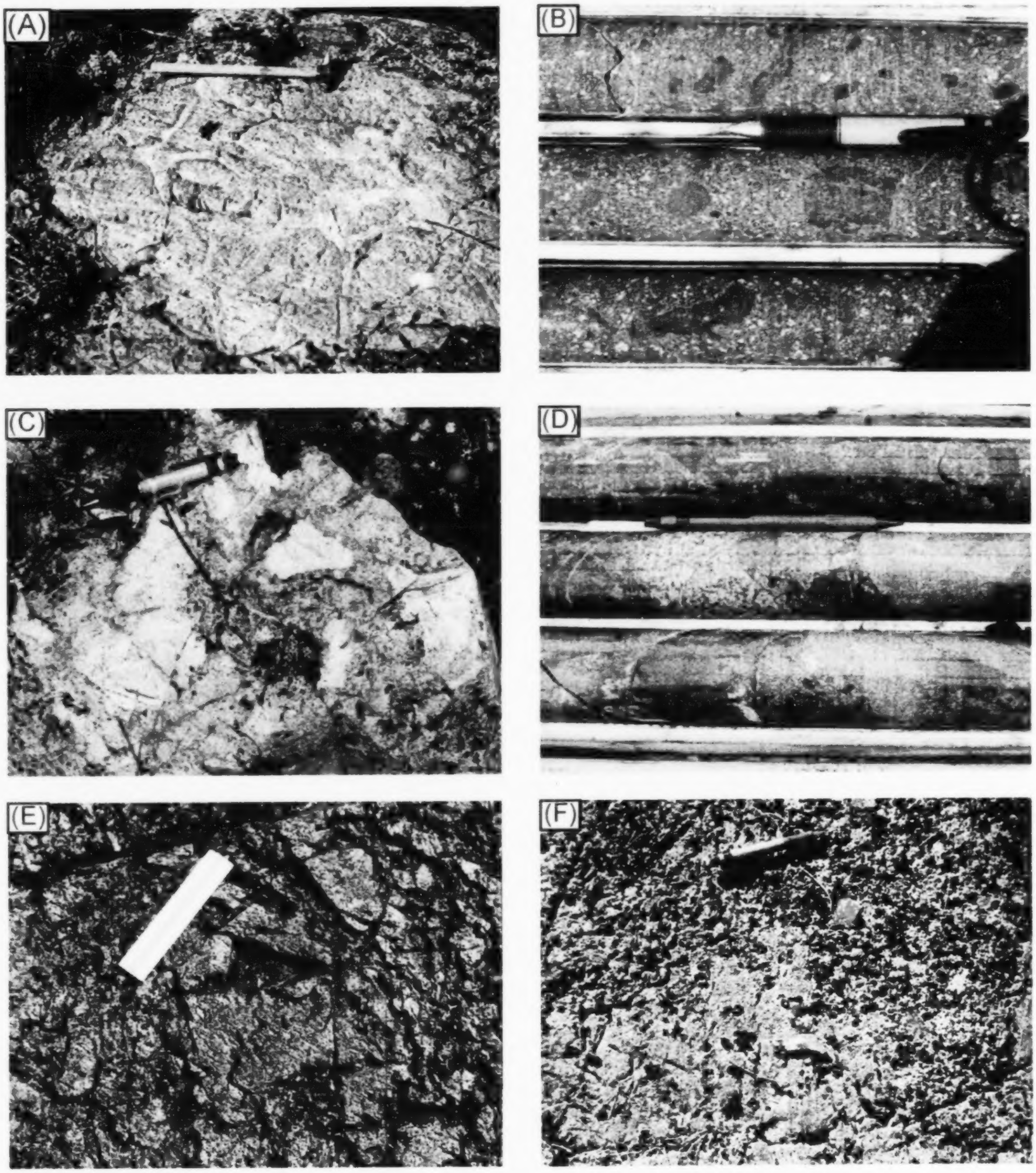

Photo 3.1. Photographs of rocks from the Blake River Group: A) typical pillowed basaltic andesite flows from cycle 1, unit 1 of the Blake River Group, B) cycle I, unit 2 lapilli tuff to tuff breccia with feldspar phenocrysts and angular (black) fragments of andesite; C) cycle 1, unit 3 polylithic tuff breccia with angular fragments of rhyolite and andesite; D) cycle 1, unit 3 clast-supported polylithic breccia in drill core; E) monolithic carapace breccia of rhyolite with polygonally jointed, flow banded rhyolite clasts from eastern Clifford Township; and F) synvolcanic rhyolite dike (bottom of photo) with irregular margins intruding into flow-banded rhyolite carapace breccia.

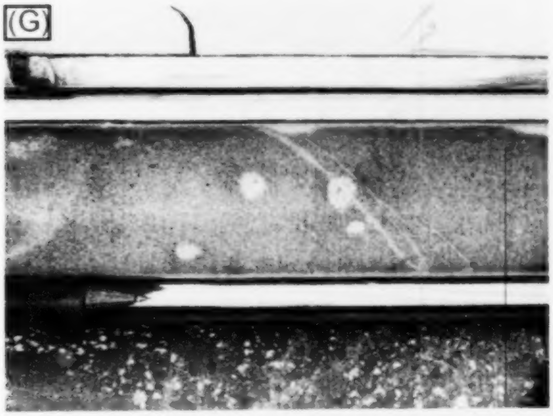

Photo 3.1, continued. Photographs of rocks from the Blake River Group: G) synvolcanic diabase dike with amygdules that are filled with epidote.

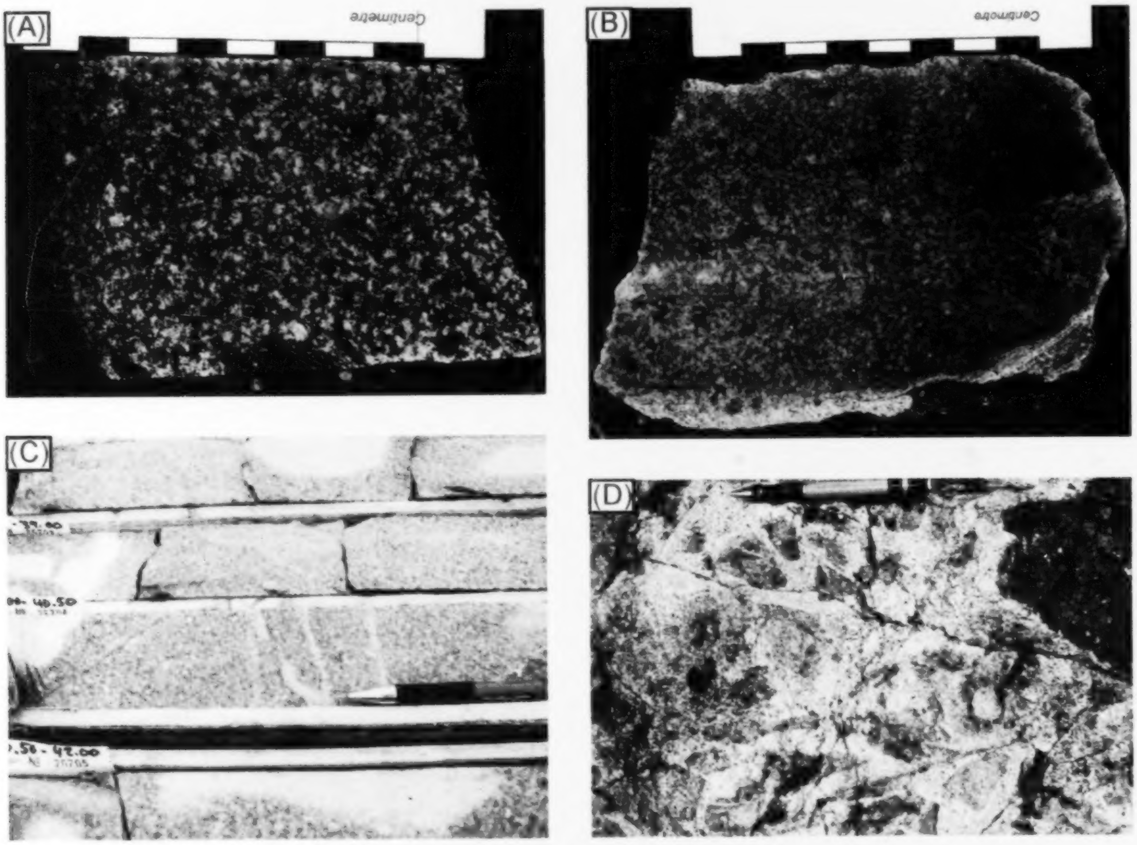

Photo 3.2. Photographs of rocks from the Clifford stock and equivalent units: A) typical hornblende tonalite from the Clifford stock; B) finer grained border phase from the western margin of the Clifford stock ; C) typical finer grained porphyry dikes from drill core that are equivalent to the Clifford stock; and D) typical dike with brecciated xenoliths of surrounding wall rock suggesting a forceful emplacement.

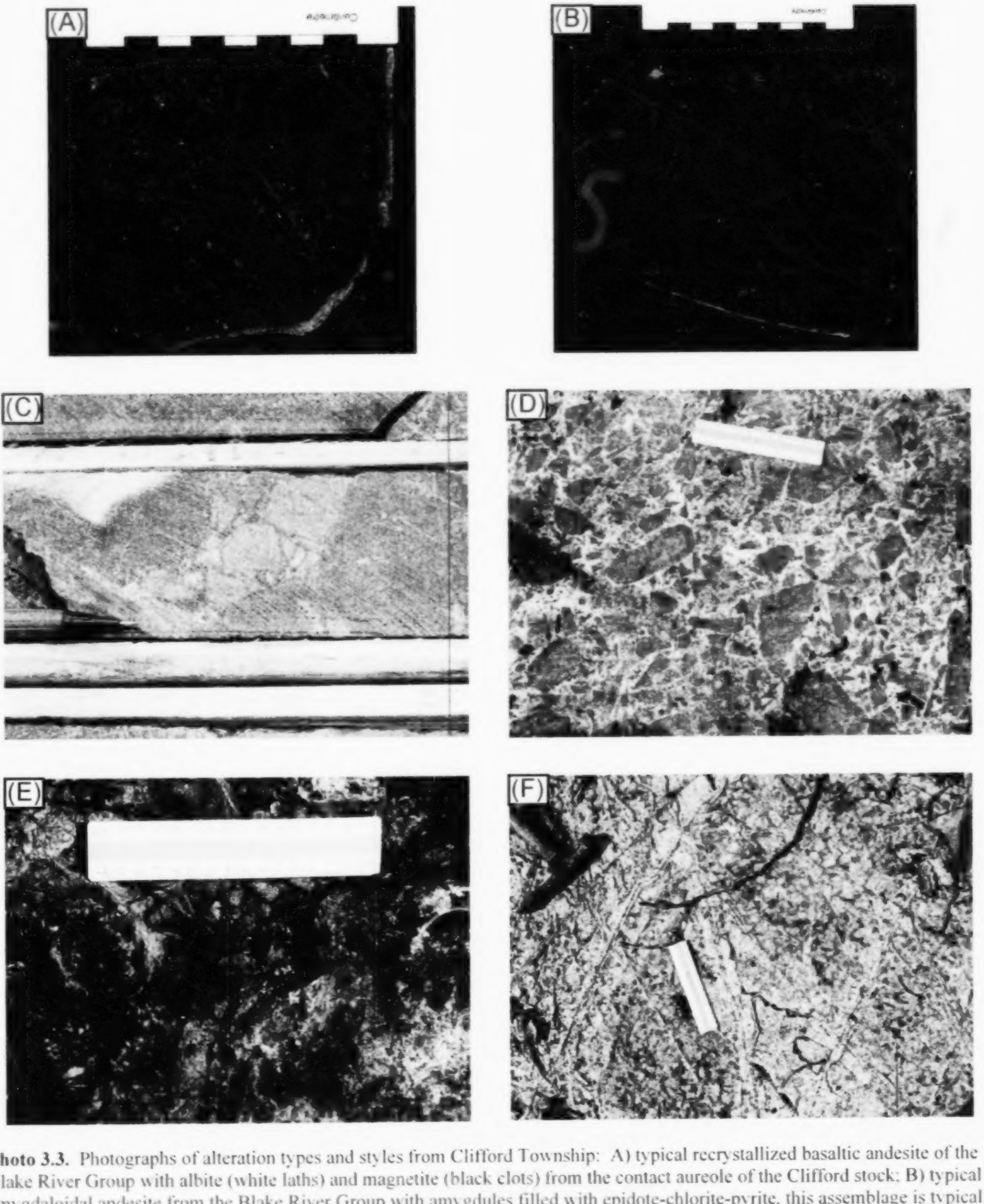

Photo 3.3. Photographs of alteration types and styles from Clifford Township: A) typical recrystallized basaltic andesite of the Blake River Group with albite (white laths) and magnetite (black clots) from the contact aureole of the Clifford stock; B) typical amygdaloidal andesite from the Blake River Group with amygdules filled with epidote-chlorite-pyrite, this assemblage is typical of VMS-related regional semi-conformable alteration (e.g., Galley 1993); C) pillow lava with chlorite alteration of the edge of the pillow with silicification of the hyaloclastite (white fragments), and an sulphide assemblage of pyrite-chalcopyrite; this is typical of pipe-like VMS-related alteration; D) breccia pipe occurrence from the Brett-Trethway (Croxall) prospect with angular andesite fragments within a sea of quartz and sulphide; this style of alteration is interpreted to represent a younger magmatic-hydrothermal event; E) typical pyrite-rich assemblage associated with the breccia pipe at the Brett–Trethway prospect; and F) randomly oriented epidote-quartz veins that are associated with the younger, magmatic-hydrothermal event (i.e., these veins crosscut the Clifford stock as well, thus must be younger than circa 2690 Ma).

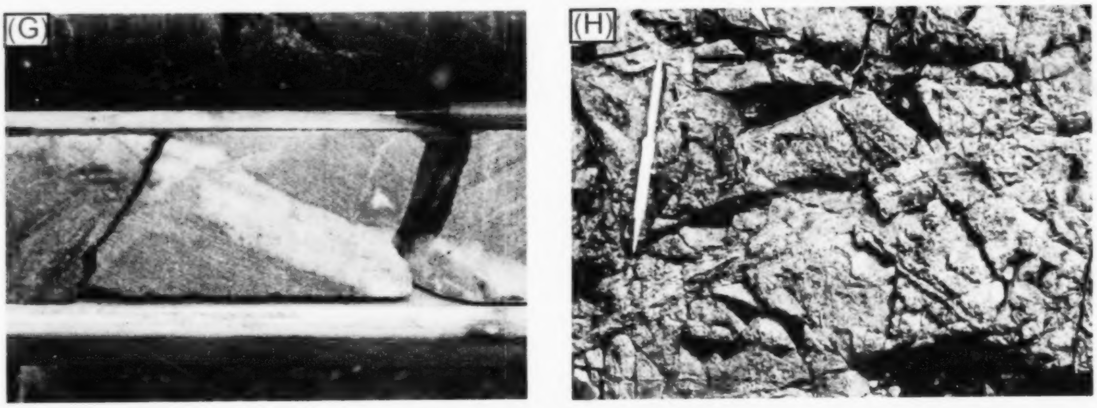

Photo 3.3, continued. Photographs of alteration types and styles from Clifford Township: G) typical medium to dark grey quartz veins that contain pyrite, molybdenite and gold; these veins typically form stockworks and are interpreted to reflect a magmatic (porphyry)-style of mineralization; and H) typical late "J-veins" of potassium feldspar, calcite, and hematite; these veins are the latest in the magmatic hydrothermal paragenesis and crosscut all other alteration and/or mineralization styles.

Table 3.1. Geochemical data for rocks of the Blake River Group and Clifford stock and equivalents

Sample	03SJP044-2	03SJP077-1	03SJP017-1	03SJP027-1	03SJP090-1	P03-005	WC04-08. 13.10 13.20	03SJP046-1	03SJP046-2	03SJP047-1-1
Easting	591145	592356	588861	588900	591996	591250	591510	591080	591080	590849
Northing	5351472	5349524	5349923	5350525	5350686	5350623	5350267	5351814	5351814	5351742
Drill Hole	-	-	-	-	-	-	WC04-08	-	-	-
Depth 2	-	-	-	-	-	-	13.10-13.20	-	-	-
Rock Type 1	basalt dyke	gabbro dyke	pillowed andesite	pillowed andesite	basaltic-andesite	andesite	amygdaloidal andesite	amygdaloidal pillow basalt	amygdaloidal (hornfelsed) basalt	amygdaloidal pillow basalt
Cycle	-	-	1	1	1	1	1	1	1	1
Unit	Matachewan	Matachewan	1	1	1	1	1	1	1	1
Affinity			Contaminated E-MORB-like	Contaminated E-MORB-like	Contaminated E-MORB-like	Contaminated E-MORB-like	Contaminated E-MORB-like	E-MORB-like	E-MORB-like	E-MORB-like
SiO2 (wt%)	60.74	44.92	61.31	56.09	52.49	55.9	58.62	50.48	49.58	54.5
TiO2	0.61	2.56	0.63	0.71	0.88	0.97	0.72	1.29	1.26	1.13
Al2O3	17.43	14.88	16.25	16.45	15.76	16.01	14.92	16.21	15.9	15.61
Fe2O3	5.14	16.34	5.52	7.26	8.98	8.73	6.68	10.01	11.13	8.64
MnO	0.07	0.21	0.11	0.14	0.15	0.16	0.066	0.26	0.26	0.23
MgO	3.03	8.61	4.33	5.54	6.76	6.25	5.26	5.04	4.68	5.08
CaO	4.54	8.44	6.52	7.58	8.61	6.9	5.23	11.1	12.82	9.42
Na2O	4.74	3.05	3.43	3.58	2.33	2.62	3.18	3.14	2.52	3.2
K2O	1.38	0.97	0.86	0.93	1.12	0.76	1.60	0.67	0.48	0.85
P2O5	0.15	0.59	0.11	0.14	0.14	0.17	0.16	0.16	0.16	0.18
LOI	2.36	0.17	1.77	2.39	2.85	2.67	2.68	1.73	1.65	1.77
Total	100.18	100.75	100.85	100.8	100.07	101.15	99.12	100.1	100.44	100.6
Ni (ppm)	32	141	108	152	66	139	114	120	122	116
Cr	27.31	70.07	91.39	128.11	186.33	120.98	107	148.67	123.61	139.94
Co	17	58	21	25	35	29	46.00	35	32	28
V	84.4	224	100.9	124.7	73.9	131.2	103	170.7	161.4	131.1
Sc	6.3	19.5	10.6	13.6	16.9	15.1	13.8	19.9	18.8	16.4
Cu	99	1002	78	110	458	31	10	290	138	552
Pb										
Zn	60	209	67	96	129	100	85	118	107	192
Cd	N.D	N.D.	N.D.	N.D.	N.D.	N.D.	N.D.	N.D	N.D.	N.D.
Mo	ND	ND	ND	ND	ND	ND	N.D	ND	ND	ND
W	5	N.D.	4	10	N.D.	N.D	N.D.	8	7	4
S	65	>400	188	145	88	128	>400	97	121	>400
Nb (XRF)	6	13	6	6	9	7	6	6	6	8
Y (XRF)	8	24	20	20	35	28	27	28	28	26
Zr (XRF)	83	156	128	150	152	150	138	124	121	140
Zr	77.9	163.6	137.5	149.2	162.7	153.1	152.9	127.3	122.8	131.1
Hf	2.2	3.9	3.6	3.9	4.1	3.9	3.8	3.5	3.4	3.4
Nb	5.1	13.6	5.7	6	6.9	6.9	6.7	5.6	5.6	5.9
Ta	0.39	0.85	0.49	0.52	0.52	0.51	0.49	0.42	0.41	0.42
Y	7.36	25.05	18.86	21.02	25.75	24.41	28.1	28.37	28.63	24.58
Be	0.49	0.66	0.45	0.43	0.44	0.52	0.48	0.38	0.38	0.44
Li	20	11	7	6	14	12	15	16	13	19
Cs	0.97	0.579	0.732	0.765	1.34	0.802	1.001	0.635	0.529	0.725
Rb	49.98	14.02	24.16	29.87	43.08	23.24	57.75	23.5	15.96	26.63
Ba	281	453	210	196	187	155	216	132	98	220
Sr	383.1	536.4	206.3	199.2	236.9	167.2	132.2	184	203.9	197.7
Th	1.08	1.14	1.5	1.66	1.3	1.15	2.52	0.65	0.65	0.8
U	0.343	0.295	0.395	0.513	0.35	0.335	0.659	0.182	0.176	0.227
La	9.53	22.38	10.21	13.6	12.98	10.94	23.35	9.01	8.89	11.06
Ce	20.64	51.75	22.3	28.73	29.77	26.61	53.01	23.51	22.58	27.57
Pr	2.584	7.204	2.857	3.399	3.963	3.591	6.502	3.485	3.298	3.766
Nd	10.35	32.35	12.3	13.73	17.33	15.82	26.97	16.37	15.84	17.13
Sm	2.15	6.99	2.99	3.2	4	3.92	5.62	4.47	4.38	4.28
Eu	0.709	2.388	0.9	0.938	1.148	1.137	1.134	1.526	1.378	1.4
Gd	1.954	6.435	3.304	3.57	4.458	4.385	5.361	5.32	5.135	4.641
Tb	0.267	0.922	0.545	0.591	0.726	0.698	0.818	0.879	0.84	0.74
Dy	1.448	5.094	3.385	3.762	4.523	4.393	4.996	5.476	5.203	4.674
Ho	0.272	0.991	0.727	0.801	0.962	0.931	1.042	1.161	1.114	0.954
Er	0.725	2.601	2.175	2.363	2.872	2.729	3.079	3.349	3.293	2.768
Tm	0.105	0.355	0.314	0.355	0.42	0.399	0.46	0.48	0.466	0.403
Yb	0.8	2.24	2.05	2.34	2.76	2.65	3.09	3.15	3.02	2.61
Lu	0.098	0.327	0.313	0.361	0.428	0.415	0.477	0.472	0.462	0.396

Table 3.1. Geochemical data for rocks of the Blake River Group and Clifford stock and equivalents

Sample	WC04-08, 168.34-168.52	WC04-08, 171.03-171.26	03SJP019	WC04-03, 79.43-79.57	WC04-03, 150.63-150.79	P03-001	P03-003	03SJP031-1-1	WC04-03, 62.65-62.79	WC04-03, 68.12-68.25
Easting	591510	591510	589121	591513	591513	591319	591335	591846	591513	591513
Northing	5350267	5350267	5350008	5350066	5350066	5349924	5350300	5349969	5350066	5350066
Drill Hole	WC04-08	WC04-08	-	WC04-03	WC04-03	-	-	-	WC04-03	WC04-03
Depth 2	168.34-168.52	171.03-171.26	-	79.43-79.57	150.63-150.79	-	-	-	62.65-62.79	68.12-68.25
Rock Type 1	amygdaloidal basaltic andesite	amygdaloidal basaltic andesite	Hbl-Bio basalt (hornfelsed)	basaltic lapilli tuff	basaltic lapilli tuff	andesitic to dacitic tuff	andesitic to dacitic tuff	dacite	andesitic tuff	andesitic tuff
Cycle	1	1	1	1	1	1	1	1	1	1
Unit	1	1	1	2	2	2	2	2	2	2
Affinity	E-MORB-like	E-MORB-like	E-MORB-like	Contaminated E-MORB-like	Contaminated E-MORB-like	Contaminated E-MORB-like	Contaminated E-MORB-like	Contaminated E-MORB-like	Contaminated E-MORB-like	Contaminated E-MORB-like
SiO2 (wt%)	52.56	53.19	49.8	43.43	48.68	62.16	65.86	64.44	61.38	65.77
TiO2	1.17	1.18	1.42	0.62	0.58	0.7	0.52	0.49	0.62	0.56
Al2O3	15.68	15.08	17.61	16.17	17.41	15.03	14.3	13.92	14.48	13.31
Fe2O3	10.24	11.08	10.76	17.57	12.31	6.79	5.2	4.76	6.28	6.11
MnO	0.120	0.100	0.2	0.032	0.029	0.05	0.06	0.12	0.081	0.047
MgO	6.32	6.53	6.87	1.29	0.79	3.98	2.56	2.6	3.67	2.25
CaO	6.50	5.74	6.45	4.61	6.23	4.68	4.62	3.93	4.68	3.19
Na2O	2.85	3.20	2.43	5.29	3.64	4	4.21	1.02	3.74	3.88
K2O	0.87	0.86	1.39	1.10	2.20	1.5	1.35	3.4	1.05	1.18
P2O5	0.21	0.20	0.21	0.14	0.12	0.14	0.11	0.1	0.14	0.13
LOI	2.51	2.69	3.13	9.39	6.66	2.34	1.77	5.27	3.43	2.88
Total	99.03	99.85	100.27	99.64	98.65	101.38	100.56	100.05	99.55	99.31
Ni (ppm)	121	109	176	19	15	97	64	55	87	41
Cr	145	175	150.97	53	18	88.57	52.55	45.14	162	48
Co	23.00	29.00	45	17	22	14	15	12	22	23
V	175	169	172.3	96	60	99	61.5	60	95	68
Sc	18.6	18.1	20.4	6.4	7.5	11.9	8.5	8.5	11.7	10
Cu	15	55	70	63	841	777	681	383	12	30
Pb										
Zn	77	53	115	45	30	90	99	145	88	63
Cd	N.D	N.D	N.D	N.D	N.D	N.D	N.D	N.D	N.D	N.D.
Mo	N.D.	N.D	ND	N.D	N.D	ND	ND	ND	N.D	N.D.
W	N.D	N.D.	5	5	11	N.D	N.D	8	5	4
S	>400	>400	243	>400	>400	>400	59	>400	>400	>400
Nb (XRF)	5	4	9	6	9	8	9	8	5	7
Y (XRF)	25	26	29	29	32	33	36	35	30	34
Zr (XRF)	123	115	164	171	169	152	141	135	137	142
Z	132.9	123.7	177.3	179.1	182.7	160.6	147.5	142.7	144.3	154.7
Hf	3.4	3.2	4.6	4.8	5.1	4.2	4.3	4.3	3.9	4.3
Nb	6.3	5.9	8.4	8.1	10	7.8	8.6	8	7.3	8
Ta	0.38	0.36	0.58	0.86	1.05	0.73	0.94	0.9	0.63	0.75
Y	27.25	25.94	29.82	28.76	33.49	32.89	36.23	35.33	30.75	34.41
Be	0.39	0.39	0.61	0.31	0.58	0.68	0.68	0.57	0.56	0.46
Li	13	13	16	7	4	10	9	16	14	9
Cs	0.883	1.315	1.755	0.672	1.36	0.916	0.607	2.018	0.697	0.523
Rb	26.95	20.35	52.72	38.75	78.72	69.49	45.97	113.24	32.67	38.57
Ba	290	273	333	98	247	205	247	210	227	141
Sr	178.7	138.2	182.9	141.3	301.5	126	133.2	24.8	151.7	124
Th	0.84	0.68	0.78	5.99	6.16	3.[illegible]	5.63	5.41	3.4	4.4
U	0.222	0.225	0.224	1.264	2.312	1.035	1.714	1.514	0.985	1.326
La	10.29	10.53	11.92	24.23	21.07	16.53	19.76	20.21	17.68	13.05
Ce	25.74	25.32	29.46	50.18	46.65	36.43	42.06	44.2	38.46	30.4
Pr	3.65	3.549	4.156	6.241	5.508	4.661	5.196	5.496	4.892	3.894
Nd	16.6	16.38	18.82	24.3	21.05	20.02	21.62	22.52	20.66	15.84
Sm	4.27	4.06	4.8	5.5	4.82	4.85	5.17	5.5	4.84	4.2
Eu	1.293	1.36	1.385	1.44	1.306	1.139	1.086	1.219	1.125	1.074
Gd	4.786	4.72	5.465	5.593	5.103	5.229	5.703	5.874	5.279	4.903
Tb	0.789	0.776	0.879	0.892	0.875	0.876	0.96	0.991	0.85	0.897
Dy	4.847	4.855	5.504	5.142	5.724	5.546	6.158	6.148	5.37	5.84
Ho	1.03	1.017	1.17	1.024	1.262	1.18	1.329	1.321	1.154	1.261
Er	2.995	2.994	3.381	2.942	3.887	3.518	4.048	4.037	3.452	3.916
Tm	0.443	0.431	0.493	0.445	0.587	0.541	0.636	0.608	0.526	0.607
Yb	2.92	2.84	3.14	3.09	4.02	3.64	4.4	4.16	3.56	4.13
Lu	0.443	0.424	0.479	0.526	0.675	0.578	0.695	0.665	0.559	0.647

Table 3.1. Geochemical data for rocks of the Blake River Group and Clifford stock and equivalents

Sample	WC04-03, 76.27 76.41	WC04-03, 131.59-131.7	WC04-03, 146.0 146.16	WC04-03, 154.75-154.90	WC04-08, 25.05 25.18	WC04-08, 26.81 26.97	WC04-08, 64.53 64.69	WC04-08, 123.7 123.9	WC04-08, 132.4 132.55	WC04-08 158.61-158.94
Easting	591513	591513	591513	591513	591510	591510	591510	591510	591510	591510
Northing	5350066	5350066	5350066	5350066	5350267	5350267	5350267	5350267	5350267	5350267
Drill Hole	WC04-03	WC04-03	WC04-03	WC04-03	WC04-08	WC04-08	WC04-08	WC04-08	WC04-08	WC04-08
Depth 2	76.27-76.41	131.59-131.7	146.0-146.16	154.75-154.90	25.05-25.18	26.81-26.97	64.53-64.69	123.7-123.9	132.4-132.55	158.61-158.94
Rock Type 1	andesitic lapilli tuff	andesitic lapilli tuff	andesitic lapilli tuff	andesitic lapilli tuff	andesitic tuff	andesitic tuff	andesite	andesitic lapilli tuff	andesitic lapilli tuff	andesitic lapillistone
Cycle	1	1	1	1	1	1	1	1	1	1
Unit	2	2	2	2	2	2	2	2	2	2
Affinity	Contaminated E-MORB-like	Contaminated E-MORB-like	Contaminated E-MORB-like	Contaminated E-MORB-like	Contaminated E-MORB-like	Contaminated E-MORB-like	Contaminated E-MORB-like	Contaminated E-MORB-like	Contaminated E-MORB-like	Contaminated E-MORB-like
SiO2 (wt%)	62.50	66.18	68.32	69.62	59.51	59.47	60.37	67.15	66.69	67.00
TiO2	0.62	0.60	0.57	0.42	0.72	0.76	0.74	0.59	0.47	0.51
Al2O3	14.75	14.47	14.23	13.10	15.56	15.52	15.54	14.06	13.97	16.11
Fe2O3	6.89	4.63	5.01	3.69	6.74	6.88	6.85	5.92	4.08	4.85
MnO	0.058	0.045	0.041	0.033	0.076	0.075	0.115	0.051	0.040	0.034
MgO	2.97	2.34	2.16	1.59	4.69	4.94	4.01	1.94	1.95	1.03
CaO	5.58	3.56	3.51	4.00	5.73	4.81	6.14	4.84	3.83	3.23
Na2O	3.49	4.96	4.26	3.77	3.03	4.79	3.03	3.90	3.83	4.90
K2O	0.56	0.75	0.75	1.10	1.75	1.12	1.54	0.53	1.50	1.22
P2O5	0.14	0.15	0.14	0.11	0.15	0.15	0.16	0.14	0.11	0.11
LOI	2.62	2.44	2.00	1.99	2.21	2.04	1.80	1.68	3.77	1.82
Total	100.18	100.13	100.99	99.42	100.17	100.56	100.30	100.80	100.24	100.81
Ni (ppm)	54	33	23	23	111	110	87	24	32	<4
Cr	102	29	23	23	117	103	66	22	27	<8
Co	22	8	8	14	23	24.00	18.00	8.00	6.00	6.00
V	78	58	46	39	122	132	116	55	48	<5
Sc	11.3	10.4	9.4	8.2	15	15	13.6	9.6	7.7	10.1
Cu	8	38	34	46	N.D.	N.D.	19	N.D.	4	N.D.
Pb										
Zn	69	71	72	51	128	57	85	43	35	39
Cd	N.D.	N.D.	N.D.	N.D.	N.D.	N.D.	N.D.	N.D.	N.D.	N.D.
Mo	N.D.	N.D.	N.D.	N.D.	N.D.	N.D.	N.D.	N.D.	N.D.	N.D.
W	3	6	3	4	N.D.	N.D.	2	N.D.	N.D.	N.D.
S	>400	>400	144	>400	134	279	183	69	165	>400
Nb (XRF)	7	6	7	7	4	5	5	7	7	8
Y (XRF)	37	36	38	37	28	29	28	34	42	43
Zr (XRF)	153	156	143	123	158	148	183	150	129	280
Zr	167.6	162.6	168.1	144.3	169.6	160.7	191.2	166.3	152.9	297.8
Hf	4.5	4.6	4.7	4.1	4.3	4.1	4.8	4.7	4.4	8
Nb	8.4	8.7	8.9	8.5	7.1	6.9	7.6	8.9	8.6	12.3
Ta	0.74	0.81	0.84	0.83	0.53	0.5	0.54	0.84	0.86	0.96
Y	39.83	37.7	39.32	38.68	28.74	31.15	27.38	36.07	44.64	45.35
Be	0.59	0.55	0.58	0.51	0.62	0.51	0.56	0.56	0.51	0.78
Li	13	11	10	6	12	12	8	9	14	6
Cs	0.393	0.539	0.608	0.732	1.397	0.876	1.005	0.41	0.958	0.666
Rb	20.14	24.79	28.05	36.44	72.46	38.34	56.87	18.28	52.65	34.02
Ba	82	101	132	189	237	196	251	66	262	520
Sr	261	102	130.7	136.6	134.1	126.4	149.6	189.2	68	178.4
Th	4.28	4.88	5.3	5.06	2.19	1.92	2.09	5.18	5.58	5.37
U	1.373	1.411	1.536	1.74	0.675	0.653	0.614	1.447	1.661	1.37
La	20.52	15.39	18.69	15.19	11.88	12.56	14.4	14.31	25.83	25.66
Ce	45.5	35.38	42.3	34.02	27.09	27.95	32.34	33.22	55.48	56.3
Pr	5.743	4.569	5.358	4.263	3.524	3.617	4.108	4.217	7.052	7.11
Nd	23.65	19.28	21.96	17.36	15.03	15.26	17.29	17.24	29.65	29.69
Sm	5.72	4.97	5.56	4.51	3.77	4.09	3.99	4.41	7.52	6.99
Eu	1.232	1.124	1.182	1.045	1.039	0.989	1.084	0.965	1.733	1.731
Gd	6.338	5.664	6.237	5.313	4.449	4.946	4.424	5.155	8.33	7.645
Tb	1.083	1.004	1.059	0.974	0.754	0.851	0.732	0.915	1.333	1.263
Dy	6.846	6.454	6.596	6.493	4.833	5.397	4.703	6.091	7.871	8.044
Ho	1.447	1.402	1.426	1.388	1.038	1.17	1.019	1.344	1.602	1.713
Er	4.414	4.32	4.384	4.412	3.196	3.504	3.071	4.204	4.631	5.288
Tm	0.675	0.664	0.682	0.679	0.487	0.522	0.462	0.663	0.7	0.815
Yb	4.55	4.55	4.67	4.62	3.32	3.4	3.08	4.55	4.8	5.51
Lu	0.714	0.716	0.742	0.718	0.507	0.527	0.477	0.709	0.718	0.865

Table 3.1. Geochemical data for rocks of the Blake River Group and Clifford stock and equivalents

Sample	03SJP088-1	WC04-08, 134.45-134.61	03SJP011-1	03SJP070-2-1	03SJP095-1	03SJP096-1-1	03SJP052-1	03SJP053-1	03SJP056-1	03SJP065-1
Easting	591815	591510	590898	591805	591979	591934	590119	590153	590216	590904
Northing	5350056	5350267	5349546	5349956	5351476	5351663	5348846	5248894	5349027	5349046
Drill Hole	-	WC04-08	-	-	-	-	-	-	-	-
Depth 2	-	134.45-134.61	-	-	-	-	-	-	-	-
Rock Type 1	andesitic tuff	andesitic lapilli tuff	andesitic lapilli tuff	andesite	basaltic andesite	andesite	andesite	andesite	andesite	basaltic andesit
Cycle	1	1	1	1	1	1	2	2	2	2
Unit	2	2	2	2	2	2	4	4	4	4
Affinity	Contaminated E-MORB-like	Intensely Altered E-MORB-like	E-MORB-like	E-MORB-like	E-MORB-like	E-MORB like	Contaminated E-MORB-like	Contaminated E-MORB-like	Contaminated E-MORB-like	Contaminated E-MORB-like
SiO2 (wt%)	65.05	62.44	53.75	50.44	56.07	50.37	57.29	64.24	63.96	56.61
TiO2	0.65	0.43	1.3	1.12	0.92	1.16	0.94	0.61	0.56	0.96
Al2O3	14.73	13.49	15.12	15.24	15.4	16.22	16.44	15.92	13.72	16.69
Fe2O3	6.36	3.32	10.82	11.7	7.01	10.98	8.38	4.78	7.72	7.41
MnO	0.06	0.040	0.19	0.2	0.11	0.19	0.09	0.04	0.08	0.1
MgO	3.39	1.54	6.74	8.91	6.45	7.8	3.93	1.75	3.93	4.42
CaO	2.8	9.16	5.21	6.49	7.57	8.61	5.93	3.28	2.93	5.31
Na2O	3.59	0.31	2.96	1.87	2.54	2.67	3.32	2.75	2.29	4.61
K2O	1.23	3.16	0.95	0.8	1.3	0.75	1.45	2.76	1.7	1.13
P2O5	0.13	0.11	0.18	0.18	0.17	0.18	0.11	0.11	0.06	0.11
LOI	2.55	8.76	4.04	2.34	2.4	2.4	2.43	3.35	3.52	2.44
Total	100.54	102.76	101.25	99.29	99.93	101.33	100.31	99.59	100.47	99.78
Ni (ppm)	128	39	128	246	181	165	51	11	89	68
Cr	55.88	28	164.39	209.64	142.8	158.04	12.39	9.62	27.63	13.42
Co	17	4.00	26	38	54	39	27	6	50	36
V	148.8	49	157.6	155.8	138.1	131.8	174.5	68	106.5	193.6
Sc	10.2	7.5	19.4	18.4	15.9	17.8	17.4	8.6	9.4	17.3
Cu	298	N.D.	68	4977	1067	119	330	33	275	847
Pb										
Zn	148	27	182	386	118	110	72	53	77	144
Cd	N.D.	N.D.	N.D.	N.D.	N.D.	N.D.	N.D.	N.D.	N.D.	N.D.
Mo	ND	N.D.	ND	ND	ND	ND	ND	ND	ND	ND
W	N.D.	N.D.	3	2	2	N.D.	8	9	6	8
S	>400	156	>400	>400	>400	>400	>400	>400	>400	>400
Nb (XRF)	6	6	7	6	7	7	7	9	5	6
Y (XRF)	29	27	29	25	24	21	25	36	15	25
Zr (XRF)	133	121	133	122	155	149	138	197	128	138
Zr	166.3	137	131.4	126.4	154.3	157.6	136.2	198.8	129.7	139.2
Hf	4.6	4	3.4	3.2	3.9	4.2	3.7	5.6	3.5	3.9
Nb	8.5	8	6.2	6	6.7	7	6	9	4.6	6
Ta	0.86	0.81	0.46	0.43	0.5	0.53	0.49	0.91	0.51	0.53
Y	35.84	28.95	28.36	25.85	22.12	28.76	24.75	35.56	14.88	24.02
Be	0.7	0.43	0.38	0.38	0.43	0.6	0.41	0.59	0.44	0.55
Li	17	15	14	10	13	17	6	11	14	7
Cs	1.013	1.861	0.28	1.102	1.263	1.403	0.871	1.899	1.408	1.003
Rb	48.3	117.27	16.48	27.48	54.32	25.67	54.36	87.6	63.99	40.84
Ba	180	419	178	96	182	180	230	545	386	174
Sr	162.1	19.6	247.4	128.2	167.8	195.1	141.9	94.8	138.3	164.9
Th	4.52	5.44	0.86	0.75	1.22	1.06	1.6	5.39	2.89	1.6
U	1.325	1.453	0.287	0.253	0.378	0.303	0.392	1.476	0.758	0.445
La	19.2	2.68	15.28	8.24	6.66	13.5	13.21	20.23	8.46	15.76
Ce	42.58	6.48	38.7	20.74	14.46	32.66	28.56	43.04	19.47	33.36
Pr	5.448	0.887	5.368	2.969	1.884	4.547	3.622	5.264	2.406	4.177
Nd	22.85	4.02	73.68	13.95	8.75	20.98	15.37	20.75	9.53	17.34
Sm	5.27	1.51	5.78	3.82	2.56	5.11	3.65	4.92	2.33	4.12
Eu	1.422	0.377	1.354	1.141	1.263	0.795	1.042	1.182	0.64	1.282
Gd	5.732	2.682	5.744	4.388	3.271	5.378	4.182	5.277	2.499	4.337
Tb	0.96	0.573	0.898	0.747	0.56	0.885	0.693	0.943	0.425	0.704
Dy	6.176	4.136	5.512	4.691	3.634	5.395	4.403	6.015	2.658	4.445
Ho	1.285	0.977	1.154	0.988	0.803	1.146	0.945	1.309	0.572	0.938
Er	3.853	3.171	3.286	2.892	2.35	3.316	2.81	3.993	1.766	2.793
Tm	0.593	0.504	0.473	0.42	0.363	0.486	0.423	0.606	0.27	0.412
Yb	4.08	3.74	3.01	2.79	2.46	3.26	2.79	4.14	1.8	2.69
Lu	0.659	0.623	0.449	0.429	0.392	0.497	0.426	0.642	0.289	0.41

Table 3.1. Geochemical data for rocks of the Blake River Group and Clifford stock and equivalents

Sample	03SJP055-1-2	03SJP055-1	03SJP068-1-1	03SJP068-36	03SJP110-2	03SJP112-1	03SJP037-1	03SJP080-1-1	03SJP109-2-1	03SJP84-1
Easting	590904	590175	591261	591261	593171	593182	592278	592497	593437	592470
Northing	5349046	5349090	5348588	5348588	5350838	5350691	5350685	5349867	5350948	5350306
Drill Hole	-	-	-	-	-	-	-	-	-	-
Depth 2	-	-	-	-	-	-	-	-	-	-
Rock Type 1	basaltic andesite	andesite	rhyolite	rhyolite	diabase / diorite	diabase / diorite	diorite porphyry	diabase / gabbro	diabase	diabase
Cycle	2	2	2	2	-	-	-	-	-	-
Unit	4	4	5	5	synvolcanic intrusions	synvolcanic intrusions	synvolcanic intrusions	synvolcanic intrusions	synvolcanic intrusions	synvolcanic intrusions
Affinity	Contaminated E-MORB-like	E-MORB-like	Transitional Rhyolite	Transitional Rhyolite	E-MORB-like	E-MORB-like	Contaminated E-MORB-like	Contaminated E-MORB-like	Contaminated E-MORB-like	E-MORB-like
SiO2 (wt%)	58.29	52.49	75.04	70.4	51.52	49.92	71.32	52.67	65.54	51.05
TiO2	1.04	1.25	0.17	0.4	1.21	1.16	0.43	0.56	0.5	1.24
Al2O3	16.87	16.91	12.91	14.93	15.5	14.88	13.63	9.23	15.42	15.92
Fe2O3	7.16	10.05	1.35	1.89	11.39	11.77	3.98	10.92	5.37	11.8
MnO	0.11	0.22	0.03	0.02	0.17	0.16	0.05	0.16	0.09	0.19
MgO	4.74	6.27	0.52	0.35	6.51	7.65	0.4	14.67	2.3	6.42
CaO	4.36	7.62	1.81	2.15	8.01	7.45	1.55	4.44	2.83	7.51
Na2O	3.88	2.44	4.29	6.27	2.02	1.87	4.88	1.65	5.32	1.7
K2O	1	1.05	1.67	1.85	0.69	0.28	2.76	0.32	1.1	0.38
P2O5	0.12	0.24	0.06	0.07	0.18	0.14	0.09	0.09	0.1	0.18
LOI	2.96	1.78	2.18	1.11	3.62	5.77	1.18	4.22	2.09	4.3
Total	100.53	100.32	100.04	99.45	100.8	101.05	100.27	98.93	100.66	100.69
Ni (ppm)	54	109	6	5	36	167	7	463	67	179
Cr	11.24	132.79	9.32	9.04	167.24	172.69	10.23	>400.00	37.41	147.02
Co	28	19	2	2	43	43	4	56	17	38
V	189.3	162.7	4.7	4	64.7	150.3	N.D.	113.4	105.5	172.2
Sc	17.3	18.9	2	6.4	20.1	18.7	8.4	18.3	8.9	18.7
Cu	491	222	185	89	114	110	34	167	490	442
Pb										
Zn	122	78	40	22	86	130	33	112	210	103
Cd	N.D.	N.D.	N.D.	N.D.	N.D.	N.D.	N.D.	N.D.	N.D.	N.D.
Mo	ND	ND	ND	ND	ND	ND	ND	ND	ND	ND
W	5	5	3	N.D.	N.D.	5	8	N.D.	3	N.D.
S	>400	>400	>400	>400	126	92	45	58	53	191
Nb (XRF)	7	8	11	10	8	6	10	5	8	5
Y (XRF)	26	28	10	39	30	27	39	16	8	23
Zr (XRF)	148	152	94	247	170	117	237	93	120	105
Zr	147.4	147.3	100.8	250.8	122.6	108.9	245.7	97.4	175.4	142.6
Hf	4	3.9	3	7.1	3.2	2.9	6.8	2.5	5	3.7
Nb	6.4	7	11.5	9.9	5.8	4.9	10.2	3.9	7.4	6.4
Ta	0.53	0.5	0.96	0.96	0.41	0.36	0.88	0.34	0.75	0.45
Y	23.51	27.51	10.28	38.67	27.27	23.24	39.35	15.99	30.6	30.11
Be	0.53	0.47	0.59	0.78	0.55	0.36	0.71	0.28	0.66	0.4
Li	12	4	7	3	25	20	4	14	17	19
Cs	0.798	0.956	0.756	0.489	0.589	0.61	0.483	2.418	0.393	0.783
Rb	35.69	38.96	57.87	32.28	19.07	8.56	44.69	13.02	25.93	11.96
Ba	163	122	449	795	244	76	796	99	327	101
Sr	169.6	176.7	95.1	72.3	218.1	161.7	99	95.7	173.6	173.1
Th	1.68	0.84	3.71	5.62	0.7	0.58	4.54	0.85	4.21	0.79
U	0.431	0.243	1.063	1.362	0.194	0.163	1.168	0.228	1.105	0.216
La	12.25	12.06	16.54	25.73	9.21	7.77	22.66	8.25	21.2	10.26
Ce	26.29	30.24	33.56	54.4	23.86	19.79	49.43	18.49	44.91	25.84
Pr	3.4	4.163	3.852	6.595	3.453	2.962	6.191	2.411	5.413	3.743
Nd	14.71	18.74	14	26.86	16.36	13.85	25.78	10.22	22.36	17.47
Sm	3.53	4.54	2.49	6.23	4.27	3.53	6.28	2.51	5.02	4.68
Eu	1.127	1.415	0.549	1.336	1.069	1.297	1.363	0.707	0.85	1.151
Gd	4.033	5.036	2.127	6.7	4.919	4.24	6.744	2.783	5.39	5.305
Tb	0.683	0.813	0.319	1.105	0.808	0.678	1.148	0.456	0.886	0.87
Dy	4.272	5.098	1.796	7.012	4.957	4.27	7.127	2.847	5.53	5.456
Ho	0.915	1.065	0.355	1.491	1.065	0.896	1.508	0.618	1.163	1.133
Er	2.765	3.151	1.098	4.463	3.049	2.577	4.527	1.843	3.494	3.23
Tm	0.416	0.461	0.166	0.69	0.438	0.379	0.684	0.273	0.534	0.475
Yb	2.74	2.98	1.15	4.84	2.84	2.48	4.61	1.89	3.6	3.14
Lu	0.422	0.453	0.178	0.744	0.436	0.378	0.705	0.303	0.561	0.478

Table 3.1. Geochemical data for rocks of the Blake River Group and Clifford stock and equivalents

Sample	WC04-03, 212.49-212.63	WC04-04, 51.62-51.92	WC04-04, 70.65-70.84	WC04-04, 130.88-131.04	WC04-04, 166.52-166.67	WC04-08, 176.74-176.96	WC04-08, 227.76-227.93	WC04-08, 236.47-236.52	03SJP013-2-1	03SJP013-2-1(2)
Easting	591513	591517	591517	591517	591517	591510	591510	591510	590880	590880
Northing	5350066	5349643	5349643	5349643	5349643	5350267	5350267	5350267	5349453	5349453
Drill Hole	WC04-03	WC04-04	WC04-04	WC04-04	WC04-04	WC04-08	WC04-08	WC04-08	-	-
Depth 2	212.49-212.63	51.62-51.92	70.65-70.84	130.88-131.04	166.52-166.67	176.74-176.96	227.76-227.93	236.47-236.52	-	-
Rock Type 1	diabase / diorite dyke	diabase / diorite	diabase / diorite	diabase / diorite	diabase / diorite	diabase / diorite	diabase / diorite	diabase / diorite	diorite porphyry	diorite porphyry
Cycle	-	-	-	-	-	-	-	-	-	-
Unit	synvolcanic intrusions	synvolcanic intrusions	synvolcanic intrusions	synvolcanic intrusions	synvolcanic intrusions	synvolcanic intrusions	synvolcanic intrusions	synvolcanic intrusions	Clifford Stock and Equivalents	Clifford Stock and Equivalents
Affinity	E-MORB-like	E-MORB-like	E-MORB-like	E-MORB-like	E-MORB-like	Contaminated E-MORB-like	E-MORB-like	E-MORB-like	TTG	TTG
SiO2 (wt%)	57.74	53.47	52.67	53.28	65.14	58.74	51.84	54.20	70.18	61.95
TiO2	0.95	1.17	1.14	1.24	0.67	0.78	1.25	1.17	0.57	0.62
Al2O3	12.19	15.69	15.76	15.94	11.48	16.19	16.17	14.94	13.63	16.84
Fe2O3	10.09	10.04	9.14	9.13	6.41	7.36	10.70	9.08	3.47	5.17
MnO	0.112	0.090	0.109	0.092	0.059	0.119	0.097	0.095	0.02	0.07
MgO	6.15	7.20	6.95	6.96	5.06	4.58	6.31	6.16	2.3	3.11
CaO	5.87	3.50	6.48	4.92	4.22	5.64	8.36	7.87	2.61	4.9
Na2O	0.98	3.08	2.23	3.22	2.04	3.66	2.41	3.76	3.92	3.98
K2O	0.40	0.85	2.19	1.33	0.81	0.84	1.28	0.63	1.16	1.07
P2O5	0.19	0.20	0.18	0.22	0.15	0.17	0.21	0.20	0.07	0.15
LOI	4.95	4.88	2.64	3.11	3.37	1.67	2.14	1.83	2.35	2.22
Total	99.62	100.17	99.49	99.44	99.41	99.75	100.77	99.94	100.28	100.1
Ni (ppm)	160	108	136	125	120	98	99	91	31	42
Cr	190	154	189	181	177	90	135	158	21	31.08
Co	31	30	31	29	21	20.00	21.00	16.00	20	17
V	152	191	162	156	88	136	167	177	69.6	86
Sc	16.3	14.7	18.5	18.4	12	12.9	19	18.3	8.1	7.2
Cu	583	844	271	654	509	33	41	N.D.	281	153
Pb										
Zn	204	106	70	88	140	63	62	61	50	67
Cd	N.D.	N.D.	N.D.	N.D.	N.D.	N.D.	N.D.	N.D.	N.D.	N.D.
Mo	N.D.	N.D.	N.D.	13	N.D.	N.D.	N.D.	N.D.	ND	ND
W	2	9	5	6	4	N.D.	N.D.	N.D.	8	4
S	>400	>400	>400	>400	>400	203	155	111	>400	114
Nb (XRF)	5	5	5	6	5	5	6	5	7	7
Y (XRF)	22	29	26	25	18	25	27	28	19	12
Zr (XRF)	102	123	124	136	99	159	127	120	160	112
Zr	110.5	127.8	130.8	145.6	107.3	163	138.9	129	163.8	114.1
Hf	2.8	3.3	3.2	3.7	2.8	4.1	3.5	3.3	4.5	3.2
Nb	5.2	6.2	6	6.8	5.2	6.6	6.4	6.2	6.8	5.7
Ta	0.32	0.38	0.38	0.42	0.32	0.48	0.38	0.37	0.63	0.47
Y	22.53	24.9	26.05	25.82	17.03	24.8	28.31	29	18.03	10.5
Be	0.58	0.52	0.48	0.51	0.46	0.43	0.39	0.48	0.65	0.54
Li	32	34	10	23	22	9	13	6	11	16
Cs	0.527	1.403	1.872	1.641	0.509	0.96	1.816	0.922	0.966	1.072
Rb	14.76	31	99.64	55.62	22.29	23.29	61.62	22.25	46.29	33.47
Ba	47	115	225	156	62	138	153	69	166	311
Sr	268.2	215.8	159.1	220.8	233	167.2	170.6	225	143.5	271.6
Th	0.65	0.78	0.78	0.89	0.94	1.85	0.79	0.83	3.58	1.92
U	0.258	0.564	0.303	0.625	0.457	0.487	0.194	0.624	0.888	0.408
La	10.94	8.79	10.47	11.08	9.83	14.66	9.1	7.42	16.24	11.53
Ce	26.8	22.64	25.87	27.36	24.39	32.85	24.14	18.11	33.79	25.1
Pr	3.719	3.354	3.722	3.915	3.381	4.128	3.506	2.674	3.913	3.102
Nd	16.67	15.7	17.03	18.11	14.8	17.42	16.54	13.06	15.22	12.24
Sm	4.07	4.21	4.31	4.61	3.52	4.05	4.25	4.02	3.3	2.63
Eu	1.2	1.058	1.274	1.288	0.862	1.118	1.048	1.141	0.875	0.74
Gd	4.331	4.847	4.755	5.065	3.538	4.38	4.719	4.967	3.177	2.357
Tb	0.665	0.795	0.78	0.812	0.553	0.701	0.783	0.858	0.529	0.337
Dy	4.094	4.82	4.769	4.823	3.173	4.269	4.926	5.418	3.191	2.041
Ho	0.84	1.015	0.999	0.999	0.642	0.911	1.058	1.152	0.678	0.397
Er	2.457	2.956	2.94	2.905	1.858	2.697	3.153	3.367	2.034	1.129
Tm	0.355	0.434	0.424	0.427	0.264	0.41	0.465	0.493	0.309	0.166
Yb	2.35	2.83	2.8	2.83	1.72	2.71	3.07	3.22	2.08	1.06
Lu	0.366	0.417	0.424	0.436	0.262	0.421	0.467	0.486	0.319	0.165

Table 3.1. Geochemical data for rocks of the Blake River Group and Clifford stock and equivalents

Sample	03SJP020-2	03SJP022-1	03SJP047-2-1	03SJP059-2	03SJP096-2-1	P03-007A	P03-007B	WC04-03 180.95-181.14	WC04-03 192.67-192.81	WC04-03 209.63-209.82
Easting	589170	589444	590849	590369	591934	590938	590938	591513	591513	591513
Northing	5350097	5350567	5351742	5349181	5351663	5360770	5360770	5350066	5350066	5350066
Drill Hole	-	-	-	-	-	-	-	WC04-03	WC04-03	WC04-03
Depth 2	-	-	-	-	-	-	-	180.95-181.14	192.67-192.81	209.63-209.82
Rock Type 1	tonalite / granodiorite	tonalite / granodiorite	tonalite / granodiorite	diorite porphyry	diorite	diorite	diorite	quartz-feldspar porphyry	quartz-feldspar porphyry	quartz-feldspar porphyry
Cycle	-	-	-	-	-	-	-	-	-	-
Unit	Clifford Stock and Equivalents	Clifford Stock and Equivalents	Clifford Stock and Equivalents	Clifford Stock and Equivalents	Clifford Stock and Equivalents	Clifford Stock and Equivalents	Clifford Stock and Equivalents	Clifford Stock and Equivalents	Clifford Stock and Equivalents	Clifford Stock and Equivalents
Affinity	TTG	TTG	TTG	TTG	TTG	TTG	TTG	TTG	TTG	TTG
SiO2 (wt%)	62.86	60.59	60.82	62.91	58.63	60.36	61.27	66.96	68.86	69.66
TiO2	0.59	0.64	0.59	0.44	0.68	0.62	0.63	0.39	0.38	0.33
Al2O3	16.64	17.98	17.53	16.29	17.53	17.66	17.95	14.74	14.50	13.01
Fe2O3	5.01	5.4	5.03	3.38	5.93	5.28	5.07	3.50	3.65	3.52
MnO	0.06	0.09	0.07	0.09	0.07	0.07	0.07	0.040	0.046	0.036
MgO	2.42	3.15	2.83	1.61	3.03	2.84	2.86	1.46	1.53	1.24
CaO	3.95	5.95	5.45	3.93	6.82	6.97	6.04	2.84	2.31	2.97
Na2O	4.93	3.74	4.27	3.44	4.67	4.39	4.25	5.01	4.84	3.87
K2O	1.12	1.01	1.42	2.97	1.11	0.92	1.05	1.45	1.63	1.57
P2O5	0.12	0.14	0.14	0.11	0.16	0.15	0.14	0.13	0.12	0.09
LOI	2.23	2.18	2.27	4.61	2.34	1.65	1.93	2.39	2.57	2.75
Total	99.92	100.87	100.43	99.79	100.98	100.9	101.26	98.91	100.44	99.05
Ni (ppm)	32	41	38	24	172	36	38	17	11	13
Cr	28.17	34.45	27.58	19.34	36.17	29.36	31.21	8	<8	<8
Co	16	20	17	12	22	17	16	9	8	9
V	76.5	94	81.7	54.4	154.2	87.6	91.5	42	44	48
Sc	5.5	7.9	6.9	4.3	8.8	7.5	7.9	3.3	3.5	3.3
Cu	19	102	115	229	2199	13	5	593	697	404
Pb										
Zn	54	100	69	244	117	37	42	66	68	47
Cd	N.D	N.D	N.D	N.D	N.D	N.D	N.D	N.D	N.D	N.D
Mo	ND	ND	ND	ND	ND	ND	ND	N.D.	N.D	N.D
W	5	10	7	12	N.D	N.D	4	3	N.D.	6
S	>400	130	69	>400	101	90	127	>400	>400	>400
Nb (XRF)	6	7	7	4	8	5	5	4	3	3
Y (XRF)	13	8	9	8	29	8	8	10	10	7
Zr (XRF)	90	90	95	95	158	89	93	94	83	77
Zr	94.1	97.5	89.1	105	125.8	78.5	88.4	98.6	98.2	83.2
Hf	2.7	2.8	2.7	3	3.3	2.3	2.4	2.9	2.8	2.3
Nb	5.3	5.7	6.1	3.5	6.9	5.9	5.2	4.7	4.2	2.8
Ta	0.47	0.48	0.54	0.34	0.5	0.46	0.41	0.38	0.29	0.19
Y	12.96	8.65	8.97	6.58	8.82	8.69	8.26	7.55	7.64	4.34
Be	0.38	0.5	0.53	0.61	0.52	0.52	0.52	0.42	0.37	0.39
Li	10	12	17	8	20	16	24	11	12	9
Cs	0.934	1.247	1.54	1.933	0.835	0.717	0.758	0.817	0.891	0.879
Rb	45.17	27.44	49.58	83.16	38.95	24.53	31.33	40.82	42.18	52.85
Ba	242	296	332	422	247	231	248	264	257	175
Sr	232.3	299.7	240.4	195.9	266	341.4	324.5	183.2	112.5	150
Th	2.31	1.84	2.51	1.6	1.58	1.55	1.27	1.73	1.18	1.07
U	0.648	0.467	0.526	0.511	0.452	0.359	0.362	0.35	0.329	0.307
La	10.17	11.57	10.7	11.54	10.17	11.5	10.75	6.68	6.84	5.06
Ce	24.01	25.27	23.7	22.22	24.5	24.12	22.94	14.66	15.58	10.58
Pr	3.103	3.145	3.107	2.955	3.151	3.023	2.854	1.93	2.053	1.292
Nd	12.94	12.58	12.84	12.27	12.89	12.07	11.58	8.73	9.08	5.48
Sm	2.88	2.6	2.6	2.42	2.67	2.44	2.39	1.94	2.09	1.16
Eu	0.781	0.78	0.818	0.81	1.588	0.787	0.751	0.617	0.611	0.528
Gd	2.686	2.267	2.325	2.1	2.344	2.172	2.144	1.827	1.882	1.056
Tb	0.419	0.317	0.326	0.294	0.325	0.306	0.297	0.243	0.258	0.144
Dy	2.457	1.769	1.742	1.615	1.765	1.707	1.606	1.354	1.414	0.795
Ho	0.494	0.335	0.337	0.312	0.336	0.323	0.304	0.264	0.274	0.156
Er	1.449	0.918	0.913	0.862	0.892	0.867	0.829	0.734	0.747	0.451
Tm	0.212	0.132	0.128	0.125	0.126	0.124	0.114	0.104	0.11	0.068
Yb	1.35	0.81	0.86	0.83	0.81	0.82	0.75	0.69	0.7	0.44
Lu	0.199	0.121	0.13	0.125	0.124	0.117	0.113	0.105	0.102	0.07

Table 3.1. Geochemical data for rocks of the Blake River Group and Clifford stock and equivalents

Sample	WC04-03, 244.38-244.61	WC04-03, 246.34-246.57	WC04-04, 9.37-9.48	WC04-04, 34.71 34.95	WCO4-04, 43.72 43.89	WC04-04, 63.14 63.29	WC04-04 102.07-102.23	WC04-04, 104.75-104.94	WC04-04, 139.65-139.85	WC04-04 163.78-163.94
Easting	591513	591513	591517	591517	591517	591517	591517	591517	591517	591517
Northing	5350066	5350066	5349643	5349643	5349643	5349643	5349643	5349643	5349643	5349643
Drill Hole	WC04-03	WC04-03	WC04-04	WC04-04	WCO4-04	WC04-04	WC04-04	WC04-04	WC04-04	WC04-04
Depth 2	244.38-244.61	246.34-246.57	9.37-9.48	34.71-34.95	43.72-43.89	63.14-63.29	102.07-102.23	104.75-104.94	139.65-139.85	163.78-163.94
Rock Type 1	quartz-feldspar porphyry	quartz-feldspar porphyry	feldspar porphyry	feldspar porphyry	feldspar porphyry	feldspar porphyry	amygdaloidal andesite (dyke?)	amygdaloidal andesite (dyke?)	feldspar porphyry	feldspar porphyry
Cycle	-	-	-	-	-	-	-	-	-	-
Unit	Clifford Stock and Equivalents	Clifford Stock and Equivalents	Clifford Stock and Equivalents	Clifford Stock and Equivalents	Clifford Stock and Equivalents	Clifford Stock and Equivalents	Clifford Stock and Equivalents	Clifford Stock and Equivalents	Clifford Stock and Equivalents	Clifford Stock and Equivalents
Affinity	TTG	TTG	TTG	TTG	TTG	TTG	TTG	TTG	TTG	TTG
SiO2 (wt%)	63.28	68.42	67.08	67.45	68.81	63.12	60.19	60.65	67.89	77.54
TiO2	0.44	0.38	0.35	0.38	0.37	0.52	0.41	0.40	0.44	0.29
Al2O3	16.84	14.16	15.45	15.48	15.52	16.41	15.75	15.48	15.00	10.13
Fe2O3	4.17	4.73	3.60	3.40	3.21	5.61	3.84	3.19	3.12	3.16
MnO	0.034	0.032	0.021	0.025	0.026	0.031	0.136	0.124	0.025	0.018
MgO	1.83	1.41	1.28	1.30	1.36	2.29	1.97	1.58	1.64	1.25
CaO	3.61	2.32	2.43	2.67	2.67	3.57	5.41	5.12	2.24	1.82
Na2O	2.19	4.72	4.69	4.65	4.74	3.92	1.32	0.97	5.00	3.08
K2O	4.00	1.27	1.66	1.50	1.48	2.00	3.94	4.13	1.78	1.08
P2O5	0.11	0.11	0.09	0.10	0.09	0.15	0.13	0.12	0.11	0.09
LOI	6.30	2.48	2.76	2.33	2.04	3.29	7.85	7.22	2.14	2.19
Total	102.80	100.03	99.41	99.29	100.32	100.91	100.95	98.98	99.39	100.65
Ni (ppm)	14	11	7	7	9	21	34	17	15	17
Cr	13	12	16	<8	35	10	12	14	11	<8
Co	15	11	14	11	9.00	20	29	11	11	16
V	61	47	50	52	38	66	65	64	37	30
Sc	5.4	3.6	3.5	4.5	3.6	4.6	4.6	4.4		3.1
Cu	34	314	940	294	583	1279	20	98		1017
Pb										
Zn	54	68	50	31	37	44	346	94		30
Cd	N.D	N.D	N.D	N.D	N.D	N.D	N.D	N.D		N.D
Mo	N.D	N.D	N.D	10	N.D	N.D	N.D	N.D		N.D
W	3	N.D	7	12	14	N.D	11	12		11
S	>400	>400	>400	>400	>400	>400	>400	>400		>400
Nb (XRF)	3	4	5	5	6	5	3	3	3	3
Y (XRF)	8	10	11	11	10	11	7	8	10	6
Zr (XRF)	77	90	93	92	93	100	78	77	92	47
Zr	83.2	94.8	100	102.3	104.3	107.9	86.7	84	99.6	57.7
Hf	2.3	2.7	3	3.1	3	3	2.3	2.3	2.7	1.6
Nb	3.1	4.2	5.6	5.2	5.1	5.3	3.3	3.3	4.4	2.9
Ta	0.22	0.32	0.47	0.47	0.43	0.4	0.28	0.24	0.29	0.19
Y	5.92	6.99	7.92	8.92	7.11	8.48	5.14	5.31	7.88	4.38
Be	0.56	0.7	0.79	0.61	0.71	0.62	0.5	0.49		0.45
Li	12	12	11	9	10	14	6	5		10
Cs	1.845	1.016	1.324	0.954	0.942	1.479	2.704	2.903	0.979	0.602
Rb	108.94	37.9	51.1	43.2	45.09	76.73	117.05	122.82	58.79	36.36
Ba	300	266	392	244	306	306	269	254		131
Sr	54	190	257.4	243.4	237.4	252.9	61.8	58.1	160.9	129.8
Th	1.32	1.56	2.08	2.17	2.08	1.49	1.45	1.46	1.51	0.9
U	0.454	0.375	0.649	0.739	0.633	0.564	0.474	0.524	0.574	0.391
La	7.16	7.36	11.51	12.05	9.86	11.2	10.39	10.56	10.14	4.76
Ce	15.92	16.16	24.58	25.44	21.53	24.9	21.94	22.42	23.7	10.94
Pr	2.027	2.089	3.067	3.25	2.702	3.147	2.731	2.838	3.134	1.462
Nd	8.43	9.06	12.4	12.96	10.78	12.79	10.88	11.17	13.13	6.05
Sm	1.79	2	2.57	2.76	2.26	2.6	1.98	2	2.65	1.29
Eu	0.577	0.68	0.783	0.839	0.764	0.828	0.494	0.604	0.799	0.475
Gd	1.51	1.706	2.175	2.37	1.961	2.209	1.517	1.59	2.272	1.124
Tb	0.212	0.244	0.301	0.331	0.267	0.309	0.202	0.2	0.3	0.155
Dy	1.16	1.327	1.575	1.766	1.412	1.667	1.008	1.038	1.543	0.856
Ho	0.219	0.257	0.299	0.336	0.266	0.315	0.191	0.192	0.294	0.163
Er	0.61	0.717	0.831	0.938	0.754	0.871	0.531	0.54	0.822	0.477
Tm	0.084	0.103	0.122	0.138	0.113	0.127	0.076	0.077	0.113	0.068
Yb	0.54	0.68	0.83	0.9	0.75	0.82	0.49	0.51	0.93	0.44
Lu	0.08	0.101	0.125	0.135	0.113	0.124	0.072	0.076	0.113	0.067

Table 3.1. Geochemical data for rocks of the Blake River Group and Clifford stock and equivalents

Sample	WC04-04 191.62-191.88	WCO4-04 192.17-192.30	WC04-08, 49.25 49.42	03SJP038-1
Easting	591517	591517	591510	592158
Northing	5349643	5349643	5350267	5350781
Drill Hole	WC04-04	WCO4-04	WC04-08	-
Depth 2	191.62-191.88	192.17-192.30	49.25-49.42	-
Rock Type 1	feldspar porphyry	feldspar porphyry	feldspar porphyry	dacite porphyry
Cycle	-	-	-	-
Unit	Clifford Stock and Equivalents	Clifford Stock and Equivalents	Clifford Stock and Equivalents	Clifford Stock and Equivalents
Affinity	TTG	TTG	TTG	TTG
SiO2 (wt%)	58.70	63.80	66.70	60.63
TiO2	0.40	0.39	0.40	0.69
Al2O3	15.53	14.10	16.21	17.19
Fe2O3	3.40	3.72	2.53	5.56
MnO	0.120	0.032	0.038	0.09
MgO	1.92	1.53	1.44	2.68
CaO	6.09	4.00	2.16	6.71
Na2O	2.10	4.17	6.21	2.36
K2O	3.19	2.01	1.19	1.47
P2O5	0.10	0.11	0.11	0.19
LOI	7.17	5.13	2.51	2.73
Total	98.72	98.99	99.50	100.28
Ni (ppm)	23	14	6	36
Cr	15	17	<8	30.01
Co	14.00	16.00	4.00	19
V	63	50	51	86.8
Sc	4.6	3.6	3.8	6.2
Cu	N.D	2446	621	301
Pb				
Zn	186	58	79	84
Cd	N.D	N.D	N.D	N.D
Mo	N.D	400	N.D	ND
W	3	10	N.D	5
S	148	>400	>400	70
Nb (XRF)	2	1	3	9
Y (XRF)	8	11	9	9
Zr (XRF)	77	90	97	114
Zr	82.8	88.9	109.8	118.8
Hf	2.2	2.5	3	3.3
Nb	3.2	4.8	3.8	8.2
Ta	0.22	0.34	0.27	0.57
Y	5.91	8.67	6.94	8.86
Be	0.47	0.49	0.75	0.47
Li	18	13	13	12
Cs	2.238	0.991	1.172	0.906
Rb	104.74	52.45	43.01	50.04
Ba	291	214	124	384
Sr	105.8	165.8	154.4	275.3
Th	1.36	1.78	1.55	1.65
U	0.455	0.41	0.565	0.476
La	8.51	16.56	8.5	13.5
Ce	18.8	34.31	19.7	29.22
Pr	2.352	4.101	2.554	3.57
Nd	9.57	16.82	10.61	14.09
Sm	2.05	3.24	2.19	2.78
Eu	0.713	0.771	0.556	0.875
Gd	1.701	2.615	1.786	2.36
Tb	0.23	0.338	0.235	0.324
Dy	1.157	1.779	1.295	1.792
Ho	0.215	0.33	0.251	0.341
Er	0.565	0.906	0.717	0.945
Tm	0.079	0.127	0.104	0.135
Yb	0.51	0.81	0.72	0.87
Lu	0.075	0.128	0.109	0.128

Table 3.2. Key element ratios for rocks of the Blake River Group and Clifford stock and equivalents.

Sample	03SJP044-2	03SJP077-1	03SJP017-1	03SJP027-1	03SJP090-1	P03-005
Easting	591145	592356	588861	588900	591996	591250
Northing	5351472	5349524	5349923	5350525	5350686	5350623
Drill Hole	-	-	-	-	-	-
Depth 2	-	-	-	-	-	-
Rock Type 1	basalt dyke	gabbro dyke	pillowed andesite	pillowed andesite	basaltic-andesite	andesite
Cycle	-	-	1	1	1	1
Unit	Matachewan	Matachewan	1	1	1	1
Affinity			Contaminated E-MORB-like	Contaminated E-MORB-like	Contaminated E-MORB-like	Contaminated E-MORB-like
Al2O3/Na20	3.7	4.9	4.7	4.6	6.8	6.1
Hashi	32.2	45.5	34.3	36.7	41.9	42.4
CCPI	57.2	86.1	69.7	73.9	82.0	81.6
Nb/Y	0.69	0.54	0.30	0.29	0.27	0.28
Zr/Y	10.6	6.5	7.3	7.1	6.3	6.3
Zr/Ti	0.02	0.01	0.04	0.04	0.03	0.03
Zr/Sc	12.4	8.4	13.0	11.0	9.6	10.1
La/Yb	11.9	10.0	5.0	5.8	4.7	4.1
Th/Yb	1.35	0.51	0.73	0.71	0.47	0.43
Nb/ThUCN	4.2	10.6	3.4	3.2	4.7	5.4
La/SmUCN	0.66	0.48	0.51	0.64	0.49	0.42
Nb/Ta	13.1	16.0	11.6	11.5	13.3	13.5
Nb/U	14.9	46.1	14.4	11.7	19.7	20.6
Nb/Thpm	0.56	1.42	0.45	0.43	0.63	0.72
Nb/Lapm	0.52	0.59	0.54	0.43	0.51	0.61
Ti/Sc	580	787	356	313	312	385
La/Sm	4.4	3.2	3.4	4.3	3.2	2.8
Sm/Yb	2.7	3.1	1.5	1.4	1.4	1.5
Sc/Y	0.86	0.78	0.56	0.65	0.66	0.62
Al2O3/Yb	22	7	8	7	6	6

Table 3.2. Key element ratios for rocks of the Blake River Group and Clifford stock and equivalents.

Sample	WC04-08, 13.10-13.20	03SJP046-1	03SJP046-2	03SJP047-1-1	WC04-08, 168.34-168.52	WC04-08, 171.03-171.26
Easting	591510	591080	591080	590849	591510	591510
Northing	5350267	5351814	5351814	5351742	5350267	5350267
Drill Hole	WC04-08	-	-	-	WC04-08	WC04-08
Depth 2	13.10-13.20	-	-	-	168.34-168.52	171.03-171.26
Rock Type 1	amygdaloidal andesite	amygdaloidal pillow basalt	amygdaloidal (hornfelsed) basalt	amygdaloidal pillow basalt	amygdaloidal basaltic andesite	amygdaloidal basaltic andesite
Cycle	1	1	1	1	1	1
Unit	1	1	1	1	1	1
Affinity	Contaminated E-MORB-like	E-MORB-like	E-MORB-like	E-MORB-like	E-MORB-like	E-MORB-like
Al2O3/Na20	4.7	5.2	6.3	4.9	5.5	4.7
Hashi	44.9	28.6	25.2	32.0	43.5	45.3
CCPI	71.4	79.8	84.1	77.2	81.7	81.3
Nb/Y	0.24	0.20	0.20	0.24	0.23	0.23
Zr/Y	5.4	4.5	4.3	5.3	4.9	4.8
Zr/Ti	0.04	0.02	0.02	0.02	0.02	0.02
Zr/Sc	11.1	6.4	6.5	8.0	7.1	6.8
La/Yb	7.6	2.9	2.9	4.2	3.5	3.7
Th/Yb	0.82	0.21	0.22	0.31	0.29	0.24
Nb/ThUCN	2.4	7.7	7.7	6.6	6.7	7.7
La/SmUCN	0.62	0.30	0.30	0.39	0.36	0.39
Nb/Ta	13.7	13.3	13.7	14.0	16.6	16.4
Nb/U	10.2	30.8	31.8	26.0	28.4	26.2
Nb/Thpm	0.32	1.03	1.03	0.88	0.89	1.03
Nb/Lapm	0.28	0.60	0.61	0.51	0.59	0.54
Ti/Sc	313	389	402	413	377	391
La/Sm	4.2	2.0	2.0	2.6	2.4	2.6
Sm/Yb	1.8	1.4	1.5	1.6	1.5	1.4
Sc/Y	0.49	0.70	0.66	0.67	0.68	0.70
Al2O3/Yb	5	5	5	6	5	5

Table 3.2. Key element ratios for rocks of the Blake River Group and Clifford stock and equivalents.

Sample	03SJP019	WC04-03, 79.43-79.57	WC04-03, 150.63-150.79	P03-001	P03-003	03SJP031-1-1
Easting	589121	591513	591513	591319	591335	591846
Northing	5350008	5350066	5350066	5349924	5350300	5349969
Drill Hole	-	WC04-03	WC04-03	-	-	-
Depth 2	-	79.43-79.57	150.63-150.79	-	-	-
Rock Type 1	Hbl-Bio basalt (hornfelsed)	basaltic lapilli tuff	basaltic lapilli tuff	andesitic to dacitic tuff	andesitic to dacitic tuff	dacite
Cycle	1	1	1	1	1	1
Unit	1	2	2	2	2	2
Affinity	E-MORB-like	Contaminated E-MORB-like	Contaminated E-MORB-like	Contaminated E-MORB-like	Contaminated E-MORB-like	Contaminated E-MORB-like
Al2O3/Na20	7.2	3.1	4.8	3.8	3.4	13.6
Hashi	48.2	19.4	23.3	38.7	30.7	54.8
CCPI	82.2	74.7	69.2	66.2	58.3	62.5
Nb/Y	0.28	0.28	0.30	0.24	0.24	0.23
Zr/Y	5.9	6.2	5.5	4.9	4.1	4.0
Zr/Ti	0.02	0.05	0.05	0.04	0.05	0.05
Zr/Sc	8.7	28.0	24.4	13.5	17.4	16.8
La/Yb	3.8	7.8	5.2	4.5	4.5	4.9
Th/Yb	0.25	1.94	1.53	0.92	1.28	1.30
Nb/ThUCN	9.6	1.2	1.4	2.1	1.4	1.3
La/SmUCN	0.37	0.66	0.66	0.51	0.57	0.55
Nb/Ta	14.5	9.4	9.5	10.7	9.1	8.9
Nb/U	37.5	6.4	4.3	7.5	5.0	5.3
Nb/Thpm	1.28	0.16	0.19	0.28	0.18	0.18
Nb/Lapm	0.68	0.32	0.46	0.45	0.42	0.38
Ti/Sc	417	581	464	353	367	346
La/Sm	2.5	4.4	4.4	3.4	3.8	3.7
Sm/Yb	1.5	1.8	1.2	1.3	1.2	1.3
Sc/Y	0.68	0.22	0.22	0.36	0.23	0.24
Al2O3/Yb	6	5	4	4	3	3

Table 3.2. Key element ratios for rocks of the Blake River Group and Clifford stock and equivalents.

Sample	WC04-03, 62.65-62.79	WC04-03, 68.12-68.25	WC04-03, 76.27-76.41	WC04-03, 131.59-131.7	WC04-03, 146.0-146.16	WC04-03, 154.75-154.90
Easting	591513	591513	591513	591513	591513	591513
Northing	5350066	5350066	5350066	5350066	5350066	5350066
Drill Hole	WC04-03	WC04-03	WC04-03	WC04-03	WC04-03	WC04-03
Depth 2	62.65-62.79	68.12-68.25	76.27-76.41	131.59-131.7	146.0-146.16	154.75-154.90
Rock Type 1	andesitic tuff	andesitic tuff	andesitic lapilli tuff	andesitic lapilli tuff	andesitic lapilli tuff	andesitic lapilli tuff
Cycle	1	1	1	1	1	1
Unit	2	2	2	2	2	2
Affinity	Contaminated E-MORB-like	Contaminated E-MORB-like	Contaminated E-MORB-like	Contaminated E-MORB-like	Contaminated E-MORB-like	Contaminated E-MORB-like
Al2O3/Na20	3.9	3.4	4.2	2.9	3.3	3.5
Hashi	35.9	32.7	28.0	26.6	27.2	25.7
CCPI	67.5	62.3	70.9	55.0	58.9	52.0
Nb/Y	0.24	0.23	0.21	0.23	0.23	0.22
Zr/Y	4.7	4.5	4.2	4.3	4.3	3.7
Zr/Ti	0.04	0.05	0.05	0.05	0.05	0.06
Zr/Sc	12.3	15.5	14.8	15.6	17.9	17.6
La/Yb	5.0	3.2	4.5	3.4	4.0	3.3
Th/Yb	0.96	1.07	0.94	1.07	1.13	1.10
Nb/ThUCN	1.9	1.6	1.8	1.6	1.5	1.5
La/SmUCN	0.55	0.47	0.54	0.46	0.50	0.51
Nb/Ta	11.6	10.7	11.4	10.7	10.6	10.2
Nb/U	7.4	6.0	6.1	6.2	5.8	4.9
Nb/Thpm	0.26	0.22	0.23	0.21	0.20	0.20
Nb/Lapm	0.40	0.59	0.39	0.54	0.46	0.54
Ti/Sc	318	336	329	346	364	307
La/Sm	3.7	3.1	3.6	3.1	3.4	3.4
Sm/Yb	1.4	1.0	1.3	1.1	1.2	1.0
Sc/Y	0.38	0.29	0.28	0.28	0.24	0.21
Al2O3/Yb	4	3	3	3	3	3

Table 3.2. Key element ratios for rocks of the Blake River Group and Clifford stock and equivalents.

Sample	WC04-08, 25.05-25.18	WC04-08, 26.81-26.97	WC04-08, 64.53-64.69	WC04-08, 123.7-123.9	WC04-08, 132.4-132.55	WC04-08, 158.61-158.94
Easting	591510	591510	591510	591510	591510	591510
Northing	5350267	5350267	5350267	5350267	5350267	5350267
Drill Hole	WC04-08	WC04-08	WC04-08	WC04-08	WC04-08	WC04-08
Depth 2	25.05-25.18	26.81-26.97	64.53-64.69	123.7-123.9	132.4-132.55	158.61-158.94
Rock Type 1	andesitic tuff	andesitic tuff	andesite	andesitic lapilli tuff	andesitic lapilli tuff	andesitic lapillistone
Cycle	1	1	1	1	1	1
Unit	2	2	2	2	2	2
Affinity	Contaminated E-MORB-like	Contaminated E-MORB-like	Contaminated E-MORB-like	Contaminated E-MORB-like	Contaminated E-MORB-like	Contaminated E-MORB-like
Al2O3/Na20	5.1	3.2	5.1	3.6	3.6	3.3
Hashi	42.4	38.7	37.7	22.0	31.1	21.7
CCPI	70.5	66.7	70.4	64.0	53.1	49.0
Nb/Y	0.25	0.22	0.28	0.25	0.19	0.27
Zr/Y	5.9	5.2	7.0	4.6	3.4	6.6
Zr/Ti	0.04	0.04	0.04	0.05	0.05	0.10
Zr/Sc	11.3	10.7	14.1	17.3	19.9	29.5
La/Yb	3.6	3.7	4.7	3.1	5.4	4.7
Th/Yb	0.66	0.56	0.68	1.14	1.16	0.97
Nb/ThUCN	2.9	3.2	3.2	1.5	1.4	2.0
La/SmUCN	0.47	0.46	0.54	0.49	0.52	0.55
Nb/Ta	13.4	13.8	14.1	10.6	10.0	12.8
Nb/U	10.5	10.6	12.4	6.2	5.2	9.0
Nb/Thpm	0.39	0.43	0.43	0.20	0.18	0.27
Nb/Lapm	0.58	0.53	0.51	0.60	0.32	0.46
Ti/Sc	288	304	326	368	366	303
La/Sm	3.2	3.1	3.6	3.2	3.4	3.7
Sm/Yb	1.1	1.2	1.3	1.0	1.6	1.3
Sc/Y	0.52	0.48	0.50	0.27	0.17	0.22
Al2O3/Yb	5	5	5	3	3	3

Table 3.2. Key element ratios for rocks of the Blake River Group and Clifford stock and equivalents.

Sample	03SJP088-1	WC04-08, 134.45-134.61	03SJP011-1	03SJP070-2-1	03SJP095-1	03SJP096-1-1
Easting	591815	591510	590898	591805	591979	591934
Northing	5350056	5350267	5349546	5349956	5351476	5351663
Drill Hole	-	WC04-08	-	-	-	-
Depth 2	-	134.45-134.61	-	-	-	-
Rock Type 1	andesitic tuff	andesitic lapilli tuff	andesitic lapilli tuff	andesite	basaltic andesite	andesite
Cycle	1	1	1	1	1	1
Unit	2	2	2	2	2	2
Affinity	Contaminated E-MORB-like	Intensely Altered E-MORB-like	E-MORB-like	E-MORB-like	E-MORB-like	E-MORB like
Al2O3/Na20	4.1	43.5	5.1	8.1	6.1	6.1
Hashi	42.0	33.2	48.5	53.7	43.4	43.1
CCPI	66.9	58.3	81.8	88.5	77.8	84.6
Nb/Y	0.24	0.28	0.22	0.23	0.30	0.24
Zr/Y	4.6	4.7	4.6	4.9	7.0	5.5
Zr/Ti	0.04	0.05	0.02	0.02	0.03	0.02
Zr/Sc	16.3	18.3	6.8	6.9	9.7	8.9
La/Yb	4.7	0.7	5.1	3.0	2.7	4.1
Th/Yb	1.11	1.45	0.29	0.27	0.50	0.33
Nb/ThUCN	1.7	1.3	6.4	7.1	4.9	5.9
La/SmUCN	0.55	0.27	0.40	0.32	0.39	0.40
Nb/Ta	9.9	9.9	13.5	14.0	13.4	13.2
Nb/U	6.4	5.5	21.6	23.7	17.7	23.1
Nb/Thpm	0.22	0.18	0.86	0.95	0.65	0.79
Nb/Lapm	0.43	2.88	0.39	0.70	0.97	0.50
Ti/Sc	382	344	402	365	347	391
La/Sm	3.6	1.8	2.6	2.2	2.6	2.6
Sm/Yb	1.3	0.4	1.9	1.4	1.0	1.6
Sc/Y	0.28	0.26	0.68	0.71	0.72	0.62
Al2O3/Yb	4	4	5	5	6	5

Table 3.2. Key element ratios for rocks of the Blake River Group and Clifford stock and equivalents.

Sample	03SJP052-1	03SJP053-1	03SJP056-1	03SJP065-1	03SJP065-1-2	03SJP055-1
Easting	590119	590153	590216	590904	590904	590175
Northing	5348846	5248894	5349027	5349046	5349046	5349090
Drill Hole	-	-	-	-	-	-
Depth 2	-	-	-	-	-	-
Rock Type 1	andesite	andesite	andesite	basaltic andesite	basaltic andesite	andesite
Cycle	2	2	2	2	2	2
Unit	4	4	4	4	4	4
Affinity	Contaminated E-MORB-like	Contaminated E-MORB-like	Contaminated E-MORB-like	Contaminated E-MORB-like	Contaminated E-MORB-like	E-MORB-like
Al2O3/Na20	5.0	5.8	6.0	3.6	4.3	6.9
Hashi	36.8	42.8	51.9	35.9	41.1	42.1
CCPI	72.1	54.2	74.5	67.3	70.9	82.4
Nb/Y	0.24	0.25	0.31	0.25	0.27	0.25
Zr/Y	5.5	5.6	8.7	5.8	6.3	5.4
Zr/Ti	0.02	0.05	0.04	0.02	0.02	0.02
Zr/Sc	7.8	23.1	13.8	8.0	8.5	7.8
La/Yb	4.7	4.9	4.7	5.9	4.5	4.0
Th/Yb	0.57	1.30	1.61	0.59	0.61	0.28
Nb/ThUCN	3.3	1.5	1.4	3.3	3.4	7.4
La/SmUCN	0.54	0.62	0.54	0.57	0.52	0.40
Nb/Ta	12.2	9.9	9.0	11.3	12.1	14.0
Nb/U	15.3	6.1	6.1	13.5	14.8	28.8
Nb/Thpm	0.45	0.20	0.19	0.45	0.45	0.99
Nb/Lapm	0.44	0.43	0.52	0.37	0.50	0.56
Ti/Sc	324	425	357	333	360	396
La/Sm	3.6	4.1	3.6	3.8	3.5	2.7
Sm/Yb	1.3	1.2	1.3	1.5	1.3	1.5
Sc/Y	0.70	0.24	0.63	0.72	0.74	0.69
Al2O3/Yb	6	4	8	6	6	6

Table 3.2. Key element ratios for rocks of the Blake River Group and Clifford stock and equivalents.

Sample	03SJP068-1-1	03SJP068-36	03SJP110-2	03SJP112-1	03SJP037-1	03SJP080-1-1
Easting	591261	591261	593171	593182	592278	592497
Northing	5348588	5348588	5350838	5350691	5350685	5349867
Drill Hole	-	-	-	-	-	-
Depth 2	-	-	-	-	-	-
Rock Type 1	rhyolite	rhyolite	diabase / diorite	diabase / diorite	diorite porphyry	diabase / gabbro
Cycle	2	2	-	-	-	-
Unit	5	5	synvolcanic intrusions	synvolcanic intrusions	synvolcanic intrusions	synvolcanic intrusions
Affinity	Transitional Rhyolite	Transitional Rhyolite	E-MORB-like	E-MORB-like	Contaminated E-MORB-like	Contaminated E-MORB-like
Al2O3/Na20	3.0	2.4	7.7	8.0	2.8	5.6
Hashi	26.4	20.7	41.8	46.0	33.0	71.1
CCPI	23.9	21.6	86.9	90.0	36.4	92.9
Nb/Y	1.12	0.26	0.21	0.21	0.26	0.24
Zr/Y	9.8	6.5	4.5	4.7	6.2	6.1
Zr/Ti	0.10	0.10	0.02	0.02	0.10	0.03
Zr/Sc	50.4	39.2	6.1	5.8	29.3	5.3
La/Yb	14.4	5.3	3.2	3.1	4.9	4.4
Th/Yb	3.23	1.16	0.25	0.23	0.98	0.45
Nb/ThUCN	2.8	1.6	7.4	7.5	2.0	4.1
La/SmUCN	1.00	0.62	0.32	0.33	0.54	0.49
Nb/Ta	12.0	10.3	14.1	13.6	11.6	11.5
Nb/U	10.8	7.3	29.9	30.1	8.7	17.1
Nb/Thpm	0.37	0.21	0.99	1.01	0.27	0.55
Nb/Lapm	0.67	0.37	0.61	0.61	0.43	0.46
Ti/Sc	510	375	361	372	307	183
La/Sm	6.6	4.1	2.2	2.2	3.6	3.3
Sm/Yb	2.2	1.3	1.5	1.4	1.4	1.3
Sc/Y	0.19	0.17	0.74	0.80	0.21	1.14
Al2O3/Yb	11	3	5	6	3	5

Table 3.2. Key element ratios for rocks of the Blake River Group and Clifford stock and equivalents.

Sample	03SJP109-2-1	03SJP84-1	WC04-03, 212.49-212.63	WC04-04, 51.62-51.92	WC04-04, 70.65-70.84	WC04-04, 130.88-131.04
Easting	593437	592470	591513	591517	591517	591517
Northing	5350948	5350306	5350066	5349643	5349643	5349643
Drill Hole	-	-	WC04-03	WC04-04	WC04-04	WC04-04
Depth 2	-	-	212.49-212.63	51.62-51.92	70.65-70.84	130.88-131.04
Rock Type 1	diabase	diabase	diabase / diorite dyke	diabase / diorite	diabase / diorite	diabase / diorite
Cycle	-	-	-	-	-	-
Unit	synvolcanic intrusions	synvolcanic intrusions	synvolcanic intrusions	synvolcanic intrusions	synvolcanic intrusions	synvolcanic intrusions
Affinity	Contaminated E-MORB-like	E-MORB-like	E-MORB-like	E-MORB-like	E-MORB-like	E-MORB-like
Al2O3/Na20	2.9	9.4	12.4	5.1	7.1	5.0
Hashi	29.4	42.5	48.9	55.0	51.2	50.5
CCPI	54.4	89.8	92.2	81.4	78.4	78.0
Nb/Y	0.24	0.21	0.23	0.25	0.23	0.26
Zr/Y	5.7	4.7	4.9	5.1	5.0	5.6
Zr/Ti	0.06	0.02	0.02	0.02	0.02	0.02
Zr/Sc	19.7	7.6	6.8	8.7	7.1	7.9
La/Yb	5.9	3.3	4.7	3.1	3.7	3.9
Th/Yb	1.17	0.25	0.28	0.28	0.28	0.31
Nb/ThUCN	1.6	7.2	7.1	7.1	6.9	6.8
La/SmUCN	0.63	0.33	0.40	0.31	0.36	0.36
Nb/Ta	9.9	14.2	16.3	16.3	15.8	16.2
Nb/U	6.7	29.6	20.2	11.0	19.8	10.9
Nb/Thpm	0.21	0.97	0.95	0.95	0.92	0.91
Nb/Lapm	0.34	0.60	0.46	0.68	0.55	0.59
Ti/Sc	337	398	349	477	369	404
La/Sm	4.2	2.2	2.7	2.1	2.4	2.4
Sm/Yb	1.4	1.5	1.7	1.5	1.5	1.6
Sc/Y	0.29	0.62	0.72	0.59	0.71	0.71
Al2O3/Yb	4	5	5	6	6	6

Table 3.2. Key element ratios for rocks of the Blake River Group and Clifford stock and equivalents.

Sample	WC04-04, 166.52-166.67	WC04-08, 176.74-176.96	WC04-08, 227.76-227.93	WC04-08, 236.47-236.52	03SJP013-2-1	03SJP013-2-1(2)
Easting	591517	591510	591510	591510	590880	590880
Northing	5349643	5350267	5350267	5350267	5349453	5349453
Drill Hole	WC04-04	WC04-08	WC04-08	WC04-08	-	-
Depth 2	166.52-166.67	176.74-176.96	227.76-227.93	236.47-236.52	-	-
Rock Type 1	diabase / diorite	diabase / diorite	diabase / diorite	diabase / diorite	diorite porphyry	diorite porphyry
Cycle	-	-	-	-	-	-
Unit	synvolcanic intrusions	synvolcanic intrusions	synvolcanic intrusions	synvolcanic intrusions	Clifford Stock and Equivalents	Clifford Stock and Equivalents
Affinity	E-MORB-like	Contaminated E-MORB-like	E-MORB-like	E-MORB-like	TTG	TTG
Al2O3/Na20	5.6	4.4	6.7	4.0	3.5	4.2
Hashi	48.4	36.8	41.3	36.9	34.6	32.0
CCPI	80.1	72.6	82.2	77.6	53.2	62.1
Nb/Y	0.31	0.27	0.23	0.21	0.38	0.54
Zr/Y	6.3	6.6	4.9	4.4	9.1	10.9
Zr/Ti	0.03	0.03	0.02	0.02	0.05	0.03
Zr/Sc	8.9	12.6	7.3	7.0	20.2	15.8
La/Yb	5.7	5.4	3.0	2.3	7.8	10.9
Th/Yb	0.55	0.68	0.26	0.26	1.72	1.81
Nb/ThUCN	4.9	3.2	7.2	6.7	1.7	2.6
La/SmUCN	0.42	0.54	0.32	0.28	0.74	0.66
Nb/Ta	16.3	13.8	16.8	16.8	10.8	12.1
Nb/U	11.4	13.6	33.0	9.9	7.7	14.0
Nb/Thpm	0.66	0.43	0.97	0.89	0.23	0.35
Nb/Lapm	0.51	0.43	0.68	0.81	0.40	0.48
Ti/Sc	335	362	394	383	422	516
La/Sm	2.8	3.6	2.1	1.8	4.9	4.4
Sm/Yb	2.0	1.5	1.4	1.2	1.6	2.5
Sc/Y	0.70	0.52	0.67	0.63	0.45	0.69
Al2O3/Yb	7	6	5	5	7	16

Table 3.2. Key element ratios for rocks of the Blake River Group and Clifford stock and equivalents.

Sample	03SJP020-2	03SJP022-1	03SJP047-2-1	03SJP059-2	03SJP096-2-1	P03-007A
Easting	589170	589444	590849	590369	591934	590938
Northing	5350097	5350567	5351742	5349181	5351663	5360770
Drill Hole	-	-	-	-	-	-
Depth 2	-	-	-	-	-	-
Rock Type 1	tonalite / granodiorite	tonalite / granodiorite	tonalite / granodiorite	diorite porphyry	diorite	diorite
Cycle	-	-	-	-	-	-
Unit	Clifford Stock and Equivalents	Clifford Stock and Equivalents	Clifford Stock and Equivalents	Clifford Stock and Equivalents	Clifford Stock and Equivalents	Clifford Stock and Equivalents
Affinity	TTG	TTG	TTG	TTG	TTG	TTG
Al2O3/Na20	3.4	4.8	4.1	4.7	3.8	4.0
Hashi	28.5	30.0	30.4	38.3	26.5	24.9
CCPI	55.1	64.3	58.0	43.8	60.8	60.5
Nb/Y	0.41	0.66	0.68	0.41	0.78	0.68
Zr/Y	7.3	11.3	9.9	12.2	14.3	9.0
Zr/Ti	0.03	0.03	0.03	0.04	0.03	0.02
Zr/Sc	17.1	12.3	12.9	24.4	14.3	10.5
La/Yb	7.5	14.3	12.4	13.9	12.6	14.0
Th/Yb	1.71	2.27	2.92	1.93	1.95	1.89
Nb/ThUCN	2.0	2.8	2.2	2.0	3.9	3.4
La/SmUCN	0.53	0.67	0.62	0.72	0.57	0.71
Nb/Ta	11.3	11.9	11.3	10.3	13.8	12.8
Nb/U	8.2	12.2	11.6	6.8	15.3	16.4
Nb/Thpm	0.27	0.37	0.29	0.26	0.52	0.45
Nb/Lapm	0.50	0.47	0.55	0.29	0.65	0.49
Ti/Sc	643	486	513	613	463	496
La/Sm	3.5	4.5	4.1	4.8	3.8	4.7
Sm/Yb	2.1	3.2	3.0	2.9	3.3	3.0
Sc/Y	0.42	0.91	0.77	0.50	1.00	0.86
Al2O3/Yb	12	22	20	20	22	22

Table 3.2. Key element ratios for rocks of the Blake River Group and Clifford stock and equivalents.

Sample	P03-007B	WC04-03, 180.95-181.14	WC04-03, 192.67-192.81	WC04-03, 209.63-209.82	WC04-03, 244.38-244.61	WC04-03, 246.34-246.57
Easting	590938	591513	591513	591513	591513	591513
Northing	5360770	5350066	5350066	5350066	5350066	5350066
Drill Hole	-	WC04-03	WC04-03	WC04-03	WC04-03	WC04-03
Depth 2	-	180.95-181.14	192.67-192.81	209.63-209.82	244.38-244.61	246.34-246.57
Rock Type 1	diorite	quartz-feldspar porphyry	quartz-feldspar porphyry	quartz-feldspar porphyry	quartz-feldspar porphyry	quartz-feldspar porphyry
Cycle	-	-	-	-	-	-
Unit	Clifford Stock and Equivalents	Clifford Stock and Equivalents	Clifford Stock and Equivalents	Clifford Stock and Equivalents	Clifford Stock and Equivalents	Clifford Stock and Equivalents
Affinity	TTG	TTG	TTG	TTG	TTG	TTG
Al2O3/Na20	4.2	2.9	3.0	3.4	7.7	3.0
Hashi	27.5	27.0	30.6	29.1	50.1	27.6
CCPI	59.9	43.4	44.5	46.7	49.2	50.6
Nb/Y	0.63	0.62	0.55	0.65	0.52	0.60
Zr/Y	10.7	13.1	12.9	19.2	14.1	13.6
Zr/Ti	0.02	0.04	0.04	0.04	0.03	0.04
Zr/Sc	11.2	29.9	28.1	25.2	15.4	26.3
La/Yb	14.3	9.7	9.8	11.5	13.3	10.8
Th/Yb	1.69	2.51	1.69	2.43	2.44	2.29
Nb/ThUCN	3.7	2.4	3.2	2.3	2.1	2.4
La/SmUCN	0.67	0.52	0.49	0.65	0.60	0.55
Nb/Ta	12.7	12.4	14.5	14.7	14.1	13.1
Nb/U	14.4	13.4	12.8	9.1	6.8	11.2
Nb/Thpm	0.49	0.32	0.42	0.31	0.28	0.32
Nb/Lapm	0.47	0.68	0.59	0.53	0.42	0.55
Ti/Sc	478	709	651	600	488	633
La/Sm	4.5	3.4	3.3	4.4	4.0	3.7
Sm/Yb	3.2	2.8	3.0	2.6	3.3	2.9
Sc/Y	0.96	0.44	0.46	0.76	0.91	0.52
Al2O3/Yb	24	21	21	30	31	21

Table 3.2. Key element ratios for rocks of the Blake River Group and Clifford stock and equivalents.

Sample	WC04-04, 9.37-9.48	WC04-04, 34.71-34.95	WCO4-04, 43.72-43.89	WC04-04, 63.14-63.29	WC04-04, 102.07-102.23	WC04-04, 104.75-104.94
Easting	591517	591517	591517	591517	591517	591517
Northing	5349643	5349643	5349643	5349643	5349643	5349643
Drill Hole	WC04-04	WC04-04	WCO4-04	WC04-04	WC04-04	WC04-04
Depth 2	9.37-9.48	34.71-34.95	43.72-43.89	63.14-63.29	102.07-102.23	104.75-104.94
Rock Type 1	feldspar porphyry	feldspar porphyry	feldspar porphyry	feldspar porphyry	amygdaloidal andesite (dyke?)	amygdaloidal andesite (dyke?)
Cycle	-	-	-	-	-	-
Unit	Clifford Stock and Equivalents	Clifford Stock and Equivalents	Clifford Stock and Equivalents	Clifford Stock and Equivalents	Clifford Stock and Equivalents	Clifford Stock and Equivalents
Affinity	TTG	TTG	TTG	TTG	TTG	TTG
Al2O3/Na20	3.3	3.3	3.3	4.2	11.9	16.0
Hashi	29.2	27.7	27.7	36.4	46.8	48.4
CCPI	43.5	43.3	42.4	57.2	52.5	48.3
Nb/Y	0.71	0.58	0.72	0.63	0.64	0.62
Zr/Y	12.6	11.5	14.7	12.7	16.9	15.8
Zr/Ti	0.05	0.04	0.05	0.03	0.04	0.04
Zr/Sc	28.6	22.7	29.0	23.5	18.8	19.1
La/Yb	13.9	13.4	13.1	13.7	21.2	20.7
Th/Yb	2.51	2.41	2.77	1.82	2.96	2.86
Nb/ThUCN	2.4	2.1	2.2	3.2	2.0	2.0
La/SmUCN	0.67	0.65	0.65	0.65	0.79	0.79
Nb/Ta	11.9	11.1	11.9	13.3	11.8	13.8
Nb/U	8.6	7.0	8.1	9.4	7.0	6.3
Nb/Thpm	0.32	0.29	0.29	0.42	0.27	0.27
Nb/Lapm	0.47	0.42	0.50	0.46	0.31	0.30
Ti/Sc	600	506	616	678	534	545
La/Sm	4.5	4.4	4.4	4.3	5.2	5.3
Sm/Yb	3.1	3.1	3.0	3.2	4.0	3.9
Sc/Y	0.44	0.50	0.51	0.54	0.89	0.83
Al2O3/Yb	19	17	21	20	32	30

Table 3.2. Key element ratios for rocks of the Blake River Group and Clifford stock and equivalents.

Sample	WC04-04, 139.65-139.85	WC04-04, 163.78-163.94	WC04-04, 191.62-191.88	WCO4-04, 192.17-192.30	WC04-08, 49.25-49.42	03SJP038-1
Easting	591517	591517	591517	591517	591510	592158
Northing	5349643	5349643	5349643	5349643	5350267	5350781
Drill Hole	WC04-04	WC04-04	WC04-04	WCO4-04	WC04-08	-
Depth 2	139.65-139.85	163.78-163.94	191.62-191.88	192.17-192.30	49.25-49.42	-
Rock Type 1	feldspar porphyry	feldspar porphyry	feldspar porphyry	feldspar porphyry	feldspar porphyry	dacite porphyry
Cycle	-	-	-	-	-	-
Unit	Clifford Stock and Equivalents	Clifford Stock and Equivalents	Clifford Stock and Equivalents	Clifford Stock and Equivalents	Clifford Stock and Equivalents	Clifford Stock and Equivalents
Affinity	TTG	TTG	TTG	TTG	TTG	TTG
Al2O3/Na20	3.0	3.3	7.4	3.4	2.6	7.3
Hashi	32.1	32.2	38.4	30.2	23.9	31.4
CCPI	41.2	51.5	50.1	45.9	34.9	68.3
Nb/Y	0.56	0.66	0.54	0.55	0.55	0.93
Zr/Y	12.6	13.2	14.0	10.3	15.8	13.4
Zr/Ti	0.04	0.03	0.03	0.04	0.05	0.03
Zr/Sc	-	18.6	18.0	24.7	28.9	19.2
La/Yb	10.9	10.8	16.7	20.4	11.8	15.5
Th/Yb	1.62	2.05	2.67	2.20	2.15	1.90
Nb/ThUCN	2.6	2.9	2.1	2.4	2.2	4.4
La/SmUCN	0.57	0.55	0.62	0.77	0.58	0.73
Nb/Ta	15.2	15.3	14.5	14.1	14.1	14.4
Nb/U	7.7	7.4	7.0	11.7	6.7	17.2
Nb/Thpm	0.35	0.38	0.28	0.32	0.29	0.59
Nb/Lapm	0.42	0.59	0.36	0.28	0.43	0.59
Ti/Sc	-	561	521	649	631	667
La/Sm	3.8	3.7	4.2	5.1	3.9	4.9
Sm/Yb	2.8	2.9	4.0	4.0	3.0	3.2
Sc/Y	-	0.71	0.78	0.42	0.55	0.70
Al2O3/Yb	16	23	30	17	23	20

This page left blank intentionally

Appendix A

Lithogeochemical Analytical Methods, Quality Control and Quality Assurance

Samples for the Discover Abitibi Project were collected during field work in 2003 and 2004. Samples were ~5 kg and were taken from either surface exposures or from drill core. Weathered surfaces from surface samples were either removed in the field or later with a diamond saw. Samples were crushed using a steel jaw crusher and subsequently pulverized; samples from 2003 were pulverized in an agate mortar at the Ontario Geoscience Laboratories (GeoLabs) in Sudbury, Ontario, and samples from 2004 were pulverized in mild (carbon) steel at Activation Laboratories Limited (ActLabs) in Ancaster, Ontario. Powders from the previous step were subsequently analyzed using a combination of X-ray fluorescence (XRF), inductively coupled plasma emission spectroscopy (ICP–ES), and inductively coupled plasma mass spectrometry (ICP–MS).

Major elements (SiO_2, Al_2O_3, TiO_2, Fe_2O_3T, MnO, MgO, CaO, Na_2O, K_2O and P_2O_5) were determined by wavelength dispersive XRF using fused discs at both the Ontario Geoscience Laboratories (2003 samples) and Activation Laboratories (2004 samples); loss-on-ignition (LOI) was determined via conventional heating and weight difference methods at both GeoLabs and ActLabs. Trace elements were analyzed via inductively coupled plasma mass spectrometry (ICP–MS: Nb, Ta, Zr, Hf, Y, Cs, Th, U, La, Ce, Pr, Nd, Sm, Eu, Gd, Tb, Dy, Ho, Er, Tm, Yb, Lu) and inductively coupled plasma emission spectroscopy (ICP–ES: Ba, Be, Cd, Co, Cr, Cu, Li, Mo, Ni, S, Sc, Sr, V, W, Zn) using a closed-beaker multi-acid digestion prior to analysis (Burnham et al. 2002; Burnham and Schweyer 2004; Tomlinson, Bowins and Hechler 1998; Tomlinson et al. 1999) at the GeoLabs. Some trace elements were also determined by pressed powder pellet XRF at the GeoLabs (2003 samples: Nb, Zr and Y) and ActLabs (2004 samples: Nb, Zr, Y, Ni, Cr and V). Niobium, Zr and Y were all determined by XRF pressed pellet analysis to test whether digestions were complete for ICP–ES and ICP–MS methods; for most samples, the XRF Nb, Zr and Y analyses were within 10% of the values obtained by ICP–MS, suggesting that the dissolutions for ICP–ES and ICP–MS were complete. We have utilized Nb, Zr and Y data by ICP–MS in this report because of the superior detection limits and sensitivity for these elements by ICP–MS as compared to XRF. The 2003 samples have Ni, Cr and V values via ICP–ES from the GeoLabs, whereas the 2004 samples have utilized Ni, Cr and V via pressed pellet XRF from ActLabs. For most samples, the Ni, Cr and V values via XRF are within 10% of the samples analyzed by ICP–ES.

PRECISION

Precision was calculated using replicate analysis a variety of known and unknown reference materials, and by utilization of analytical duplicates and scatterplots and Thompson–Howarth plots (Fletcher 1981, 1986; Stanley 2003; Thompson and Howarth 1978).

Using replicate analysis of reference materials, the measure of precision is given by the percent relative standard deviation:

$$\%RSD_i = 100 \times \frac{s_i}{\mu_i} \qquad (1)$$

where
$\%RSD_i$ = percent relative standard deviation for element i
s_i = standard deviation of the mean from the series of analytical runs for element i
μ_i = mean value of element i over a series of analytical runs.

In general, %RSD values between 0 and 3% are excellent, 3 to 7% are very good, 7 to 10% are good, and above 10% are poor (e.g., Jenner 1996). In general, %RSD increases as one approaches the limit of detection (LOD) for an instrument (e.g., Jenner 1996) and this must be considered for each standard (i.e., as one gets closer to the LOD the precision will decrease). Furthermore, values that lie between the LOD and the limit of quantification (LOQ = 3.3×LOD; Jenner 1996), are also subject to poor precision; thus, %RSD values in Tables A1 to A6 should only be considered valid for elemental concentrations above the LOQ.

Analytical error for each element calculated from replicate analysis of standards is given in Tables A1 to A6, and is presented as the 2σ error:

$$2\sigma_i = \frac{2 \times s_i}{\sqrt{n}} \qquad (2)$$

where
σ_i = standard error of the mean of analytical runs for element i
s_i = standard deviation of the mean of analytical runs for element i
n = number of measurements of element i.

The $2\sigma_i$ value implies that if a sample was repeatedly analyzed, the value of element i in that sample will have a value between $\mu_i \pm 2\sigma_i$ 95% of the time (i.e., the 95% confidence level).

Percent relative standard deviation and 2σ errors for each analytical method for reference materials run at the GeoLabs during this project are presented in Tables A1, A3, A5 and A6, and for ActLabs these data are presented in Tables A2 and A4.

A second gauge of the precision that is independent of reference materials is the utilization of the random analytical duplicates and a combination of scatterplots and Thompson–Howarth plots. Scatterplots involve logarithmic graphs of the original analyses on the X-axis against the duplicate analyses on the Y-axis with a 1:1 control line and bounding lines at a given precision (i.e., 5%, 10%, etc.; Figure A1a). We have also employed the Thompson–Howarth short method and related plots (Fletcher 1981, 1986; Stanley 2003; Thompson and Howarth 1978). Thompson–Howarth short method plots involve plotting the duplicate data on a control graph with a control line (Figure A1b). The control graph involves plotting the duplicate data (X_1 = original analysis, X_2 = duplicate analysis) in the form of the X-axis equal to $(X_1+X_2)/2$ and the Y-axis equal to $|X_1-X_2|$ (Figure A1b); these are estimates of the average and standard deviation or median of the replicate analyses, respectively. The control line is constructed based on the assumption of the probability of randomly distributed errors in the analytical data and the probability that samples will lie below the control line a prescribed level of precision if they are precise to that level of precision (Fletcher 1981, 1986; Thompson and Howarth 1978). In essence, the control line is set at a given precision and if all the duplicate data lie below the line, the data are precise to that given precision (Fletcher 1981, 1986; Thompson and Howarth 1978). Details on constructing the control line are presented in Thompson and Howarth (1978), Fletcher (1981, 1986) and Stanley (2003). Utilizing scatterplots and Thompson–Howarth methods percent precision for major elements by fused disc XRF at the GeoLabs are SiO_2 (2%), Al_2O_3 (2%), TiO_2 (4%), Fe_2O_3T (4%), MgO (7%), MnO (2%) CaO (5%), Na_2O (5%), K_2O (5%), P_2O_5 (10%) and LOI (3%); the higher values for MgO and P_2O_5 are due to these elements being close to the limit of detection in the duplicate samples and the values are likely <5% (O.M. Burnham and J. Schweyer, Ontario Geoscience Laboratories, personal communication, 2004). Percent precision of traces by pressed pellet XRF at the GeoLabs are Nb (~10%), Zr (5%) and Y (10%). Percent precision for major elements by fused disc XRF at ActLabs are SiO_2 (2%), Al_2O_3 (1%), TiO_2 (3%), Fe_2O_3T (2%), MgO (6%), MnO (4%) CaO (2%), Na_2O (4%), K_2O (10%), P_2O_5 (1%) and LOI (2%); the high values for K_2O, however, are due to being close to the limit of detection in most duplicate analysis and are likely <5% (O.M. Burnham and J. Schweyer, Ontario Geoscience Laboratories, personal communication, 2004). Precision for trace elements by pressed pellet XRF at ActLabs are Nb (~5%), Zr (8%), Y (10%), Ni (10%), Cr (7%) and V (4%). Precision for trace elements by ICP–ES analysis at the GeoLabs are Ba (5%), Be (5%), Cd (90%), Co (15%), Cr (15%), Cu (15%), Li (10%), Mo (not detected), Ni (10%), S (20%), Sc (10%), Sr (10%), V (10%), W (90%) and Zn (10%). Values that were severely imprecise, including Cd, Mo and W, are not considered reliable via this method and are not used in this report. Precision for trace elements by ICP–MS at the GeoLabs are Nb (5%), Ta (5%), Zr (10%), Hf (10%), Y (10%), Cs (10%), Th (7%), U (7%) and REE (<10-12%).

ACCURACY

Accuracy was determined using reference materials with known or accepted values. Both international and internal reference materials were utilized, and internal reference materials from the GeoLabs are compared to the long term averages for said reference materials. The measure of accuracy is given the percent relative difference of the mean value of the analytical runs for an element as compared to the accepted value for the standard, and is given by:

$$\%RD = 100 \times \frac{\mu_i - STD_i}{STD_i} \qquad (3)$$

where:
μ_i = mean value of element i in the standard over a number of analytical runs
STD_i = "known" or "certified" value of i in the standard or reference material

Values for %RD can be negative or positive as values can be less than the known value (i.e., %RD<0), or greater than the known value (i.e., %RD>0). In general, values of %RD values that are ±0–3% are considered to have excellent accuracy, values from 3 to 7% are considered to represent very good accuracy, and 7 to 10% good accuracy. Values above 10% should be considered indicators of poor accuracy. Notably, accuracy decreases as on approaches the LOD (e.g., Jenner 1996) and this must be considered for each standard (i.e., as one gets closer to the LOD the accuracy will decrease). Furthermore, values that lie between the LOD and the LOQ are also subject to poor accuracy; thus, %RD values in Tables A1 to A6 should only be considered valid for elemental concentrations above the LOQ.

Reference materials run at the GeoLabs for XRF included in-house standards (for precision) MRB-31 (basalt), NPD-1 (diabase) and MRB-15 (rhyolite); international reference materials GSD-11 (stream sediment), GSR-2 (hornblende andesite) and BIR-1 (basalt); and 3 blind standards PER-1 (rhyolite), BAMAP-01 (basalt) and CHA-2 (andesite) from the Multi-National Andean Project of the Geological Survey of Canada (J. Getsinger, Geological Survey of Canada, personal communication, 2004). Reference materials run at ActLabs for XRF included the international reference materials W-2 (diabase), SY-3 (syenite), SGR-1 (shale), BE-N (basalt), DNC-1 (dolerite), MRG-1 (gabbro), MAG-1 (mud); and 3 blind, in-house reference materials from the OGS, including OKUM-1 (komatiite), NPD-1 (diabase) and MRB-15 (rhyolite). Reference materials run at the GeoLabs for ICP–ES include the in-house standard MRB-29 (basalt); the international reference materials BIR-1 (basalt), BHVO-2 (basalt), NBS-688 (basalt), AGV-2 (andesite), GSR-2 (hornblende andesite), RGM-1 (rhyolite), SY-4 (syenite), GSP-2 (granodiorite), GSR-1 (biotite granite); and the blind standards PER-1 (rhyolite), BAMAP-01 (basalt) (J. Getsinger, Geological Survey of Canada, personal communication, 2004). Reference materials run at the GeoLabs for ICP–MS include the international reference materials BIR-1 (basalt), BHVO-2 (basalt), NBS-688 (basalt), GSR-1 (biotite granite), GSR-2 (hornblende andesite), GSR-3 (olivine basalt) and GSP-2 (granodiorite); in-house standard MRB-29 (basalt), MRB-32 (weakly mineralized peridotite) and NPD-1 (diabase); and the blind standards PER-1 (rhyolite), BAMAP-01 (basalt) and CHA-2 (andesite) from the Multi-National Andean Project of the Geological Survey of Canada (J. Getsinger, Geological Survey of Canada, personal communication, 2004). Reference values for these international reference materials were obtained directly from the certificates from the issuing agencies (e.g., USGS, GeoLabs, CANMET) and from compilations such as Govindaraju (1994). In-house reference values were from

Burnham and Schweyer (2004) and Schweyer (GeoLabs, personal communication, 2004). Results for analytical accuracy for the various analytical techniques and standards are given in Tables A1 to A6.

REFERENCES

Burnham, O.M., Hechler, J., Semenyna, L. and Schweyer, J. 2002. Mineralogical controls on the determination of trace elements following mixed-acid dissolution; *in* Summary of Field Work and Other Activities, 2002, Ontario Geological Survey, Open File Report 6100, p36-1 to 36-12.

Burnham, O.M. and Schweyer, J. 2004. Trace element analysis of geological samples by inductively coupled plasma mass spectrometry at the Geoscience Laboratories: revised capabilities due to improvements to instrumentation; *in* Summary of Field Work and Other Activities 2004, Ontario Geological Survey, Open File Report 6145, p.54-1 to 54-20.

Fletcher, W.K. 1981. Analytical methods in geochemical prospecting; Elsevier, Amsterdam, Handbook of exploration geochemistry, v.1, 255p.

——— 1986. Analysis of soil samples; *in* Exploration geochemistry: design and interpretation of soil surveys, Society of Economic Geologists, Reviews in Economic Geology v.3, p.79-96.

Govindaraju, K. 1994. 1994 compilation of working values and sample description for 383 geostandards; Geostandards Newsletter, v.18, July, 158 pages (special issue).

Jenner, G.A. 1996. Trace element geochemistry of igneous rocks: geochemical nomenclature and analytical geochemistry; *in* Trace element geochemistry of volcanic rocks: applications for massive sulfide exploration, Geological Association of Canada, Short Course Notes, v.12, p.51-77.

Stanley, C.R. 2003. THPLOT.M: a MATLAB function to implement generalized Thompson–Howarth error analysis using replicate data; Computers & Geosciences, v.29, p.225-237.

Thompson, M. and Howarth, R.J. 1978. A new approach to the estimation of analytical precision; Journal of Geochemical Exploration, v.9, p.23-30.

Tomlinson, K.Y., Bowins, R. and Hechler, J. 1998. Refinement of hafnium (Hf) and zirconium (Zr) analysis by improvement to digestion procedure; *in* Summary of Field Work 1997, Ontario Geological Survey, Miscellaneous Paper 169, p.189-192.

Tomlinson, K.Y., Hughes, D.J., Thurston, P.C. and Hall, R.P. 1999. Plume magmatism and crustal growth at 2.9 to 3.0 Ga in the Steep Rock and Lumby Lake area, western Superior Province; Lithos, v.46, p.103-136.

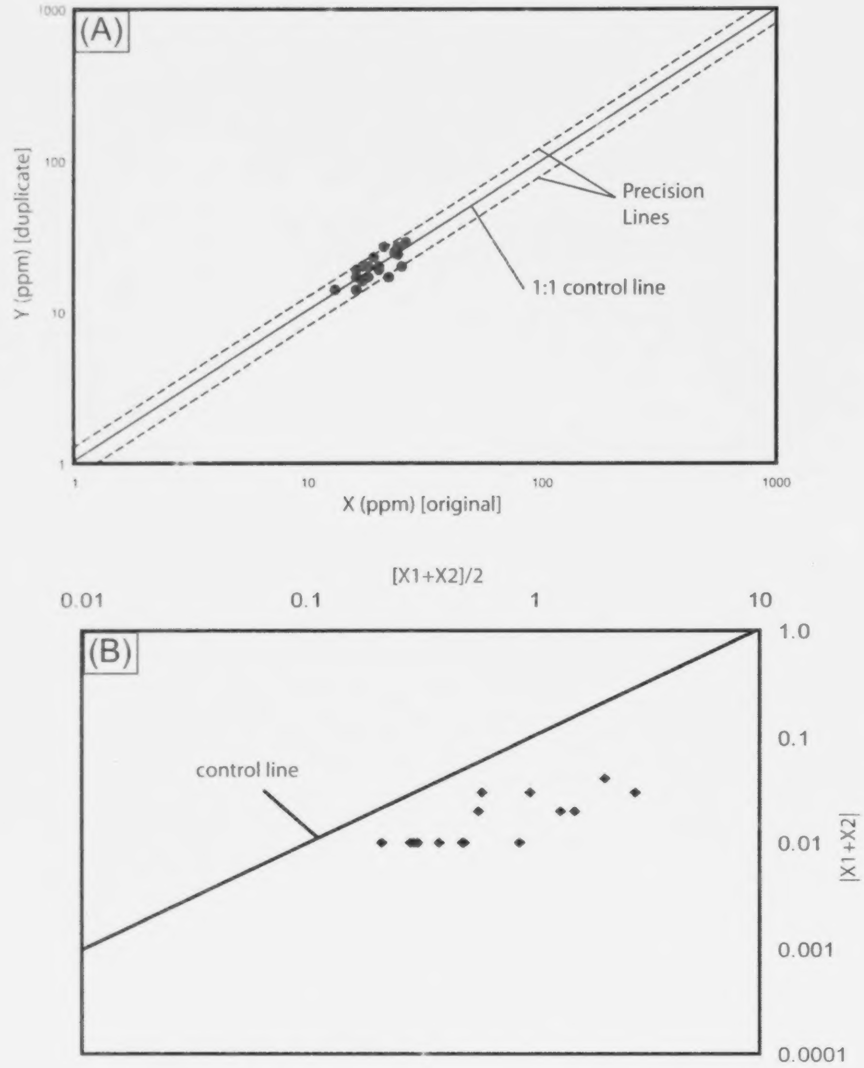

Figure A1. Schematic of the standard scatterplot (A) and Thompson–Howarth plot (B). In the scatterplot, if duplicate samples lie within the precision lines, the precision for the given element is at that prescribed level (A). On the Thompson–Howarth plot, if the samples lie below the control line at a given precision, they are precise to that precision (B).

Table A1. Precision and accuracy data for reference materials analyzed by fused disc XRF at the Ontario Geoscience Laboratories.

	LOD	**GSD-11** Mean (n=18)	STD	%RSD	Accepted	%RD	2σ
Al2O3	**0.01**	10.70	0.02	0.15	10.37	3.17	0.01
CaO	**0.01**	0.50	0.02	3.85	0.47	5.67	0.01
Fe2O3	**0.01**	4.34	0.00	0.10	-	-	0.00
K2O	**0.01**	3.43	0.01	0.21	3.28	4.64	0.00
MgO	**0.01**	0.61	0.01	2.15	0.62	-1.16	0.01
MnO	**0.01**	0.34	0.00	1.44	0.32	5.21	0.00
Na2O	**0.01**	0.41	0.05	12.34	0.46	-11.96	0.02
P2O5	**0.01**	0.06	0.00	7.34	0.06	6.40	0.00
SiO2	**0.01**	76.30	0.06	0.08	76.25	0.06	0.03
TiO2	**0.01**	0.36	0.00	1.06	0.35	3.33	0.00
TOTAL	-	100.40	0.10	0.10	-	-	0.05
LOI	**0.05**	3.36	0.00	0.00	-	-	0.00

	LOD	**GSR-2** Mean (n=8)	STD	%RSD	Accepted	%RD	2σ
Al2O3	**0.01**	16.58	0.05	0.28	16.17	2.50	0.03
CaO	**0.01**	5.56	0.06	1.08	5.20	6.83	0.04
Fe2O3	**0.01**	5.00	0.01	0.26	na	-	0.01
K2O	**0.01**	1.83	0.00	0.25	1.89	-3.31	0.00
MgO	**0.01**	1.67	0.01	0.75	1.72	-2.83	0.01
MnO	**0.01**	0.08	0.00	0.00	0.08	0.00	0.00
Na2O	**0.01**	3.99	0.04	0.92	3.86	3.27	0.03
P2O5	**0.01**	0.24	0.01	2.19	0.24	-1.56	0.00
SiO2	**0.01**	60.22	0.13	0.21	60.62	-0.66	0.09
TiO2	**0.01**	0.52	0.00	0.68	0.52	-0.24	0.00
TOTAL	-	100.42	0.15	0.15	na	-	0.11
LOI	**0.05**	4.75	0.00	0.00	n/a	-	0.00

	LOD	**BIR-1** Mean (n=2)	STD	%RSD	Accepted	%RD	2σ
Al2O3	**0.01**	15.87	0.03	0.18	15.35	3.39	0.04
CaO	**0.01**	13.52	0.03	0.21	13.24	2.11	0.04
Fe2O3	**0.01**	11.71	0.01	0.12	-	-	0.02
K2O	**0.01**	0.03	0.00	0.00	-	-	0
MgO	**0.01**	9.73	0.01	0.07	9.68	0.46	0.01
MnO	**0.01**	0.18	0.00	0.00	0.17	5.26	0
Na2O	**0.01**	1.97	0.03	1.44	1.75	12.57	0.04
P2O5	**0.01**	0.03	0.00	0.00	-	-	0
SiO2	**0.01**	47.74	0.11	0.24	47.77	-0.06	0.16
TiO2	**0.01**	0.98	0.01	0.73	-	-	0.01
TOTAL	-	101.29	0.23	0.22	-	-	0.32
LOI	**0.05**						

Table A1, continued.

	LOD	**MRB-31** Mean (n=7)	STD	%RSD	Accepted	%RD	2σ
Al2O3	**0.01**	15.20	0.06	0.40	-	-	0.05
CaO	**0.01**	3.72	0.01	0.38	-	-	0.01
Fe2O3	**0.01**	9.14	0.02	0.19	-	-	0.01
K2O	**0.01**	2.22	0.02	0.82	-	-	0.01
MgO	**0.01**	2.95	0.01	0.46	-	-	0.01
MnO	**0.01**	0.15	0.00	2.54	-	-	0.00
Na2O	**0.01**	3.85	0.04	0.94	-	-	0.03
P2O5	**0.01**	0.17	0.00	2.20	-	-	0.00
SiO2	**0.01**	60.54	0.25	0.40	-	-	0.19
TiO2	**0.01**	0.79	0.00	0.62	-	-	0.00
TOTAL	-	100.50	0.33	0.33	-	-	0.25
LOI	**0.05**	1.72	0.04	2.52	-	-	0.03

	LOD	**NPD-1** Mean (n=4)	STD	%RSD	Accepted	%RD	2σ
Al2O3	**0.01**	14.31	0.03	0.24	14.24	0.50	0.03
CaO	**0.01**	8.44	0.01	0.11	8.19	3.10	0.01
Fe2O3	**0.01**	12.95	0.02	0.15	12.81	1.09	0.02
K2O	**0.01**	1.38	0.01	0.91	1.40	-1.72	0.01
MgO	**0.01**	4.84	0.02	0.36	4.85	-0.30	0.02
MnO	**0.01**	0.19	0.01	2.60	0.19	0.38	0.01
Na2O	**0.01**	2.81	0.04	1.34	2.84	-1.29	0.04
P2O5	**0.01**	0.13	0.01	3.92	0.12	5.77	0.01
SiO2	**0.01**	53.59	0.06	0.12	53.77	-0.34	0.06
TiO2	**0.01**	1.18	0.01	0.42	1.17	1.05	0.01
TOTAL	-	101.08	0.06	0.06	100.84	0.23	0.06
LOI	**0.05**	1.27	0.03	2.32	1.27	0.00	0.03

	LOD	**MRB-15** Mean (n=5)	STD	%RSD	Accepted	%RD	2σ
Al2O3	**0.01**	11.64	0.05	0.44	11.58	0.52	0.05
CaO	**0.01**	1.26	0.03	2.51	1.21	3.76	0.03
Fe2O3	**0.01**	2.88	0.01	0.25	2.88	0.11	0.01
K2O	**0.01**	2.33	0.01	0.56	2.30	1.09	0.01
MgO	**0.01**	0.22	0.01	3.84	0.24	-7.74	0.01
MnO	**0.01**	0.06	0.00	0.00	0.06	2.70	0.00
Na2O	**0.01**	3.75	0.02	0.48	3.73	0.40	0.02
P2O5	**0.01**	0.05	0.01	11.91	0.04	23.47	0.00
SiO2	**0.01**	75.39	0.23	0.31	75.53	-0.18	0.21
TiO2	**0.01**	0.43	0.00	0.00	0.43	-0.60	0.00
TOTAL	-	99.69	0.25	0.25	99.69	0.00	0.22
LOI	**0.05**	1.70	0.06	3.73	1.69	0.47	0.06

Table A1, continued.

	LOD	**PER-1**	Accepted	%RD
		n=1		
Al2O3	**0.01**	12.71	12.53	1.44
CaO	**0.01**	1.24	1.18	5.08
Fe2O3	**0.01**	1.6	1.60	0.00
K2O	**0.01**	4.4	4.37	0.69
MgO	**0.01**	0.34	0.35	-2.86
MnO	**0.01**	0.04	0.04	0.00
Na2O	**0.01**	3.34	3.29	1.52
P2O5	**0.01**	0.04	0.03	33.33
SiO2	**0.01**	75.49	75.09	0.53
TiO2	**0.01**	0.16	0.15	6.67
TOTAL	-	100.33	99.81	0.52
LOI	**0.05**	0.96	1.17	-17.95

	LOD	**BAMAP-1**	Accepted	%RD
		n=1		
Al2O3	**0.01**	15.56	15.24	2.10
CaO	**0.01**	8.78	8.33	5.40
Fe2O3	**0.01**	12.56	12.34	1.78
K2O	**0.01**	1.54	1.57	-1.91
MgO	**0.01**	8.31	8.18	1.59
MnO	**0.01**	0.16	0.16	0.00
Na2O	**0.01**	4.01	4	0.25
P2O5	**0.01**	0.46	0.45	2.22
SiO2	**0.01**	48.08	47.91	0.35
TiO2	**0.01**	2.35	2.31	1.73
TOTAL	-	101.42	100.13	1.29
LOI	**0.05**	N.D.	<0.05	-

	LOD	**CHA-2**	Accepted	%RD
		n=1		
Al2O3	**0.01**	17.81	17.75	0.34
CaO	**0.01**	6.08	5.88	3.40
Fe2O3	**0.01**	5.7	5.67	0.53
K2O	**0.01**	2.06	2.02	1.98
MgO	**0.01**	2.44	2.46	-0.81
MnO	**0.01**	0.1	0.10	0.00
Na2O	**0.01**	3.99	4.02	-0.75
P2O5	**0.01**	0.23	0.22	4.55
SiO2	**0.01**	59.66	60.42	-1.26
TiO2	**0.01**	0.72	0.72	0.00
TOTAL	-	99.55	100.02	-0.47
LOI	**0.05**	0.75	0.76	-1.32

Table A2. Precision and accuracy data for reference materials analyzed by fused disc XRF at Activation Laboratories.

		W-2	STD	%RSD	Accepted	%RD	2σ
	LOD	Mean (n=3)					
Al2O3	**0.01**	15.38	0.09	0.55	15.35	0.22	0.10
CaO	**0.01**	10.88	0.02	0.18	10.87	0.09	0.02
Cr2O3	**0.01**	0.02	0.01	34.64	0.01	66.67	0.01
Fe2O3	**0.01**	10.88	0.03	0.28	10.74	1.30	0.03
K2O	**0.01**	0.67	0.03	4.82	0.63	5.82	0.04
MgO	**0.01**	6.46	0.02	0.32	6.37	1.36	0.02
MnO	**0.01**	0.17	0.00	0.35	0.160	3.96	0.00
Na2O	**0.01**	2.23	0.05	2.03	2.14	4.05	0.05
P2O5	**0.01**	0.13	0.00	0.00	0.13	0.00	0.00
SiO2	**0.01**	52.14	0.25	0.49	52.44	-0.57	0.29
TiO2	**0.01**	1.08	0.01	1.07	1.06	2.20	0.01
LOI	**0.01**	-	-	-	-	-	-

		SY-3	STD	%RSD	Accepted	%RD	2σ
	LOD	Mean (n=3)					
Al2O3	**0.01**	11.72	0.07	0.62	11.76	-0.31	0.08
CaO	**0.01**	8.31	0.04	0.43	8.25	0.73	0.04
Cr2O3	**0.01**	<0.01	-	-	-	-	-
Fe2O3	**0.01**	6.47	0.02	0.24	6.49	-0.26	0.02
K2O	**0.01**	4.20	0.01	0.28	4.23	-0.79	0.01
MgO	**0.01**	2.67	0.03	1.21	2.67	-0.12	0.04
MnO	**0.01**	0.32	0.00	0.36	0.32	-0.42	0.00
Na2O	**0.01**	4.10	0.04	0.92	4.12	-0.40	0.04
P2O5	**0.01**	0.54	0.01	1.06	0.54	0.62	0.01
SiO2	**0.01**	59.47	0.37	0.62	59.68	-0.35	0.43
TiO2	**0.01**	0.15	0.00	0.00	0.15	0.00	0.00
LOI	**0.01**	-	-	-	-	-	-

		SGR-1	STD	%RSD	Accepted	%RD	2σ
	LOD	Mean (n=3)					
Al2O3	**0.01**	6.60	0.02	0.32	6.52	1.28	0.02
CaO	**0.01**	8.39	0.03	0.32	8.38	0.12	0.03
Cr2O3	**0.01**	<0.01	-	-	-	-	-
Fe2O3	**0.01**	3.00	0.01	0.19	3.03	-1.10	0.01
K2O	**0.01**	1.58	0.01	0.37	1.66	-5.02	0.01
MgO	**0.01**	4.43	0.01	0.26	4.44	-0.15	0.01
MnO	**0.01**	0.03	0.00	1.77	0.03	-3.92	0.00
Na2O	**0.01**	3.04	0.04	1.16	2.99	1.56	0.04
P2O5	**0.01**	0.28	0.00	0.00	0.33	-14.63	0.00
SiO2	**0.01**	28.36	0.10	0.37	28.24	0.42	0.12
TiO2	**0.01**	0.25	0.00	0.00	0.26	-5.30	0.00
LOI	**0.01**	-	-	-	-	-	-

Table A2, continued.

		BE-N	STD	%RSD	Accepted	%RD	2σ
	LOD	Mean (n=3)					
Al2O3	**0.01**	10.13	0.09	0.92	10.07	0.56	0.11
CaO	**0.01**	14.08	0.05	0.34	13.87	1.49	0.05
Cr2O3	**0.01**	0.05	0.01	10.83	0.05	0.63	0.01
Fe2O3	**0.01**	13.09	0.02	0.18	12.84	1.92	0.03
K2O	**0.01**	1.42	0.01	0.41	1.39	2.40	0.01
MgO	**0.01**	13.28	0.02	0.13	13.15	0.99	0.02
MnO	**0.01**	0.20	0.00	0.76	0.20	0.67	0.00
Na2O	**0.01**	3.18	0.02	0.65	3.18	0.10	0.02
P2O5	**0.01**	1.08	0.01	0.54	1.05	2.54	0.01
SiO2	**0.01**	38.76	0.25	0.65	38.20	1.47	0.29
TiO2	**0.01**	2.72	0.01	0.21	2.61	4.09	0.01
LOI	**0.01**	-	-	-	-	-	-

		DNC-1	STD	%RSD	Accepted	%RD	2σ
	LOD	Mean (n=3)					
Al2O3	**0.01**	18.76	0.18	0.97	18.30	2.50	0.21
CaO	**0.01**	11.32	0.03	0.27	11.27	0.44	0.03
Cr2O3	**0.01**	0.04	0.00	0.00	0.04	-4.76	0.00
Fe2O3	**0.01**	10.05	0.01	0.11	9.93	1.24	0.01
K2O	**0.01**	0.25	0.01	2.34	0.23	7.71	0.01
MgO	**0.01**	10.29	0.03	0.26	10.05	2.39	0.03
MnO	**0.01**	0.15	0.00	0.78	0.15	-0.45	0.00
Na2O	**0.01**	1.99	0.07	3.34	1.87	6.60	0.08
P2O5	**0.01**	0.08	0.01	7.53	0.09	-9.80	0.01
SiO2	**0.01**	47.12	0.38	0.81	47.04	0.18	0.44
TiO2	**0.01**	0.50	0.01	1.16	0.48	3.47	0.01
LOI	**0.01**	-	-	-	-	-	-

		OKUM-1	STD	%RSD	Accepted	%RD	2σ
	LOD	Mean (n=7)					
Al2O3	**0.01**	8.01	0.04	0.49	8.05	-0.48	0.03
CaO	**0.01**	7.81	0.04	0.48	8.06	-3.08	0.03
Cr2O3	**0.01**	0.36	0.00	0.00	-	-	0.00
Fe2O3	**0.01**	11.86	0.06	0.48	12.14	-2.32	0.04
K2O	**0.01**	0.08	0.02	22.81	0.04	107.14	0.01
MgO	**0.01**	21.48	0.13	0.61	22.37	-3.97	0.10
MnO	**0.01**	0.18	0.00	0.71	0.18	-0.79	0.00
Na2O	**0.01**	1.12	0.02	1.89	1.15	-2.73	0.02
P2O5	**0.01**	0.03	0.00	0.00	0.02	50.00	0.00
SiO2	**0.01**	43.83	0.19	0.43	43.57	0.59	0.14
TiO2	**0.01**	0.38	0.00	1.27	0.40	-4.29	0.00
LOI	**0.01**	4.89	0.03	0.55	4.66	4.83	0.02

Table A2, continued.

		MRB-15	STD	%RSD	Accepted	%RD	2σ
	LOD	Mean (n=7)					
Al2O3	**0.01**	11.61	0.07	0.58	11.58	0.26	0.05
CaO	**0.01**	1.18	0.02	1.47	1.21	-2.82	0.01
Cr2O3	**0.01**	0.02	0.00	28.46	-	-	0.00
Fe2O3	**0.01**	2.87	0.02	0.70	2.88	-0.23	0.02
K2O	**0.01**	2.24	0.01	0.60	2.30	-2.67	0.01
MgO	**0.01**	0.24	0.01	4.01	0.24	0.36	0.01
MnO	**0.01**	0.06	0.00	2.73	0.06	-4.15	0.00
Na2O	**0.01**	3.57	0.03	0.74	3.73	-4.43	0.02
P2O5	**0.01**	0.05	0.00	7.78	0.04	30.37	0.00
SiO2	**0.01**	75.73	0.23	0.30	75.53	0.27	0.17
TiO2	**0.01**	0.43	0.00	0.00	0.43	-0.60	0.00
LOI	**0.01**	1.77	0.11	6.32	1.69	4.97	0.08

		NPD-21	STD	%RSD	Accepted	%RD	2σ
	LOD	Mean (n=7)					
Al2O3	**0.01**	13.86	0.11	0.80	14.24	-2.69	0.08
CaO	**0.01**	8.04	0.05	0.66	8.19	-1.80	0.04
Cr2O3	**0.01**	0.02	0.00	28.46	-	-	0.00
Fe2O3	**0.01**	12.75	0.07	0.53	12.81	-0.42	0.05
K2O	**0.01**	1.39	0.01	0.90	1.40	-0.62	0.01
MgO	**0.01**	4.85	0.05	0.97	4.85	-0.05	0.04
MnO	**0.01**	0.19	0.00	0.51	0.19	-3.38	0.00
Na2O	**0.01**	2.71	0.02	0.67	2.84	-4.56	0.01
P2O5	**0.01**	0.13	0.00	3.67	0.12	10.21	0.00
SiO2	**0.01**	53.58	0.41	0.76	53.77	-0.36	0.31
TiO2	**0.01**	1.17	0.01	0.91	1.17	0.29	0.01
LOI	**0.01**	1.38	0.03	2.33	1.27	8.49	0.02

Table A3. Precision and accuracy data for reference materials analyzed by pressed pellet XRF at the Ontario Geoscience Laboratories.

	LOD	**BIR-1** Mean (n= 10)	STD	%RSD	Accepted	%RD	2σ
Nb	2	ND	-	-	ND	-	-
Y	1	14.4	0.52	3.6	16	-10.0	0.3
Zr	3	15.7	0.95	6.0	18	-12.8	0.6

	LOD	**RGM-1** Mean (n=9)	STD	%RSD	Accepted	%RD	2σ
Nb	2	7.3	0.68	9.3	8.9	-17.7	0.5
Y	1	22.5	0.93	4.1	-	-	0.6
Zr	3	218.2	3.87	1.8	219	-0.4	2.6

	LOD	**NPD-1** Mean (n=5)	STD	%RSD	Accepted	%RD	2σ
Nb	2	4.8	0.45	9.3	6.3	-23.8	0.4
Y	1	24.0	0.00	0.0	25.3	-5.1	0.0
Zr	3	107.6	1.52	1.4	116	-7.2	1.4

	LOD	**OKUM-1** Mean (n=6)	STD	%RSD	Accepted	%RD	2σ
Nb	2	ND	-	-	0.4	-	-
Y	1	8.8	0.50	5.7	10.33	-15.3	0.4
Zr	3	17.8	0.50	2.8	19	-6.6	0.4

Table A4. Precision and accuracy data for reference materials analyzed by pressed pellet XRF at Activation Laboratories.

	LOD	**OKUM-1** Mean (n=7)	STD	%RSD	Accepted	%RD	2σ
Y	**2**	11.1	0.7	6.2	10.33	7.9	0.5
Zr	**5**	16.6	5.4	32.7	19	-12.8	4.1
Nb	**2**	<1	-	-	0.4	-	-
V	**5**	167.9	4.3	2.6	166	1.1	3.3
Cr	**5**	2413.3	12.2	0.5	2120	13.8	9.3
Ni	**5**	933.7	5.0	0.5	780	19.7	3.7

	LOD	**MRB-15** Mean (n=7)	STD	%RSD	Accepted	%RD	2σ
Y	**2**	115.4	0.5	0.5	-	-	0.4
Zr	**5**	635.9	9.1	1.4	-	-	6.9
Nb	**2**	24.3	3.5	14.6	-	-	2.7
V	**5**	-	-	-	-	-	-
Cr	**5**	115.3	5.7	5.0	-	-	4.3
Ni	**5**	-	-	-	-	-	-

	LOD	**NPD-1** Mean (n=7)	STD	%RSD	Accepted	%RD	2σ
Y	**2**	22.7	0.5	2.1	25.3	-10.2	0.4
Zr	**5**	106.7	1.9	1.8	116	-8.0	1.4
Nb	**2**	5.3	0.5	9.2	6.3	-16.1	0.4
V	**5**	250.4	6.5	2.6	283	-11.5	4.9
Cr	**5**	108.3	7.3	6.7	135.4	-20.0	5.5
Ni	**5**	53.1	2.2	4.1	69.9	-24.0	1.7

	LOD	**MRG-1** Mean (n=2)	STD	%RSD	Accepted	%RD	2σ
Y	**2**	14.5	0.7	4.9	14	3.6	0.5
Zr	**5**	100.0	2.8	2.8	108	-7.4	2.0
Nb	**2**	21.5	0.7	3.3	20	7.5	0.5
V	**5**	530.0	33.9	6.4	526	0.8	24.0
Cr	**5**	478.0	26.9	5.6	430	11.2	19.0
Ni	**5**	175.0	4.2	2.4	193	-9.3	3.0

	LOD	**MAG-1** Mean (n=2)	STD	%RSD	Accepted	%RD	2σ
Y	**2**	28.0	2.8	10.1	28	0.0	2.0
Zr	**5**	123.0	4.2	3.4	126	-2.4	3.0
Nb	**2**	12.5	0.7	5.7	12	4.2	0.5
V	**5**	140.0	11.3	8.1	140	0.0	8.0
Cr	**5**	94.0	5.7	6.0	97	-3.1	4.0
Ni	**5**	47.5	0.7	1.5	53	-10.4	0.5

	LOD	**DNC-1** Mean (n=3)	STD	%RSD	Accepted	%RD	2σ
Y	**2**	17.7	0.6	3.3	18	-1.9	0.3
Zr	**5**	40.3	2.3	5.7	41	-1.6	1.3
Nb	**2**	<1	-	-	3	-	-
V	**5**	133.0	3.6	2.7	148	-10.1	2.1
Cr	**5**	251.7	8.5	3.4	285	-11.7	4.9
Ni	**5**	236.3	1.5	0.6	247	-4.3	0.9

Table A5. Precision and accuracy data for reference materials analyzed by solution ICP–ES at the Ontario Geoscience Laboratories.

		AGV-2					
	LOD	Mean (n=5)	STD	%RSD	Accepted	%RD	2σ
Ba	3	1097.3	68.1	6.2	1140.0	-3.7	60.9
Be	3	<3	-	-	2.3	-	-
Cd	2	8.7	4.2	48.0	-	-	3.7
Co	3	21.6	5.4	25.0	16.0	-	4.8
Cr	4	22.2	2.5	11.3	17.0	30.4	2.2
Cu	5	45.4	3.2	7.1	53.0	-14.3	2.9
Li	3	12.0	1.0	8.3	-	-	0.9
Mo	8	<8	-	-	-	-	-
Ni	5	25.2	1.6	6.5	19.0	32.6	1.5
S	30	184.0	108.0	58.7	-	-	96.6
Sc	1	10.2	0.9	8.5	13.0	-21.8	0.8
Sr	1	588.7	29.4	5.0	658.0	-10.5	26.3
V	5	108.7	4.5	4.1	120.0	-9.4	4.0
W	35	<35	-	-	-	-	-
Zn	2	93.6	4.2	4.5	86.0	8.8	3.8

		BIR-1					
	LOD	Mean (n=5)	STD	%RSD	Accepted	%RD	2σ
Ba	3	8.7	1.6	18.2	-	-	1.4
Be	3	<3	-	-	-	-	-
Cd	2	10.0	4.0	40.0	-	-	3.6
Co	3	55.6	8.7	15.7	52.0	6.9	7.8
Cr	4	338.8	31.3	9.2	370.0	-8.4	28.0
Cu	5	115.6	7.8	6.8	125.0	-7.5	7.0
Li	3	<3	-	-	3.6	-	-
Mo	8	<8	-	-	-	-	-
Ni	5	171.6	14.9	8.7	170.0	0.9	13.3
S	30	381.8	311.4	81.6	-	-	278.5
Sc	1	34.5	6.4	18.5	44.0	-21.5	5.7
Sr	1	91.7	16.9	18.4	110.0	-16.7	15.1
V	5	281.0	33.2	11.8	310.0	-9.4	29.7
W	35	<35	-	-	-	-	-
Zn	2	78.0	6.2	7.9	70.0	11.4	5.5

		MRB-29					
	LOD	Mean (n=32)	STD	%RSD	Accepted	%RD	2σ
Ba	3	261.2	14.9	5.7	291.0	-10.2	5.3
Be	3	<3	-	-	-	-	-
Cd	2	11.9	3.7	31.0	-	-	1.3
Co	3	52.8	11.1	21.0	51.5	2.6	3.9
Cr	4	236.0	12.1	5.1	291.0	-18.9	4.3
Cu	5	134.9	19.4	14.4	149.0	-9.5	6.9
Li	3	12.5	1.4	11.3	12.2	2.7	0.5
Mo	8	<8	-	-	-	-	-
Ni	5	111.5	5.5	5.0	115.1	-3.1	2.0
S	30	295.4	174.8	59.2	-	-	61.8
Sc	1	25.9	1.8	6.8	33.2	-22.1	0.6
Sr	1	271.7	13.4	4.9	316.0	-14.0	4.8
V	5	272.6	10.4	3.8	317.0	-14.0	3.7
W	35	<35	-	-	0.2	-	-
Zn	2	113.1	4.6	4.1	106.0	6.7	1.6

Table A5, continued.

		NBS-688					
	LOD	Mean (n=2)	STD	%RSD	Accepted	%RD	2σ
Ba	3	163.7	12.2	7.5	200.0	-18.2	17.3
Be	3	<3	-	-	-	-	-
Cd	2	14.5	3.5	24.4	-	-	5.0
Co	3	56.3	3.2	5.7	49.7	13.2	4.5
Cr	4	277.8	7.3	2.6	332.0	-16.3	10.4
Cu	5	86.0	9.9	11.5	96.0	-10.4	14.0
Li	3	6.0	0.0	0.0	0.3	1664.7	0.0
Mo	8	<8	-	-	-	-	-
Ni	5	151.5	0.7	0.5	150.0	1.0	1.0
S	30	633.5	46.0	7.3	-	-	65.0
Sc	1	31.7	0.4	1.2	38.1	-16.7	0.5
Sr	1	153.5	3.5	2.3	169.2	-9.3	5.0
V	5	220.8	0.3	0.2	250.0	-11.7	0.5
W	35	<35	-	-	-	-	-
Zn	2	81.0	2.8	3.5	58.0	39.7	4.0

		SY-4					
	LOD	Mean (n=2)	STD	%RSD	Accepted	%RD	2σ
Ba	3	339.8	25.8	7.6	340.0	-0.1	36.5
Be	3	<3	-	-	2.6	-	-
Cd	2	8.5	0.7	8.3	-	-	1.0
Co	3	5.8	0.3	5.1	2.8	106.8	0.4
Cr	4	24.0	9.8	41.0	12.0	100.3	13.9
Cu	5	<5	-	-	7.0	-	-
Li	3	48.5	0.7	1.5	37.0	31.1	1.0
Mo	8	<8	-	-	-	-	-
Ni	5	15.5	6.4	41.1	9.0	72.2	9.0
S	30	494.5	20.5	4.1	-	-	29.0
Sc	1	<1	-	-	1.1	-	-
Sr	1	1069.5	57.3	5.4	1191.0	-10.2	81.0
V	5	<5	-	-	8.0	-	-
W	35	<35	-	-	-	-	-
Zn	2	99.5	4.9	5.0	93.0	7.0	7.0

		BHVO-2					
	LOD	Mean (n=4)	STD	%RSD	Accepted	%RD	2σ
Ba	3	120.8	7.3	6.0	130.0	-7.1	7.3
Be	3	<3	-	-	-	-	-
Cd	2	9.5	2.1	22.3	-	-	2.1
Co	3	48.5	16.1	33.3	45.0	7.8	16.1
Cr	4	259.2	12.1	4.7	280.0	-7.4	12.1
Cu	5	124.8	9.7	7.8	127.0	-1.8	9.7
Li	3	5.0	1.4	28.3	-	-	1.4
Mo	8	<8	-	-	-	-	-
Ni	5	122.8	7.8	6.4	119.0	3.2	7.8
S	30	344.7	296.9	86.1	-	-	296.9
Sc	1	26.6	2.6	9.9	32.0	-17.0	2.6
Sr	1	357.6	25.2	7.0	389.0	-8.1	25.2
V	5	287.4	12.0	4.2	317.0	-9.4	12.0
W	35	<35	-	-	-	-	-
Zn	2	114.0	5.8	5.1	103.0	10.7	5.8

Table A5, continued.

		RGM-1					
	LOD	Mean (n=2)	STD	%RSD	Accepted	%RD	2σ
Ba	**3**	788.4	10.8	1.4	807.0	-2.3	15.3
Be	**3**	<3	-	-	2.4	-	-
Cd	**2**	<2	-	-	-	-	-
Co	**3**	<5	-	-	2.0	-	-
Cr	**4**	11.5	1.3	11.5	-	-	1.9
Cu	**5**	8.5	0.7	8.3	11.6	-26.7	1.0
Li	**3**	67.0	4.2	6.3	57.0	17.5	6.0
Mo	**8**	<8	-	-	2.3	-	-
Ni	**5**	<5	-	-		-	-
S	**30**	83.5	9.2	11.0	-	-	13.0
Sc	**1**	3.5	0.2	6.4	4.4	-19.8	0.3
Sr	**1**	94.0	2.8	3.0	108.0	-13.0	4.0
V	**5**	9.5	0.1	0.9	13.0	-26.9	0.1
W	**35**	>35	-	-	1.5	-	-
Zn	**2**	32.0	0.0	0.0	-	-	0.0

		GSP-2					
	LOD	Mean (n=4)	STD	%RSD	Accepted	%RD	2σ
Ba	**3**	1333.2	53.3	4.0	1340.0	-0.5	53.3
Be	**3**	<3	-	-	-	-	-
Cd	**2**	<2	-	-	-	-	-
Co	**3**	10.0	3.3	33.1	7.3	36.5	3.3
Cr	**4**	24.2	3.2	13.3	20.0	21.0	3.2
Cu	**5**	39.5	1.7	4.4	43.0	-8.1	1.7
Li	**3**	37.3	2.2	6.0	-	-	2.2
Mo	**8**	<8	-	-	-	-	-
Ni	**5**	21.0	0.8	3.9	17.0	23.5	0.8
S	**30**	466.0	11.7	2.5	-	-	11.7
Sc	**1**	5.7	0.4	6.2	6.3	-8.9	0.4
Sr	**1**	217.2	2.3	1.1	240.0	-9.5	2.3
V	**5**	48.7	1.6	3.3	52.0	-6.4	1.6
W	**35**	<35	-	-	-	-	-
Zn	**2**	117.5	3.9	3.3	120.0	-2.1	3.9

		GSR-1					
	LOD	Mean (n=5)	STD	%RSD	Accepted	%RD	2σ
Ba	**3**	308.2	7.6	2.5	343.0	-10.1	6.8
Be	**3**	8.0	0.6	7.2	12.4	-35.3	0.5
Cd	**2**	<2	-	-	-	-	-
Co	**3**	<5	-	-	3.4	-	-
Cr	**4**	7.6	2.4	32.1	-	-	2.2
Cu	**5**	<5	-	-	3.2	-	-
Li	**3**	137.8	13.4	9.7	131.0	5.2	12.0
Mo	**8**	<8	-	-	3.5	-	-
Ni	**5**	<5	-	-	2.3	-	-
S	**30**	300.0	154.4	51.5	-	-	138.1
Sc	**1**	4.8	0.1	2.9	6.1	-21.3	0.1
Sr	**1**	96.8	1.7	1.7	106.0	-8.7	1.5
V	**5**	19.8	0.5	2.6	24.0	-17.5	0.5
W	**35**	<35	-	-	8.4	-	-
Zn	**2**	26.6	1.3	5.0	28.0	-5.0	1.2

Table A5, continued.

		GSR-2					
	LOD	Mean (n=2)	STD	%RSD	Accepted	%RD	2σ
Ba	**3**	846.0	128.7	15.2	1020.0	-17.1	182.0
Be	**3**	<3	-	-	1.1	-	-
Cd	**2**	<2	-	-	0.6	-	-
Co	**3**	14.0	1.4	10.1	13.2	6.1	2.0
Cr	**4**	30.7	0.4	1.5	32.4	-5.3	0.6
Cu	**5**	45.0	1.4	3.1	55.4	-18.8	2.0
Li	**3**	19.0	19.0	-	18.3	3.8	26.9
Mo	**8**	<8	-	-	0.5	-	-
Ni	**5**	19.0	4.2	22.3	17.0	11.8	6.0
S	**30**	168.0	-	-	-	-	-
Sc	**1**	6.3	0.4	6.7	9.5	-33.7	0.6
Sr	**1**	667.1	53.8	8.1	790.0	-15.6	76.1
V	**5**	80.9	5.4	6.7	24.0	236.9	7.7
W	**35**	<35	-	-	-	-	-
Zn	**2**	66.5	4.9	7.4	71.0	-6.3	7.0

		BAMAP-01					
	LOD	Mean (n=3)	STD	%RSD	Accepted	%RD	2σ
Ba	**3**	257.0	4.2	1.7	339.0	-24.2	6.0
Be	**3**	0.9	0.1	5.8	-	-	0.1
Cd	**2**	<2	-	-	-	-	-
Co	**3**	42.7	2.9	6.8	49.0	-12.9	4.1
Cr	**4**	229.1	3.8	1.7	-	-	5.4
Cu	**5**	35.0	1.0	2.9	57.0	-38.6	1.4
Li	**3**	7.5	0.7	9.4	8.0	-6.3	1.0
Mo	**8**	<8	-	-	3.0	-	-
Ni	**5**	178.3	3.1	1.7	187.0	-4.6	4.3
S	**30**	188.5	27.6	14.6	-	-	39.0
Sc	**1**	14.2	0.5	3.3	20.1	-29.2	0.7
Sr	**1**	510.4	23.5	4.6	<450	-	33.2
V	**5**	180.0	6.9	3.8	216.0	-16.7	9.7
W	**35**	<35	-	-	0.4	-	-
Zn	**2**	118.3	2.9	2.4	116.0	2.0	4.1

		PER-1					
	LOD	Mean (n=3)	STD	%RSD	Accepted	%RD	2σ
Ba	**3**	762.0	17.0	2.2	823.0	-7.4	24.0
Be	**3**	0.9	0.0	3.8	-	-	0.0
Cd	**2**	<2	-	-	-	-	-
Co	**3**	2.7	0.6	21.7	2.0	33.3	0.8
Cr	**4**	205.3	1.4	0.7	-	-	1.9
Cu	**5**	<5	-	-	4.0	-	-
Li	**3**	31.5	0.7	2.2	36.0	-12.5	1.0
Mo	**8**	<8	-	-	3.0	-	-
Ni	**5**	5.3	0.6	10.8	<5	-	0.8
S	**30**	83.0	32.5	39.2	-	-	46.0
Sc	**1**	2.1	0.1	4.8	2.7	-22.2	0.1
Sr	**1**	103.1	2.5	2.4	126.0	-18.2	3.6
V	**5**	10.5	0.2	1.5	19.0	-44.9	0.2
W	**35**	<35	-	-	1.7	-	-
Zn	**2**	26.7	0.6	2.2	22.0	21.2	0.8

Table A5, continued.

	LOD	CHA-2 Mean (n=3)	STD	%RSD	Accepted	%RD	2σ
Ba	**3**	392.0	11.3	2.9	472.9	-17.1	16.0
Be	**3**	1.1	0.0	3.8	-	-	0.1
Cd	**2**	<2	-	-	-	-	-
Co	**3**	14.3	0.6	4.0	13.8	3.8	0.8
Cr	**4**	57.4	0.8	1.3	-	-	1.1
Cu	**5**	14.3	0.6	4.0	21.9	-34.7	0.8
Li	**3**	19.5	0.7	3.6	24.1	-19.2	1.0
Mo	**8**	<8	-	-	-	-	-
Ni	**5**	18.0	0.0	0.0	14.1	27.6	0.0
S	**30**	111.0	21.2	19.1	-	-	30.0
Sc	**1**	8.9	0.7	7.4	13.2	-32.7	0.9
Sr	**1**	428.0	9.2	2.1	524.5	-18.4	13.0
V	**5**	99.2	1.8	1.8	124.9	-20.6	2.5
W	**35**	<35	-	-	1.3	-	-
Zn	**2**	78.7	2.1	2.6	74.9	5.0	2.9

Table A6. Precision and accuracy data for reference materials analyzed by solution ICP–MS at the Ontario Geoscience Laboratories.

		BHVO-2					
	LOD	Mean (n=4)	STD	%RSD	Accepted	%RD	2σ
Ce	**0.30**	38.49	0.92	2.38	37.50	2.65	0.92
Cs	**0.01**	0.17	0.01	6.45	-	-	0.01
Dy	**0.01**	5.39	0.20	3.69	5.31	1.47	0.20
Er	**0.006**	2.536	0.134	5.276	2.540	-0.177	0.134
Eu	**0.004**	2.251	0.088	3.925	2.070	8.720	0.088
Gd	**0.03**	6.49	0.14	2.08	6.24	4.07	0.14
Hf	**0.10**	4.66	0.30	6.42	4.60	1.25	0.30
Ho	**0.002**	1.029	0.048	4.675	0.972	5.890	0.048
La	**0.20**	15.87	0.45	2.84	15.20	4.38	0.45
Lu	**0.001**	0.279	0.030	10.830	0.274	1.642	0.030
Nb	**0.08**	19.26	0.58	3.01	18.00	6.97	0.58
Nd	**0.20**	25.40	0.98	3.88	24.50	3.67	0.98
Pr	**0.03**	5.54	0.11	2.06	5.29	4.79	0.11
Rb	**0.20**	10.28	0.46	4.44	9.10	12.91	0.46
Sm	**0.03**	6.26	0.18	2.87	6.07	3.05	0.18
Ta	**0.30**	1.14	0.08	7.05	1.40	-18.75	0.08
Tb	**0.001**	0.952	0.043	4.480	0.936	1.736	0.043
Th	**0.05**	1.25	0.06	4.46	1.20	3.96	0.06
Tm	**0.005**	0.341	0.017	4.841	0.341	0.073	0.017
U	**0.01**	0.43	0.02	5.64	-	-	0.02
Y	**0.20**	26.58	1.09	4.12	26.00	2.22	1.09
Yb	**0.01**	2.00	0.12	5.90	2.00	0.00	0.12
Zr	**6.00**	181.69	7.41	4.08	172.00	5.63	7.41

		GSR-1					
	LOD	Mean (n=7)	STD	%RSD	Accepted	%RD	2σ
Ce	**0.30**	111.46	7.36	6.60	108.00	3.20	5.56
Cs	**0.01**	38.63	1.32	3.43	38.40	0.59	1.00
Dy	**0.01**	10.42	0.24	2.28	10.20	2.15	0.18
Er	**0.006**	6.841	0.220	3.210	6.500	5.244	0.166
Eu	**0.004**	0.876	0.037	4.241	0.850	3.059	0.028
Gd	**0.03**	9.28	0.19	2.08	9.30	-0.17	0.15
Hf	**0.10**	5.86	0.27	4.53	6.30	-6.92	0.20
Ho	**0.002**	2.189	0.091	4.179	2.050	6.794	0.069
La	**0.20**	54.85	2.16	3.94	54.00	1.57	1.63
Lu	**0.001**	1.223	0.055	4.522	1.150	6.373	0.042
Nb	**0.08**	43.03	1.70	3.95	40.00	7.57	1.28
Nd	**0.20**	46.36	1.28	2.77	47.00	-1.35	0.97
Pr	**0.03**	13.05	0.36	2.75	12.70	2.75	0.27
Rb	**0.20**	-	-	-	-	-	-
Sm	**0.03**	9.94	0.32	3.19	9.70	2.44	0.24
Ta	**0.30**	35.45	48.88	137.90	7.20	392.34	36.95
Tb	**0.001**	1.646	0.032	1.935	1.650	-0.234	0.024
Th	**0.05**	55.64	2.60	4.67	54.00	3.04	1.97
Tm	**0.005**	1.137	0.042	3.695	1.060	7.305	0.032
U	**0.01**	19.27	0.41	2.11	18.80	2.48	0.31
Y	**0.20**	66.91	2.90	4.33	62.00	7.92	2.19
Yb	**0.01**	7.86	0.25	3.21	7.40	6.18	0.19
Zr	**6.00**	166.06	4.63	2.79	167.00	-0.56	3.50

Table A6, continued.

		GSR-2					
	LOD	Mean (n=4)	STD	%RSD	Accepted	%RD	2σ
Ce	**0.30**	39.40	1.18	3.00	40.00	-1.51	1.18
Cs	**0.01**	1.79	0.38	21.43	2.30	-22.10	0.38
Dy	**0.01**	1.73	0.09	5.31	1.80	-3.83	0.09
Er	**0.006**	0.826	0.045	5.400	0.850	-2.853	0.045
Eu	**0.004**	1.022	0.078	7.676	1.020	0.172	0.078
Gd	**0.03**	2.58	0.18	7.02	2.70	-4.39	0.18
Hf	**0.10**	2.62	0.22	8.41	2.90	-9.57	0.22
Ho	**0.002**	0.318	0.019	5.929	0.340	-6.544	0.019
La	**0.20**	20.78	0.96	4.62	21.80	-4.70	0.96
Lu	**0.001**	0.111	0.009	8.152	0.120	-7.292	0.009
Nb	**0.08**	5.96	0.61	10.32	6.80	-12.43	0.61
Nd	**0.20**	18.15	0.69	3.78	19.00	-4.47	0.69
Pr	**0.03**	4.70	0.23	4.85	4.90	-4.07	0.23
Rb	**0.20**	37.00	0.91	2.45	37.60	-1.60	0.91
Sm	**0.03**	3.26	0.15	4.66	3.40	-4.26	0.15
Ta	**0.30**	-	-	-	-	-	-
Tb	**0.001**	0.347	0.044	12.564	0.410	-15.305	0.044
Th	**0.05**	2.46	0.18	7.41	2.60	-5.58	0.18
Tm	**0.005**	0.114	0.007	6.242	-	-	0.007
U	**0.01**	0.91	0.03	3.31	-	-	0.03
Y	**0.20**	8.63	0.55	6.39	9.30	-7.23	0.55
Yb	**0.01**	0.70	0.03	4.34	-	-	0.03
Zr	**6.00**	97.78	4.07	4.16	99.00	-1.24	4.07

		GSR-3					
	LOD	Mean (n=2)	STD	%RSD	Recommended	%RD	2σ
Ce	**0.30**	108.09	61.72	57.11	105.00	2.94	87.29
Cs	**0.01**	0.46	0.05	10.86	-	-	0.07
Dy	**0.01**	5.50	3.13	56.83	5.60	-1.80	4.42
Er	**0.006**	2.005	1.134	56.559	2.000	0.250	1.604
Eu	**0.004**	3.293	1.856	56.385	3.200	2.891	2.625
Gd	**0.03**	8.68	4.92	56.64	8.50	2.16	6.96
Hf	**0.10**	6.40	3.57	55.77	6.50	-1.54	5.05
Ho	**0.002**	0.879	0.497	56.564	0.880	-0.114	0.703
La	**0.20**	55.81	31.67	56.74	56.00	-0.34	44.79
Lu	**0.001**	0.159	0.087	54.533	0.190	-16.316	0.123
Nb	**0.08**	75.30	43.12	57.27	68.00	10.74	60.98
Nd	**0.20**	51.66	29.43	56.98	54.00	-4.34	41.63
Pr	**0.03**	12.81	7.26	56.73	13.20	-2.99	10.27
Rb	**0.20**	38.68	21.81	56.39	37.00	4.54	30.85
Sm	**0.03**	10.24	5.83	56.90	10.20	0.39	8.24
Ta	**0.30**	-	-	-	4.30	-	-
Tb	**0.001**	1.121	0.622	55.506	1.200	-6.625	0.880
Th	**0.05**	5.99	3.36	56.08	6.00	-0.25	4.75
Tm	**0.005**	0.230	0.129	55.981	0.280	-17.857	0.182
U	**0.01**	1.45	0.82	56.61	1.40	3.54	1.16
Y	**0.20**	22.63	12.74	56.33	22.00	2.84	18.02
Yb	**0.01**	1.29	0.72	56.37	1.50	-14.33	1.02
Zr	**6.00**	297.10	169.25	56.97	277.00	7.26	239.35

Table A6. continued.

		GSP-2					
	LOD	Mean (n=4)	STD	%RSD	Accepted	%RD	2σ
Ce	**0.30**	>200	-	-	410.00	-	-
Cs	**0.01**	1.25	0.05	4.13	1.20	3.83	0.05
Dy	**0.01**	5.87	0.36	6.10	6.10	-3.79	0.36
Er	**0.006**	2.420	0.102	4.214	2.200	10.000	0.102
Eu	**0.004**	2.370	0.177	7.487	2.300	3.022	0.177
Gd	**0.03**	12.49	1.01	8.06	12.00	4.06	1.01
Hf	**0.10**	13.93	0.61	4.40	14.00	-0.54	0.61
Ho	**0.002**	0.988	0.054	5.438	1.000	-1.175	0.054
La	**0.20**	>100	-	-	180.00	-	-
Lu	**0.001**	0.238	0.011	4.778	0.230	3.478	0.011
Nb	**0.08**	26.71	0.93	3.47	27.00	-1.09	0.93
Nd	**0.20**	>100	-	-	200.00	-	-
Pr	**0.03**	>25	-	-	51.00	-	-
Rb	**0.20**	>150	-	-	245.00	-	-
Sm	**0.03**	26.29	1.76	6.69	27.00	-2.62	1.76
Ta	**0.30**	0.87	0.04	4.88	-	-	0.04
Tb	**0.001**	1.335	0.116	8.681	-	-	0.116
Th	**0.05**	>100	-	-	105.00	-	-
Tm	**0.005**	0.303	0.014	4.593	0.290	4.310	0.014
U	**0.01**	2.55	0.13	5.17	2.40	6.28	0.13
Y	**0.20**	25.78	1.63	6.33	28.00	-7.94	1.63
Yb	**0.01**	1.74	0.09	5.33	1.60	8.44	0.09
Zr	**6.00**	531.85	17.18	3.23	550.00	-3.30	17.18

		BIR-1					
	LOD	Mean (n=4)	STD	%RSD	Accepted	%RD	2σ
Ce	**0.30**	2.03	0.12	5.83	1.95	3.97	0.12
Cs	**0.01**	0.06	0.02	33.33	-	-	0.02
Dy	**0.01**	2.61	0.13	4.79	2.50	4.52	0.13
Er	**0.006**	1.755	0.126	7.193	1.700	3.250	0.126
Eu	**0.004**	0.558	0.044	7.859	0.540	3.287	0.044
Gd	**0.03**	1.93	0.08	3.94	1.85	4.24	0.08
Hf	**0.10**	0.67	0.06	9.20	0.60	12.08	0.06
Ho	**0.002**	0.593	0.045	7.565	0.570	4.079	0.045
La	**0.20**	0.69	0.05	7.20	0.62	11.29	0.05
Lu	**0.001**	0.253	0.028	11.062	0.260	-2.692	0.028
Nb	**0.08**	0.60	0.09	14.34	0.60	0.00	0.09
Nd	**0.20**	2.49	0.12	4.79	2.50	-0.40	0.12
Pr	**0.03**	0.40	0.02	5.38	0.38	4.54	0.02
Rb	**0.20**	0.22	0.06	29.46	0.25	-12.00	0.06
Sm	**0.03**	1.14	0.06	5.31	1.10	3.64	0.06
Ta	**0.30**	<0.3	-	-	-	-	-
Tb	**0.001**	0.371	0.019	5.202	0.360	3.125	0.019
Th	**0.05**	<0.05	-	-	-	-	-
Tm	**0.005**	0.256	0.022	8.734	0.260	-1.635	0.022
U	**0.01**	0.01	0.00	30.86	-	-	0.00
Y	**0.20**	14.98	2.00	13.36	16.00	-6.39	2.00
Yb	**0.01**	1.63	0.15	9.27	1.65	-1.52	0.15
Zr	**6.00**	16.32	0.70	4.31	18.00	-9.32	0.70

Table A6, continued.

		NBS-688					
	LOD	Mean (n=4)	STD	%RSD	Accepted	%RD	2σ
Ce	**0.30**	12.50	0.26	2.07	13.30	-6.00	0.26
Cs	**0.01**	0.09	0.04	39.54	-	-	0.04
Dy	**0.01**	3.55	0.11	3.18	-	-	0.11
Er	**0.006**	2.211	0.084	3.787	-	-	0.084
Eu	**0.004**	1.135	0.084	7.424	1.070	6.075	0.084
Gd	**0.03**	3.16	0.14	4.56	-	-	0.14
Hf	**0.10**	1.63	0.09	5.46	1.60	1.87	0.09
Ho	**0.002**	0.783	0.046	5.878	-	-	0.046
La	**0.20**	5.45	0.13	2.31	-	-	0.13
Lu	**0.001**	0.345	0.020	5.904	0.340	1.324	0.020
Nb	**0.08**	4.29	0.21	4.90	-	-	0.21
Nd	**0.20**	8.71	0.31	3.58	-	-	0.31
Pr	**0.03**	1.82	0.06	3.18	-	-	0.06
Rb	**0.20**	2.19	0.25	11.21	1.91	14.53	0.25
Sm	**0.03**	2.52	0.11	4.23	2.79	-9.86	0.11
Ta	**0.30**	0.30	0.04	12.47	-	-	0.04
Tb	**0.001**	0.541	0.023	4.231	0.450	20.222	0.023
Th	**0.05**	0.35	0.03	7.38	0.33	6.06	0.03
Tm	**0.005**	0.331	0.017	4.987	-	-	0.017
U	**0.01**	0.30	0.02	7.99	0.37	-17.91	0.02
Y	**0.20**	20.34	0.85	4.16	-	-	0.85
Yb	**0.01**	2.21	0.08	3.68	2.09	5.50	0.08
Zr	**6.00**	57.20	1.93	3.38	-	-	1.93

		MRB-29					
	LOD	Mean (n=40)	STD	%RSD	Accepted	%RD	2σ
Ce	**0.30**	50.70	1.32	2.61	51.20	-0.98	0.42
Cs	**0.01**	0.29	0.04	14.41	0.25	15.91	0.01
Dy	**0.01**	5.38	0.15	2.76	5.37	0.10	0.05
Er	**0.006**	2.899	0.089	3.068	2.900	-0.030	0.028
Eu	**0.004**	2.002	0.100	5.012	1.950	2.665	0.032
Gd	**0.03**	6.23	0.19	3.09	6.22	0.21	0.06
Hf	**0.10**	4.65	0.16	3.50	4.59	1.30	0.05
Ho	**0.002**	1.059	0.038	3.623	1.050	0.829	0.012
La	**0.20**	22.64	0.50	2.20	22.70	-0.25	0.16
Lu	**0.001**	0.371	0.016	4.242	0.370	0.196	0.005
Nb	**0.08**	13.44	0.43	3.18	13.30	1.02	0.14
Nd	**0.20**	28.96	0.72	2.49	29.10	-0.47	0.23
Pr	**0.03**	6.75	0.15	2.18	6.74	0.08	0.05
Rb	**0.20**	15.19	0.96	6.32	15.20	-0.09	0.30
Sm	**0.03**	6.37	0.18	2.80	6.39	-0.26	0.06
Ta	**0.30**	0.82	0.04	5.34	0.81	1.10	0.01
Tb	**0.001**	0.929	0.029	3.157	0.930	-0.113	0.009
Th	**0.05**	2.70	0.09	3.22	2.69	0.34	0.03
Tm	**0.005**	0.404	0.015	3.648	0.400	1.088	0.005
U	**0.01**	0.66	0.02	3.23	0.66	0.19	0.01
Y	**0.20**	26.88	0.85	3.16	26.80	0.32	0.27
Yb	**0.01**	2.52	0.09	3.53	2.54	-0.60	0.03
Zr	**6.00**	178.94	4.38	2.45	179.00	-0.03	1.39

Table A6. continued.

		MRB-32					
	LOD	Mean (n=2)	STD	%RSD	Accepted	%RD	2σ
Ce	**0.30**	4.40	0.15	3.38	4.50	-2.33	0.21
Cs	**0.01**	0.78	0.01	1.55	0.90	-13.61	0.02
Dy	**0.01**	1.23	0.00	0.35	1.25	-1.76	0.01
Er	**0.006**	0.703	0.026	3.724	0.700	0.357	0.037
Eu	**0.004**	0.283	0.006	2.253	0.284	-0.528	0.009
Gd	**0.03**	1.20	0.03	2.24	1.23	-2.60	0.04
Hf	**0.10**	0.75	0.07	9.43	0.76	-1.32	0.10
Ho	**0.002**	0.254	0.004	1.395	0.252	0.595	0.005
La	**0.20**	1.60	0.06	3.54	1.65	-3.03	0.08
Lu	**0.001**	0.094	0.003	3.009	0.094	0.000	0.004
Nb	**0.08**	1.35	0.07	5.24	1.41	-4.26	0.10
Nd	**0.20**	3.29	0.09	2.80	3.37	-2.52	0.13
Pr	**0.03**	0.67	0.01	0.96	0.69	-3.55	0.01
Rb	**0.20**	1.69	0.02	1.26	1.79	-5.87	0.03
Sm	**0.03**	1.01	0.01	0.70	1.02	-1.47	0.01
Ta (n=1)	**0.30**	0.17	-	-	0.17	0.00	-
Tb	**0.001**	0.196	0.006	2.886	0.204	-3.922	0.008
Th	**0.05**	0.21	0.04	17.25	0.19	10.81	0.05
Tm	**0.005**	0.102	0.001	1.386	0.100	2.000	0.002
U	**0.01**	0.06	0.00	2.57	0.06	-5.17	0.00
Y	**0.20**	6.26	0.30	4.74	6.27	-0.16	0.42
Yb	**0.01**	0.64	0.03	4.42	0.64	0.00	0.04
Zr	**6.00**	27.65	2.62	9.46	27.00	2.41	3.70

		NPD-1					
	LOD	Mean (n=3)	STD	%RSD	Accepted	%RD	2σ
Ce	**0.30**	35.17	0.43	1.21	35.90	-2.03	0.49
Cs	**0.01**	1.10	0.02	2.13	1.09	0.64	0.03
Dy	**0.01**	4.65	0.08	1.73	4.77	-2.42	0.09
Er	**0.006**	2.788	0.027	0.974	2.830	-1.496	0.031
Eu	**0.004**	1.299	0.009	0.672	1.310	-0.814	0.010
Gd	**0.03**	4.70	0.12	2.51	4.76	-1.22	0.14
Hf	**0.10**	3.17	0.12	3.65	3.19	-0.73	0.13
Ho	**0.002**	0.959	0.011	1.162	0.980	-2.109	0.013
La	**0.20**	16.53	0.23	1.37	16.90	-2.17	0.26
Lu	**0.001**	0.386	0.014	3.514	0.398	-2.931	0.016
Nb	**0.08**	6.17	0.06	0.94	6.30	-2.12	0.07
Nd	**0.20**	18.17	0.19	1.05	18.70	-2.83	0.22
Pr	**0.03**	4.37	0.05	1.09	4.48	-2.50	0.06
Rb	**0.20**	48.41	0.15	0.32	48.00	0.85	0.18
Sm	**0.03**	4.30	0.06	1.28	4.38	-1.90	0.06
Ta	**0.30**	0.48	0.04	7.94	0.49	-2.72	0.04
Tb	**0.001**	0.748	0.007	0.949	0.770	-2.900	0.008
Th	**0.05**	4.50	0.12	2.74	4.70	-4.18	0.14
Tm	**0.005**	0.400	0.011	2.785	0.409	-2.119	0.013
U	**0.01**	1.51	0.04	2.88	1.54	-1.69	0.05
Y	**0.20**	24.91	0.16	0.64	25.30	-1.55	0.18
Yb	**0.01**	2.57	0.03	1.12	2.65	-3.14	0.03
Zr	**6.00**	115.50	6.19	5.36	116.00	-0.43	7.15

Table A6, continued.

		PER-1					
	LOD	Mean (n=5)	STD	%RSD	Accepted	%RD	2σ
Ce	**0.30**	44.11	0.88	1.99	45.10	-2.19	0.79
Cs	**0.01**	7.27	0.11	1.48	7.20	1.03	0.10
Dy	**0.01**	1.67	0.02	1.15	1.60	4.66	0.02
Er	**0.006**	1.130	0.012	1.030	1.020	10.784	0.010
Eu	**0.004**	0.359	0.012	3.453	0.500	-28.280	0.011
Gd	**0.03**	1.82	0.08	4.27	1.80	1.11	0.07
Hf	**0.10**	2.62	0.08	3.19	2.61	0.38	0.07
Ho	**0.002**	0.358	0.005	1.364	0.300	19.200	0.004
La	**0.20**	25.46	0.43	1.70	26.00	-2.06	0.39
Lu	**0.001**	0.218	0.007	3.210	0.210	3.619	0.006
Nb	**0.08**	5.90	0.14	2.40	6.58	-10.33	0.13
Nd	**0.20**	14.62	0.19	1.29	13.80	5.97	0.17
Pr	**0.03**	4.50	0.03	0.65	4.20	7.06	0.03
Rb	**0.20**	144.37	2.77	1.92	127.00	13.67	2.47
Sm	**0.03**	2.36	0.02	0.72	2.20	7.39	0.02
Ta	**0.30**	0.58	0.04	7.58	0.60	-4.17	0.04
Tb	**0.001**	0.277	0.004	1.414	<0.5	-	0.004
Th	**0.05**	15.91	0.22	1.38	14.30	11.22	0.20
Tm	**0.005**	0.187	0.004	2.329	<0.3	-	0.004
U	**0.01**	2.76	0.04	1.39	2.52	9.56	0.03
Y	**0.20**	10.49	0.26	2.52	11.55	-9.16	0.24
Yb	**0.01**	1.34	0.03	2.06	1.20	11.46	0.02
Zr	**6.00**	84.70	2.57	3.04	90.00	-5.89	2.30

		BAMAP-01					
	LOD	Mean (n=5)	STD	%RSD	Recommended	%RD	2σ
Ce	**0.30**	49.87	0.54	1.08	47.70	4.55	0.48
Cs	**0.01**	0.36	0.02	6.33	0.37	-3.14	0.02
Dy	**0.01**	4.18	0.05	1.14	4.37	-4.42	0.04
Er	**0.006**	1.887	0.028	1.480	2.090	-9.722	0.025
Eu	**0.004**	1.942	0.027	1.384	1.950	-0.421	0.024
Gd	**0.03**	5.62	0.11	2.02	5.25	6.96	0.10
Hf	**0.10**	4.26	0.05	1.29	4.50	-5.33	0.05
Ho	**0.002**	0.749	0.008	1.038	0.850	-11.882	0.007
La	**0.20**	24.42	0.31	1.28	25.20	-3.09	0.28
Lu	**0.001**	0.198	0.003	1.288	0.230	-13.913	0.002
Nb	**0.08**	29.12	0.49	1.67	31.13	-6.46	0.44
Nd	**0.20**	25.99	0.14	0.55	26.00	-0.03	0.13
Pr	**0.03**	6.13	0.06	0.95	6.78	-9.55	0.05
Rb	**0.20**	22.24	0.34	1.52	26.10	-14.80	0.30
Sm	**0.03**	5.74	0.06	1.10	5.77	-0.55	0.06
Ta	**0.30**	1.73	0.03	1.80	2.00	-13.40	0.03
Tb	**0.001**	0.776	0.010	1.314	0.810	-4.198	0.009
Th	**0.05**	2.75	0.03	1.11	2.91	-5.64	0.03
Tm	**0.005**	0.242	0.004	1.619	0.270	-10.519	0.003
U	**0.01**	0.71	0.01	0.99	0.77	-8.29	0.01
Y	**0.20**	18.96	0.25	1.31	21.30	-10.99	0.22
Yb	**0.01**	1.45	0.04	2.47	1.41	2.55	0.03
Zr	**6.00**	180.48	1.61	0.89	178.00	1.39	1.44

Table A6. continued.

		CHA-2					
	LOD	Mean (n=5)	STD	%RSD	Accepted	%RD	2s
Ce	**0.30**	47.08	5.43	11.53	51.53	-8.64	4.85
Cs	**0.01**	4.16	0.03	0.62	4.53	-8.15	0.02
Dy	**0.01**	3.59	0.42	11.66	3.87	-7.26	0.37
Er	**0.006**	2.124	0.220	10.381	2.180	-2.578	0.197
Eu	**0.004**	1.101	0.124	11.269	1.190	-7.462	0.111
Gd	**0.03**	4.02	0.51	12.82	4.30	-6.60	0.46
Hf	**0.10**	4.46	0.05	1.23	4.36	2.29	0.05
Ho	**0.002**	0.719	0.076	10.501	0.780	-7.769	0.068
La	**0.20**	22.38	2.58	11.53	24.62	-9.09	2.31
Lu	**0.001**	0.320	0.037	11.407	0.340	-5.824	0.033
Nb	**0.08**	9.96	0.18	1.82	9.92	0.40	0.16
Nd	**0.20**	22.55	2.76	12.26	24.91	-9.48	2.47
Pr	**0.03**	5.72	0.69	12.06	6.18	-7.49	0.62
Rb	**0.20**	73.81	0.77	1.05	75.93	-2.80	0.69
Sm	**0.03**	4.45	0.56	12.64	4.85	-8.33	0.50
Ta	**0.30**	0.87	0.04	4.30	0.86	1.16	0.03
Tb	**0.001**	0.601	0.058	9.600	0.670	-10.358	0.052
Th	**0.05**	7.20	0.58	8.06	7.49	-3.85	0.52
Tm	**0.005**	0.315	0.032	10.203	0.380	-17.158	0.029
U	**0.01**	2.84	0.03	0.90	2.72	4.40	0.02
Y	**0.20**	20.03	1.99	9.93	23.30	-14.02	1.78
Yb	**0.01**	2.09	0.22	10.40	2.26	-7.70	0.19
Zr	**6.00**	173.08	1.62	0.93	171.53	0.90	1.45

Appendix B

Analytical Methods for Uranium–Lead Geochronology

Uranium-lead geochronological samples for this project were collected during field work in 2003 and 2004 and analyzed at the Jack Satterly Geochronology Laboratory (JSGL) at the University of Toronto. All samples had weathered surfaces removed in the field using a hammer and chisel, and each piece was subsequently washed and dried in the laboratory before further processing. Total rock sample weights committed to crushing were generally in the 10 to 15 kg range. Samples were initially reduced using a jaw crusher, and then taken down to sand-size particles using a disk mill. Wilfley™ (shaking) table, heavy liquid (bromoform and methylene iodide) and magnetic separation (Frantz™ isodynamic separator) techniques were then employed to obtain an initial concentration of zircon and other minerals of high density.

From the least paramagnetic groups, highest quality zircon grains were handpicked under alcohol using a binocular microscope, with preferential individual grain selection made on the basis of clarity, and the absence of cores, cracks, alteration, and (lead-bearing) inclusions. All zircon fractions were subjected to an air abrasion treatment (Krogh 1982) in order to remove exterior portions of grains that may have experienced post-crystallization lead loss. Prior to dissolution, weights of abraded zircons were estimated by use of a scaled digital photographic measurement of the length and breadth of each grain and an estimate of the maximum thickness, together with the known density.

Selected zircons were washed briefly in warm 4N HNO_3, given a brief second cleaning in 7N HNO_3, and then transferred in a single drop of 7N HNO_3 into clean Teflon™ dissolution vessels together with concentrated hydrofluoric acid and a measured quantity of mixed ^{205}Pb–^{235}U isotopic tracer solution (Krogh 1973). Complete sample dissolution was accomplished over a period of approximately 4 days at a temperature of 195°C. In all cases, zircon grain sizes were sufficiently small such that no ion exchange column chemical isolation and purification of lead and uranium was necessary. Instead, fractions were dried down, redissolved in 6N HCl, dried down again with phosphoric acid and loaded directly with silica gel onto outgassed single Re filaments. All of the isotopic compositions of lead and uranium were determined on a VG354 mass spectrometer using a Daly detector equipped with a digital ion counting system. System deadtime corrections during the analytical period were 19.5 ns for both lead and uranium. Corrections for Daly mass discrimination were 0.05%/a.m.u., while that for thermal mass discrimination was estimated at 0.1%/a.m.u.

Laboratory procedural blanks at the JSGL are routinely at the 0.5 pg and 0.1 pg level or less for lead and uranium, respectively. In most cases, the measured total common lead in the samples was negligible and was assigned the isotopic composition of the lab blank; in a few cases, however, higher common Pb contents could be correlated with the presence of inclusions or minor cracks, and can be interpreted to represent initial common lead, estimated here after Stacey and Kramers (1975). Comprehensive error estimation was made by propagating all known sources of analytical error, including internal (within-run) ratio variability, uncertainty in the fractionation corrections for lead and uranium (based on long-term monitoring of standards), and uncertainties in the quantities and isotopic compositions of the laboratory blank and initial common lead. The decay constants used for the U–Pb system are those of Jaffey et al. (1971). Age errors in the text, tables and figures are all presented at the 95% confidence level. Error ellipses in the concordia diagrams are shown at the 2σ level. For concordant and near-concordant data having overlapping $^{207}Pb/^{206}Pb$ errors, weighted mean ages were calculated by forcing a regression through the origin of concordia, according to the method of Davis (1982). Other discordia lines and concordia intercept ages were also determined by the regression methods outlined in Davis (1982), using the in-house program ROMAGE. In most cases, the calculated ages and errors using either the Davis (1982) or IsoPlot/Ex (Ludwig 2001) algorithms are equivalent. Uranium–lead concordia diagrams were generated using the IsoPlot/Ex program of Ludwig (2001).

REFERENCES

Davis, D.W. 1982. Optimum linear regression and error estimation applied to U-Pb data; Canadian Journal of Earth Sciences, v.19, p.2141-2149.

Jaffey, A.H., Flynn, K.F., Glendenin, L.E., Bentley, W.C. and Essling, A.M. 1971. Precision measurement of half-lives and specific activities of 235U and 238U; Physical Review C, v.4, p.1889-1906.

Krogh, T.E. 1973. A low contamination method for hydrothermal decomposition of zircon and extraction of U and Pb for isotopic age determinations; Geochimica et Cosmochimica Acta, v.37, p.485-494.

——— 1982. Improved accuracy of U-Pb zircon ages by the creation for more concordant systems using an air abrasion technique; Geochimica et Cosmochimica Acta, v.46, p.637-649.

Ludwig, K.E. 2001. Users manual for Isoplot/Ex v.2.49: a geochronological toolkit for Microsoft® Excel; University of California–Berkeley, Berkeley, California, Berkeley Geochronology Center, Special Publication No. 1a.

Stacey, J.S. and Kramers, J.D. 1975. Approximation of terrestrial lead isotope evolution by a two-stage model; Earth and Planetary Science Letters, v.26, p.207-221.

Metric Conversion Table

Conversion from SI to Imperial			Conversion from Imperial to SI		
SI Unit	*Multiplied by*	*Gives*	*Imperial Unit*	*Multiplied by*	*Gives*
LENGTH					
1 mm	0.039 37	inches	1 inch	**25.4**	mm
1 cm	0.393 70	inches	1 inch	**2.54**	cm
1 m	3.280 84	feet	1 foot	**0.304 8**	m
1 m	0.049 709	chains	1 chain	20.116 8	m
1 km	0.621 371	miles (statute)	1 mile (statute)	**1.609 344**	km
AREA					
1 cm^2	0.155 0	square inches	1 square inch	**6.451 6**	cm^2
1 m^2	10.763 9	square feet	1 square foot	**0.092 903 04**	m^2
1 km^2	0.386 10	square miles	1 square mile	2.589 988	km^2
1 ha	2.471 054	acres	1 acre	0.404 685 6	ha
VOLUME					
1 cm^3	0.061 023	cubic inches	1 cubic inch	**16.387 064**	cm^3
1 m^3	35.314 7	cubic feet	1 cubic foot	0.028 316 85	m^3
1 m^3	1.307 951	cubic yards	1 cubic yard	0.764 554 86	m^3
CAPACITY					
1 L	1.759 755	pints	1 pint	0.568 261	L
1 L	0.879 877	quarts	1 quart	1.136 522	L
1 L	0.219 969	gallons	1 gallon	**4.546 090**	L
MASS					
1 g	0.035 273 962	ounces (avdp)	1 ounce (avdp)	28.349 523	g
1 g	0.032 150 747	ounces (troy)	1 ounce (troy)	**31.103 476 8**	g
1 kg	2.204 622 6	pounds (avdp)	1 pound (avdp)	**0.453 592 37**	kg
1 kg	0.001 102 3	tons (short)	1 ton (short)	**907.184 74**	kg
1 t	1.102 311 3	tons (short)	1 ton (short)	**0.907 184 74**	t
1 kg	0.000 984 21	tons (long)	1 ton (long)	**1016.046 908 8**	kg
1 t	0.984 206 5	tons (long)	1 ton (long)	**1.016 046 90**	t
CONCENTRATION					
1 g/t	0.029 166 6	ounce (troy)/ ton (short)	1 ounce (troy)/ ton (short)	34.285 714 2	g/t
1 g/t	0.583 333 33	pennyweights/ ton (short)	1 pennyweight/ ton (short)	1.714 285 7	g/t

OTHER USEFUL CONVERSION FACTORS

	Multiplied by	
1 ounce (troy) per ton (short)	31.103 477	grams per ton (short)
1 gram per ton (short)	0.032 151	ounces (troy) per ton (short)
1 ounce (troy) per ton (short)	20.0	pennyweights per ton (short)
1 pennyweight per ton (short)	0.05	ounces (troy) per ton (short)

Note: Conversion factors which are in bold type are exact. The conversion factors have been taken from or have been derived from factors given in the Metric Practice Guide for the Canadian Mining and Metallurgical Industries, published by the Mining Association of Canada in co-operation with the Coal Association of Canada.

ISSN 0826-9580
ISBN 0-7794-7615-8